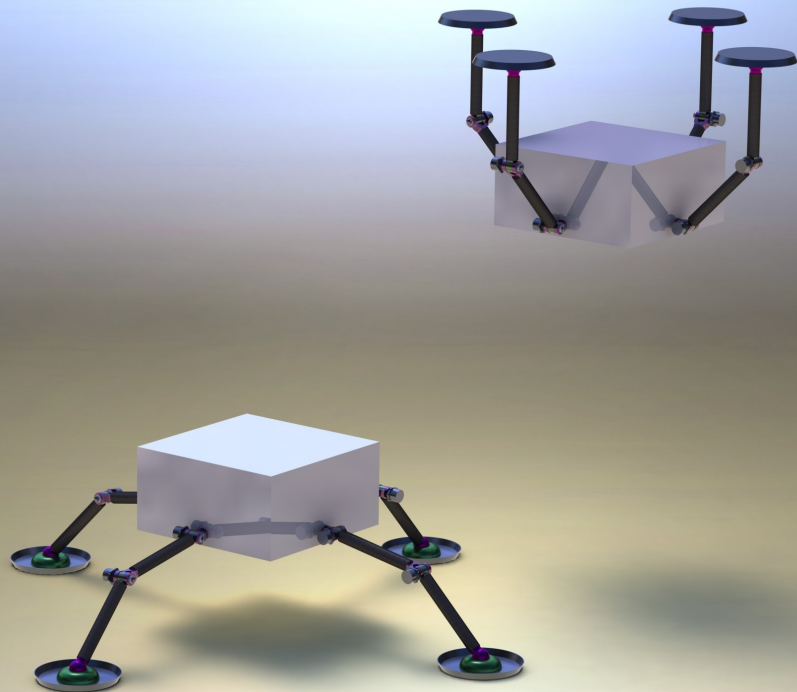


Europa Lander Landing System

Study on Deployment,
Landing and
Preliminary Design

Pietro Squillace



Europa Lander Landing System

Study on Deployment, Landing and
Preliminary Design

by

Pietro Squillace

To obtain the degree of Master of Science
at the Delft University of Technology.
to be defended publicly on Monday January 31st, 2022 at 2:00 PM.

Student number: 5011116
Project duration: December 8, 2020 – January 31 , 2022
Thesis Committee: Dr. J. Guo, TU Delft, Committee Chair
Prof. Chiara Bisagni, TU Delft, Supervisor
Ir. Barry Zandbergen, TU Delft, Supervisor
Ir. M. C. Naeije, TU Delft, External Examiner

An electronic version of this thesis will be available at <http://repository.tudelft.nl/>.

Acknowledgments

First and foremost I would like to thank my family. Thank you so much for supporting me throughout the highs and lows of my 2.5 years of master. Giving me the opportunity to study abroad both for my bachelor and master is something I will always be thankful for.

A special thank has to go to both my supervisors: Barry and Chiara. Your guidelines have made sure that I delivered the best project that I could think of. It's a pity our meetings were only online due to the measures, but they were incredibly useful nevertheless.

It wouldn't be TU Delft without its engineering student projects, of which I had the opportunity to be part of in many. I would like to thank the student teams that I have been part of: Formula Student Team Delft, Project Inspiration and Lunar Zebro. Thank you for all the lessons that you taught me about how to be a real engineer, even though my sleeping schedule has been affected by these multiple times. Being able to call myself one of your engineers is priceless.

And finally I'd like to thank my flatmates that have accompanied me throughout the last tough 2.5 years: Edoardo, Dominik, Willem, Kaushik, Emily, Marco, Elina and Sarah. Spending the lockdowns, curfew, movie and board game nights and dinners with you has helped me stay focused for the past thesis year and for that I am incredibly thankful.

Pietro Squillace
Delft, January 2022

Abstract

The Europa Lander is a mission by NASA to land scientific instruments on the Jovian Moon by 2030. The current design of the landing system envisions fixed landing legs with the lander being lowered down at very low velocities (≈ 0.1 m/s) by use of a Skycrane. This latter system not only adds mass, but also requires complicated moving parts and a high reliance on control systems to work properly. This thesis wants to propose an alternative design to the Europa Lander Landing System that uses sturdier legs that can withstand landing at higher velocities than originally envisioned. This eliminates the need to use a Skycrane system. In order to pack them in a more efficient way while coasting, the landing legs are of the deployable type.

In order to track the deployment dynamics of the landing system a 2-dimensional Matlab deployment model based on double pendulum motion with damping is created. Furthermore, in order to prove the landability with a prescribed landing case, a landing model is created using FEA software Abaqus. The landing model is used to make sure that stresses, strains and G forces applied to the rest of the lander don't exceed prescribed values as dictated by requirements. The implementation of both models is verified by comparing models found in literature with the ones made for the purpose of this thesis. Good correlation is shown with less than 10% of difference between literature results and results for this thesis.

The result through the modelling found a specific geometry with parameters that include, but are not limited to: length of leg elements, joint damping and maximum deployment angles. The 2-dimensional geometry features output by the Matlab deployment model are fed into the Abaqus landing model in order to assess the landing performance with a single leg landing. The landing case has been chosen as a worst case scenario. 2 landing leg designs, with the same geometry, but one made of metallic parts and the other made of composite materials are compared in the landing model. In this model it was found that both designs pass the stress (or strain for the composite leg design) and G forces requirements when a shock absorber is attached to the leg and when they land on deformable Lunar like soil. On the other hand, the landing legs don't pass G forces requirements when landing on stiff soil.

Through the modelling, it was also possible to give preliminary design guidelines over the subsystems making the landing system. Therefore, system engineering practices have been used in order to initiate the design of some of the subsystems such as the landing damping, the leg joints and the locking mechanism to lock the legs at the desired angle and make sure they don't retract.

Simplifications have been made in order to model some of the landing and deployment aspects of the system for this thesis. Matters related to the adaptability and the detailed design of each of the subsystems have been left as future work.

In the end, a comparison between the design developed in this thesis and the current Europa Lander Landing System design is made difficult by the lack of technical data on the latter related to mass. Nevertheless, a design that uses the decelerations of the engine module before touchdown is developed and the suggested material for the leg elements is CFRP. The design, though, didn't pass mass fraction requirements when computing the mass of the extra subsystems. Even so, locations where potential gains through mass optimization can be performed for future studies have been pointed out.

Contents

List of Figures	ix
List of Tables	xiii
Glossary	xv
1 Introduction and Research Questions	1
1.1 Literature Review	2
1.2 Problem Statement	9
1.3 Research Questions	9
1.4 Thesis Organisation	10
2 Requirements	11
2.1 Design Requirements for the Europa Lander Landing System	11
2.2 Deployment Modelling Tool Requirements	12
2.3 Landing Modelling Tool Requirements	13
3 Deployment Modelling	15
3.1 Landing System Matlab Parametrised Model	15
3.2 Assumptions for Deployment Model	17
3.3 Pendulum Model for Deployment Analyses	17
3.4 Numerical Values to be Fed in Models	21
4 Landing Modelling	23
4.1 Landing Modelling Assumptions	23
4.2 Landing Stability Modelling on Matlab	24
4.3 Finite Element Model	25
5 Verification	31
5.1 Verification of Deployment Model	31
5.2 Verification of Landing Stability	41
5.3 Verification of Landing Model	43
5.4 Conclusion on Verification	50
6 Deployment Analyses Results	51
6.1 Deployment Model Sensitivity Analyses	51
6.2 Sensitivity Analysis 1: Damping vs. Deployment Time	52
6.3 Sensitivity Analysis 2: Cutoff Deployment Angle vs. Deployment Time	55
6.4 Sensitivity Analysis 3: Leg Mass vs. Deployment Time	58
6.5 Sensitivity Analysis 4: Leg Element Length vs. Deployment Time	63
6.6 Sensitivity Analysis 5: Footprint vs. Landing Stability	66
6.7 Sensitivity Analysis 6: COM Height vs. Landing Stability	67
6.8 Conclusions Drawn from Sensitivity Analyses	68
6.9 Detailed Deployment Analyses	69
6.10 Conclusion and Limitations on Deployment Analyses	72
7 Landing Analyses Results	75
7.1 Types of Analyses	75
7.2 Geometry	75
7.3 Mesh Convergence Analysis	77
7.4 Detailed Landing Analyses	77
7.5 Conclusion and Findings on Landing Analyses	84

8	System Design Guidelines	85
8.1	Systems to Be Selected and Tradeoff Methodology	85
8.2	Leg Joints	86
8.3	Damping	88
8.4	Locking Mechanism	92
8.5	Preliminary Landing System Design.	94
8.6	Conclusions on System Design Guidelines	96
9	Conclusions and Recommendations	97
9.1	Conclusions.	97
9.2	Further Work	99
A	Matlab Deployment Modelling Code and Extra Figures	105
A.1	Matlab Deployment Modelling and Landing Stability Tool	105
A.2	Detailed Deployment Modelling Figures.	116
A.3	Landing Performances vs. Increasing Payload Mass	122
B	Thesis proposal	125
C	Tabulated Data for Future Verification Purposes	139

List of Figures

1.1	The current Europa Lander Stage Configuration [50].	2
1.2	Diagram of Europa Lander showing the width of the payload module [16].	3
1.3	Timeline of descent of the Europa Lander [16].	4
1.4	Stage distribution of Europa Lander mission [44].	4
1.5	Deployed state (on the left) and stowed state (on the right) of the multi particle approximation method for the IKAROS deployable boom [5].	5
1.6	Philae Landing System [52].	6
1.7	Model of Phoenix terminal descent configuration [15].	6
1.8	Technical drawing of Viking 1 landing system (all dimensions are in inches) [36].	7
1.9	Example of landing FEM results from [22].	7
1.10	Vectors involved in stability criterion calculation [12].	8
1.11	Landing success/failure maps of a lander design at different terrain slope angles β , the red circle signifies landing success, while the blue cross means landing failure and tip over [28].	9
3.1	Naming convention of coordinates used for the landing system (shown in here in the deployed configuration).	15
3.2	Naming convention of Matlab deployment model characteristics.	16
3.3	Adaptability of legs with 2 leg elements as seen in current Europa Lander design [46].	18
3.4	Deployment model implementation flowchart.	19
3.5	General initial leg configuration for deployment modelling studies.	20
3.6	Lander rectangle with leg elements around it to be packed in an efficient configuration.	22
4.1	FBD showing a diagram of a stable landing on an inclined surface.	24
4.2	FBD showing a diagram of an unstable landing on an inclined surface.	24
4.3	Detail of mesh in landing leg elements with S4R elements.	26
4.4	Detail of mesh S4R element of the landing leg's footpad.	27
4.5	Mesh distribution on the deformable soil cuboid.	27
4.6	Abaqus simulation assembly.	27
4.7	Detail of the FEA setup with concentrated mass (at RP1 as seen with Green square) interacting with the top of the landing leg.	28
5.1	Naming convention for double pendulum for verification studies.	32
5.2	Variation of angular rate against variation of angular displacement in [9].	33
5.3	Variation of angular displacement with respect to time in [9].	33
5.4	Variation of angular rate against variation of angular displacement in Matlab algorithm developed for this thesis.	34
5.5	Variation of angular displacement with respect to time in the deployment Matlab algorithm used for this thesis.	34
5.6	Variation of angular displacement with respect to angular rate in double pendulum algorithm in [9] with markings of angular rate when the angle is -0.5 rad.	35
5.7	Variation of angular rate with respect to variation of angular displacement in [9] with lower damping.	36
5.8	Variation of angular displacement with respect to time in [9] with lower damping.	37
5.9	Variation of angular rate against variation of angular displacement in deployment Matlab algorithm used for this thesis with lower damping.	37
5.10	Variation of angular displacement with respect to time in the deployment Matlab algorithm used for this thesis with lower damping.	38

5.11	Variation of angular displacement with respect to time in double pendulum algorithm in [9] with markings of the third oscillation when displacement is at +1 rad.	39
5.12	Analysis of implication of position of center of mass over leg element length assumption.	40
5.13	Geometry used for landing stability algorithm verification.	42
5.14	Visualisation of angles at which geometry is stable (in blue circles) and unstable (in red circles).	42
5.15	Geometry parameters of the landing leg as seen in [27].	43
5.16	Geometry of the landing leg as sketched on Abaqus with SI units.	44
5.17	Material assignments for each landing leg section.	45
5.18	Load displacement curve of different models as shown in [27].	45
5.19	Top part of Abaqus model showing the reference point where the model is loaded and the rigid body interaction that connects the point to the top part of the model.	46
5.20	Detail of the boundary conditions at the bottom of the Abaqus model.	46
5.21	Detail of mesh elements at the top of the model.	47
5.22	Comparison of shortening vs. loading results between Mason [27] and the 3 studies made for this thesis written above.	48
6.1	Relation between deployment time and damping with changing damping for V1 of Sensitivity analysis #1.	53
6.2	Output geometries for V1 of Sensitivity analysis #1.	53
6.3	Relation between deployment time and damping with changing damping for V2 of Sensitivity analysis #1.	54
6.4	Output geometries for V2 of Sensitivity analysis #1.	55
6.5	Relation between Cutoff deployment angle and deployment time with changing CDA for V1 of Sensitivity analysis # 2.	56
6.6	Output geometries for V1 of Sensitivity analysis #2.	56
6.7	Relation between Cutoff deployment angle and deployment time with changing CDA and damping for V2 of Sensitivity analysis #2.	57
6.8	Relation between Cutoff deployment angle and deployment time with changing CDA and damping for V2 of Sensitivity analysis #2.	58
6.9	Variation of deployment time when mass of first leg element is changed in the V1 of sensitivity analysis 3.	59
6.10	Leg configurations output in V1 of sensitivity analysis 3.	60
6.11	Variation of deployment time when mass of second leg element is changed in the V2 of sensitivity analysis 3.	61
6.12	Leg configurations output in V2 of sensitivity analysis 3.	61
6.13	Variation of deployment time when masses of both leg elements is changed in the V3 of sensitivity analysis 3.	62
6.14	Variation of deployment time when masses of both leg elements is changed in the V4 of sensitivity analysis 3.	63
6.15	Variation of deployment time when leg element lengths are changed in the V1 of sensitivity analysis 4.	64
6.16	Leg configurations output in V1 of sensitivity analysis 4.	64
6.17	Variation of deployment time when leg element lengths are changed in the V1 of sensitivity analysis 4.	65
6.18	Leg configurations output in V2 of sensitivity analysis 4.	66
6.19	Stability plot of lander at different soil inclinations and footprint values.	67
6.20	Stability plot of lander at different soil inclinations and CDA values.	67
6.21	Output geometries for V1 of sensitivity analysis 5.	67
6.22	Variation of landing stability when COM height is changed in the V1 of sensitivity analysis 6.	68
6.23	1st timestep of deployment of aluminum landing leg.	70
6.24	2nd timestep of deployment of aluminum landing leg.	70
6.25	Second to last timestep of deployment of aluminum landing leg.	71
6.26	Last timestep of deployment modelling of aluminum landing leg.	71
6.27	Landing stability at different soil inclination angles for developed geometry.	72

6.28 Initial leg configuration with inward facing legs.	73
7.1 Geometry of landing system as developed by Matlab at the end of chapter 6 as a sketch.	76
7.2 3D Geometry of landing system.	76
7.3 Mesh convergence analysis.	77
7.4 Max Von Mises stress experienced by aluminum leg during landing with no dashpot and deformable soil (soil has been suppressed for better viewing of the landing leg).	78
7.5 Vertical deceleration profile (in mm/s^2) over time in landing of aluminum leg with no dashpot and deformable soil.	79
7.6 Deformation in vertical direction at moment of max sinking (landing leg has been suppressed for better viewing of the deformed floor).	79
7.7 Max Von Mises stress experienced by aluminum leg during landing with dashpot and deformable soil (soil has been suppressed for better viewing of the landing leg).	80
7.8 Vertical deceleration profile (in mm/s^2) over time in landing of aluminum leg with dashpot and deformable soil.	81
7.9 Max principal strain experienced by CFRP leg during landing with dashpot and deformable soil (soil has been suppressed for better viewing of the landing leg).	81
7.10 Vertical deceleration profile (in mm/s^2) over time in landing of CFRP leg with dashpot and deformable soil.	82
7.11 Max Von Mises stress experienced by aluminum leg during landing with dashpot and stiff soil (soil has been suppressed for better viewing of the landing leg).	82
7.12 Vertical deceleration profile (in mm/s^2) over time in landing of aluminum leg with dashpot and stiff soil.	83
7.13 Max principal strain experienced by CFRP leg during landing with dashpot and stiff soil (soil has been suppressed for better viewing of the landing leg).	83
7.14 Vertical deceleration profile (in mm/s^2) over time in landing of CFRP leg with dashpot and stiff soil.	84
8.1 Example of universal joint [7].	86
8.2 Ball joint in Lunar lander model of footpad [23].	86
8.3 Tradeoff table for leg joint concept selection.	87
8.4 Visualisation on SolidWorks of pin joint subassembly.	88
8.5 Envisioned application example of a rotary damper [21].	89
8.6 Hinge-like design for a rotational passive damper [1].	89
8.7 Tradeoff table for deployment damping concept selection.	90
8.8 Tradeoff table for landing damping concept selection.	91
8.9 Dampers based on plastic deformation of aluminum honeycomb [38].	91
8.10 CAD model of honeycomb damper.	92
8.11 Diagram of simplified ratchet mechanism.	93
8.12 Tradeoff table for locking mechanism concept selection.	93
8.13 Detailed CAD model of aluminum leg design.	94
8.14 Detailed CAD model of CFRP leg design.	95
8.15 Particular of pin joint (without rotary dashpot) between leg elements in detailed CFRP CAD model of the landing leg.	96
A.1 Variation of internal stresses experienced by the landing leg with varying payload mass.	122
A.2 Variation of G forces experienced by the lander COM with varying payload mass.	122
A.3 Variation of soil sinkage experienced by the footpad with varying payload mass.	123

List of Tables

4.1	Abaqus aluminum alloy 7075-T6 material table [2].	26
4.2	Elastic and physical material properties used to model the Lunar like soil on Abaqus. . .	26
4.3	Plastic properties of lunar like soil used for Abaqus simulations [32].	26
5.1	Pendulum characteristics for double pendulum first verification study, masses are located at the tips of each pendulum element.	33
5.2	Pendulum characteristics for verification study with lower damping, masses are located at the tips of each pendulum element.	36
5.3	Physical parameters' values as found in [27] with the original values and ones turned in SI units.	43
5.4	Material properties as found in [27].	44
5.5	Table summarising differences in the modelling done by [27] and the one made for this thesis for the verification of landing modelling.	47
5.6	Tabulated data from Figure 5.22.	48
5.7	Data from Figure 5.22 of dynamic implicit thesis analysis (separated from the previous table because of more data points available).	49
6.1	Landing system elements for V1 of Sensitivity analysis 1, done by changing the joint damping.	52
6.2	Landing system elements for V2 of Sensitivity analysis 1, done by changing the joint damping with a higher range than V1.	54
6.3	Landing system elements for V1 of Sensitivity analysis 2, done by changing the CDA. . .	55
6.4	Landing system elements for V2 of Sensitivity analysis 2, done by changing the damping and CDA.	57
6.5	Landing system elements for V1 of sensitivity analysis 3, done by changing only the mass of the first leg elements.	59
6.6	Landing system elements for V2 of sensitivity analysis 3, done by changing only the mass of the lower leg elements.	60
6.7	Landing system elements for V3 of sensitivity analysis 3, done by changing both the mass of the first and second leg elements.	62
6.8	Landing system elements for V4 of sensitivity analysis 3, done by changing both the mass of the first and second leg elements.	62
6.9	Landing system elements for V1 of sensitivity analysis 4, done by changing both the leg element lengths.	63
6.10	Landing system elements for V2 of sensitivity analysis 4, done by changing both the leg element lengths.	65
6.11	Landing system elements for V1 of Sensitivity analysis 5, done by changing the CDA. . .	66
6.12	Landing system elements for V1 of Sensitivity analysis 6, done by changing the CDA. . .	68
6.13	Feasible ranges for deployable landing system elements.	69
6.14	Landing system elements for the aluminum design of the landing system.	70
8.1	Mass breakdown of landing leg with aluminum leg elements.	94
8.2	Mass breakdown of landing leg with CFRP leg elements.	95
9.1	Design requirements acceptance.	98
9.2	Modelling requirements acceptance.	98
C.1	Tabulated and filtered data for Figure 5.4	141
C.2	Tabulated and filtered data for Figure 5.5	143

C.3	Tabulated and filtered data for Figure 5.9	145
C.4	Tabulated and filtered data for Figure 5.10	147

Glossary

b_i Landing System Joint Damping of Joint i

g Gravitational Acceleration

l_i Landing System Element length of Element i

m_i Leg Element Mass of Element i

P_{xy} Coordinate of Payload Point P in 2-Dimensional x-y Plane

θ_i Deployment Angle of Joint i

CAD Computer Aided Design

CDA Cutoff Deployment Angle

CFRP Carbon Fibre Reinforced Polymers

COG Center of Gravity

COM Center of Mass

DEP Deployment

DES Design

DS Descent Stage

EL Europa Lander

ELLS Europa Lander Landing System

FEA Finite Element Analysis

FEM Finite Element Modelling

FBD Free Body Diagram

GNC Guidance, Navigation and Control

HDA Hazard Detection and Avoidance

LAN Landing

MBD Multi Body Dynamics

NASA National Aeronautics and Space Administration

ODE Ordinary Differential Equation

PAY Payload

SCR Script

TRL Technology Readiness Level

TRN Terrain Relative Navigation

UTS Ultimate Tensile Strength

2D Two-Dimensional

3D Three-Dimensional

Introduction and Research Questions

Since the first successful controlled landing on another planetary body in 1966 by the Soviet Union [10], interplanetary landers have increased human capabilities to study the surface of other planetary bodies. In the following years, many aspects of a planet's surface have been studied by either robotic landers, rovers that were deployed from a lander, or by human themselves in the case of, for example, the Apollo Moon landings. These investigations range from looking for basic signs of life (as is the case for the Mars Perseverance rover [26]), to the investigations of the solar system's origins through the Rosetta-Philae lander [52]. Due to this, it is clear that it is important to provide safe landing to payloads (or humans) through a safe lander's landing system. With "safe" landing it is meant a landing that doesn't lead to high decelerations imparted to the spacecraft's instruments (in the case of this thesis, but also to humans in the case of manned landing capsules) that damage the internal payload, instruments and electronics. Furthermore, a "safe" landing is one that is stable within the prescribed soil inclination angles. Meaning that it doesn't lead the lander to tip over at the slope angles that are expected to be found in the planetary body of arrival. In the end, a safe landing is a landing that doesn't lead to damages to the landing legs.

In space engineering, deployable structures have been used in multiple instances. Some examples include the use of a folding mechanism to store during launch and subsequently deploy solar arrays for small and bigger satellites [35]. Also, space deployable structures have been used to deploy reflectors in order to design space based antennas [8]. The main loads that these structures will have to survive for are the ones that happen during launch inside the launch vehicle. Landing systems, on the other hand, will see the biggest of their loads coming from the action of landing itself [40].

One of the defining aspects of space based deployable structures is the means of actuation. Generally, a satellite's deployable structure would be actuated by either unlocking stored energy inside the material property, as is the case for the so called "tape springs" [24], or by using motors to move the structure move into the desired position.

The unique advantage that landers have is that they will have forces acting upon them because of their mission profile. These forces will be due to the decelerations imparted by the retro-rockets when the lander is slowing down to land on the target body's surface. This deceleration can be used to the lander's advantage when actuating the deployable landing system. The thesis will focus on the deployment dynamics and the landability of an alternative design of the Europa Lander Landing System (ELLS) whose deployment is aided by the decelerating forces of landing. Therefore, by using the negative G forces to actuate the deployment of the landing legs, no motor would need to be added to do the same task, which leads to the advantage of not using power from the spacecraft's supply for this action. The Europa Lander has been chosen because of the fact that this project is still in the preliminary stages [50], therefore offering a design variation is still beneficial for the success of the mission. Some data is present on design parameters of the lander, other types of data are missing. In the case of missing data, parameters or characteristics taken from similar landers such as the Viking Mars lander will be used [36]. As will be better seen in subsection 1.1.1, the Europa Lander Landing System design currently involves the use of a Skycrane [50]. This project does not look into it, but it does look into a design alternative and doesn't involve the hovering above the lander of a spacecraft that can deposit

material that can inherently tamper with the possible findings of the lander's instruments.

Designing a deployable landing system that has the decelerating G forces as a mean of actuation is a novel aspect. A similar project has been researched with regards to designing satellite's deployable structures using the spinning of satellites. This type of deployment is called "Centrifugal Deployment". In [57] and [20], the dynamic modelling of such a deployable structure applied to solar sails is laid out. In [57], the model is first set up analytically by deriving expressions on the rotational and translational motion of the tip masses, which are small masses at the corners of the solar sail. Using spinning to actuate the deployment is similar to the envisioned methodology for the actuation of the Europa Lander Landing System that will be analysed in this thesis since, in both cases, the inertia of the structure is used as a mean for its proper actuation. By using a structure's inertia to actuate its deployment, no motors are needed, therefore it is hypothesized that this leads to mass savings and to incurring a lower probability of failure due to the absence of components that require a control strategy that can be tampered by the radiation rich environment around Jupiter.

1.1. Literature Review

In this section of the thesis, the main findings from the Literature study are laid out. This thesis focuses on deployment and landing modelling and from those, a preliminary design is reached. The application to the deployable landing system concept is the Europa Lander, of which the current aspects of the mission and design of it are also laid out in this section. The following section has the aim of introducing aspects related to these matters so that the reader has an overview before seeing the work done for this thesis.

1.1.1. The Europa Lander

The Europa Lander (EL) is a mission to the Jovian Moon of Europa currently in the conceptual phase and envisioned by National Aeronautics and Space Administration (NASA) [50]. Launch date is expected for the end of the 2020 decade [50]. Europa is of particular scientific interest because of the fact that it is highly likely to hold a liquid ocean beneath its frozen surface [33]. A lander on Europa would pave the way, with its surface samples measurements, for a potential subsequent mission to the same moon with an autonomous submarine probe to also explore the European ocean, which has the potential of harboring life [14].

As of June 2019, the Europa Lander design is the one shown in Figures 1.1 and 1.2.

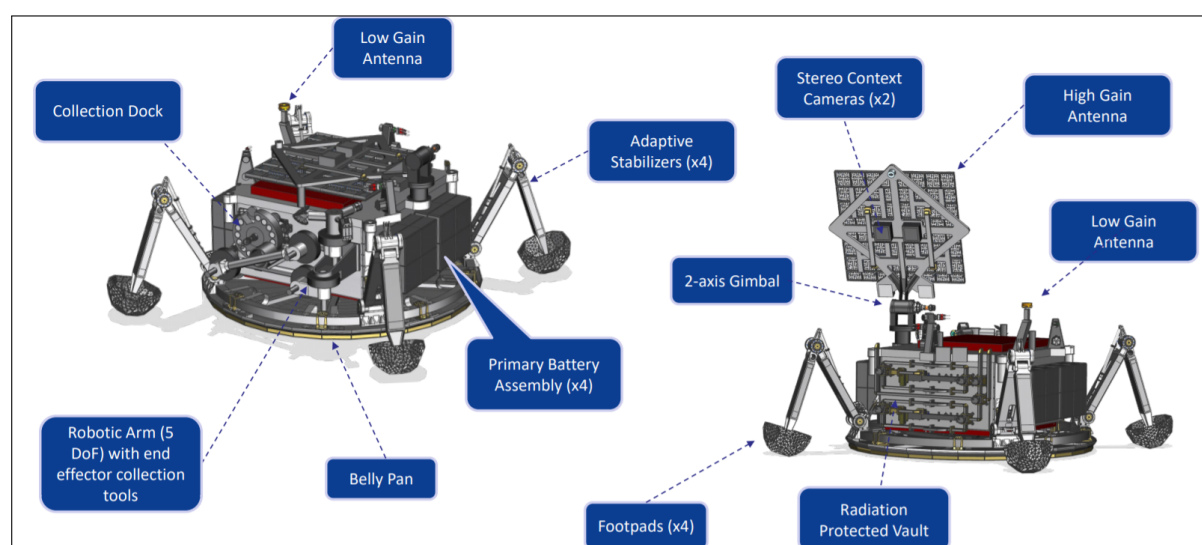


Figure 1.1: The current Europa Lander Stage Configuration [50].

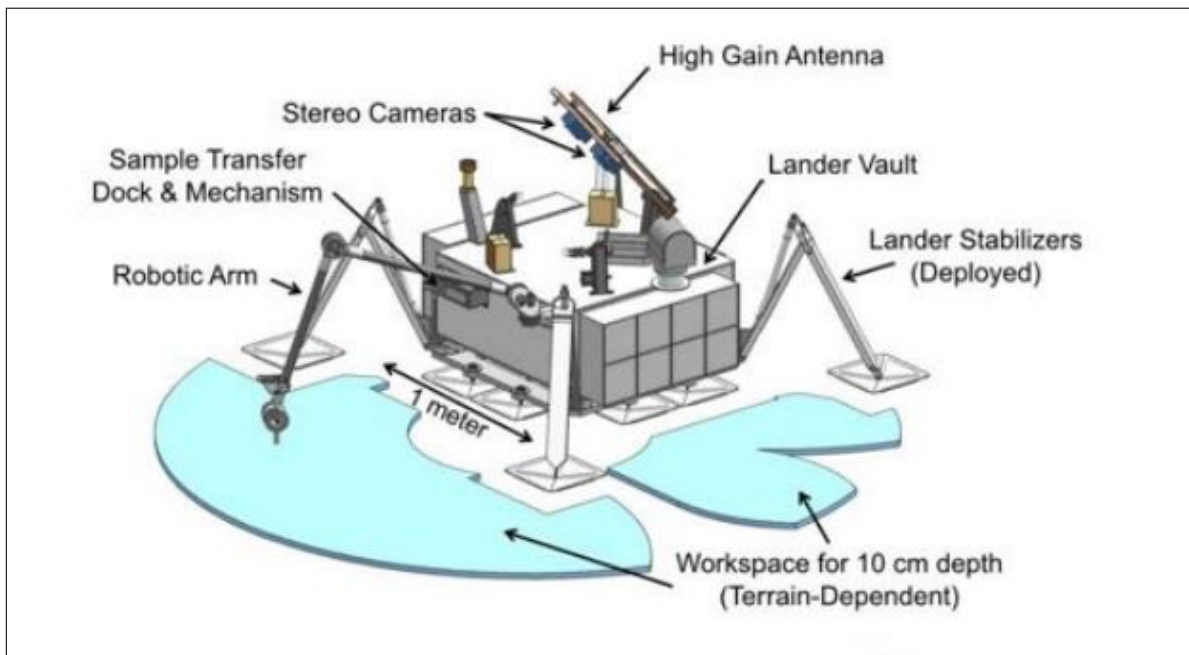


Figure 1.2: Diagram of Europa Lander showing the width of the payload module [16].

The design seen in Figure 1.1 is currently envisioned by NASA for this lander. From a payload perspective, it is supposed to carry scientific instruments to give scientists a better understanding of Europa as a moon and as a potential location for harboring life in the solar system. Instruments to study the surface of Europa from a geological point of view include a camera (for both visible, near visible and infrared spectra), a Raman spectrometer to study molecular activity, a seismometer and an instrument to measure aqueous chemistry [33]. On the other hand, to perform astrobiology studies and assess the possibility of the European subsurface ocean to harbor life, an optical microscope and an elemental analysis instrument are also planned as part of the mission's payloads [14]. In order to collect samples, a robotic arm is placed on the lander.

There are multiple challenges that the Europa Lander faces both when approaching the moon's surface and when performing scientific tasks. The topography of the Jovian moon's surface is not well known and it is likely that it will involve the presence of boulders in the orders of up to dozens of meters high. This means that the Guidance, Navigation and Control (GNC) and Hazard Detection and Avoidance (HDA) system will have to be able to identify those and come up with a manoeuvre to avoid them [41].

Another challenge will be related to the shielding of all electronic components. In fact, due to the ionizing radiation rich environment that Jupiter imparts on its moons, radiation absorption levels for the Europa Lander are estimated to be around 2 Mrad [14], or 20 kJ/kg. Radiation hardening can be achieved by either physically placing a barrier that stops the required level of radiation or by making the software running the lander's systems and its instruments redundant.

The current estimate on the landed mass of the Europa Lander is 575 kg [16].

The current version of the ELLS has a Skycrane, as seen in Figure 1.3. The landing sequence starts with the deorbit burn. After that the deorbit engine is jettisoned and the terrain relative navigation starts looking for a suitable place to land based on slope angle and the presence of boulders. After a suitable landing location has been found, it is at this point that the retro-rockets fire up in order to bring the lander to an almost still position. Then, from here, the Skycrane lowers down the lander until this reaches the ground at an expected velocity of 0.1 m/s.

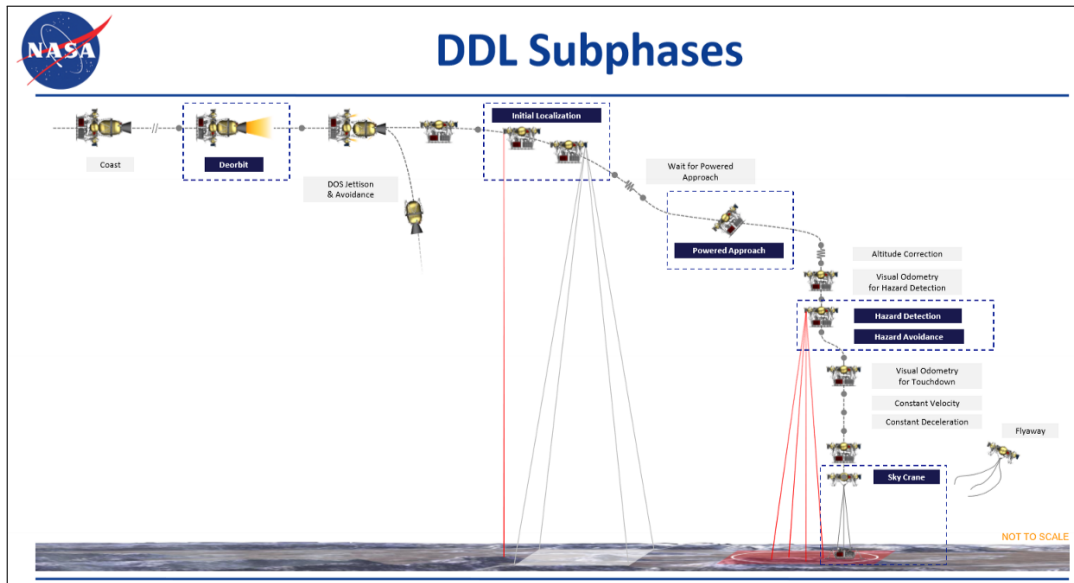


Figure 1.3: Timeline of descent of the Europa Lander [16].

The stage distribution is important to be known because, by scrapping some mass from the Skycrane, which is part of the Descent Stage (DS), it is possible to have a bigger allocation of instruments inside the lander.

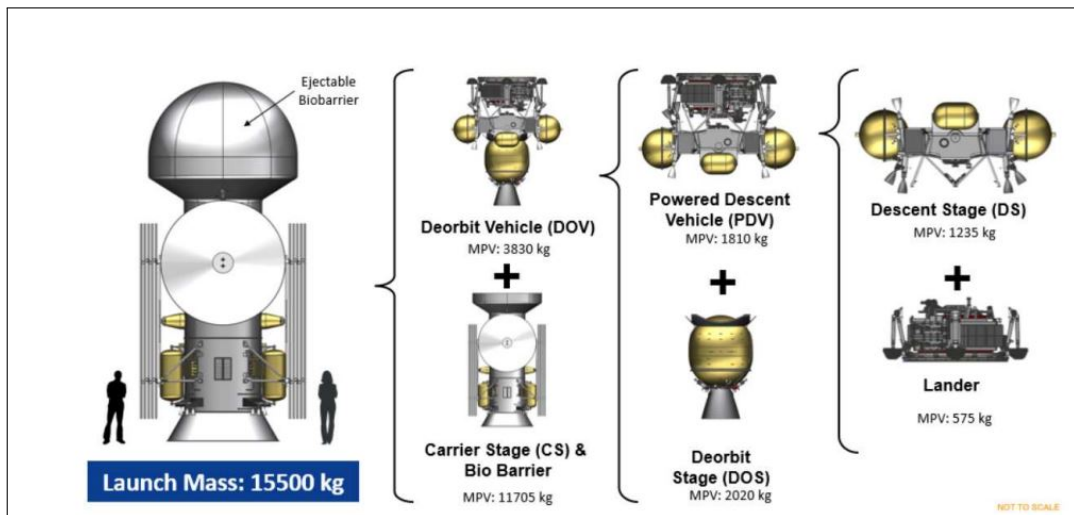


Figure 1.4: Stage distribution of Europa Lander mission [44].

The masses from each stage of the Europa Lander mission are seen in Figure 1.4, the important masses for the purpose of this project are the Descent Stage mass of 1235 kg and the actual Lander mass of 575 kg. Furthermore, this value is input in the landing simulations in order to make sure that inertia is present in the modelling.

Burn time of the Descent Stage is unknown.

1.1.2. State of the Art in Deployment Modelling

The deployment analyses that will be done for this thesis will be related to tracking the dynamics of the deployable landing system when different parameters applied to its geometry are used. Another type of analysis to the deployable landing system will be the landing analyses, but that is not related to deployability and is discussed in another section.

In [5], the deployment dynamics of 4 deployable booms are explained. These are applied to the deployment of the solar sail for the Japanese IKAROS probe technology demonstrator. The modelling, in this paper, is done with the so called "multi particle approximation method". In this method, all the deployable booms are modelled as a series of springs and masses in series, as Fig. 1.5 shows.

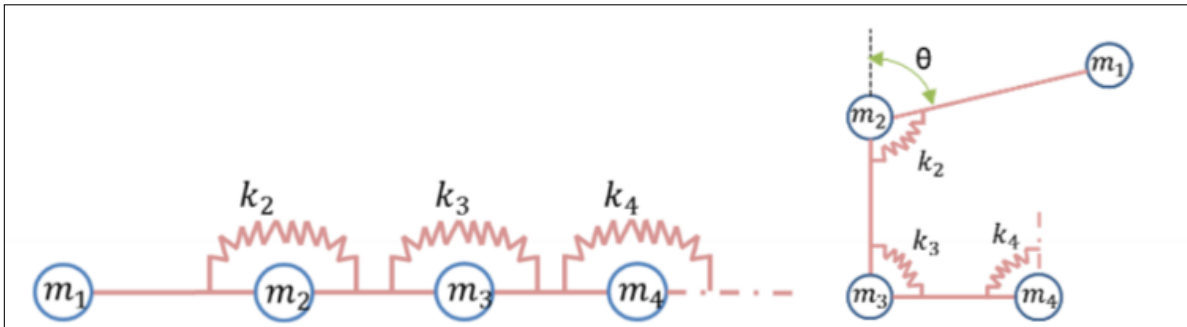


Figure 1.5: Deployed state (on the left) and stowed state (on the right) of the multi particle approximation method for the IKAROS deployable boom [5].

This method of designing tape springs, that consists in considering them as multibody systems, can be considered as reliable as it takes important values such as the virtual spring stiffness from experimental data. A similar parametrisation of the landing system as the one applied by [5] is suggested for this thesis because of the flexibility that it can give when it comes to applying a wide number of values to different parameters of the landing system like the length of each leg or their mass.

In [20] one issue of centrifugal deployment is explained and then a solution is found. One challenge with such deployment mechanisms is that, when deploying, the moment of inertia of the spacecraft also changes. Specifically, it increases, and therefore their rotational velocity decreases, so the risk is that the solar sail does not fully deploy which is the opposite from what was originally wanted. Because of this, in the paper, first a dynamic model of the solar sail is made and then a way to control the spinning of the spacecraft through attitude control is devised. An analytical model and a numerical one are set up. The physical model made in this article cannot be transposed to that of the Europa Lander landing system because of the differences in shape. The relevant information to be taken from this paper is the fact that, when deploying the landing system of the Europa Lander, its moment of inertia will change and, therefore, a way to keep track of this change shall be employed in order for this information to be relayed to the attitude dynamics algorithm.

1.1.3. State of the Art in Spacecraft Landing Methods

In this section of the thesis, an analysis of soft landing methods for planetary or other bodies lander missions is going to be outlined. This is done in order to offer an outline of how landing has been achieved, with landing legs, previously in other interplanetary missions. Furthermore, if there are similarities in landed mass and mission profile, some data can potentially be taken from the following landers in the case the data from the Europa Lander is not sufficient and cannot be found through literature.

Rosetta-Philae

The Rosetta mission was sent to study the asteroid *67P/Churyumov-Gerasimenko*. A model of the Philae Lander touchdown system can be found in Fig. 1.6.

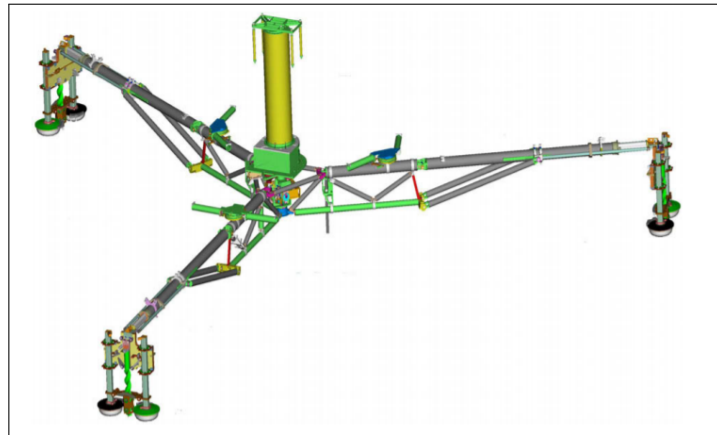


Figure 1.6: Philae Landing System [52].

In this case, the landing system consisted of a truss like structure made of Carbon Fibre Reinforced Polymers (CFRP), a central hub in which the damping system is contained and the ice screws right next to the landing footpads of each of the 3 landing legs, which were used to anchor itself to the comet's surface. This truss like landing system is of the deployable type. This landing system was tested to successfully achieve landing for a lander of up to 100 kg with an impact velocity of 1.5 m/s.

Mars Phoenix Lander

The Mars Phoenix Lander landing system consisted of a parachute and retro rockets to bring the lander to an acceptable velocity to then hand the task of the final touchdown to the landing legs. A model of the landing configuration of Phoenix is found in Fig. 1.7.

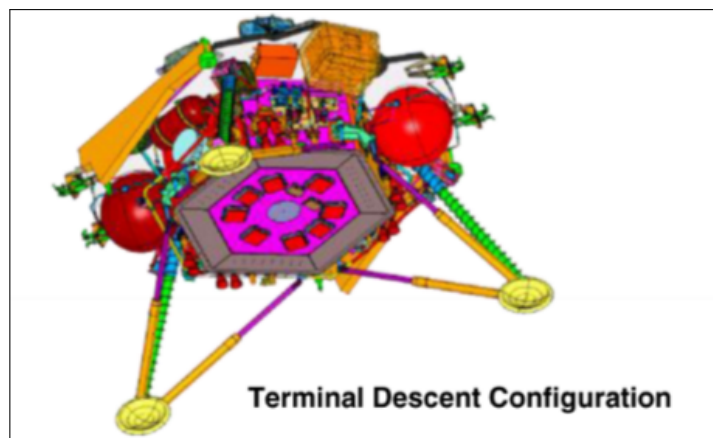


Figure 1.7: Model of Phoenix terminal descent configuration [15].

The landing legs are of the deployable type, but not much information on this is found in literature. The advantage of this landing configuration is that it leads to a precise landing location and has a lower impact velocity of 2.5 m/s when compared to that given by the airbag on the same planet with the Opportunity mission. On the other hand, it runs the risk of contaminating the lander due to the fact that the engine is turned on until the very last few meters of descent.

Mars Viking Lander

A mission with a similar mass to that of the Europa Lander is the Mars Viking lander. The lander had, in fact, a mass of 572 kg [29]. The landing was achieved by first slowing down the descent capsule from 6 to 1.6 km of height from a velocity of 250 m/s to one of 60 m/s. At that height, the parachute was cut off and the retro rockets slowed down the lander until a landing velocity of 2.4 m/s was reached.

The difference between this lander and the Europa one is the absence of atmosphere on the Jovian moon. Because of this, a parachute cannot be used on the EL. Nevertheless, because of the very similar mass and therefore very similar inertia, some parameters of the landing system of Viking can be transferred to that of the ELLS in case they are not found for the Jovian moon lander, since this is in the preliminary stages of design. On the other hand, as seen in Figure 1.8, the Viking lander system parameters are publicly available [36]:

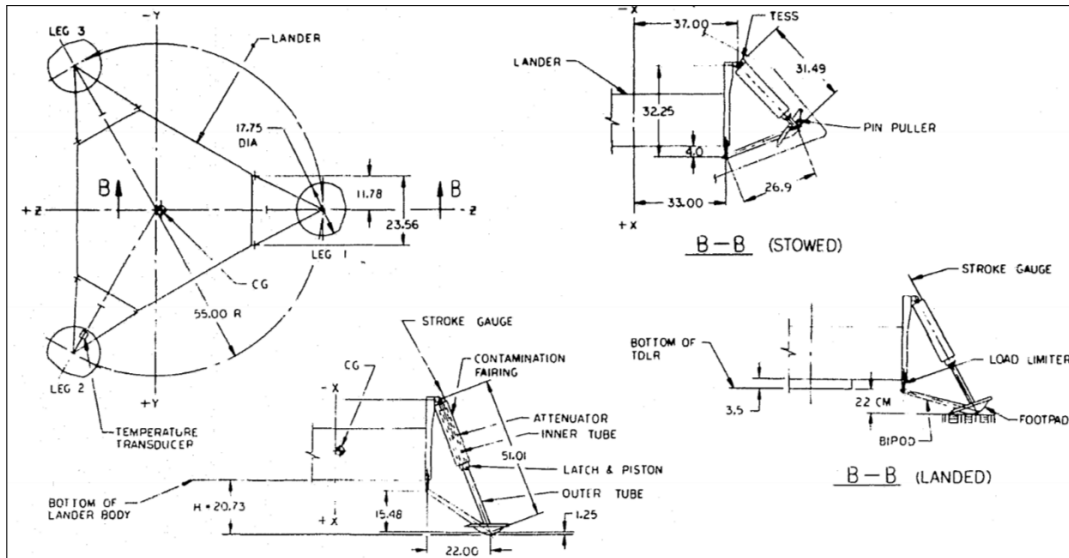


Figure 1.8: Technical drawing of Viking 1 landing system (all dimensions are in inches) [36].

1.1.4. Landing Modelling

In order for the landing system to be considered as landable, landing analyses have to be performed. Most of the analyses that were found in literature for landing systems are related to the final touchdown phase since this is the part of the mission where the lander has the highest probability to be lost. Due to this, landing analyses are of paramount importance. Of these, [22] provides a dynamic landing analysis using Abaqus on a cantilevered configuration landing leg. The properties of the lunar soil are also modelled in this paper. This paper is beneficial since it can be used as an example on how to perform landing analyses on Abaqus and also provides properties to be input in the FEA software related to the soil encountered on the Moon. An example of the results is shown in Figure 1.9:

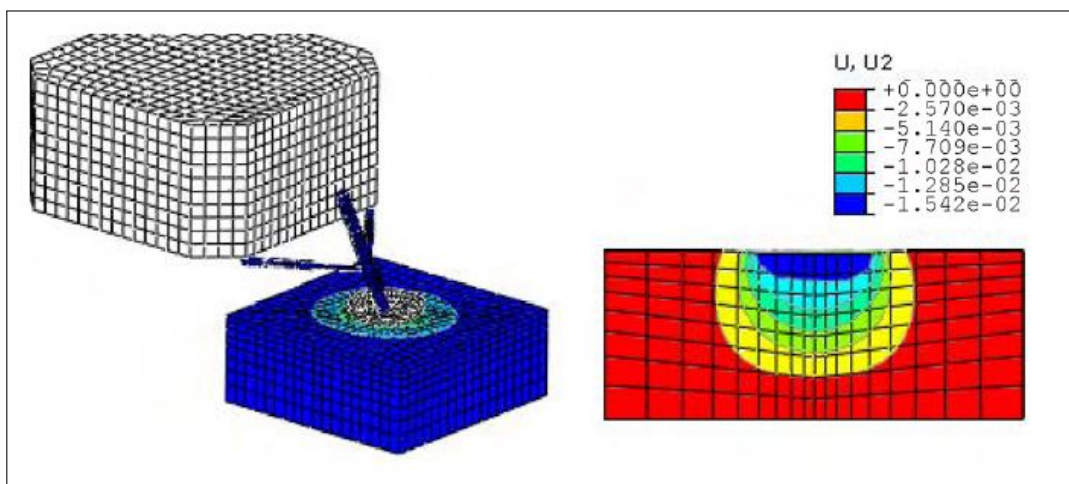


Figure 1.9: Example of landing FEM results from [22].

In [31] landing analyses for a lunar lander are performed on different conditions to account for landing

uncertainties. The different landing conditions simulated are differences in slope angle of the terrain and differences in landing mode, specifically the 1-2-1 and the 2-2 mode. The analyses are performed with MSC Adams.

In [42], a special type of legged lander is analysed by using MSC Nastran. This lander uses landing legs that plastically crush upon landing in order to dissipate the shocks of landing. The design process starts by coming up with the modelling of a single crushable landing leg. Then validation of the plastic deformation of this landing leg is performed by running material experiments on a manufactured model. Then, the leg models are assembled in a dynamic analysis software and landing analyses are performed. In this way, the analysis of an assembly of validated single components becomes more reliable. Validation won't be possible to be done, nevertheless, verification of single made models can be done by either comparing them with data found in literature with similar designs.

1.1.5. Landing Stability

In [12], a mathematical procedure is derived in order to assess a planetary lander's touchdown dynamics. The derivation is lengthy and is taken through a high number of steps as it starts with a simplified version of the lander which it is taken as a rigid body. Subsequently, more effects are added into the modelling, such as the bending of the struts when they touch the ground or the forces and moments imparted by the reaction control system to the lander.

The important section of this reference document is the one related to the establishment of a so-called stability criterion. This criterion is set up in order for computer simulations to preliminarily understand whether the spacecraft will tip over at certain design conditions, on the lander side, and physical conditions, on the surface side. In coming up with a stability criterion, an important parameter to take into account is the "stability distance" [12]. This is defined as the shortest distance between the vehicle's center of mass and the imaginary plane that is parallel to the gravity vector and that goes through 2 adjacent points that represent the footpads. The imaginary plane is also referred to as "Stability Wall". The number of stability distance vectors in a lander is equal to the number of landing legs, since a stability wall is present on the plane connecting 2 adjacent landing footpads. A visualisation of the stability distance can be better seen in Fig. 1.10.

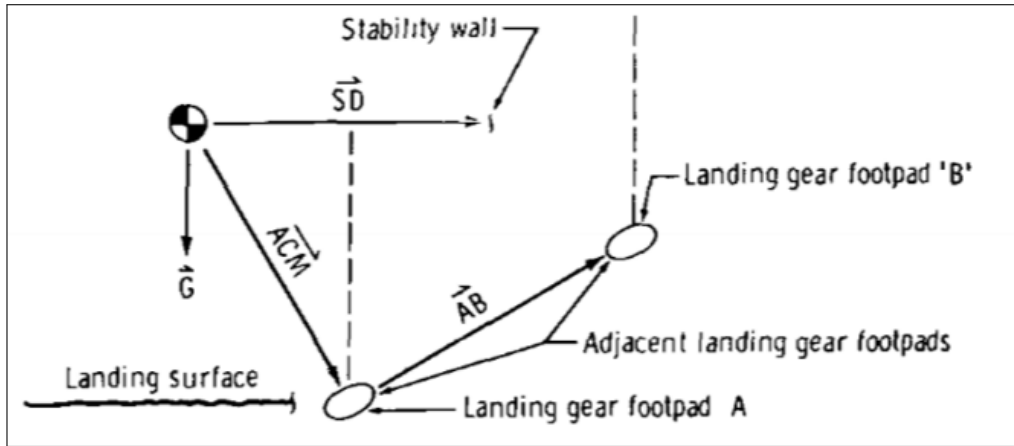


Figure 1.10: Vectors involved in stability criterion calculation [12].

The vector \vec{SD} , as seen in Fig. 1.10, is calculated as follows [12]:

$$\vec{SD} = \frac{SD(\vec{G} \times \vec{AB})}{|\vec{G} \times \vec{AB}|} \quad (1.1)$$

In which \vec{G} is the gravity vector, \vec{AB} is the vector connecting the 2 adjacent footpads and SD symbolises the magnitude of vector \vec{SD} , which is calculated as follows [12]:

$$SD = \frac{ACM \cdot (\vec{G} \times \vec{AB})}{|\vec{G} \times \vec{AB}|} \quad (1.2)$$

In which \vec{ACM} is the vector connecting the lander's Center of Mass (COM) to the footpad.

If the center of mass of the spacecraft is inside of the envelope characterised by the stability walls, then the spacecraft's landing is stable. If this is not the case, then the landing configuration, due to both the design geometry of the landing system and the surface conditions, is unstable.

In [28], the stability criterion is used to come up with a visualisation method, called "landing success maps", that is used to view the stability at different conditions of different landing legs designs for a JAXA small planetary lander. Landing success (or failure) maps from this paper can be seen in Fig. 1.11.

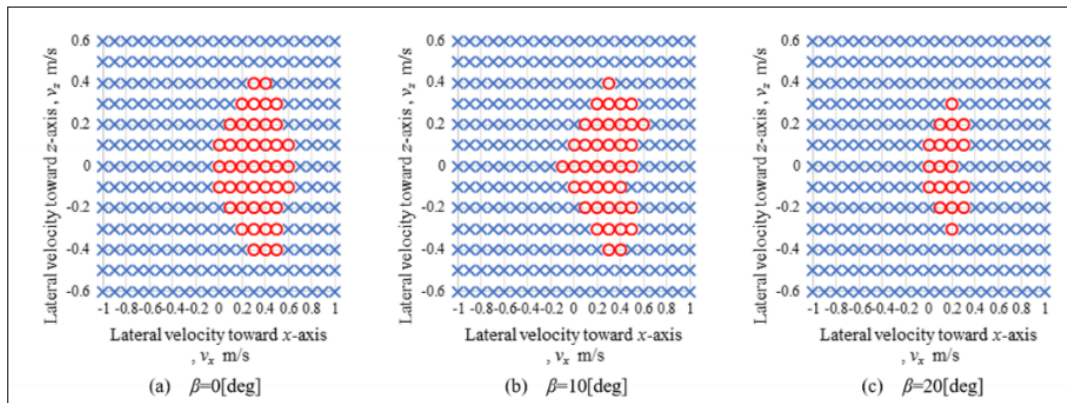


Figure 1.11: Landing success/failure maps of a lander design at different terrain slope angles β , the red circle signifies landing success, while the blue cross means landing failure and tip over [28].

Landing success maps are an efficient way of finding out and conveying information on the threshold of conditions that a landing system has to successfully land on any surface. Landing stability plots will be used, in this thesis, to assess the success or failure of landings at prescribed soil inclination angles. If the plots show that the lander is landable at a soil inclination angle higher than the maximum expected angle in the slopes of Europa (found in [43]), then the landing system will be considered as successful in fulfilling the requirement on landing at a maximum soil inclination angle.

1.2. Problem Statement

Now that the state of the art in deployment modelling, landing modelling and landing systems in space structures has been introduced, the problem encountered during the literature study that is what will be solved in this thesis, will be laid out.

The currently envisioned ELLS is made of a skycrane, as written in subsection 1.1.1. This system adds extra mass to the descent module of the Europa Lander because of the modifications that have to be made in order to accommodate the mechanisms needed in order to allow for a Skycrane to successfully lower down the Lander to the surface. Furthermore, the Skycrane system has never been tested in a radiation rich environment as the one that will be encountered at Europa (due to its vicinity to Jupiter) will be. Because of this, a system that requires complicated and lengthy control systems to function, may not be the best option.

1.3. Research Questions

In the context of this thesis, the research questions are 2.

Research Question 1: *Is it possible to model the mechanics of deployment of a Soft Landing System for Interplanetary Landers where the deployment is actuated by the decelerating force of the engine module and that can lead to the Skycrane concept being scrapped from the descent module?*

This research question makes it clear that the landing method taken in consideration is of the "soft" type, which, according to [47] is a landing that has a velocity of less than 20 m/s, although for velocities higher than 10 m/s airbags are more suitable as a landing system design choice. Hard landing models such as those for penetrators are not part of the analysis that will be performed in this project. The other matter that needs to be highlighted about this research question is what is meant by the word "possible".

It can be argued, in fact, that something that works in a model in a computational program does not necessarily work in real life. It is because of this that the modelling employed has to be verifiable. The model also has to be "landable", meaning that landing analyses will have to be performed. Therefore, if the model is verified, if it is shown that indeed the landing system geometry and predicted structural performance makes it clear that it is possible to use the decelerating forces of the lander's boosters and if it is shown, with the landing modelling, that the lander will be able to stably land, this research question will be considered as fulfilled. Design maturation of the landing system and further work will also be needed in order to come up with a more detailed design of the ELLS, as will be seen in chapter 9.

Another aspect that needs to be made clear is the aspect of mass shift. It is, in fact, hypothesised that by using a deployable landing system with sturdier legs, then the Skycrane concept can be scrapped. This would lead to a Descent module design that, without Lander, would be lighter than that of the same module, with a Skycrane. The mass saved by the absence of the Skycrane can then be shifted to the lander, by increasing it, but by keeping the same amount of combined mass (DS and Europa Lander) as seen in Figure 1.4 of 1235 kg so that the engine design would not be changed.

By scrapping the Skycrane, furthermore, the landing system becomes increasingly simpler due to the lower amount of moving parts. This, in turn, increases reliability of the landing system.

A sub-research question stemming from the previous one is also attached to the project:

Research Question 2: *What are the preliminary design guidelines that can be gathered from the model to then be used as inputs for the actual design of this specific type of deployable landing system concept that can achieve actuation using the negative g forces before landing?*

Purely performing modelling of the deployment and landing of the ELLS is not enough for the project to be successful. If such a project would be made in a company, the stakeholder would want to see what types of design choices shall be employed in order to come up with a design that behaves in an identical fashion as the one in the model.

Another fact that needs to be specified is what is meant by preliminary design. The second objective of this thesis is, in fact, to give guidelines over what types of subsystems can be placed on the deployable landing system concepts. It is beyond the scope of this thesis to figure out the precise shape and performance of these subsystems in detail. Because of this, for example, no analysis of the structural performance of the joints is offered in this thesis. At the end of the thesis, the goal is to have a geometry of the landing system, with numerical values for the size and capabilities of some of the important parameters to make the landing system deployable and landable. Design refinements, which can be in the form of the detailed design of the landing damping system, can be picked up by future researchers.

1.4. Thesis Organisation

In this section of the document, the organisation of the thesis is laid out.

In Chapter 2, the requirements dictating the design of the ELLS are laid out. Not only the design requirements, but also the modelling requirements are given in this section in order to make sure that the deployment and landing models have the right inputs and outputs.

Subsequently from this, the deployment model used for the initial investigation is explained in Chapter 3. This is a fully parametrised Matlab developed 2-dimensional model that is used to analyse the deployment dynamics of the landing system with different physical characteristics. In the chapter following this, Chapter 4, the modelling of the landing dynamics through Finite Element Analysis is explained.

After explaining the models used, first verification of both the deployment and the landing model is going to be performed in Chapter 5, then results will be found in Chapters 6 and 7. These results refer to both the deployment model developed on Matlab and the landing model used in Finite Element Analysis (FEA) software Abaqus. Following results, real life considerations related to the landing system design will be taken into account and laid out in Chapter 8. In the end chapter 9 will wrap up the findings from the previous chapters and suggest further areas of research to be taken up for future projects.

2

Requirements

In this section of the thesis, the requirements dictating the following matters, alongside their rationale, is laid out and explained:

- Design and performance requirements to dictate the development of the landing system.
- Requirements for the deployment modelling tool. Used to dictate the functionalities of this model.
- Requirements for the landing modelling tool. Also used, in this case, to dictate the functionalities of the landing modelling tool.

2.1. Design Requirements for the Europa Lander Landing System

The requirements dictating the landing system design are listed as follows:

- **LS-PAY-001:** The landing system shall support a landed mass of maximum 575 kg.
Rationale: According to the latest Europa Lander Mission Update as found in [16], the lander's dry mass is of 575 kg. Because of the fact that, in the presentation found in [16], the mass is referred as "dry", it can be assumed that this is the entirety of the landed mass. Therefore this includes the scientific instruments, the structure that holds them together and the landing system.
- **LS-PAY-002:** The decelerations of landing imparted by the landing system to the payload shall not exceed 10 Earth g.
Rationale: The internal instruments inside the Europa lander have a maximum survival value when it comes to sudden decelerations due to impact upon landing. For the Europa Lander instruments, this is at the moment not known. However, this value was found for the Mars 2001 Lander [15].
- **LS-LAN-001:** The Landing System shall survive a landing from a maximum vertical velocity of 5 m/s.
Rationale: The current idea of the ELLS has a Skycrane being envisioned as the solution to lower down the lander to a full stop. The design option investigated here wants, as written in chapter 1, to scrap the concept of a Skycrane and introduce a self standing landing system. Of course, without a Skycrane, the vertical landing velocity will be higher. The 5 m/s maximum vertical velocity requirement is placed because it is assumed that the decelerating engine is cut off from a height of 10 metres. In Europa's gravity, a free fall from 10 metres leads to a touchdown velocity of 5 m/s. 10 metres are chosen so that the engine plumes don't contaminate the soil where the lander is supposed to land. In fact, because of the fact that this mission is a lander and not a rover, it is imperative to keep the landing site pristine in order not to contaminate soil samples. For the sake of this thesis, a landing scenario with maximum velocity of 5 m/s, with a single leg landing on a higher ridge or a rock is looked at. This scenario is unlikely, but it's the most dangerous one for the survival of the leg. Therefore designing for this scenario leads to a conservative design. This requirement is an assumption and a sensitivity analysis on the variation of landing performance

parameters over landing speed is performed in section A.3. This is used to understand the trends that happen in the case this requirement is lowered or increased.

No lateral velocity requirement is added.

- **LS-LAN-002:** The landing system shall provide a stable landing for slopes of less than 15 degrees.
Rationale: According to [43], in fact, only 10 % of slopes on Europa are inclined more than 15 degrees. Because of this, from a slope landability perspective, the probe can be landed on 90 % of the Europa's surface.
- **LS-LAN-003:** The landing system shall provide a stable landing on a soil that has comparable properties to that of the Moon.
Rationale: Even if the Europa Lander is not going to the Moon, Europa soil conditions are unknown. Lunar soil properties are well known due to experience in landing and extensive literature is available on how to model them on Abaqus [22]. In order to have 2 data points on the effects of soil stiffness, a landing simulation with a stiff soil will also be run.
- **LS-LAN-004:** The stress in all Landing system members made of metal shall never exceed the Ultimate Tensile Strength (UTS) of the material with a safety factor of 1.4 for metallic structures.
Rationale: The NASA Handbook on Structural Design and Safety Factor [30] outlines that, for unmanned space structures made of metal, the safety factor between the material's UTS and the highest experienced stress by the structure shall be of 1.4.
- **LS-LAN-005:** The maximum principal strain in any composite structure shall not exceed 5000 micro strains.
Rationale: This is the same requirement that is placed in the structural analyses of composite landing struts brought forward by NASA in [19] and [27].
- **LS-DEP-001:** The deployment time of the landing system shall be of maximum 45 seconds.
Rationale: As the value of burn time is not yet known for the Europa Lander, this is taken from the Mars Perseverance Rover [25] burn time.
- **LS-DEP-002:** The landing system deployment shall not make use of any actuator to aid in its motion.
Rationale: This requirement is put here as one of the goal of the research is to use a deployment actuation method that does not use power.
- **LS-DEP-003:** Deployment of the landing system shall be started by the retro rockets of the lander firing to slow down during the approach to the designated landing spot on Europa.
Rationale: This requirement is placed here as this is one of the research goals of the thesis.
- **LS-DES-001:** The landing system shall not exceed 10% of the whole lander mass.
Rationale: On requirement LS-PAY-001, it is dictated that the lander mass is of 575 kg. The requirement written here dictates the landing system to be of a mass of maximum 57.5 kg. 10 % of the landing system mass is taken because of the study brought forward by [39]. In this Master thesis, the author found out that the average mass of a landing system is around 7 % of the whole dry mass of a space landing system itself. But, in order to account for unpredictabilities in the data found on space based landing systems, 1 standard deviation of around 3 % was added. Therefore putting a requirement to landing system mass fraction over total landed mass to 10 %.
- **LS-DES-002:** Upon maximum sinking inside the soil, the vertical distance between the bottom of the lander body and the top of the soil shall not be lower than 200 mm.
Rationale: This requirement is placed in order to make sure that enough clearance is between the bottom of the lander and the top of the soil.

2.2. Deployment Modelling Tool Requirements

The requirements that dictate the development of the deployment model are:

- **MDL-DEP-001:** The deployment model shall provide an estimate of the deployment time of the landing legs in seconds.
Rationale: Deployment is meant as the time between the moment where the actuation of the deployable landing system starts until the moment where all landing legs are locked. This is placed in order to show the acceptance of Requirement LS-DEP-001. The reason for this is that the deployment time shall be lower than the burn time that the EL descent module takes to slow down the spacecraft to an acceptable velocity.
- **MDL-DEP-002:** The model shall calculate the landing stability of the landing system.
Rationale: This requirement is in place so that requirement LS-LAN-002 can be verified.
- **MDL-DEP-003:** The deployment model shall be able to model deployment time with a 10 % accuracy.
rationale: 10 % is taken as this is a usual value for model accuracy for MSc theses [11, 55].

2.3. Landing Modelling Tool Requirements

The requirements that dictate the development of the landing model are:

- **MDL-LAN-001:** The landing model shall provide an estimate of the stresses experienced by the landing legs upon touchdown of the legs.
Rationale: This is done in order to make sure that requirement LS-LAN-004 can be proven.
- **MDL-LAN-002:** The landing model shall provide an estimate of the G forces experienced by the lander body.
Rationale: This is done in order to make sure that requirement LS-PAY-002 can be proven.
- **MDL-LAN-003:** The simulations on the landing model shall run in less than 1 hour.
Rationale: This requirement is placed so that up to 7 simulations can be uploaded in a normal working day.
- **MDL-LAN-004:** The landing model shall be able to handle both metallic and composite material inputs.
Rationale: This is because both types of materials are envisioned to be analysed in the design of the Europa Lander Landing System for this thesis.
- **MDL-LAN-005:** The landing model shall be able to model stresses, strains and deformations with a 10 % accuracy.
rationale: 10 % is taken as this is a usual value for model accuracy for MSc theses [11, 55].

3

Deployment Modelling

In this chapter of the thesis, the modelling of the deployment dynamics of the spacecraft's landing system is laid out. The aim of the deployment model is to allow for the producing of landing system geometries and to show, before the landing analyses, the acceptance of the deployment requirement on deployment time.

Since the envisioned way to actuate the deployable landing system before landing is through decelerations imparted by the lander's retro boosters, and also it is desired to put damping in between joints in order to control the deployment dynamics of the landing system, the chosen type of algorithm to track the deployment dynamics is of the pendulum type.

3.1. Landing System Matlab Parametrised Model

A 2-dimensional parametrised model has been developed in Matlab in order to track the deployment of the pendulum-like landing legs. This is seen Figure 3.1 and the picture is used to present the naming convention, so that explanation of the algorithm's implementation is made easier:

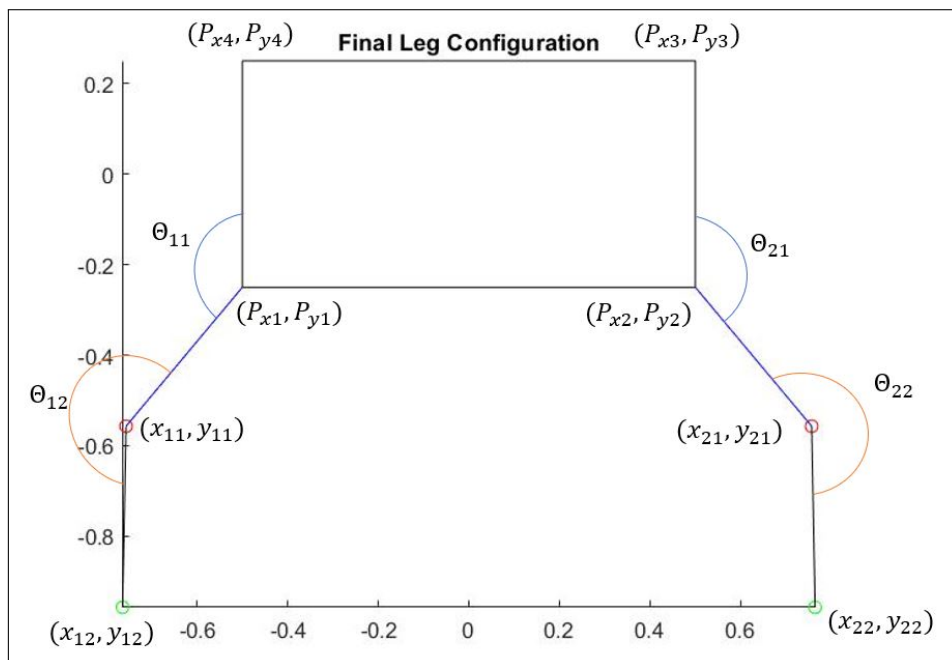


Figure 3.1: Naming convention of coordinates used for the landing system (shown in here in the deployed configuration).

The landing system is designed in a simplified way that has 2 2-dimensional landing legs and 2 leg elements per leg, the reason for this is offered in section 3.3. The landing leg elements are attached

to each others through a joint that has 1 rotational degree of freedom. Furthermore, the point of attachment between the legs and the lander body is in the lower part of the side wall of the lander body. Using this naming convention, the horizontal and vertical coordinates of leg element tips are referred only with x and y and the corresponding position number (11 for the top left, which is also the joint in between leg elements for the left leg, 12 for the bottom left, 21 for the top right, also the joint between the leg elements in the right leg and 22 for the bottom right). On the other hand, the coordinates of the corners of the payload rectangle are written with a "P" in front. When saying "Lander Body" or "Payload Rectangle", it is meant, regarding the deployment analyses performed on Matlab, the part of the lander that is not the landing system. Because of the fact that this thesis doesn't take into account the design of the lander outside of the landing system, the rest of the lander is simplified as a rectangle as seen in Figures 3.1 and 3.2.

The landing system has some characteristics embedded into it, these are seen in Figure 3.2:

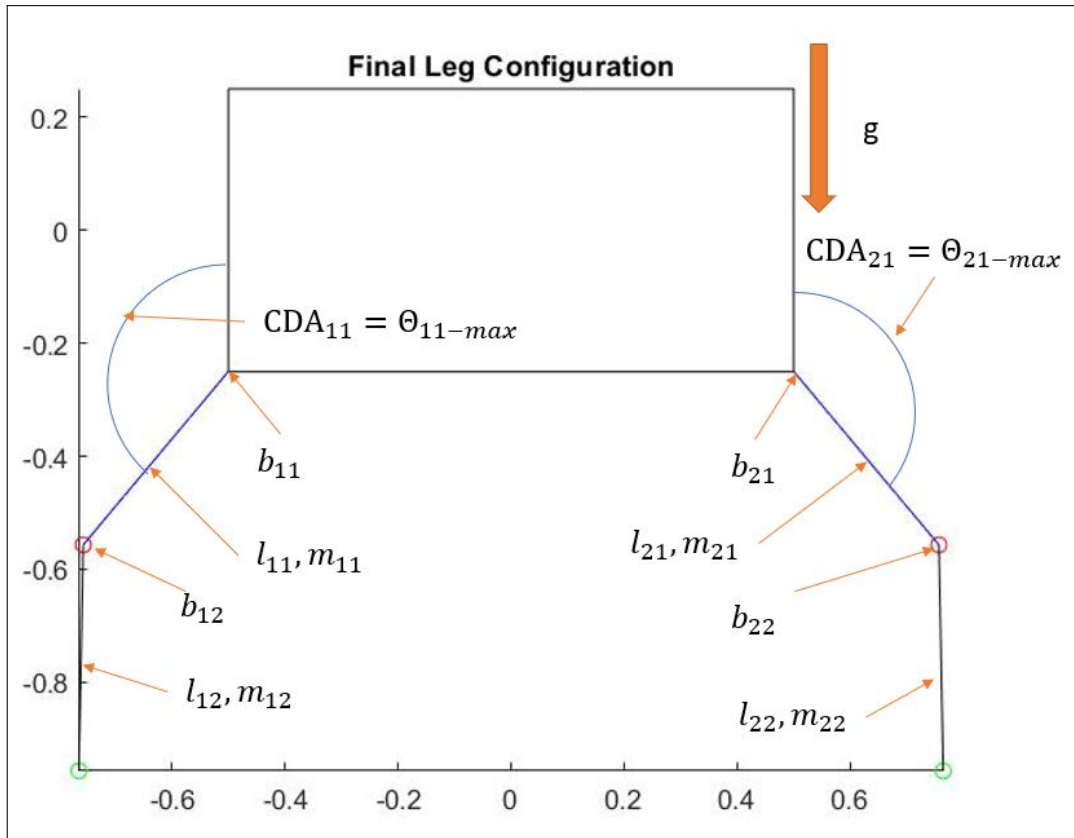


Figure 3.2: Naming convention of Matlab deployment model characteristics.

The characteristics that can be tweaked in order to model the deployability of the landing system are listed as follows and found in Figure 3.2:

- Damping of leg joints. Which refers to a resistance placed in 4 joints that acts against the deployment rate in order to control the velocity at which the leg joints rotate. Damping is referred to, in a shortened way, as b . For example, b_{11} refers to the damping value of the first joint of the first leg, which is, as seen in Figure 3.2, the top joint of the left leg. The reason why damping is introduced in the joints is because active deployment control through motors is not desired per requirement LS-DEP-002. Even so, it is still desired to control the deployment passively, therefore damping is introduced in the model. It is in fact assumed that damping plays a role in the computation of the deployment time, which is checked in future sections.
- Length of leg elements. Lengths of leg elements are referred to, with the shortened version, with the letter l . For example, l_{21} is the length of the first leg element of the second leg. As it can be seen by looking at Figure 3.2, this is the top right leg element.

- Mass of landing leg elements. These are the masses of each leg element. These are referred to, in the shortened version, with the letter m . For example, m_{22} is the mass of the second leg element of the second leg of the deployment model, which is the right leg as seen in Figure 3.2.
- Cutoff Deployment Angles between the lander body and first leg element. This is the maximum angle that the first leg elements (both left and right) make with the vertical wall of the lander body. It is referred, in a shortened way, either as θ_{ii-max} , in which ii refers to its position on the landing system or as CDA. For example θ_{11-max} is the Cutoff Deployment Angle between the first leg element of the left leg and the left side of the lander body. A CDA is not used for the 2nd deployment angle (θ_{12} or θ_{22} in Figure 3.1). On the other hand, the value of these angles at the moment when the deployment is stopped are taken as design inputs for the design of the joint and stopping mechanisms.
- G forces. Which is not the gravitational acceleration of Europa for the deployment model. The G forces, in the case of the Matlab Pendulum Deployment Model, is referred to as the amount of decelerations imparted by the retro-rockets in the final stages of landing, measured in terms of Earth's gravity.

Throughout the document, the explanation of the double pendulum algorithm will be only related to one side of the lander, this is because symmetry in the deployment dynamics is assumed.

3.2. Assumptions for Deployment Model

The following list contains the assumptions and approximations used to make the deployment model:

1. The deployment model is a 2-dimensional model, containing 2 legs. The real life version is 3-dimensional and should contain 4 landing legs.
2. Each landing leg is made of 2 straight 1-dimensional elements (called landing leg element), 2 rotary joints (1 between the lander body and the first leg element and the other between the 2 leg elements) and, at the bottom of each landing leg, a footpad shall be placed. Therefore, no cross bracing either in between leg elements or between the upper leg element and the rest of the lander body, is present. This may lead to higher stresses, but makes it possible for the landing legs to be modelled as penduli. 2-dimensional simulations related to interplanetary landing systems have been performed in works such as [54] in which, albeit landing simulations and now deployment ones, good correlation between the landing case and theory has been shown. Therefore the same simplification is applied in the case of this thesis.
3. The masses of the landing leg elements are going to be taken as point masses that contain the whole mass of the element and are located at the very tip of each penduli. This leads to big differences in pendulum dynamics if the pendulum is left oscillating throughout multiple iterations. However, because the landing system only has to go from a stowed angle to a deployed (cutoff) angle, without any rebounds, meaning that the pendulum does even less than an entire oscillation, it is assumed that this does not affect too much the results. A small analysis on how much this assumption affects deployment time for this model is placed in subsection 5.1.1.
4. Drag force are assumed to be not relevant when modelling the deployment of the landing system of the Europa Lander. This is because Europa has a very tenuous atmosphere with a pressure in the order of 10^{-12} bar [33].

3.3. Pendulum Model for Deployment Analyses

In order to track the landing system deployment dynamics, a double pendulum model is chosen because it is desired to model a system of which legs are divided into 2 leg elements, with a resistance modelled in the joints between them. The other option would be to model the dynamics of such a system using MBD software, however Matlab offers more flexibility since the program would be completely self made. Furthermore, availability of MBD software such as MSC Adams is limited within the university, however Matlab is easily accessible to students.

The reason why legs are divided into 2 leg elements is to give it a better adaptability to unknown terrains compared to if they were made of a single element. Even if adaptability is not taken care of in this

project, it is still given as a further work in case the developed landing system design of this project is further refined taking into account adaptability. If the leg would be made of a single element, in order for the lander to re-stabilise itself during touchdown, either the body would have to be tilted, or the footpads would have to slide on the terrain. However, if the landing leg is made of 2 leg elements, the 3 joints on the leg (1 between lower leg element and footpad, 1 between leg elements and 1 between upper leg element and body) can co-rotate to stabilise the Lander in uneven terrains. This is already the case for the actual current design of the ELLS as seen in Figure 3.3:

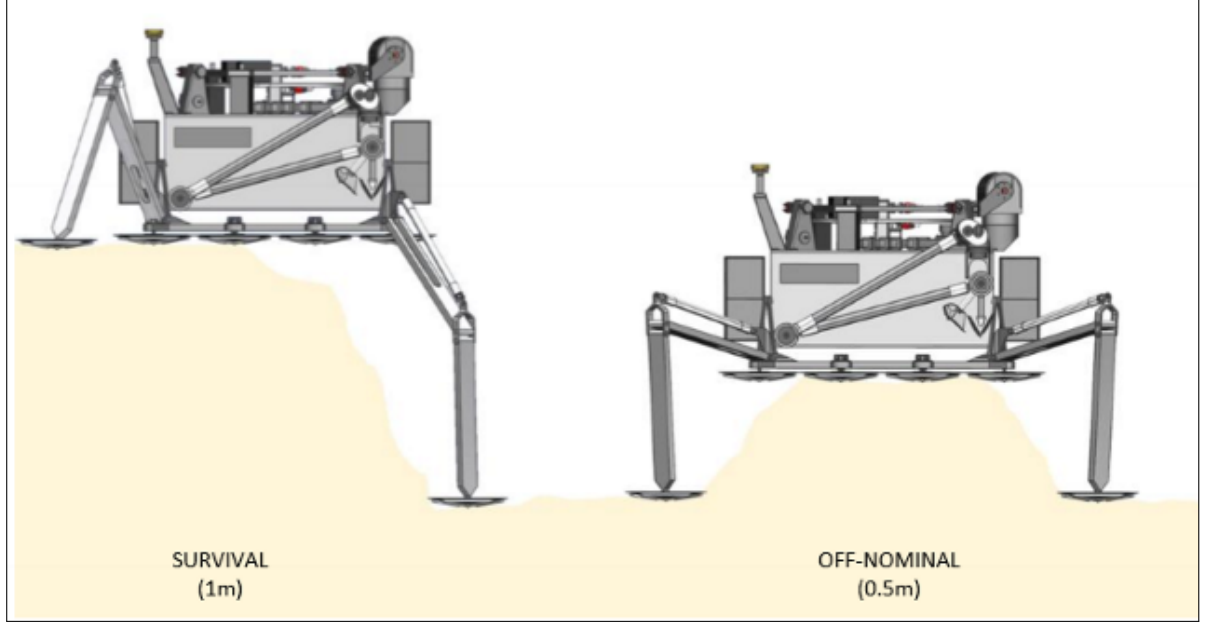


Figure 3.3: Adaptability of legs with 2 leg elements as seen in current Europa Lander design [46].

A similar degree of adaptability can also be achieved with 3 or more leg elements, however it is a good practice to keep the number of moving elements to a minimum and 2 leg elements is the prescribed minimum.

3.3.1. Algorithm for Double Pendulum with Damping

An algorithm that takes into account the dynamics of a double pendulum with damping was found in [9].

The algorithm is as follows:

$$\frac{d^2\theta_1}{dt^2} = \frac{m_2(\mu * l_1) \left(\frac{d\theta_1}{dt}\right)^2 \sin(2\Delta\theta) + 2m_2(\mu * l_2) \left(\frac{d\theta_2}{dt}\right)^2 + 2gm_2 \cos\theta_2 \sin\Delta\theta + 2gm_1 \sin\theta_1 + \gamma_1}{-2(\mu * l_1)(m_1 + m_2 \sin^2\Delta\theta)} \quad (3.1)$$

$$\frac{d^2\theta_2}{dt^2} = \frac{m_2(\mu * l_2) \left(\frac{d\theta_2}{dt}\right)^2 \sin(2\Delta\theta) + 2(m_1 + m_2)(\mu * l_1) \left(\frac{d\theta_1}{dt}\right)^2 + 2g(m_1 + m_2) \cos\theta_1 \sin\Delta\theta + \gamma_2}{2(\mu * l_2)(m_1 + m_2 \sin^2\Delta\theta)} \quad (3.2)$$

In which:

$$\gamma_1 = 2\left(b_1 \frac{d\theta_1}{dt}\right) - 2\left(b_2 \frac{d\theta_2}{dt}\right) \cos(\Delta\theta) \quad (3.3)$$

$$\gamma_2 = 2\left(b_1 \frac{d\theta_1}{dt}\right) \cos(\Delta\theta) - \frac{2(m_1 + m_2)}{m_2} \left(b_2 \frac{d\theta_2}{dt}\right) \quad (3.4)$$

$$\Delta\theta = \theta_1 - \theta_2 \quad (3.5)$$

In which:

- θ_1 and θ_2 are the angles that the first and second penduli make with the perpendicular to the horizon.
- l_1 and l_2 are the length of the first and second penduli.
- m_1 and m_2 are the masses at the end of the first and second penduli, m_2 also takes into account the footpad.
- b_1 and b_2 are the damping of the first and second penduli.
- g is the gravity acceleration.
- μ is a multiplier that is introduced for this thesis in order to change the position of the center of mass of the leg, or pendulum, elements. In [9] this multiplier is 1, meaning that the mass is concentrated at the end of the pendulum element. For this thesis, the multiplier is 0.5 for the upper leg elements, because only this item is taken into account when computing landing dynamics. For the lower leg elements this is calculated by Matlab and it's closer to 0.9, therefore very close to the tip, because of the fact that the presence of the footpad is taken into account for the lower leg element.

This algorithm takes into account the effects that one leg element's mass has on the other, which is a big instability when it comes to modelling double penduli. As it can be in fact, for example, with Eq. 3.1, the presence of m_2 is taken into account in the calculation of the acceleration of the first pendulum's deployment.

While using this algorithm, the way that the Matlab model updates the horizontal and vertical positions of each of the important points within the landing system (joint in between leg elements and leg tip) is the same as the one explained in Equations from 3.6 to 3.13.

3.3.2. Implementation of Pendulum Algorithm in Matlab Model

The way the algorithm from Equations 3.1 to 3.5 is implemented can be summarised with the flowchart in Figure 3.4:

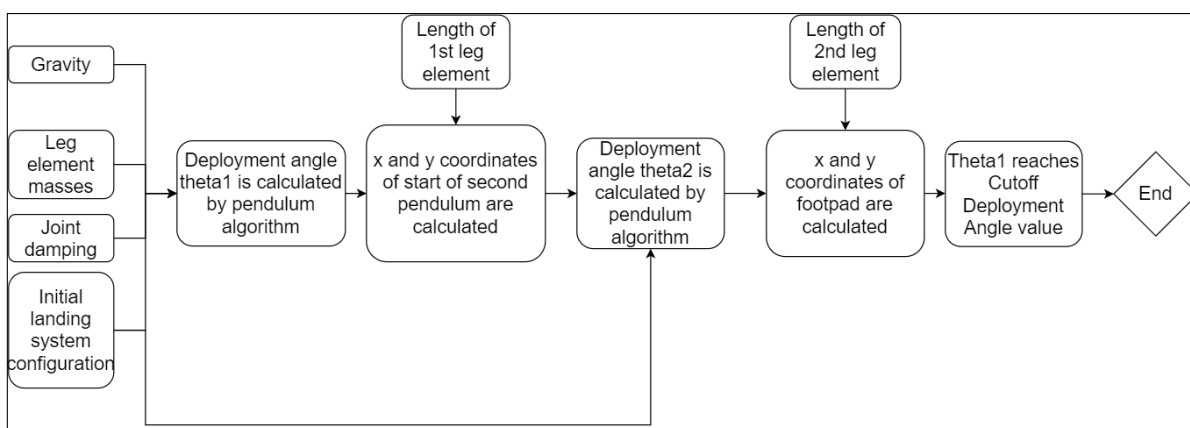


Figure 3.4: Deployment model implementation flowchart.

The variables that dictate the deployment of the legs are the angular displacements at each joint. The computation starts at time $t = 0$, where the initial position is given as in Figure 3.5:

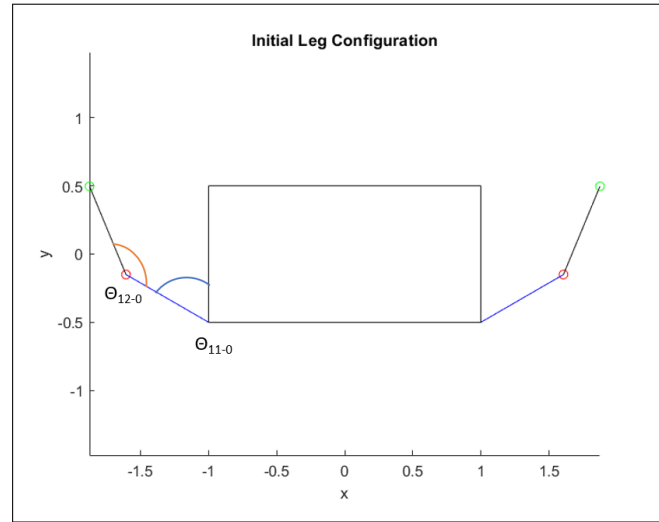


Figure 3.5: General initial leg configuration for deployment modelling studies.

The initial conditions to be given for the algorithm to properly start are the initial angles and initial angular rates. Since the landing system is stowed, it has no initial velocity before deployment, because of this, the initial angular rates of both joints are to be taken as 0. The first initial angle (seen as θ_{11-0} in Figure 3.5) is the angle that the first leg element makes with the vertical line of the payload rectangle. The second initial angle (seen as θ_{12-0} in Figure 3.5) is the angle that the first leg element makes with the second one that is less than 180 degrees. In the case of Figure 3.5 the angles are 60 degrees for θ_{11-0} and 140 degrees for θ_{12-0} . After modelling the initial positions of the ends of both elements making a leg, time-stepping starts. The program starts computing the angular displacement of the first joint at the first timestep, which corresponds to the connection between the first leg element and the payload rectangle, which is referred to as θ_{11} . Using trigonometry, by multiplying the length of the landing leg element (which is fixed) with the sine and cosine of the deployment angle, it is possible to find the horizontal and vertical position of the joint in between leg elements. Knowing the coordinates of the first joint, the program, at the same timestep, computes the updated coordinates of the second pendulum, which corresponds to the second leg element. While the coordinates of the end of the first leg element are only based on θ_{11} becoming larger in size at any timestep, this is not the case for the coordinates of the end of the second leg element. This is because the updated coordinates of footpad at the end of each timestep is the result of the compounded movement of θ_{11} and θ_{12} together due to gravity.

In more mathematical terms, the calculation for the position of the landing leg elements at each point throughout their deployment can be written as follows.

At timestep $t = 0$, the initial angles are θ_{11-0} and θ_{12-0} , while the initial positions of the ends of each of the 2 leg elements are:

$$x_{11-0} = x_{11}(t = 0) = P_{x1} + l_{11} * \sin(\theta_{11}(t_0)) \quad (3.6)$$

$$y_{11-0} = y_{11}(t = 0) = P_{y1} + l_{11} * \cos(\theta_{11}(t_0)) \quad (3.7)$$

$$x_{12-0} = x_{12}(t = 0) = x_{11-0} + l_{12} * \sin(\theta_{12}(t_0)) \quad (3.8)$$

$$y_{12-0} = y_{12}(t = 0) = y_{11-0} + l_{12} * \cos(\theta_{12}(t_0)) \quad (3.9)$$

The next timestep following the 0th one is:

$$t_i = t_0 + \Delta t$$

The horizontal position of the tip of the first leg element is calculated as follows:

$$x_{11}(t = t_i) = P_{x1} + l_{11} * \sin(\theta_{11}(t_i)) \quad (3.10)$$

The vertical position of the tip of the first leg element is calculated as follows:

$$y_{11}(t = t_i) = P_{y1} + l_{11} * \cos(\theta_{11}(t_i)) \quad (3.11)$$

The horizontal position of the tip of the second leg element is calculated as follows:

$$x_{12}(t = t_i) = x_{11} + l_{12} * \sin(\theta_{12}(t_i)) \quad (3.12)$$

The vertical position of the tip of the second leg element is calculated as follows:

$$y_{12}(t = t_i) = y_{11} + l_{12} * \cos(\theta_{12}(t_i)) \quad (3.13)$$

The same computation is done for the right side of the landing system.

In order to solve the ODE found in Equations 3.1 to 3.5 for the angles between the lander body and the first leg element (θ_{11}) and the one between leg elements (θ_{12}) the "ODE45" solver in Matlab is used. With the initial conditions given as the angles that each landing leg element has at time 0 (as seen in Figure 3.5) and the other parameters in Equations 3.1 to 3.5 (joint damping, mass and length of each leg element and gravitational) given as constants, this solver can track the variable (θ_i) in the equation of motion and its first derivative (the deployment rate) throughout the deployment procedure. The output of the deployment modelling on Matlab is an array made of 8 columns and as many rows as the amount of timestep needed to calculate the deployment from starting position until the end of deployment. The 8 columns of the array correspond to the value of the deployment angle (in *rad*) and its rotational speed (in *rad/s*) at any timestep for each of the 4 joints:

$$\left[\theta_{11}, \frac{d\theta_{11}}{dt}, \theta_{12}, \frac{d\theta_{12}}{dt}, \theta_{21}, \frac{d\theta_{21}}{dt}, \theta_{22}, \frac{d\theta_{22}}{dt} \right]$$

The end of deployment the landing system happens when a threshold value of θ_{11} is hit, this value is also referred as Cutoff Deployment Angle (CDA). The value, as an example, was set at 140 degrees for the geometry seen in Figure 3.1.

The output of the deployment Matlab model is a series of coordinates (both horizontal and vertical) that dictate the positions of each of the 4 important points of the landing system: left leg joint in between leg elements, left leg tip, right leg joint in between leg elements and right leg tip. This array is used as a starting point to sketch the landing system geometry on CAD to then transfer it to the landing model. The array is as follows and, with these values and the naming convention found in Figure 3.1, it is possible to make the geometry on CAD:

$$[x_{11}, x_{12}, x_{21}, x_{22}, y_{11}, y_{12}, y_{21}, y_{22},]$$

3.4. Numerical Values to be Fed in Models

In this section of the report, the values to be input in the deployment model are going to be laid out. They are repeated throughout the thesis, however this is a centralised spot where they can all be found. The input values for the deployment model are laid out in the following list:

- Size of the lander body. According to the figure found in 1.2, the lander body, simplified in this thesis as a rectangle, has a width of 1 metres and a height of 0.5 metres.
- The Expected G forces (Earth based) of deceleration are based on 800 N of thrust [50] and the mass of the spacecraft, using Newton's second law:

$$a = \frac{F}{m} = \frac{800 \text{ N}}{575 \text{ kg}} = 1.4 \frac{\text{m}}{\text{s}^2} \approx 0.14 \text{ Gs}$$

- Initial value of mass (counting only leg elements and footpad) used for each leg element is correspondent to half of the maximum allowable mass per the mass fraction requirement, this is:

$$m_{tot-LS} = 0.05 * 575 \text{ kg} = 28.7 \text{ kg}$$

This mass, distributed evenly for each of the 4 landing legs is:

$$m_{1-leg} = \frac{28.7}{4} \approx 7 \text{ kg}$$

This mass, assuming that both landing leg elements are the same length and geometry leads to the maximum allowable mass of a single landing leg following Requirement LS-DES-001:

$$m_{1-leg-element-max} = 3.5 \text{ kg}$$

The mass of the footpad is also taken into account. As written in subsection 4.3.1, this is made of circle of diameter 450 mm. Assuming that the footpad has a thickness of 1 cm and is made of aluminum, this becomes:

$$m_{footpad} = 0.225^2 * \pi * 0.01 * 2810 = 4.5 \text{ kg}$$

- Initial length of the leg elements is taken at 500 mm per leg element. This is because, as a desired outcome, the leg elements can be efficiently packed around the lander body, as the following figure shows:

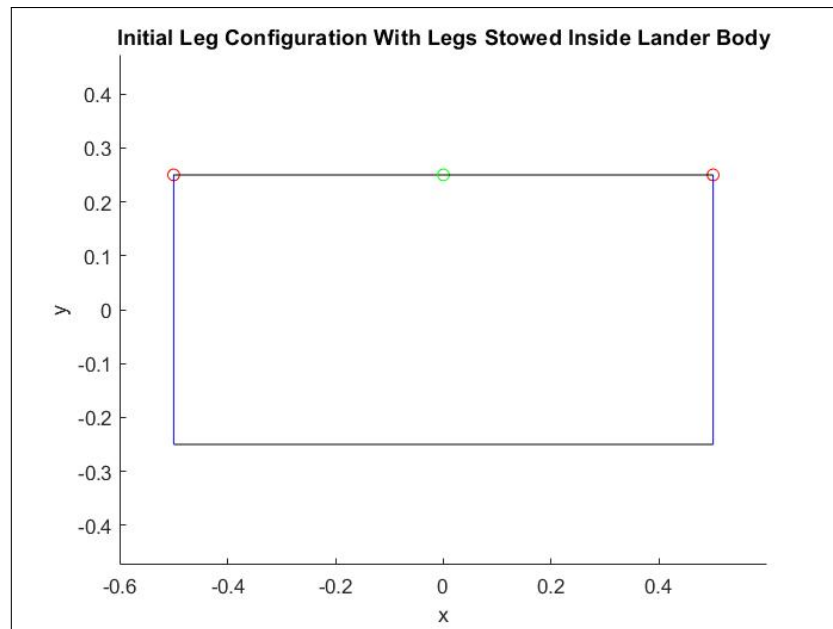
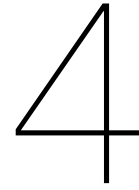


Figure 3.6: Lander rectangle with leg elements around it to be packed in an efficient configuration.

In figure 3.6, the landing legs can be seen perfectly wrapped around the payload rectangle. This is a perfect outcome that can be achieved if both leg elements are 500 mm long with a body that is 1000 mm wide and 500 mm high.

- The geometry of each landing leg element is taken as a hollow circle. The outer diameter of both the aluminum and CFRP landing legs is taken as 80 mm. The wall thickness of the CFRP landing leg elements is based on its layup. Specifically, as is explained in subsection 5.3.1 with a layup of 24 layers with each layer 0.1 mm thick, leads to a wall thickness of 2.4 mm. The wall thickness of the aluminum leg element is calculated based on the chosen mass at the end of the sensitivity analyses.
- Damping is the first item to be looked at in the sensitivity analyses, therefore a range of possible values is be found in section 6.2.



Landing Modelling

With landing modelling, for this thesis, it is meant to study the landing stability that a conceptual landing system geometry has after deployment modelling first. Landing modelling is also the part of the thesis where the stresses and decelerations are looked at. In this section of the thesis, the tools used to look into these landing performance parameters are laid out.

Regarding landing stability, Matlab is used to calculate this aspect of the landing system. Due to the availability of powerful software on behalf of the Aerospace Faculty and because of the wide acceptance of this method by industry, the modelling of the landing was performed through Finite Element Modelling (FEM). The alternative would be to use Multi Body Dynamics (MBD) software, however this type of modelling is used to track the kinematics of a system, more similar to what was done in Matlab in chapter 3. One of the requirements set on this thesis' landing model is to be able to track stresses, which FEM can successfully do [3].

In this section of the thesis, the FEA set up of the simulations is laid out. The purpose of this chapter is to explain how the simulations were set up and why choices over inputs were taken in order for them to be repeatable for future studies.

4.1. Landing Modelling Assumptions

A list of the assumptions taken for the landing analyses is laid out in the following list:

- The joints in between leg elements are taken as straight elements that don't co-rotate with regards to each others. The detailed design of the joint is, in fact, not part of the scope of this thesis, nevertheless, a small section on the leg joint design is left in Chapter 8.
- Also regarding the joints, it is assumed that the locking in position of the joints after deployment will not be compromised during landing. This means that the landing legs will no further rotationally displace with the impacts of landing.
- It is assumed that the landing will happen with a single leg touching the ground at once. This type of situation takes into account the landing system touching a soil formation, such as a rock or an icy boulder, only with a single leg. If this happen, all the weight of the lander would be focused on this leg. This is not a realistic scenario as advancements in Terrain Relative Navigation (TRN) and HDA will lead to safer landing spot selection. However, by designing a leg for this outcome, it can be inferred that this leads to a more conservative design. This is what is suggested by the study in [22], where also a single leg out of 4 is put through landing analyses.
- It is assumed that the material properties of the soil where the landing system will land are of similar properties compared to the Lunar ones as found in [22] and [32]. This is because soil properties of the European soil are not known at the moment. A sensitivity analysis with stiff soil to look at the difference in between the two results will be done nevertheless.

4.2. Landing Stability Modelling on Matlab

Landing stability of the lander, for this thesis, is calculated through Matlab by using trigonometry. On Matlab this is calculated by taking the projection of the center of mass towards the footprint at different soil inclination angles. If the projection of the lander COM is inside the footprint at a prescribed inclination angle, then the landing is deemed stable. If it is outside, then the landing is unstable.

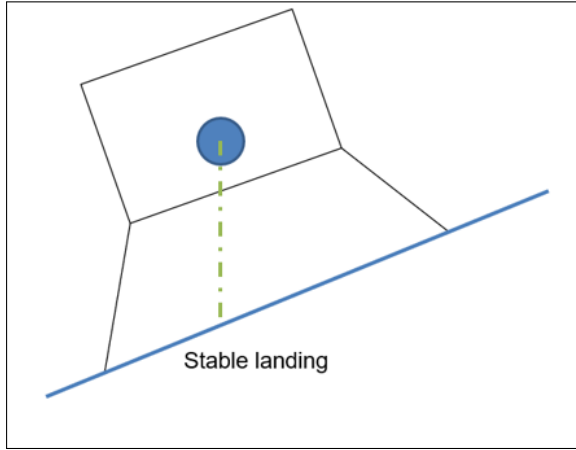


Figure 4.1: FBD showing a diagram of a stable landing on an inclined surface.

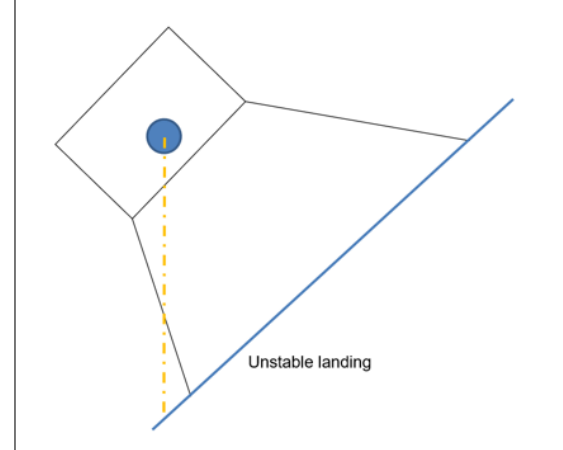


Figure 4.2: FBD showing a diagram of an unstable landing on an inclined surface.

On Matlab, stability is calculated as follows.

First the program calculates the projection on the horizontal axis of the vertical distance between the right leg tip and the COM:

$$crit = abs((y_{22} - COM_y) * tan(\theta_s)) \quad (4.1)$$

In which:

- *crit* is the name of the first criterion for calculating the stability of the landing system at the prescribed soil inclination angle,
- y_{22} is the vertical position of the right leg tip, following the naming convention laid out by Figure 3.1,
- COM_y is the vertical position of the whole lander Center of Mass, calculated by taking into account the landing system mass and the one of the payload rectangle,
- θ_s is the value of the soil inclination.

Secondly, the program calculates what is the horizontal distance between the same leg tip and the lander's COM:

$$crit1 = abs(COM_x - x_{22}) \quad (4.2)$$

In which:

- *crit1* refers to the criterion for the second computation of landing stability,
- COM_x is the horizontal position of the center of mass of the lander,
- x_{22} is the horizontal position of the landing system right leg tip.

In order for a landing to be stable, the relation:

$$crit1 > crit \quad (4.3)$$

has to be true.

A sample calculation to prove this relation is offered in section 5.2.

4.3. Finite Element Model

In this section, the setup of the FEA simulations of for the landing is laid out and explained. The scope of this is to allow for repeatability of the studies. The landing case that is modelled with the following steps is that of a landing system landing touching the ground with a single leg first, so that this leads to a conservative design. Furthermore, no horizontal velocity (or side slip) is modelled in the software.

4.3.1. Geometry

The landing system geometry is sketched on CAD software SolidWorks using the outputs from the deployment model. These outputs from deployment modelling are listed as follows:

- Landing leg element length,
- Angle between the first leg element and the lander's body vertical wall, which corresponds to the CDA,
- Vertical and horizontal distance from the payload COG (which is considered as the origin) and the landing leg tip,
- Diameter and wall thickness of the landing leg elements.

With the above items, both the CAD and FEA software can automatically compute the mass once materials are assigned. This geometry is then exported as a STEP file into Abaqus. In order to save mesh elements, only 1 leg is sketched and then moved to Abaqus.

The inner diameter of the landing legs made of aluminum is calculated backwards by having the mass, length of a landing leg element from deployment modelling and the outer diameter as a fixed value of 80 mm. Specifically, this is done by calculating backwards the area value in the Equation 4.4:

$$m_{1-leg-element} = \rho_{alu} * l_{1-leg-element} * A_{element} \quad (4.4)$$

In Equation 4.4, the components are:

- $m_{1-leg-element}$ is the mass of a single leg element, which is an input of deployment modelling, therefore an already known value, at this point,
- ρ_{alu} is the density of aluminum,
- $l_{1-leg-element}$ is the length of a leg element, also an already known value since this is an input of the deployment modelling studies,
- $A_{element}$ is the only unknown factor of this equation, therefore something that can be solved once the other values are known after deployment modelling, as will be seen at the end of chapter 6.

The footpad's geometry is borrowed from the Mars Viking footpad dimensions due to the fact that this lander had a similar payload mass to that of the Europa Lander, amounting to 572 kg [29]. A drawing of the Viking's landing leg is provided in Figure 1.8:

From Figure 1.8, specifically in the top left drawing, the size of the footpad can be produced:

$$D_{Footpad} = 17.75 \text{ in} \approx 450 \text{ mm}$$

4.3.2. Materials

Two materials are envisioned to be applied to the landing system, one is aluminum 7075-T6, and the other is a CFRP layup used by [27]. The choice of the first material is because of its popularity when it comes to designing space structures, for example the Apollo Lunar Module landing legs were made of aluminum [37]. The CFRP is chosen due to its lighter density. Other composites could be fitting, however to limit the amount of simulation iterations it is decided, for this thesis, to keep the material comparison between these two. The material properties of Aluminium alloy 7075-T6 that are input in Abaqus are grouped in Table 4.1:

Property Name	Value	Unit
Density	2810	kg/m^3
Young's Modulus	71700	MPa
Poisson Ratio	0.33	-
Ultimate Tensile Strength	572 MPa	-

Table 4.1: Abaqus aluminum alloy 7075-T6 material table [2].

The last important material to be placed in the landing model is the material of the soil. This is assumed to be deformable Lunar soil like material as found in [32] and [22].

Category	Property	Value	Unit
Cap plasticity Properties	Material Cohesion	0.0009	MPa
	Angle of Friction	0.807	Rad
	Cap Eccentricity	0.4	-
	Initial Yield Surface Position	0	-
	Transition Surface Radius Parameter	0.05	-
	Flow Stress Ratio	1	-
Mass Density	Mass Density	1580	kg/m^3
Elastic Properties	Young Modulus	182	MPa
	Poisson Ratio	0.28	-

Table 4.2: Elastic and physical material properties used to model the Lunar like soil on Abaqus.

And regarding the plasticity of the lunar like soil, this is model as a Cap Hardening material, with the properties found in Table 4.3 [32]:

Yield Stress [Mpa]	0.0069	0.011	0.021	0.06	0.102	0.2
Plastic Volumetric Strain [-]	0	0.002	0.005	0.008	0.012	0.017

Table 4.3: Plastic properties of lunar like soil used for Abaqus simulations [32].

4.3.3. Mesh Elements

The material is assigned to the leg section of the landing leg as a homogeneous 3D solid component using S4R (rectangular shell elements with 4 nodes, one per corner) mesh elements as Figure 4.3 shows:

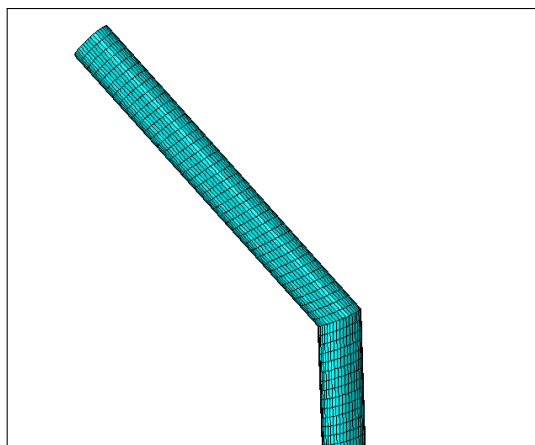


Figure 4.3: Detail of mesh in landing leg elements with S4R elements.

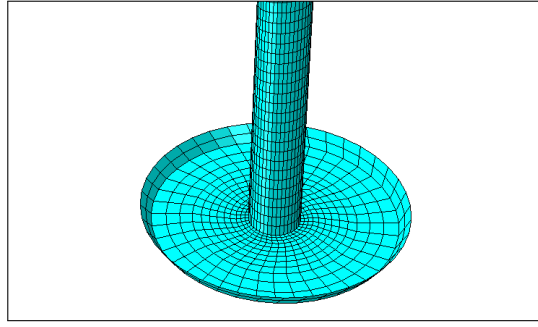


Figure 4.4: Detail of mesh S4R element of the landing leg's footpad.

The deformable soil is meshed with C3D8R elements, as Figure 4.5 shows:

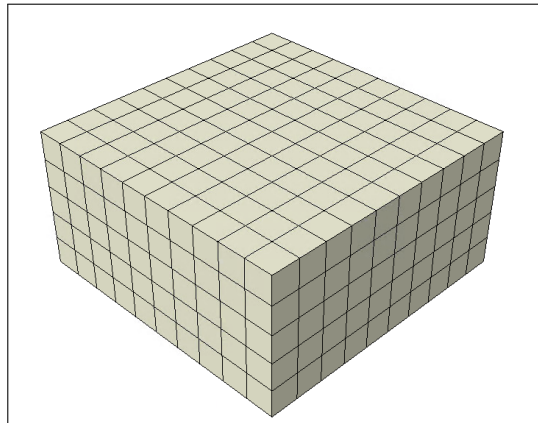


Figure 4.5: Mesh distribution on the deformable soil cuboid.

4.3.4. Simulation Assembly

At this point the 2 components of the simulation (the landing leg and the ground) are put together in the software and the assembly is seen in Figure 4.6:

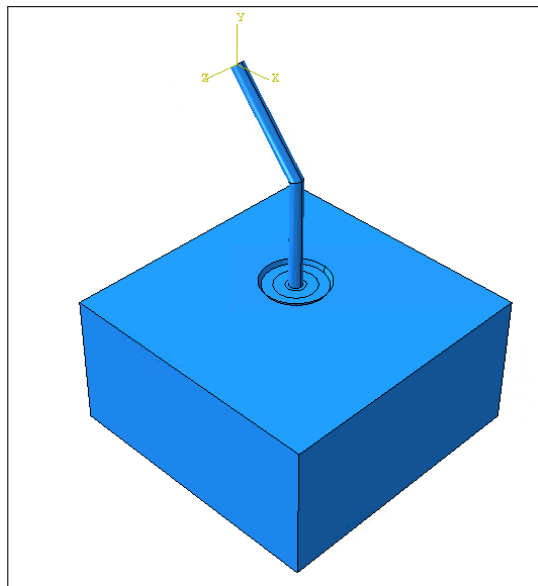


Figure 4.6: Abaqus simulation assembly.

Specifically, the footpad is placed at a height of 15 mm from the ground. This height is arbitrary and can be changed.

4.3.5. Load and Boundary Conditions

In this section of the report, the loads applied to the landing leg will be listed and explained.

To account for the lander's inertia, a point mass is placed at the same distance that it was expected to be in the Matlab model, this is at 0.5 metres of horizontal distance and 0.25 metres of vertical distance. This is because the lander body is taken to be 1 metre wide and 0.5 metres tall, therefore its COG is in the middle of its width and height. This concentrated mass has been tied to the upper part of the landing leg with a rigid body constraint:

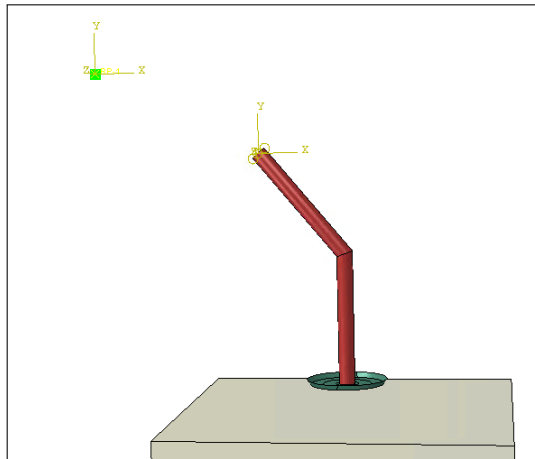


Figure 4.7: Detail of the FEA setup with concentrated mass (at RP1 as seen with Green square) interacting with the top of the landing leg.

This constraint, in the simulations that will be found in chapter 7, is substituted with a "dashpot", which is a shock absorbing mechanism that is used by the software to model landing energy dissipation. The dashpot is modelled so that it dissipates energy only in the vertical direction. By doing so, the representative of a shock absorbing mechanism that acts in the direction parallel to the landing velocity vector (or normal to the landing plane) is modelled in the simulation. This type of modelling simulates, in practice, the presence of a damping system at the interface between the upper landing leg joint and the bottom part of the lander body. The damping coefficient is chosen as 20 N/mm/s because of the fact that this achieves a % decrease of two thirds in deceleration felt by the lander's instruments compared to the same landing case with the same landing speed, but without dashpot.

The position of RP1 (Reference Point 1 and seen in green in Figure 4.7) corresponds to the position of the lander COM as found in the Matlab model. Since the lander body is simplified as a rectangle of 1 metre of width and 0.5 metres of height, this point is at an horizontal distance of 0.5 metre from the top of the landing leg and at a vertical distance of 0.25 metres from the same point.

In order to fix the assembly in Abaqus' Simulation space, a boundary condition is placed on the side and bottom walls of the deformable soil. This boundary condition constraints at all timesteps every translational and rotational degree of freedom of the side walls of the soil cuboid. This is because the soil cuboid has to have finite dimensions because of computational limitations.

In order to make sure that the landing leg is in a perfectly vertical descent, another boundary condition placed on the landing leg during the descent is to constraint the translational degrees of freedom in the x and z directions which, in Figure 4.6, can be seen that those are the horizontal directions.

Also, an initial velocity of the landing leg of 5 m/s is given as a boundary condition. This is modelled as a "predefined field" on Abaqus.

In the end, in order to model a condition more faithful to those found on Europa, gravity is added to the simulation. This is modelled as a load, selected as gravity and the value is chosen as 1.315 m/s^2 (although input as 1315 mm/s^2 in the FEM program due to the Abaqus unit convention).

4.3.6. Analysis Type

The step, in Abaqus, is what defines the type of analysis. This is clearly a dynamic analysis, as the effects of the landing shocks are different at different timesteps. Because of this the step has to be of the dynamic type. Ultimately, the choice between dynamic explicit and dynamic implicit fell on the implicit type because this was verified (in subsection 5.3.2) to be a suitable way of repeating reference results from literature.

4.3.7. Contact Modelling

Contact, in these simulations, is defined as a surface-to-surface contact between the bottom of the footpad and the top of the soil cuboid. In this case, the master surface is the footpad and the slave one is the soil's top surface. The friction coefficient is set to 0.3, as suggested by [22].

4.3.8. History and Field Outputs

Finally, the last matter to be input in the simulation are the types of field and history outputs that are desired to be analysed after results become available. In Abaqus, a field output is a type of result that shows the change of a property throughout the design space, shown as contour plots on the components making the simulation assembly. A history output, on the other hand, shows the variation of a set property in a specific place (node or element) within the design domain throughout the simulation time period. The field and history output decided for the simulations for the thesis are as follows:

1. Von Mises stress contour plots for the aluminum leg and Maximum Principal strain (for the CFRP design). It is assumed that the stress throughout the leg will be maximum at touchdown, at the moment when the footpad will touch the ground. To compare the stresses throughout different simulations, the Von Mises stresses at this moment will be looked at.
2. Acceleration history of the lander's Center of Gravity (COG). By looking at the acceleration that the lander's center of gravity, represented by the Reference Point RP1, it will be possible to assess the amount of G forces that the lander will go through.

5

Verification

In this chapter, the models used for the analyses of the deployment dynamics of the landing system and for the landing analyses, are verified. In Computer Aided Engineering, verification is concerned with the fact that inputs are properly implemented and that errors are within acceptable margins [49]. 3 models have been introduced in Chapters 3 and 4, these are:

- A Deployment model to track the deployment dynamics of the landing system using double pendulum algorithms on Matlab. Which from now will be referred to as Matlab Pendulum Deployment Model.
- A Landing Stability model in order to assess, using trigonometry, at which soil inclination angles the landing is stable and not. Also implemented on Matlab and that will be referred to as Landing Stability Matlab Model.
- A Landing model to track in detail the stresses and other effects such as decelerations experienced by the lander on Abaqus. Which, from now on, will be referred to as the Dynamic Abaqus Landing Model.

The Matlab Pendulum Deployment Model is verified by comparing its results related to the dynamics of a double pendulum with results found in a paper ([9]) that use the same algorithm to also track deployment dynamics of a double pendulum. By comparing results with the same inputs and algorithm, it is possible to conclude that the double pendulum algorithm has been properly implemented on Matlab.

Secondly, the Landing Stability Matlab Model is verified by providing sample calculations of stability at 2 different angles.

In the end, the Dynamic Abaqus Landing Model implemented for the purpose of this thesis is verified. This is done by first running an identical simulation to that found in [27], this simulation is a static analysis of a compression test of a CFRP landing strut for an interplanetary lander. In this case, by having the same results from the same inputs between the Abaqus model that is made for the verification chapter of this thesis and that is found in [27], it is possible to come with the conclusion that the Abaqus inputs have been properly implemented. Since the Dynamic Abaqus Landing Model used for coming up with landing results for this thesis uses a different type of analysis compared to that used by [27], moving from their analysis to the type of analysis for this thesis is performed to prove if the results are different. If the results do not differ or differ by less than 10%, then the methodology of using Dynamic Implicit analyses to show the effects of landing of an interplanetary lander can be considered as verified.

10 % is taken as an accuracy threshold because of the accuracy requirements as written in chapter 2.

5.1. Verification of Deployment Model

In order to keep a consistent use of the terms involved in the double pendulum algorithm, the naming convention in Figure 5.1 is used:

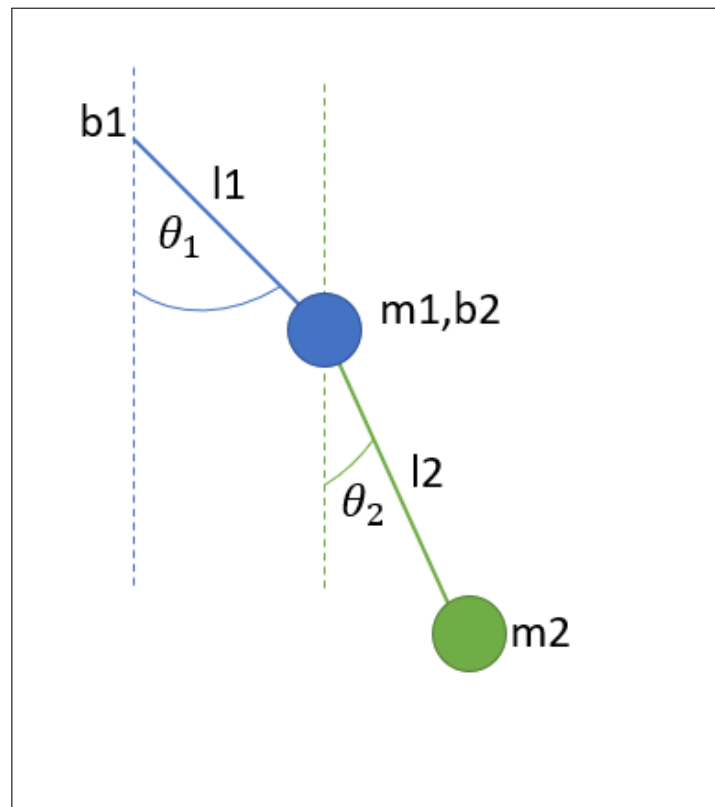


Figure 5.1: Naming convention for double pendulum for verification studies.

The parameters in Figure 5.1 are listed as follows:

- b_1 and b_2 correspond to the joint damping of the first and second pendulum elements respectively,
- θ_1 and θ_2 correspond to the displacement angles of the first and second pendulum elements. It should be noted that, in the case of this verification studies, the angles are taken as those that start from the parallel to the gravity vector and the bottom of the pendulum element beam (in the case of the deployment models the angles are taken between gravity parallel and the top of the leg element),
- m_1 and m_2 are the masses of the first and second pendulum elements respectively,
- l_1 and l_2 are the lengths of first and second pendulum elements.

In this paragraph, the verification strategy for verifying the deployment model is explained. Equations from Equation 3.1 to Equation 3.5 are taken from the paper in [9] and placed in Matlab, where an ODE45 solver solves them. This section of the verification chapter deals with the proper implementation on Matlab of these algorithms. The paper in [9] provides 2 studies where the results of the algorithm are presented. The results that are shown are in the form of the variation of angular displacement over time of the top angle of the double pendulum (θ_1 in Figure 5.1). Furthermore, the results are also in the form of phase diagrams showing the variation of angular displacement over angular rate (or rotational speed) of the same angle (θ_1 in Figure 5.1). The charts for each of the 2 studies, which are seen in Figures 5.2, 5.3, 5.7 and 5.8, are chosen because these are the presented results in the paper in [9]. The same 2 studies are run in the Matlab Pendulum Deployment Model developed for this thesis in order to prove that the algorithms and inputs have been implemented in the same way as in [9]. The difference between the first and second study performed by [9] is only the values of joint damping. All other parameters found in the list under Figure 5.1 aside from joint damping are kept the same for both studies.

The simulation characteristics (or inputs) of the first study reported in [9] are found Table 5.1:

Property	Value	Unit
Damping	1	Nm/ rad/s
Length of First Pendulum	1	m
Mass 1	1	kg
Length of Second Pendulum	1	m
Mass 2	1	kg
Gravity acceleration	9.81	m/s ²
Starting Angular Displacement of First Angle	120	Deg
Starting Angular Rate of First Angle	0	Deg/s
Starting Angular Displacement of Second Angle	0	Deg
Starting Angular Rate of Second Angle	0	Deg/s

Table 5.1: Pendulum characteristics for double pendulum first verification study, masses are located at the tips of each pendulum element.

The Figures 5.2 to 5.3 show the results of angular displacement vs. angular rate of the first pendulum angle (θ_1 in Figure 5.1) and angular displacement vs. time also of the same pendulum angle when damping is 1 N m/rad/s from [9]:

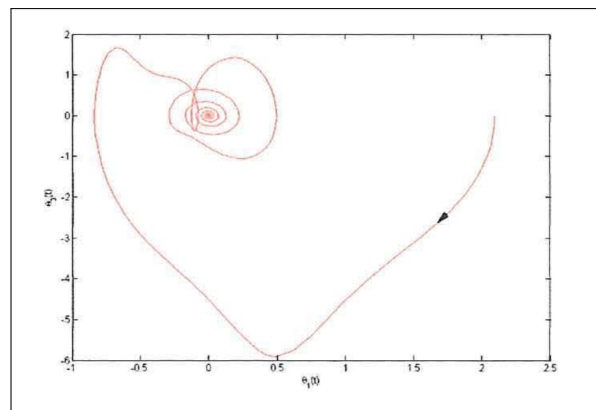


Figure 5.2: Variation of angular rate against variation of angular displacement in [9].

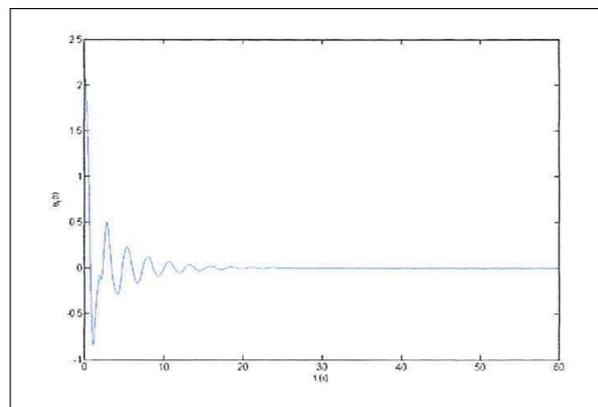


Figure 5.3: Variation of angular displacement with respect to time in [9].

Figures 5.4 and 5.5 show the same results in the Matlab Pendulum Deployment Model developed for

this thesis with double pendulum (the tabulated and filtered data to make the charts can be found in Appendix C):

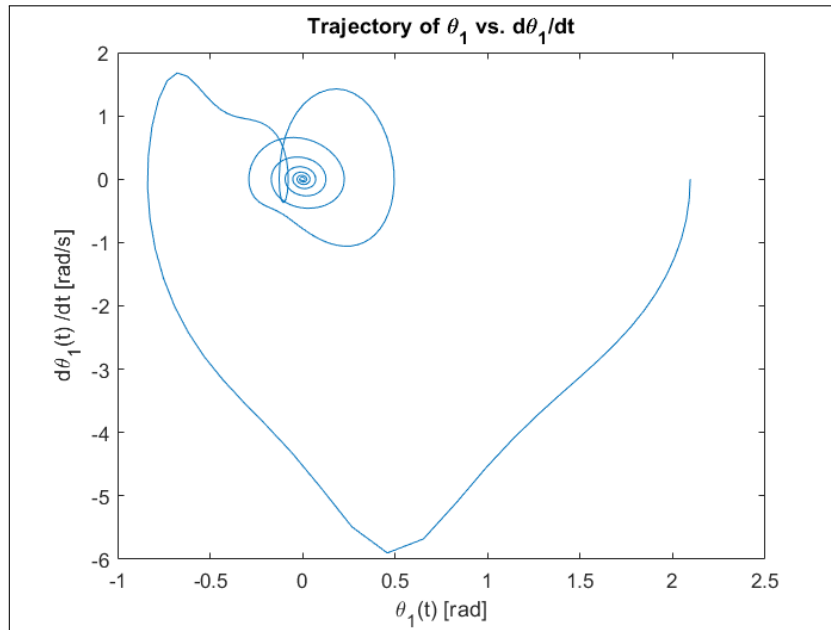


Figure 5.4: Variation of angular rate against variation of angular displacement in Matlab algorithm developed for this thesis.

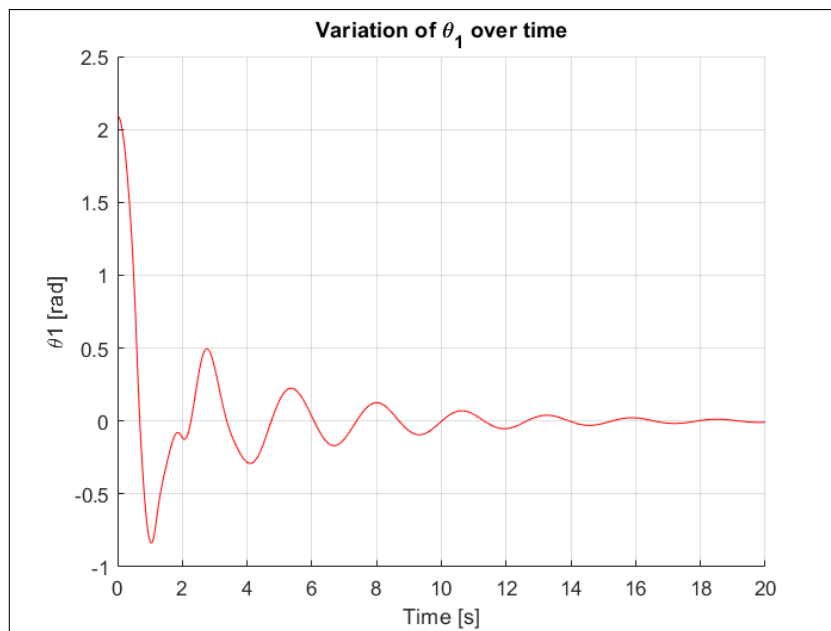


Figure 5.5: Variation of angular displacement with respect to time in the deployment Matlab algorithm used for this thesis.

The only difference between the 2 runs is, as can be seen by looking at the horizontal axis of Figure 5.3 and Figure 5.5, the running time. The author of [9] ran his model for a 60 seconds. Whereas the algorithm developed for the purpose of this thesis was ran for 20 seconds. This is because, after 20 seconds, the double pendulum becomes still because of the damping. However this doesn't prove mismatch between the Matlab Pendulum Deployment Model and the implementation of the double pendulum algorithm found in [9].

By looking at Figure 5.4 and Figure 5.2 it can be noticed that the results are almost identical, mainly noticed by the loop that is located in the top left side of the 2 graphs.

Furthermore, by looking at Figure 5.5 and Figure 5.3, it can be seen, although less noticeable due to the poor quality of the latter plot, that the variation of angle θ_1 is the same in both graphs. The most recognizing feature being the small kink at $t = 2s$.

To allow for a more quantitative comparison between the results of the deployment model made in Matlab for this thesis and the results of the double pendulum algorithm found in [9], Figures 5.2 and 5.4 are looked at more in detail. Specifically, the values of the angular rate of the pendulum when the displacement is of -0.5 radians will be compared. In the case of Figure 5.2, no numerical tables are present, therefore the graph has to be analysed by using image analyses:

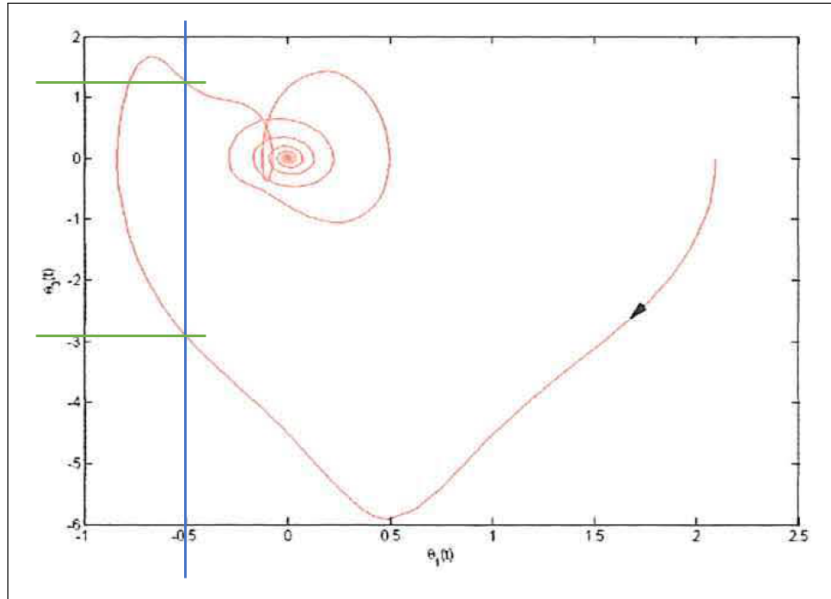


Figure 5.6: Variation of angular displacement with respect to angular rate in double pendulum algorithm in [9] with markings of angular rate when the angle is -0.5 rad.

By looking at Figure 5.6, it can be seen that the angular rate when the angle of the pendulum is displaced by -0.5 rad is of 2 values:

- $-2.90 \frac{rad}{s}$ as the lower green line shows,
- $+1.25 \frac{rad}{s}$ as the upper green line shows.

In the deployment Matlab algorithm made for this thesis, when angular displacement is at -0.5 rad, angular rate is at:

- $-3.02 \frac{rad}{s}$
- $+1.24 \frac{rad}{s}$

These two values can be found in Table C.1 and are easily recognizable as they are in bold in the Table.. These 2 data points lead to percentage differences of:

$$\epsilon_{diff_1} = 100 * \left(1 - \left(\frac{-2.9}{-3.02} \right) \right) = 3.97\%$$

$$\epsilon_{diff_1} = 100 * \left(1 - \left(\frac{1.25}{1.24} \right) \right) = -0.81\%$$

It should be pointed out that these 2 percentage differences have been calculated off values gathered from the visualisation of a graph that, as can be seen by looking at Figure 5.6, is not of high quality. On the other hand, the values in the denominators of the calculations above are easily gathered by running the Matlab deployment algorithm.

With both percentage differences below 10%, it can be said that the implementation of the double pendulum algorithm on Matlab for this thesis is very similar (if not identical) to the one found in [9]. The percentage difference is not 0 because of the fact that numerical values of the results found in [9] have been gathered by direct observation of graphs.

Since the paper offers a second study, where the types of results are the same (2 graphs where one shows angular rate vs. angular displacement and the second the angular displacement vs. time of the top pendulum angle in a double pendulum with damping), but a single input is different, a second verification study of the Matlab Pendulum Deployment Model is here performed in the same way as the one done previously. Now the damping coefficient, though, is decreased to 0.1 Nm/rad/s and the other simulation characteristics are seen in Table 5.2:

Property	Value	Unit
Damping	0.1	Nm/rad/s
Length of First Pendulum	1	m
Mass 1	1	kg
Length of Second Pendulum	1	m
Mass 2	1	kg
Gravity Acceleration	9.81	m/s^2
Starting Angular Displacement of First Angle	120	Deg
Starting Angular Rate of First Angle	0	Deg/s
Starting Angular Displacement of Second Angle	0	Deg
Starting Angular Rate of Second Angle	0	Deg/s

Table 5.2: Pendulum characteristics for verification study with lower damping, masses are located at the tips of each pendulum element.

The results are presented Figures 5.7 to 5.10 (the tabulated data to make the charts of the deployment Matlab Pendulum Deployment Model for the thesis can be found in Appendix C):

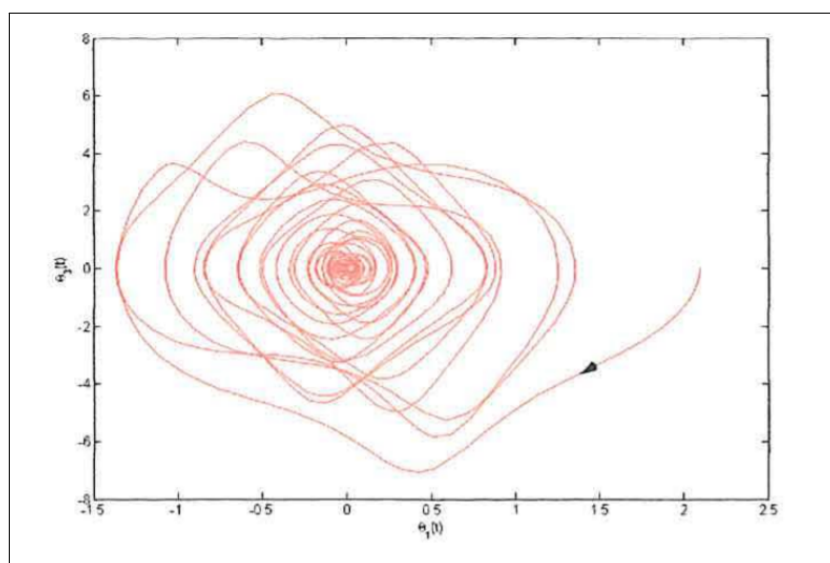


Figure 5.7: Variation of angular rate with respect to variation of angular displacement in [9] with lower damping.

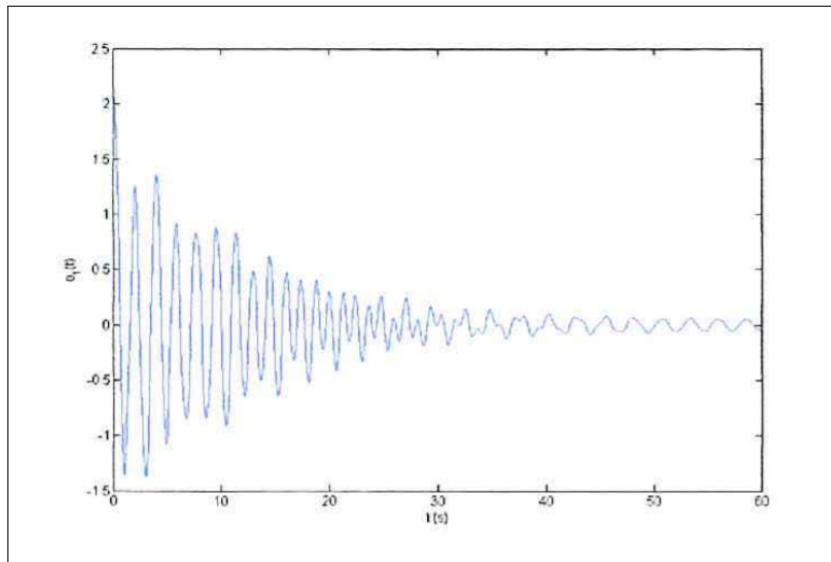


Figure 5.8: Variation of angular displacement with respect to time in [9] with lower damping.

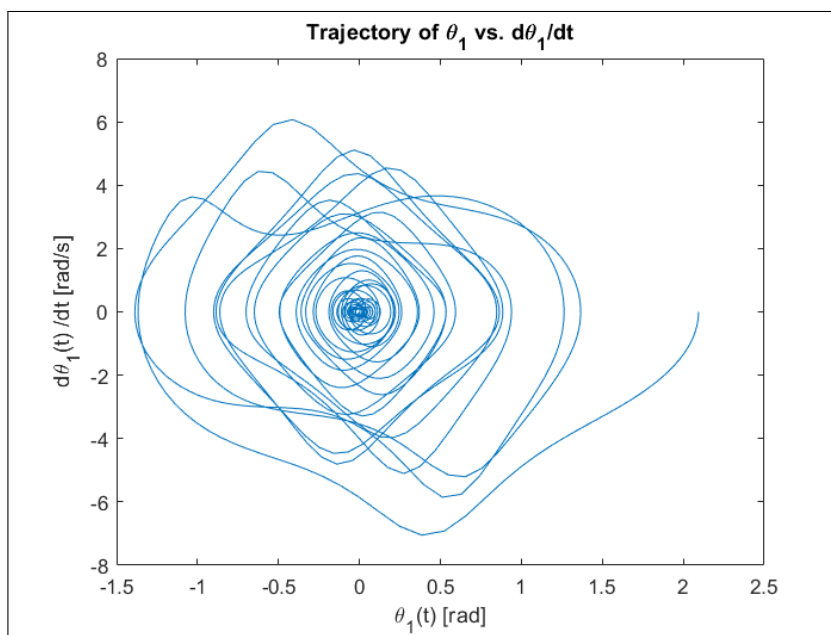


Figure 5.9: Variation of angular rate against variation of angular displacement in deployment Matlab algorithm used for this thesis with lower damping.

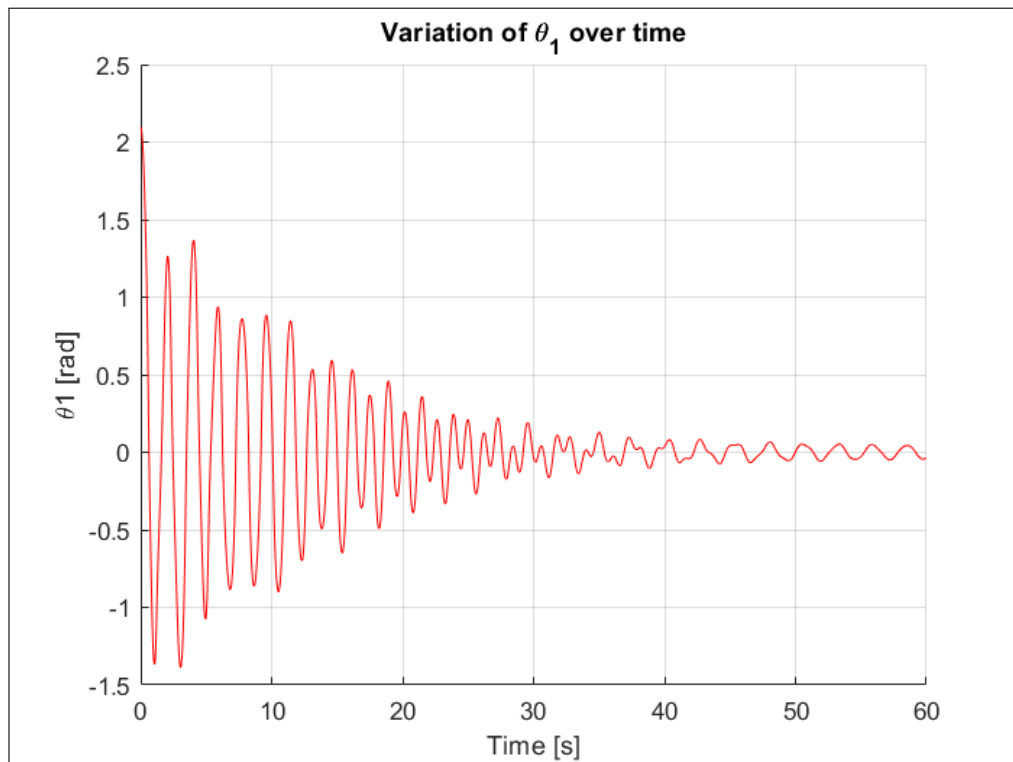


Figure 5.10: Variation of angular displacement with respect to time in the deployment Matlab algorithm used for this thesis with lower damping.

Now the Matlab Pendulum Deployment Model developed for this thesis is let run for 60 seconds as well, as can be seen in the horizontal axis of Figure 5.10. It can also be clear that the effect of lowering the damping of both joints within the double pendulum is an expected one. In charts from 5.7 to 5.10, in fact, compared to the charts from 5.2 to 5.5, the motion of the pendulum lasts for longer.

Regarding the comparison between Figure 5.7 and Figure 5.9, it can be noticed that the behaviour is the same. And the same can be said about Figure 5.8 and Figure 5.10. With minute differences due to the low quality of the images from [9].

Consequently, the model implemented on Matlab of the double simple pendulum (with mass modelled at the very tip of each pendulum) and with damping, leads to the same results with the same parameters as the one found in [9], which in itself is a peer reviewed model, meaning that the first can be considered as verified.

Unfortunately, there are no numerical values that are used to make Figures 5.2, 5.3, 5.7 and 5.8 given by [9]. Because of this, the percentage difference calculation has to be done, as performed above, with the direct visualisation and annotation of one of the graphs developed by [9]. Other than this, the comparison is also of the qualitative type, which is done by comparing the shapes of the graphs, as written in the previous chapters. Regarding the quantitative comparison, for this second verification study it'll be performed on the time angular displacement vs. time graphs as seen in Figures 5.8 and 5.10.

The one found in [9] with annotations is seen in Figure 5.11:

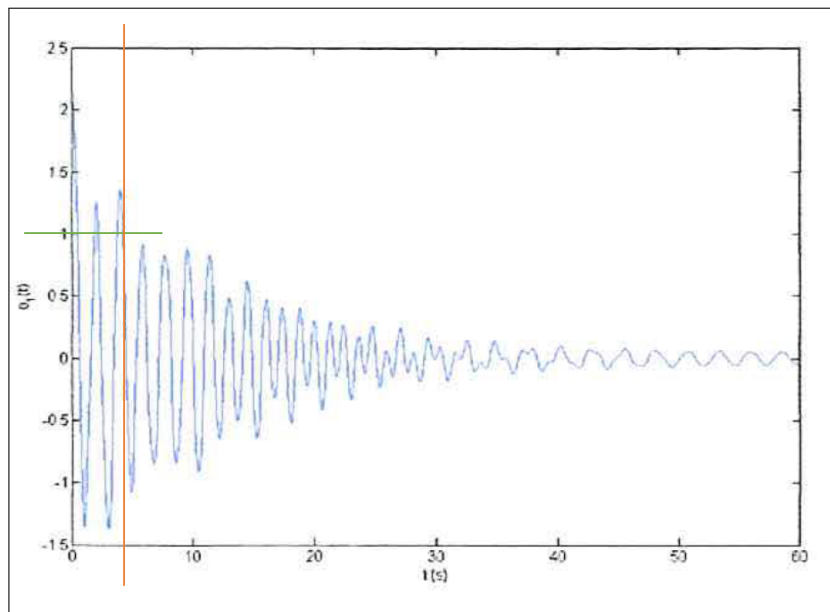


Figure 5.11: Variation of angular displacement with respect to time in double pendulum algorithm in [9] with markings of the third oscillation when displacement is at +1 rad.

Comparison between results in the second study of [9] and in the Matlab Pendulum Deployment Model will be done by comparing the time at which 1 rad of angular displacement is hit for the fifth time, or the third time where the function is decreasing after hitting this value. The difference in times at which the value of 1 rad is hit between the paper in [9] and the Matlab Pendulum Deployment Model is the percentage difference for this verification study. The time at which a displacement of 1 rad is hit after the third rotation when the pendulum's displacement is decreasing is of:

- 4.2 seconds.

In the algorithm run for this thesis, 1 radian is hit for the third time (with the function decreasing) at a time of:

- 4.26 seconds.

This value is found in Table C.4 and is marked in bold in this table for an easier search. Calculating percentage difference:

$$\epsilon_{diff_1} = 100 * \left(1 - \left(\frac{4.2}{4.26} \right) \right) = 1.41\%$$

Also this percentage difference is lower than 10 % and it is not 0 because of the fact that the numerical value placed in the denominator of the calculation above is found by direct analysis of the chart found in Figure 5.11.

After both runs of the Matlab pendulum Deployment Model, comparison of the same types of results between this model and the one found in [9] both in a qualitative way (where the shapes of the charts of the results between the 2 models were correlated) and in a quantitative way, by looking at numerical value differences at the same coordinates within the same graphs between the 2 models, minimal differences were found. These differences were still within the limits set for this thesis, below 10%, and due to the poor quality of the figures output in [9]. Because of the low differences found between the 2 models, it can be inferred that the implementation of a double pendulum algorithm with damping in between joints as done on the Matlab Pendulum Deployment Model, is reliable.

5.1.1. Effect of Deployment Assumptions

The validity of the center of mass position assumption taken for the deployment modelling implementation will be analysed. These errors are then compounded with the errors calculated by the verification and checked if the model is still within the 10 % allowable accuracy. In section 3.2, it was written that

the deployment time will not be affected too much by the fact that the landing leg element masses are at the tips and not at the center. The analysis shown in Figure 5.12 is to prove that, for the purpose of the deployment analyses with the double pendulum, the difference between putting the mass concentrated at the end of each pendulum element or at its center of mass, is less than 10 %:

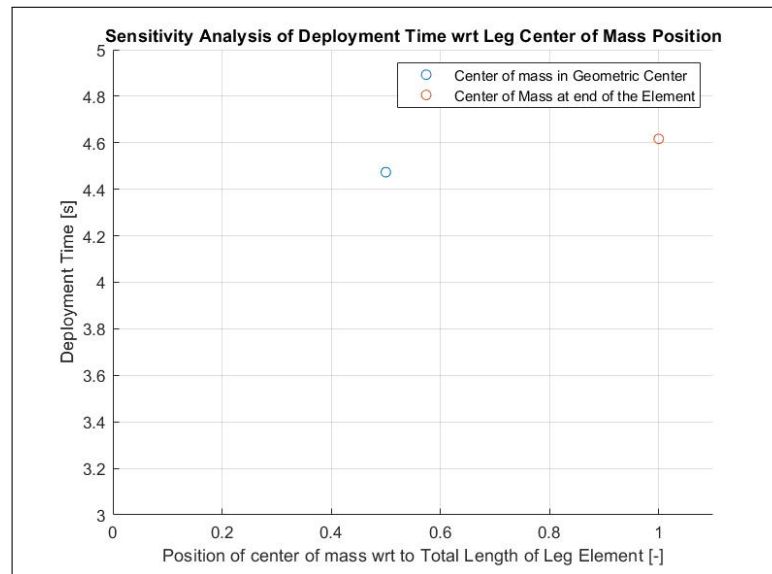


Figure 5.12: Analysis of implication of position of center of mass over leg element length assumption.

As can be seen by looking at Figure 5.12, the deployment time with the center of mass modelled in the geometric center of each leg element is 4.47 seconds. On the other hand, the deployment time when the center of mass is, similarly to a simplified pendulum, at the end of the element, of 4.61 seconds. This leads to a percentage difference of:

$$\epsilon_{err} = 100 * \left(1 - \left(\frac{4.47}{4.61} \right) \right) = 3.04\% \quad (5.1)$$

Showing that this assumption doesn't affect that much the outputs of deployment modelling. It should be reminded that this analysis is let run like all of the future deployment analyses that will be seen in this chapter, meaning that the double pendulum representing the landing legs only displaces around 100 degrees. If the 2 simulations where the center of masses are in different positions are let run for multiple oscillations, due to the highly chaotic motion of double penduli, the results would be much different. However, this is not the case for this thesis. Based on this, the requirement on deployment time's accuracy (MDL-DEP-003) is well within its limits.

5.1.2. Drag Force Calculation

Drag is calculated as follows:

$$D = \frac{1}{2} \rho S V^2 C_D \quad (5.2)$$

In which:

- ρ is the atmospheric density of Europa, measured in kg/m^3 ,
- S is the surface area of the landing legs facing in the direction of travel,
- V is the velocity of the lander, measured in m/s,
- C_D is the drag coefficient, which, for a cylinder, it's of around 1.2.

Since an indication of the density of Europa is not present, this can be calculated with the simplification that it follows Ideal Gas Law. The known matter about Europa's atmosphere is that there is oxygen

present, albeit tenuous [6]. Oxygen has a gas constant of:

$$R = 259.8 \frac{J}{kg K}$$

With a surface temperature of [6]:

$$T = 110 K$$

This leads to a surface density of:

$$\rho = \frac{p}{R \cdot T} = \frac{10^{-7}}{259.8 \cdot 110} = 3.51 \cdot 10^{-12} \frac{kg}{m^3} \quad (5.3)$$

With an assumed surface area of a cylinder, calculated by multiplying half of the circumference with the length of the leg element:

$$S_{cyl} = 0.04 \cdot \pi \cdot 0.5 = 0.0628 m^2 \quad (5.4)$$

Therefore the area of a landing system made of 4 legs and 2 leg elements per leg is of:

$$S_{tot} = 8 * 0.0628 m^2 = 0.05024 m^2 \quad (5.5)$$

According to [4], the approach velocity of the Europa Lander to Europa shall be of:

$$V = 1378 m/s$$

Even if deployment will not happen when the spacecraft velocity is this high, this is taken as a maximum value to find the maximum experienced drag on the landing legs.

All these parameters lead to a drag force of:

$$D = \frac{1}{2} 3.51 * 10^{-12} * 1378^2 * 0.05024 * 1.2 = 5.72 \cdot 10^{-7} N \quad (5.6)$$

Which can be considered as a negligible force acting on the landing system.

5.1.3. Conclusion on Deployment Modelling Verification

In this subsection, the error compounded by both the comparison with literature and the one due to the assumption analysis is going to be calculated. This error is calculated by adding the error that results from the comparison with literature and the one resulting from the assumption analyses. The error due to the drag assumption is not included as this is negligible. The compounded error is as follows:

$$\epsilon_{comp-dep} = 1.0397 * 1.0304 = 1.0713 \quad (5.7)$$

Which means that the compounded error of these 2 aspects (verification through comparison and error due to position of the COM of leg elements within the leg element and not at the tip) is of 7.13 %. This is still within the prescribed limits of the accuracy requirements.

5.2. Verification of Landing Stability

For the sake of this verification, the following geometry is used:

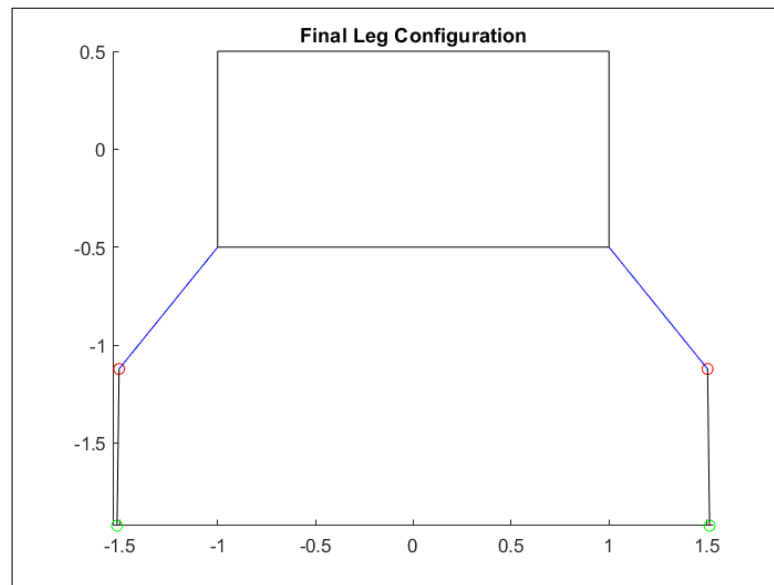


Figure 5.13: Geometry used for landing stability algorithm verification.

Through the Matlab model, the coordinates of the lander COM and of the right landing leg tip can be gathered:

$$[COM_x, COM_y] = [0, -0.0545]$$

$$[x_{22}, y_{22}] = [1.514, -1.9215]$$

In which the origin point $[0, 0]$ is the payload rectangle's COG.

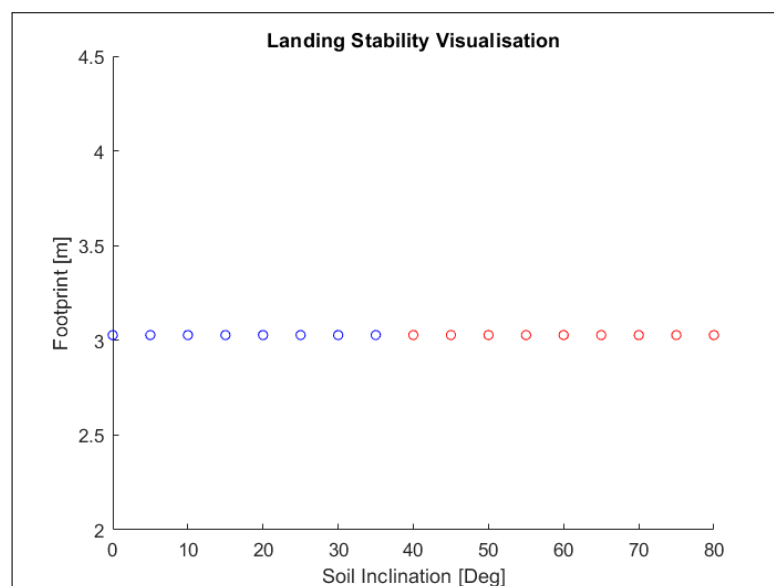


Figure 5.14: Visualisation of angles at which geometry is stable (in blue circles) and unstable (in red circles).

As can be seen by looking at Figure 5.14, the landing is still stable at 35 degrees of soil inclination, but not at 40 degrees anymore. This means that the criterion seen in Equation 4.3 is the opposite when calculated for the 2 angles. This can be calculated as:

$$crit(\theta_s = 35^\circ) = abs((-1.9215 - 0.1053) * tan(35^\circ)) = 1.419$$

$$crit1(\theta_s = 35^\circ) = abs(0 - 1.514) = 1.514$$

$$crit1 > crit \Rightarrow 1.514 > 1.419$$

Which is a true statement, therefore the landing at this angle is stable.

Subsequently the same quantities are calculated for the soil inclination at 40 degrees:

$$crit(\theta_s = 40^\circ) = abs((-1.9215 - 0.1053) * \tan(40^\circ)) = 1.701$$

$$crit1(\theta_s = 40^\circ) = abs(0 - 1.514) = 1.514$$

$$crit1 > crit \Rightarrow 1.514 > 1.701$$

Which is a false statement, therefore the program rightly outputs an unstable landing at 40 degrees.

5.3. Verification of Landing Model

In this section, the proper implementation of the composite material properties and the step used (dynamic implicit) is verified. This is done by comparing an Abaqus model set up by an article in literature dealing with the structural analysis of space based landing systems struts, with a model developed on Abaqus for this thesis that has the same geometry and material inputs. Although the landing analyses developed in this thesis and found in chapter 4 are slightly different from the ones found in literature (as is summarised in Table 5.5), the verification process brought forward in this section of the thesis has the objective of proving that the inputs related to material properties, boundary conditions and, above all, type of analysis is properly done. From the model set up in the same way as the one found in literature, a new model is made with slightly different parameters that are more similar to the ones that are used in the landing analyses for the thesis. These parameters are related to the type of analysis. In fact, in [27], the type of analysis is a static one while, for the purpose of this thesis, the analyses on Abaqus are of the dynamic implicit type.

5.3.1. Verification Study Setup

The Abaqus simulation made for the thesis verification is set up in a way that is identical to the one in [27], which also uses Abaqus to perform structural analysis studies. Not everything could be repeated from [27] because not all analysis parameters are laid out in the article, these inputs are:

- The geometry of the landing leg is that of a cylinder with a central body (of length b) and diameter D , tapered edges and final clamping regions of length f . Values for these geometrical parameters are provided by [27]:

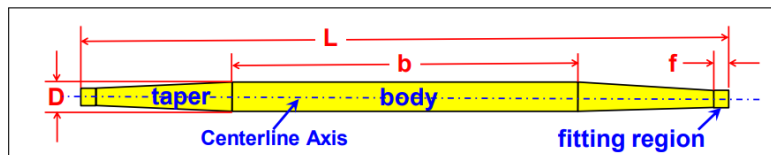


Figure 5.15: Geometry parameters of the landing leg as seen in [27].

Dimension	Original Values from [27] [in]	Values in SI Units [mm]
Strut Length (L)	77.66	1972.56
Body Length (b)	50.67	1287.02
Fitting length (f)	2.943	74.75
Inner Diameter of Body (D)	6	152.4
Fitting Wall Thickness	0.08	2
Layup Thickness	0.095	2.4

Table 5.3: Physical parameters' values as found in [27] with the original values and ones turned in SI units.

The geometry is sketched on Abaqus as a 3D deformable shell using SI units. Figure 5.16 shows the sketcher on Abaqus with the dimensions found in the table in 5.3 in millimeters:

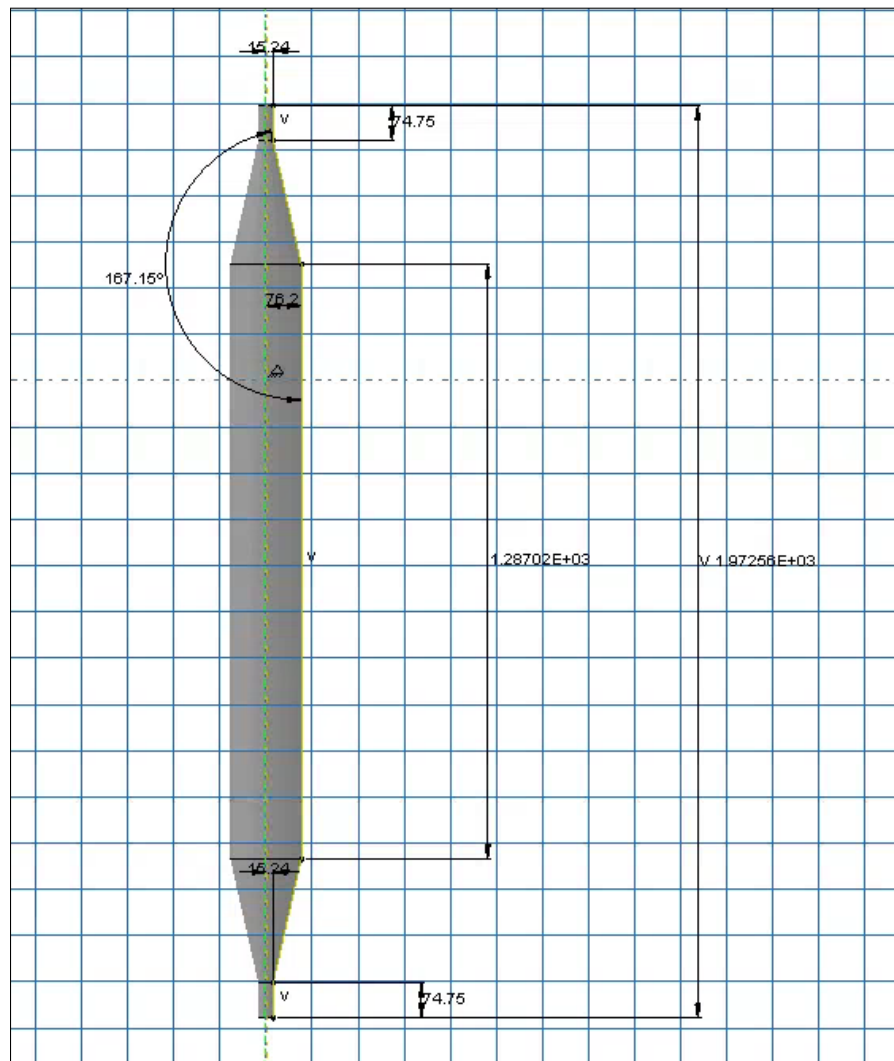


Figure 5.16: Geometry of the landing leg as sketched on Abaqus with SI units.

- The material properties of the composite layup (fibers + matrix):

Property	IM7-8552		Titanium	
Elastic Modulus - Longitudinal [Msi, GPa]	21.40	147.547	16	110.316
Elastic Modulus - Transverse [Msi, GPa]	1.46	10.066	16	110.316
Shear Modulus [MSi, GPa]	0.69	4.757	6.06	41.782
Poisson Ratio [-]	0.30		0.32	

Table 5.4: Material properties as found in [27].

- The material assignment. Since the geometry has, following the paper guidelines, its top and bottom that are made of titanium inserts and the central body made of a composite layup, different materials are assigned to different locations within the strut, as Figure 5.17 shows:

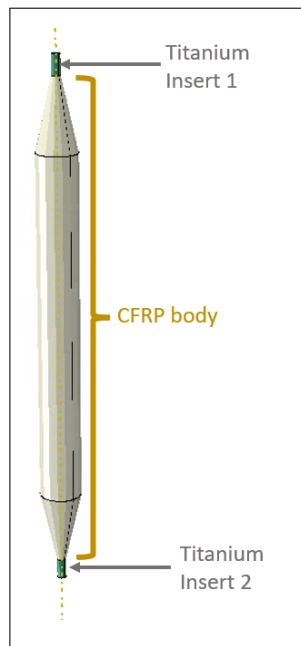


Figure 5.17: Material assignments for each landing leg section.

- The composite layup:

$$[\pm 45 / 0 / 45 / 90 / - 45 / 0_2 / 45 / 90 / - 45 / 0]_s$$

- The type of analysis was initially set as a static one as done by [27].
- The model is loaded and constrained as follows. The top titanium insert is loaded with 6 compression loads (in Newtons for the Abaqus simulation, but in lb units for the article) that are evenly spaced between 5000 and 30000 lbf. This is because it was desired to recreate a load-displacement curve similar to what is shown in Figure 5.18 and which is taken from [27]:

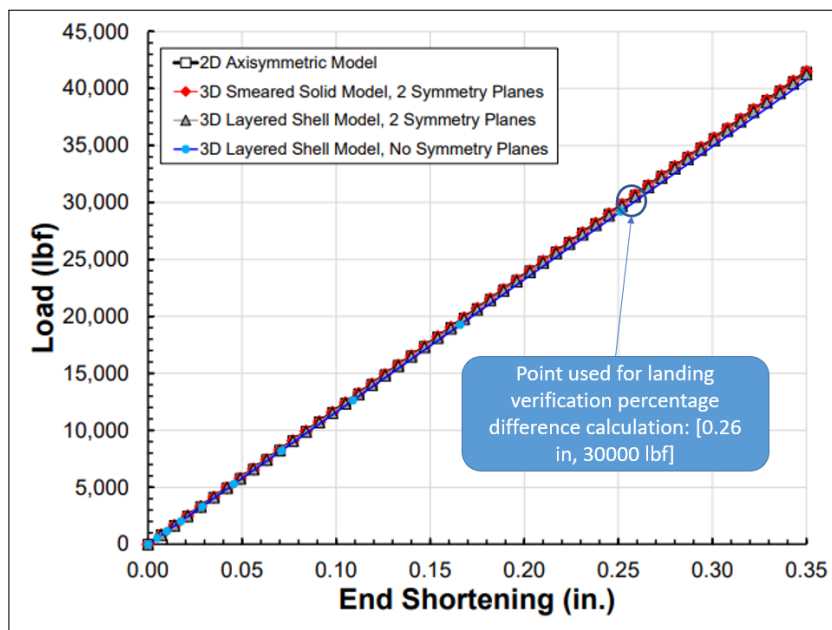


Figure 5.18: Load displacement curve of different models as shown in [27].

For comparison purposes (which will be seen in the following subsection) the line to be taken in consideration is the 3D layered shell. Although, as seen by looking at Figure 5.18, all models have roughly the same load-displacement behaviour.

Since the load has to be applied as a concentrated force, a reference point has to be created. This is placed at the center of the circle at the top of the model and then a "Rigid Body" interaction is created in between this Reference Point and the surface corresponding to the side of the top titanium insert, as Figure 5.19 shows:

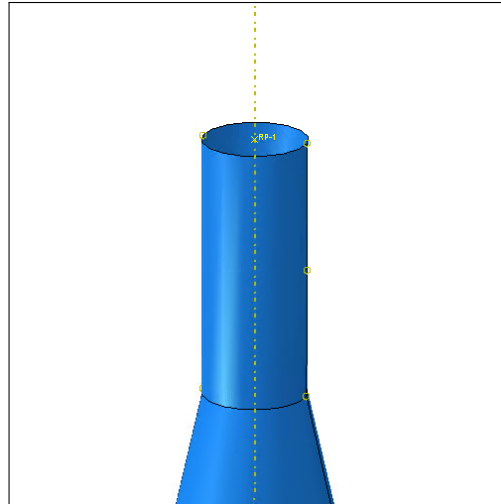


Figure 5.19: Top part of Abaqus model showing the reference point where the model is loaded and the rigid body interaction that connects the point to the top part of the model.

The bottom insert's boundary conditions are not laid out in [27], however it is assumed that it is clamped. Furthermore, the effect of this assumption was tested by taking out the boundary condition on clamping (therefore only allowing for no translation and making rotations possible), and the effect on the displacements were not noticed. This makes sense as the boundary condition is set on the surface of the small cylinder as seen in Figure 5.20 and not on an edge. Because of the fact that multiple nodes on the circumference of the cylinder and in the vertical direction as well, are fixed, this also prevents rotations from happening. If the boundary condition was set on an edge, then the difference between fixed and clamped one would be more marked. The surface on which the boundary condition is applied on is the whole bottom small cylindrical section where the titanium insert is placed and that can be seen in Figure 5.20:

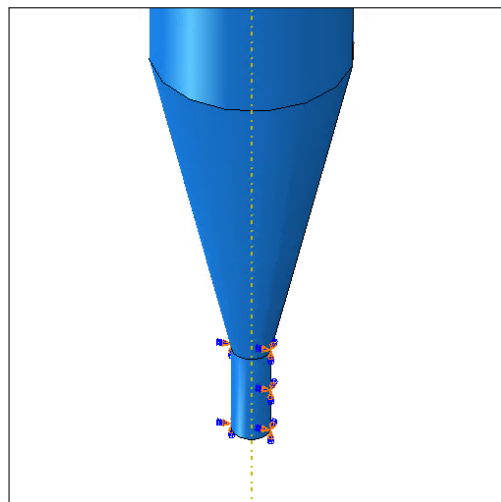


Figure 5.20: Detail of the boundary conditions at the bottom of the Abaqus model.

- The mesh in [27] was done using S8R elements, as Figure 5.21 shows:

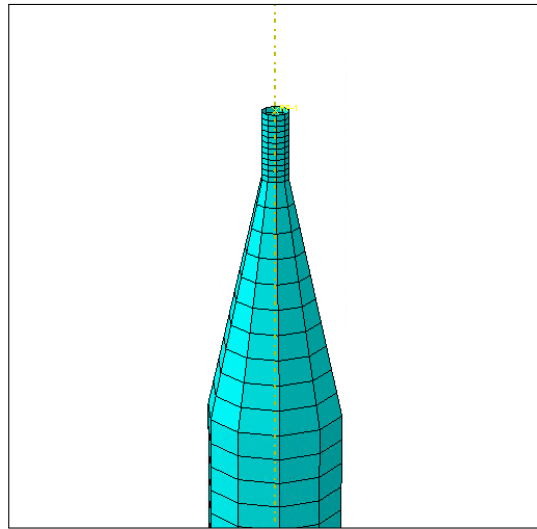


Figure 5.21: Detail of mesh elements at the top of the model.

To summarise the differences in set up between the landing strut model made for this thesis and the one performed by [27] and [19], Table 5.5 is made:

Setup Step on Abaqus	Set Up of Thesis Studies	Mason [27]	Differences?
Geometry	Tapered Cylinder with small ends	Tapered cylinder with small ends	None
Material Properties	Taken from Mason and translated to SI Units	Used as reference	None
Material Assignment	Top and bottom fitting of titanium, Center body of CFRP	Top and bottom fitting of titanium, Center body of CFRP Transition zone in between	No transition zone, in thesis model
Composite Layup	Same as Mason	Used as reference	None
Loads	From 0 to 40000 lbf, then translated to SI Units	Used as reference	None
Boundary Conditions	Clamping of bottom fitting	Unknown from Model	Unknown
Step	First static, then dynamic implicit	Only static	First none, then different
Mesh	First S8R, then S4R	Only S8R Elements	First none, then different

Table 5.5: Table summarising differences in the modelling done by [27] and the one made for this thesis for the verification of landing modelling.

5.3.2. Verification Study Results

As explained in Chapter 4, the type of landing analysis for the thesis is dynamic implicit. This is different from the type of analysis run in [27]. Furthermore, the authors in this article used S8R elements, which are not possible to be used in dynamic analyses on Abaqus due to software limitations. These are two modelling differences between the model in [27] and the landing modelling used for this project (other than the geometry). Because of this, a step by step verification through 3 studies has to be performed. This is done by first running a study on Abaqus that has all inputs in common to those from [27], then moving to 2 studies that change some inputs to those used for the Abaqus Landing Model and explained in chapter 4. Specifically, the 3 studies are:

1. The first study is of the static type with S8R elements. This is done in order to make sure that all of the inputs that are common between the thesis model and the model used by [27] are properly implemented. This includes the material properties, the boundary conditions and mesh size.
2. The second study is also of the static type, but it uses S4R elements, not S8R elements as the original study as found in [27].
3. The last study uses the same geometry and property inputs, but is of the dynamic implicit type and, like the second study, has S4R mesh elements.

The comparison between the data in [27] and the data from the 3 studies listed above is in the form of 4 load-displacement curves (similar to the ones found in Figure 5.18) and is contained in Figure 5.22:

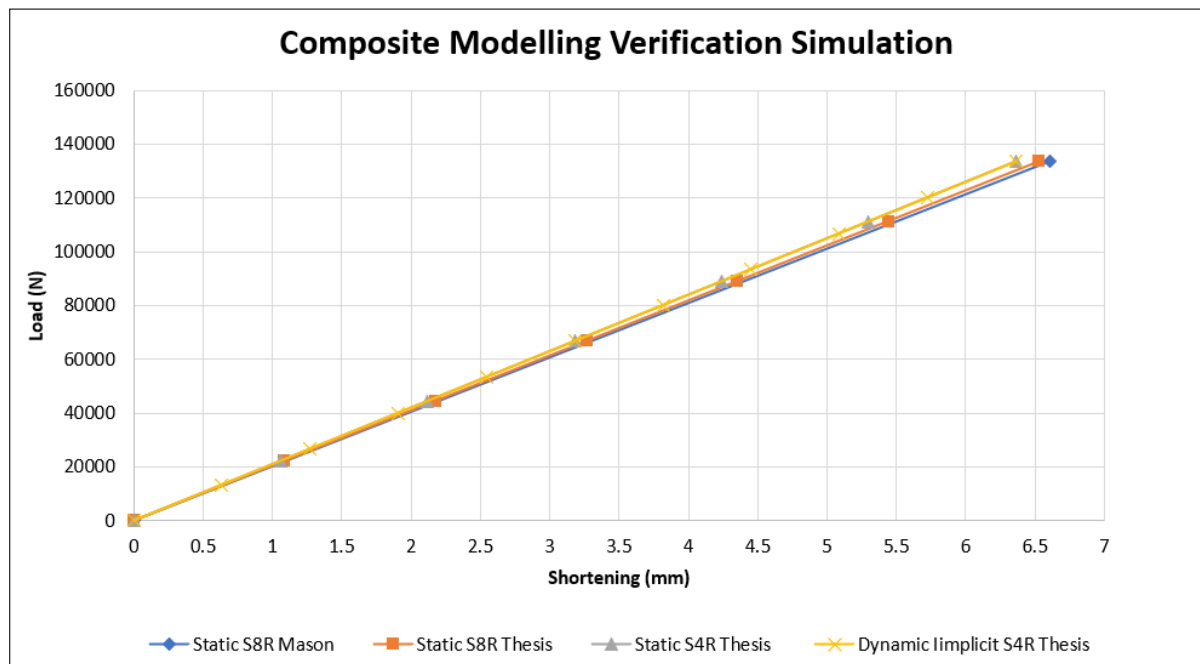


Figure 5.22: Comparison of shortening vs. loading results between Mason [27] and the 3 studies made for this thesis written above.

The data from the 3 static load displacement curves is placed in Table 5.6:

Load (N)	Shortenings (mm)		
	Static S8R Mason	Static S8R Thesis	Static S4R Thesis
0	0	0	0
22241.1	1.101	1.089	1.06
44482.2	2.201	2.177	2.12
66723.3	3.302	3.266	3.18
88964.4	4.402	4.354	4.241
111205.5	5.503	5.443	5.301
133447	6.604	6.532	6.361

Table 5.6: Tabulated data from Figure 5.22.

While the load-displacement data from the Dynamic Implicit verification study is placed in Table 5.7:

Dynamic Implicit S4R Thesis	
Load (N)	Shortening (mm)
0	0
13344.7	0.636071
26689.4	1.27219
40034.1	1.90822
53378.8	2.54436
66723.5	3.18037
80068.2	3.81654
93412.9	4.45252
106757.6	5.0887
120102.3	5.72469
133447	6.36087

Table 5.7: Data from Figure 5.22 of dynamic implicit thesis analysis (separated from the previous table because of more data points available).

As seen in Figure 5.22, the lines related to the S8R model developed for this thesis and that of the article in [27] (blue and orange lines) only slightly diverge, the percentage difference of this diversion can be calculated. Percentage error is calculated, in this section, by comparing the displacement that the strut experiences from [27] at the highest loading scenario (which is equal to 30000 lbf from the paper and translated in 133447 N for Abaqus using SI units) with the same displacement and same loading as found in the Abaqus models for the 3 different studies listed above. As can be seen by looking at Figure 5.18, the strut shortening when loaded with 30000 lbf is of 0.26 inches, which is converted to 6.604 mm. Therefore, the percentage difference between the results found in [27] and those developed in Abaqus with the same inputs is:

$$\epsilon_{diff-Mason-S8R} = 100 * \left(1 - \left(\frac{6.532}{6.604} \right) \right) = 1.09\%$$

The small difference is due to the fact that, in the model of the article, there is a small transition zone where the composite layup and the titanium inserts overlap each others, however in the Abaqus model developed for the verification of the landing modelling of this thesis, this zone is not modelled, as can be seen in Table 5.5.

Moving to the next study, as seen in the same figure above, the displacement vs. load line of the Static S4R elements simulation and that with Static S8R elements from [27] (Grey and Blue lines) diverge slightly. The percentage difference to quantify this diversion is calculated as follows:

$$\epsilon_{diff-Mason-S4R-Static} = 100 * \left(1 - \left(\frac{6.361}{6.604} \right) \right) = 3.68\%$$

And last, as seen in the same figure, the percentage difference between the dynamic S4R analysis and the one performed in the article [27] (Yellow and Blue lines) is calculated as follows:

$$\epsilon_{diff-Mason-S4R-Dynamic} = 100 * \left(1 - \left(\frac{6.36087}{6.604} \right) \right) = 3.68\%$$

Even though the geometry of the landing system used in [27] and the one developed for this thesis are different, the analyses laid out in this section of the thesis prove that there is good correlation between the modelling used with specific mesh element (S4R) and a specific modelling step (dynamic implicit) and the modelling used by NASA engineers to perform structural analysis studies on an interplanetary lander landing system.

From now on, the type of modelling used for this thesis regarding the material modelling, mesh and analysis type, can be considered as reliable because of the fact that results of validated NASA static studies can be replicated through this methodology.

5.4. Conclusion on Verification

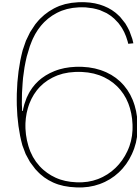
In this chapter, the Matlab Deployment Model, the Matlab landing stability model and the Abaqus landing model were verified. The first one was verified by setting up pendulum dynamic studies in the same way as the paper in [9]. Outputs were qualitatively and quantitatively compared between results gathered for the purpose of this thesis and results gathered by the paper in [9]. It was found that percentage differences between results did not go higher than 4 %. This is a satisfactory value as its value is due to poor quality images where numerical data can be gathered from. This value also means that the implementation of the double pendulum algorithm on Matlab was successfully done. Compounding the possible error with the comparison with the paper with the assumption on the position of the center of mass throughout the leg leads to a percentage difference of 7%, which is also below the required accuracy threshold.

The landing stability model was verified by showing its functioning through sample calculations.

The proper set up of a dynamic implicit analysis on Abaqus was verified by first setting up a static analysis in the same way as that done by NASA engineers and found in [27]. From the comparison between these 2 analyses, it turned out that a small percentage difference of 1% was present. This small number is due to the fact that not all inputs are laid out in the paper in [27] and therefore some of them like material transition zones, had to be eliminated from the model made for the verification purpose of this thesis. From this comparison, the geometry, material inputs, loads and boundary conditions were kept the same, but the mesh type was changed from a quadratic to a linear one (the reason for this being that Abaqus doesn't allow dynamic implicit simulations with quadratic mesh elements), and the type of analysis was changed from static to a dynamic one. This increased the percentage difference between results to 3.6 %, which is still lower than the required 10 % as laid out by accuracy requirements. This low percentage difference means that it is possible to re-create results that NASA engineers produced by using static analyses and a quadratic mesh, by using dynamic implicit analyses and a linear mesh, which are 2 inputs that are used for the structural analyses of the landing system geometry that is performed in chapter 7.

The missing procedure from this chapter is validation. This is because of lack of availability and time in performing experiments on the deployment and landing models. The final saying on the validity of these models would be reached if experiments would be performed, nevertheless, suggestion for future analyses would be to perform validation on the deployment and landing model in the following ways:

- Regarding validation of the deployment model, this can be done by building a test rig where a double pendulum with damping in between leg joints is analysed. The experiments can take the form of multiple deployment experiments where the double pendulum is deployed from different heights and, until an angle is hit, the deployment time is calculated. One thing that can be easily changed of this pendulum is the mass, which can be done by adding weights at the end of the pendulum elements.
- Regarding validation of the landing model, this can be done by making a small model of the landing system, similarly to what was done by [40] or [56]. Experiments involving drop tests from different heights can be performed on the test piece representing the scaled down version of the landing system. In order to measure experimental outputs, accelerometers can be placed inside the test piece in order to measure G forces imparted to the payload section of the lander. Furthermore, strain rosettes can be placed around the landing system in order to translate the deformation measurements into stresses.



Deployment Analyses Results

In this chapter, the results from the deployment analyses are shown. Through these analyses, a high quantity of landing system geometries will be developed, then compared against the requirements that affect the deployability of the landing systems. The requirements are, specifically, maximum deployment time of 45 seconds, soil clearance of at least 200 mm and landing stability at a soil inclination of 15 degrees or higher. In the end, one geometry will be chosen to be used as a design for Computer Aided Design (CAD) and then moved to FEA software Abaqus for the subsequent landing analyses. The objective of this section, especially of the sensitivity analyses, is to find upper and lower values for all of the inputs of the deployment model which, as written in Section 3.1 are:

- Damping of leg joints,
- Cutoff Deployment Angle,
- Length of leg elements,
- Mass of leg elements.

The types of analyses brought forward in this chapter are listed as follows:

- Sensitivity Analyses. These are performed in order to understand how the different inputs affect the outputs of the deployment model. And also they are performed to give a numerical ranges of the values of landing system parameters.
- Detailed Deployment Analyses. Which show in detail the processes happening within the modelling. This is not important when it comes to gathering a deployable design for the Europa Lander Landing System, however it is important in order to show the proper functioning of the deployment modelling tool developed for this thesis. Furthermore, these are used to prove the satisfaction of requirements.

6.1. Deployment Model Sensitivity Analyses

The model has been designed and verified. One of the goals of this study is to understand how different inputs affect outputs since, because of the complicity of the equations of motion laid out in subsection 3.3.1, this cannot be easily done with hand calculations. The following list puts together all the analyses that were brought forward when doing the sensitivity analyses on the Matlab deployment model:

- **Sensitivity analysis #1: Damping vs. deployment time.** Maximum deployment time is one of the requirements set in section 2.1. Knowing how this value can be tweaked by the input of joint damping is beneficial because, if the two quantities are strictly related, it leads to a better choice of damping subsystem that will be done in chapter 8.

- **Sensitivity analysis #2: Cutoff deployment angle vs. deployment time.** Also for this case, deployment time is a requirement set. Knowing the relation between CDA and this leads to a better choice of leg deployment locking mechanism that will be performed in chapter 8.
- **Sensitivity analysis #3: Leg mass vs. deployment time.** Same as in the case of analyses #1 and #2.
- **Sensitivity analysis #4: Leg length vs. deployment time.** Same as in the case of analyses #1, #2 and #3.
- **Sensitivity analysis #5: Footprint vs. landing stability.** Landing stability at different soil inclination angles is a requirement set in section 2.1. Knowing which footprint values can be satisfactory with a set landing stability constraint can help by scrapping some unsatisfactory designs, therefore limiting the designs output by the model.
- **Sensitivity analysis #6: COM height vs. landing stability.** Same as Sensitivity Analysis #5.

6.1.1. Methodology

The way sensitivity analyses are performed in this chapter of the thesis is by varying input parameters of the Matlab parametrised model. These parameters are the ones listed in section 3.1. Through the variation of a single parameter, a landing system geometry is developed. With the development of a landing system geometry, "success maps" are created, these are the type that can be seen in this chapter with Figures like 6.5 and 6.7 and many others. In these maps, scatter plots with different points of different colours and shapes can be seen. At each point corresponds an output landing system geometry. Regarding the different colours and shapes, in the success maps, a blue circle corresponds to a successfully developed landing system geometry, which is a geometry that satisfies design requirements. A red cross corresponds to a developed landing system geometry that does not satisfy design requirements. These design requirements are either too high of a value of deployment time (more than 45 seconds) or an unsuccessful geometry, which is one that has the joint in between leg elements lower than the leg tips or one that has the bottom of the lander too close to the top of the ground. For the landing stability maps, seen, for example, in Figures like 6.19 and 6.22, a third possible shape can be output, which is the red circle, which corresponds to an unstable landing.

6.2. Sensitivity Analysis 1: Damping vs. Deployment Time

In order to keep a consistent comparison between output landing system geometries and to allow for repeatability of results in case a future project would need to use these simulations as starting point. The characteristics that are uploaded to the model are found in Table 6.1:

Property	Value	Unit
CDA	140	Deg
Length of 1st Leg Element	0.5	m
Length of 2nd Leg Element	0.5	m
G Forces	0.14	-
Mass of 1st Leg Element	3.5	kg
Mass of 2nd Leg Element	8	kg
Joint Damping	0.5:0.5:10	Nm/rad/s

Table 6.1: Landing system elements for V1 of Sensitivity analysis 1, done by changing the joint damping.

Resulting in the relation between joint damping and deployment time as seen in Figure 6.1

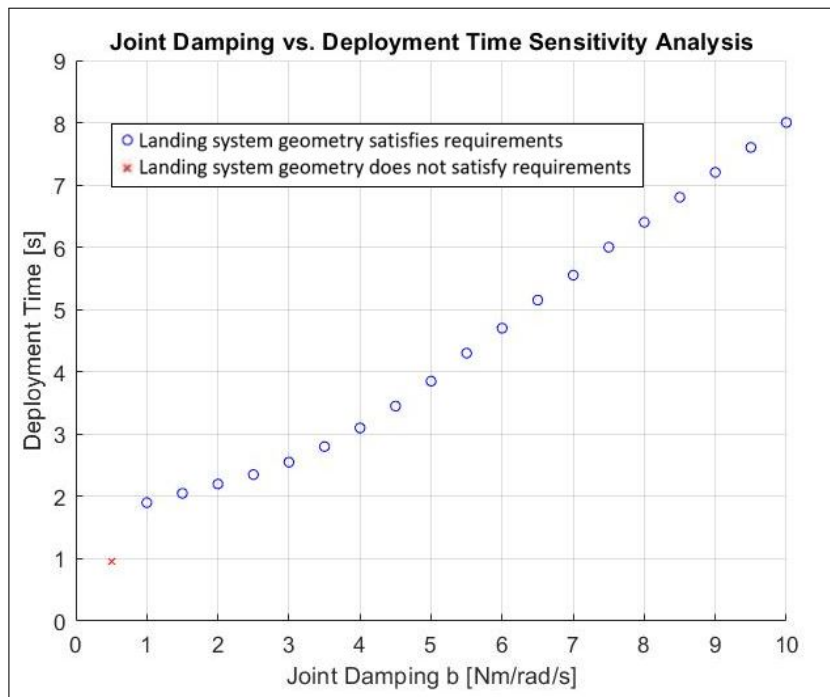


Figure 6.1: Relation between deployment time and damping with changing damping for V1 of Sensitivity analysis #1.

And the resulting output geometries are shown in Figure 6.2:

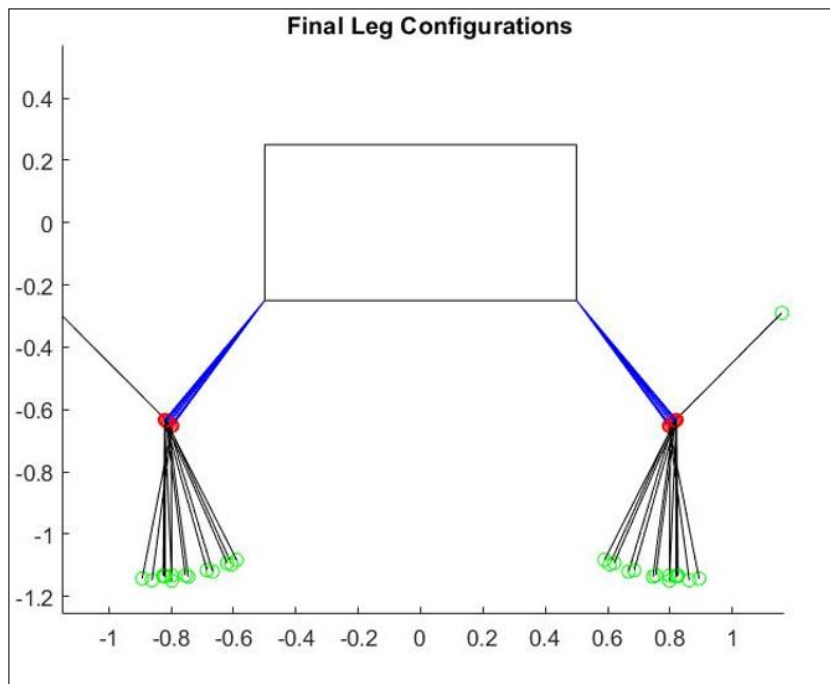


Figure 6.2: Output geometries for V1 of Sensitivity analysis #1.

It can clearly be seen in Figure 6.1 that deployment time increases the higher the joint damping is. Plus the first value of damping leads to an unsuccessful geometry (as seen with the red cross in the bottom left section of the graph). This is unsuccessful because of the fact that the program outputs a geometry where the leg tips of the lower leg elements (visualised with a green dot) are at a higher vertical position than the joints in between leg elements, as is seen with the upward facing leg elements in Figure 6.2. Furthermore, lower leg elements that taper inward, as is the case for most of the output geometries in

Figure 6.2, are not a preferable choice. This is because the rotation that would be imparted on the joints in between leg elements (visualised as red dots in figure like 6.2) when landing happens, would be in the same direction of deployment rotation. It is advised, in fact, that the rotation imparted on these joints when landing is in the opposite direction as that of deployment so that a mechanism can be placed in these joints that allows for rotation in one direction (the direction of deployment) and prevents it in the opposite.

The result of this analysis shows that, at the moment, the low range value of damping in order for the landing system to output a successful geometry is of 1 Nm/rad/s . This value leads to a deployment time of 1 second.

Now increasing the joint damping to even higher values (as seen in the last row of Table 6.2), is tried:

Property	Value	Unit
CDA	140	Deg
Length of 1st Leg Element	0.5	m
Length of 2nd Leg Element	0.5	m
G Forces	0.14	-
Mass of 1st Leg Element	3.5	kg
Mass of 2nd Leg Element	8	kg
Joint Damping	5:5:100	Nm/rad/s

Table 6.2: Landing system elements for V2 of Sensitivity analysis 1, done by changing the joint damping with a higher range than V1.

Which leads to the results shown in Figure 6.3:

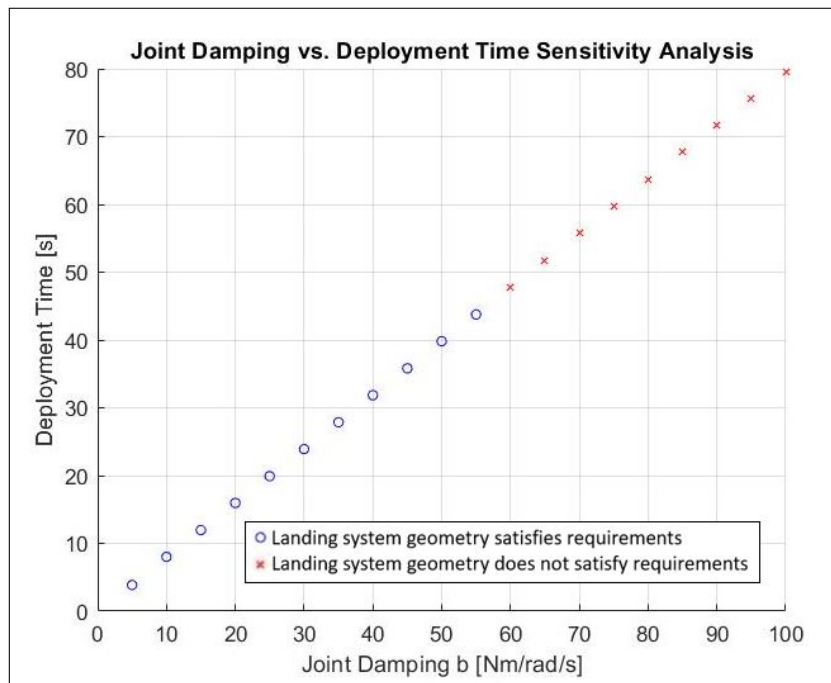


Figure 6.3: Relation between deployment time and damping with changing damping for V2 of Sensitivity analysis #1.

And the outputs of landing system geometries are found in Figure 6.4:

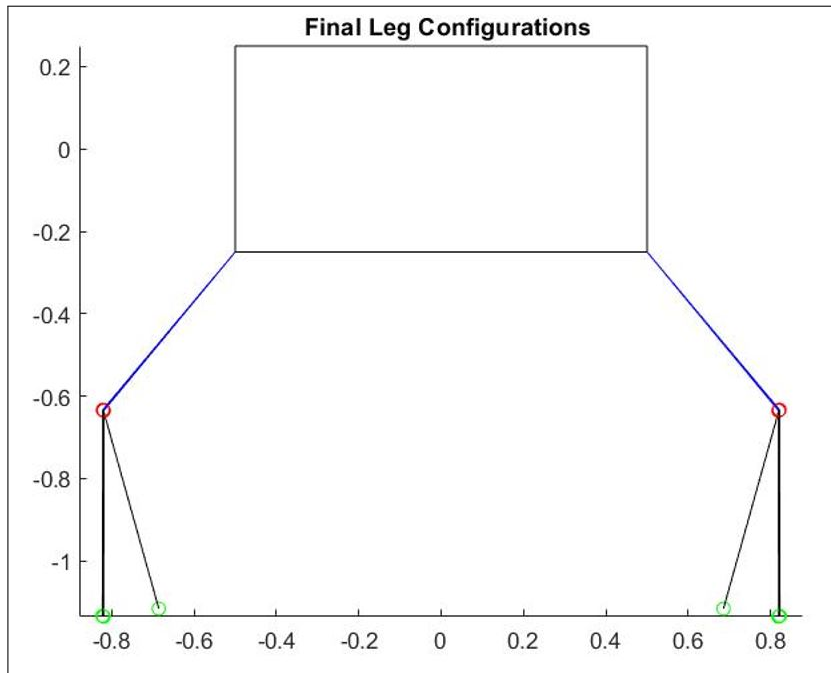


Figure 6.4: Output geometries for V2 of Sensitivity analysis #1.

Figure 6.3 also proves that deployment time and joint damping are directly proportional to each others. Furthermore, it can also be seen by looking at Figure 6.4, that further increasing the joint damping does not change the final geometry of the system. It should also be noted that the last geometries (seen in the top right section of Figure 6.3) appear as red crosses because the deployment time is higher than 45 seconds, which is one of the constraints set at the beginning of the project by the requirements.

Furthermore, from Figure 6.3, it can be inferred that the upper limit for the numerical value of damping that satisfies the maximum deployment time requirement is of 55 *Nm/rad/s*. This value leads to a deployment time 44.2 seconds.

6.3. Sensitivity Analysis 2: Cutoff Deployment Angle vs. Deployment Time

In this sensitivity analysis, the cutoff deployment angle, which is the maximum angle that the legs can make with the lander’s body after which the deployment is stopped, is changed.

Property	Value	Unit
CDA	80:5:170	Deg
Length of 1st Leg Element	0.5	m
Length of 2nd Leg Element	0.5	m
G Forces	0.14	-
Mass of 1st Leg Element	3.5	kg
Mass of 2nd Leg Element	8	kg
Joint Damping	55	Nm/rad/s

Table 6.3: Landing system elements for V1 of Sensitivity analysis 2, done by changing the CDA.

The range seen in the second row of Table 6.3 was chosen because it encloses almost all possible cases with minimal impossible geometries needed. It is shown that the feasible domain was between 90 and 140 degrees. On the low side of this range, an angle of 80 degrees between the first leg element and the vertical side of the simplified lander body would lead to an unsatisfactory geometry due to the fact that it is impossible, at this angle, for the leg tips to touch the ground. The results are as follows:

The result is found in Figure 6.5:

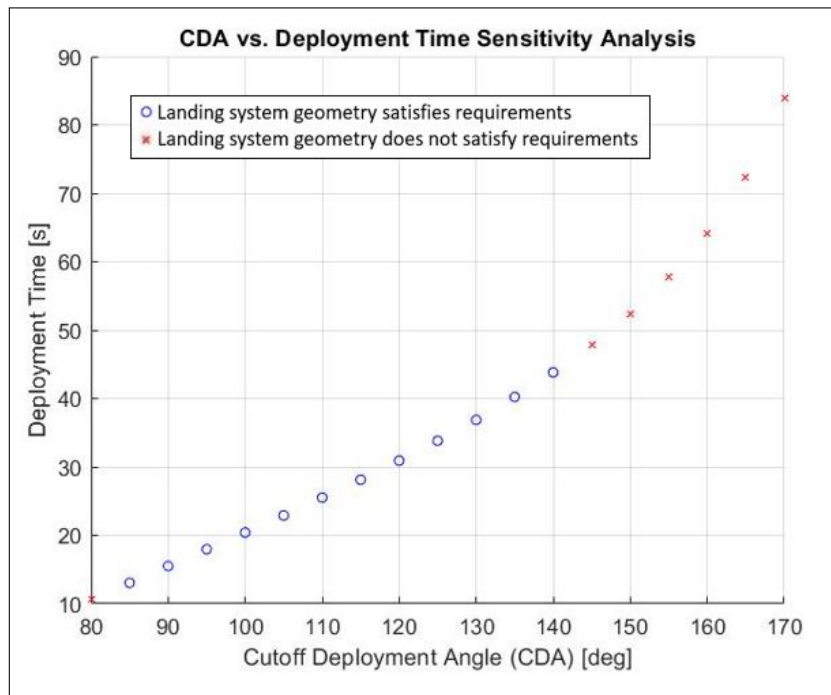


Figure 6.5: Relation between Cutoff deployment angle and deployment time with changing CDA for V1 of Sensitivity analysis # 2.

With the output geometries seen in Figure 6.6:

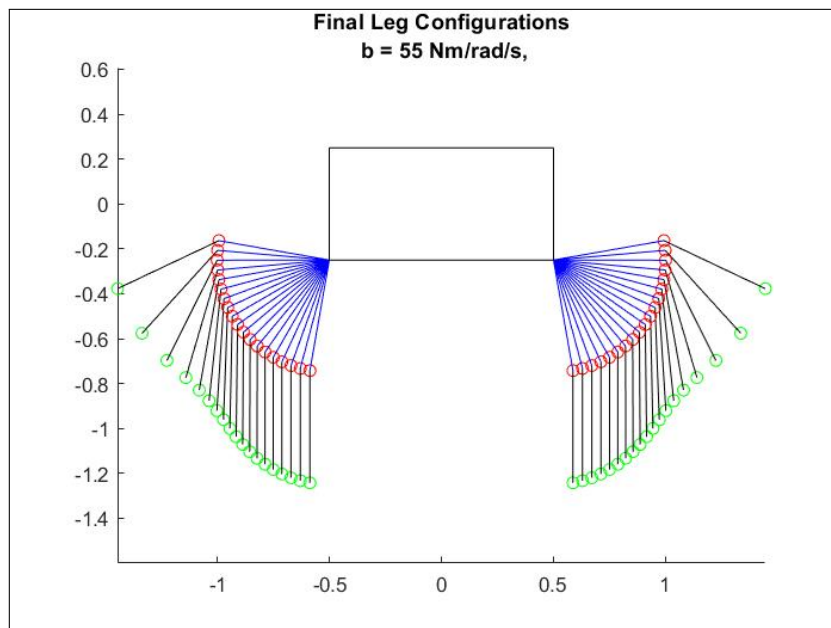


Figure 6.6: Output geometries for V1 of Sensitivity analysis #2.

As can be seen by looking at Figure 6.5, deployment time is directly proportional to cutoff deployment angle. This makes sense as the landing legs have to travel a higher amount of rotational displacement with a higher CDA compared to a lower one.

With the above figure, it can be inferred that the limits on CDA are 85 degrees (corresponding to a

deployment time of 13.8 seconds on the lower side and 140 on the upper one, leading to a deployment time of 44.5 seconds. It can also be seen, by looking at Figure 6.5, that at 80 degrees of CDA, the leg tips are within 200 mm of vertical distance compared to the bottom of the lander body. This means that, even if minimum sinking within the soil a few millimetres happens, requirement LS-DES-002 is not satisfied. Regarding the geometries with higher CDAs, these are not satisfactory because the deployment time is too high.

The following sensitivity analysis includes the effect of changing damping. This is done by changing both the CDA and the damping, as seen in Table 6.4:

Property	Value	Unit
CDA	80:10:170	Deg
Length of 1st Leg Element	0.5	m
Length of 2nd Leg Element	0.5	m
G Forces	0.14	-
Mass of 1st Leg Element	3.5	kg
Mass of 2nd Leg Element	8	kg
Joint Damping	5:5:90	Nm/rad/s

Table 6.4: Landing system elements for V2 of Sensitivity analysis 2, done by changing the damping and CDA.

Of which the results are shown in Figure 6.7 and Figure 6.8:

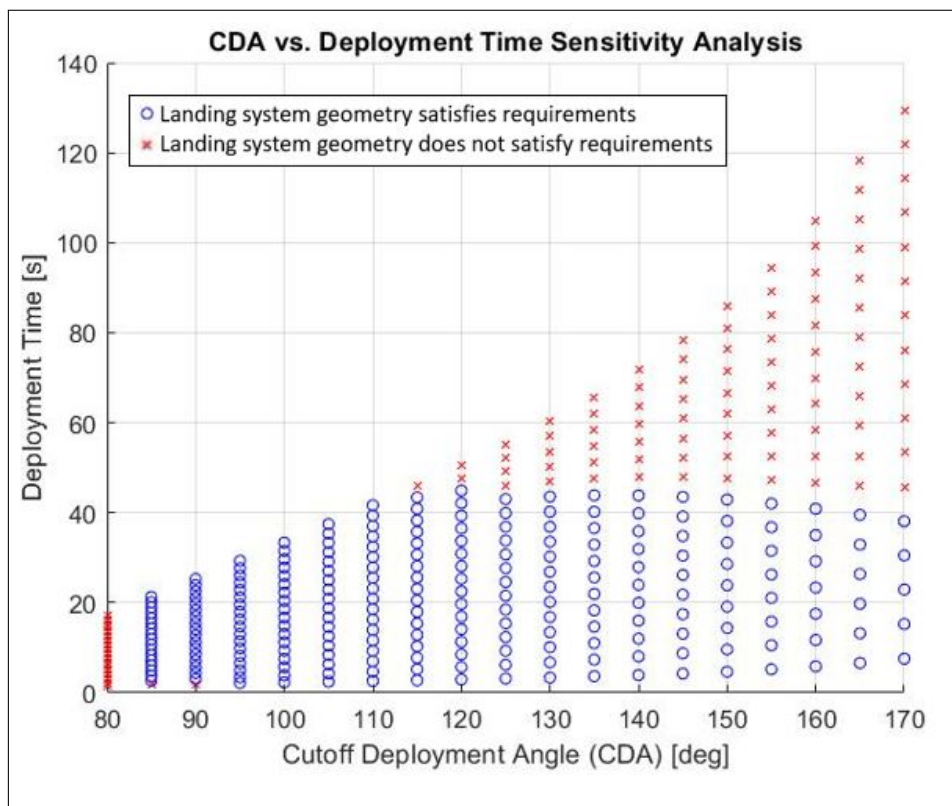


Figure 6.7: Relation between Cutoff deployment angle and deployment time with changing CDA and damping for V2 of Sensitivity analysis #2.

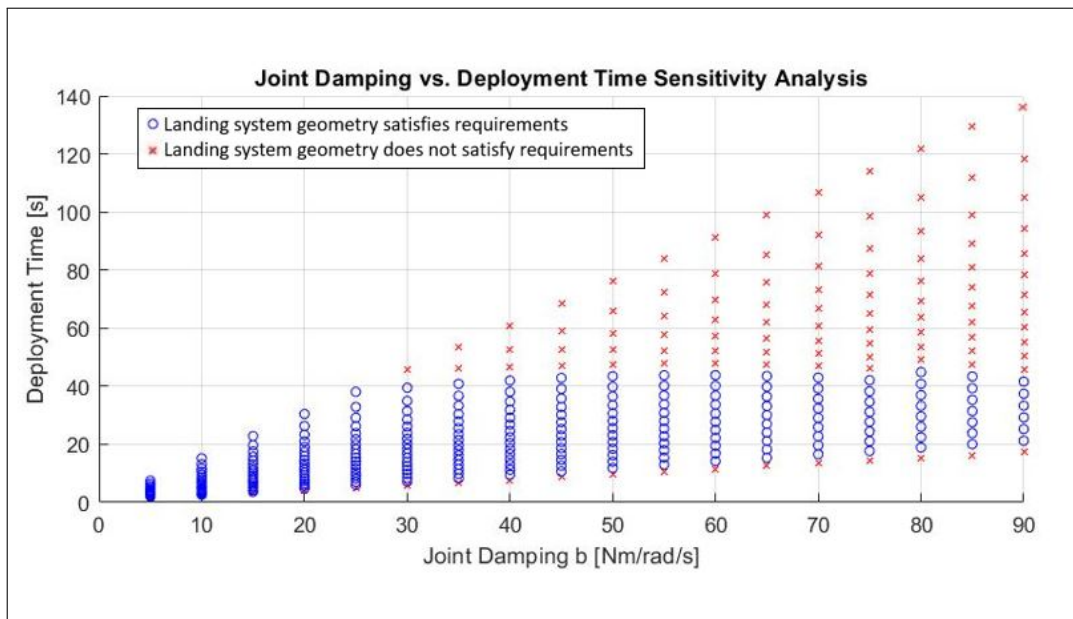


Figure 6.8: Relation between Cutoff deployment angle and deployment time with changing CDA and damping for V2 of Sensitivity analysis #2.

It is not possible to see it in Figure 6.8, but the higher the damping is the more the line that is formed by points seen in Figure 6.8 shifts upwards, therefore increasing the deployment time. As seen in both figures, a higher CDA leads to a higher deployment time, meaning that the point with the highest deployment time is the one in the top right section of the figures, that corresponds to the point where the joint damping and the CDA are also at their maximum values. As it can be seen by looking at Figure 6.7, no geometry that has a CDA of 80 degrees is feasible. This makes sense as, at this angle, the joint in between leg elements is lower than the leg tips. Nevertheless, aside from the lowest 2 damping options, geometries start being acceptable at a CDA of 85 degrees already. On the other side of the graph, top right corner, it can be seen that at high damping and high CDA, the deployment time starts becoming higher than required.

With this figure, it can be seen that all combinations are possible when damping is between 5 and 30 $Nm/rad/s$ and CDA is between 85 and 110. The areas of almost totally possible landing system geometries are found, in Figures 6.7 and 6.8, in the bottom left section of the graphs. Deployment time starts to become an issue at high damping values and also high CDA as well, but some combinations with high damping and low CDA and viceversa, are possible. These can be found in the bottom right sections of the graphs.

No geometry output figure is shown in here because there would be too many landing system 2D geometries in one figure to show them successfully.

6.4. Sensitivity Analysis 3: Leg Mass vs. Deployment Time

In this analysis, different masses of the first and second leg elements are varied to track the change in deployment time.

In order to keep a consistent comparison between output landing system geometries and to allow for repeatability of results, the characteristics found in Table 6.5 are uploaded to the model:

Property	Value	Unit
CDA	140	Deg
Length of 1st Leg Element	0.5	m
Length of 2nd Leg Element	0.5	m
G Forces	0.14	-
Mass of 1st Leg Element	2:0.5:7	kg
Mass of 2nd Leg Element	8	kg
Joint Damping	30	Nm/rad/s

Table 6.5: Landing system elements for V1 of sensitivity analysis 3, done by changing only the mass of the first leg elements.

The value of low mass from the range seen in the fifth row of Tables 6.5 to 6.8 is because it is desired to have a minimum mass for the landing legs. In fact, because the landing performance analysis have not been performed yet, it is likely that if the mass is lowered until near 0 values, the landing leg geometry would not pass strength requirements, which are verified through the landing modelling. By placing a value on minimum mass, a constraint on minimum strength is therefore inherently placed. Maximum mass is placed at 7 because adding this to the 2nd leg element mass of 8 and multiplying by 4 (the number of landing legs) leads to a mass fraction that is higher than the prescribed maximum of 10%.

This results in the relation between deployment time and 1st leg element mass are found in Figure 6.9:

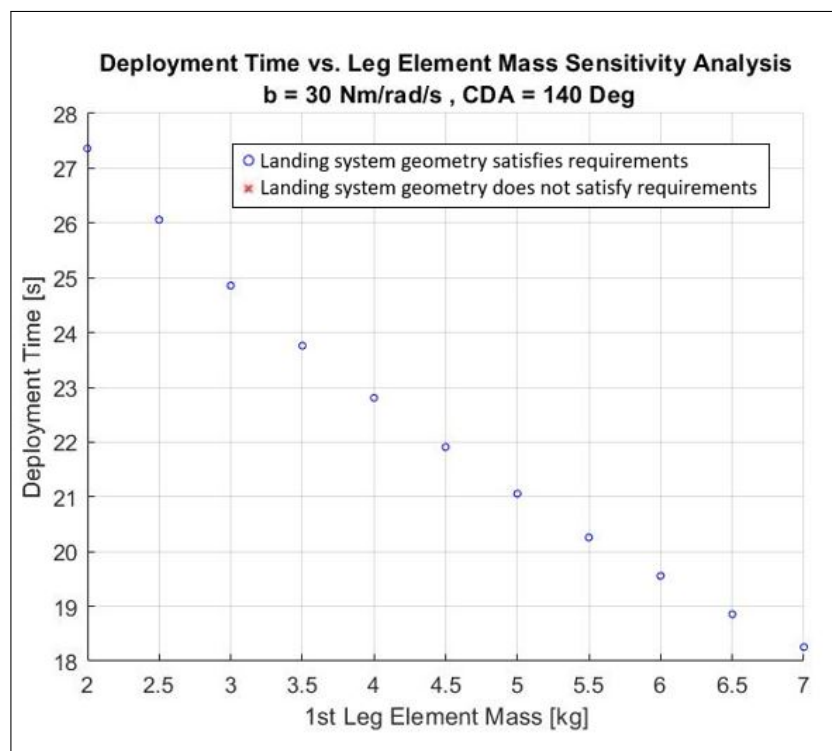


Figure 6.9: Variation of deployment time when mass of first leg element is changed in the V1 of sensitivity analysis 3.

and in the landing leg configurations as found in Figure 6.10:

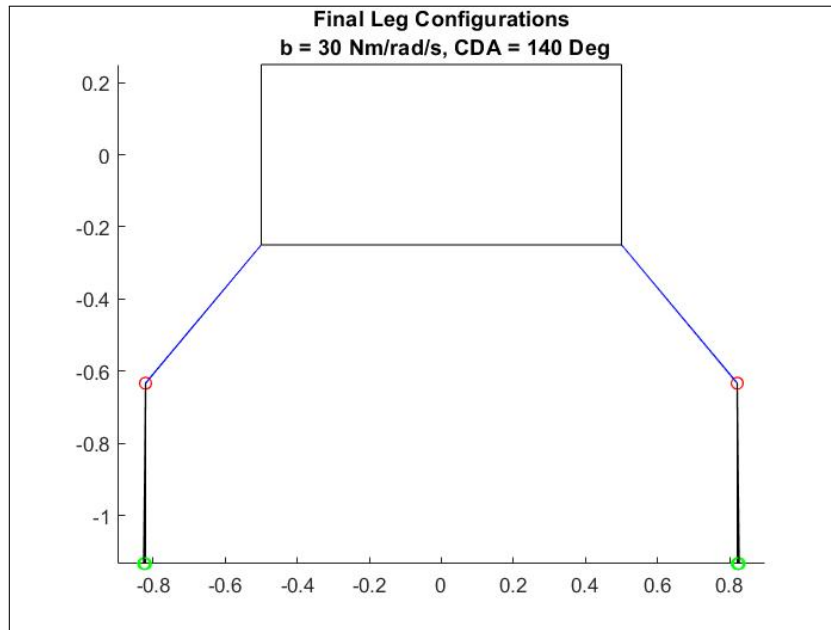


Figure 6.10: Leg configurations output in V1 of sensitivity analysis 3.

By looking at Figure 6.9 it can be seen that the higher the mass of the first leg element is, the lower the deployment time is. Furthermore, as seen in Figure 6.10, the developed geometries, have almost the same configuration (therefore footprint is also the same).

It can be noticed, in this case, that the feasible value for leg element mass for the upper leg element is between 2 and 7 kg, therefore all of the possible numbers.

For the next version of the sensitivity analysis, the mass of the first leg element is kept constant and the one of the second leg element is varied:

Property	Value	Unit
CDA	140	Deg
Length of 1st Leg Element	0.5	m
Length of 2nd Leg Element	0.5	m
G Forces	0.14	-
Mass of 1st Leg Element	3.5	kg
Mass of 2nd Leg Element	6.5:0.5:11	kg
Joint Damping	30	Nm/rad/s

Table 6.6: Landing system elements for V2 of sensitivity analysis 3, done by changing only the mass of the lower leg elements.

Leading to the deployment time/leg element mass relation found in Figure 6.11:

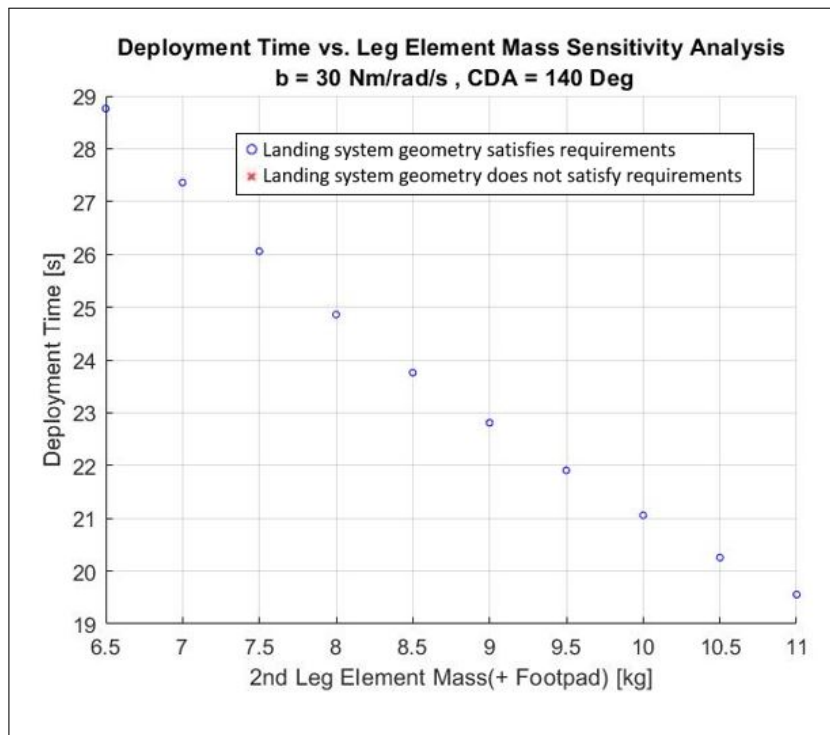


Figure 6.11: Variation of deployment time when mass of second leg element is changed in the V2 of sensitivity analysis 3.

With the following output geometries:

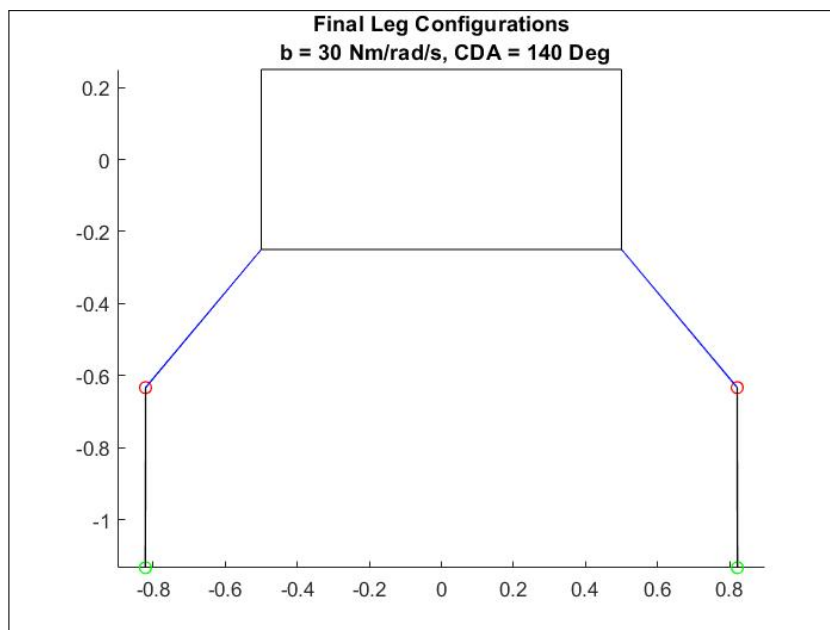


Figure 6.12: Leg configurations output in V2 of sensitivity analysis 3.

Even in this case, similarly to the V1 of this same sensitivity analysis, the higher the leg element mass of the 2nd leg element the lower the deployment time of the landing system is. Here, the masses are higher because the 4.5 kg of mass of the footpad is taken into account.

And finally, the combinations of leg masses are tried by changing both the mass of the first and second leg elements together:

Property	Value	Unit
CDA	90	Degrees
Length of 1st Leg Element	0.5	m
Length of 2nd Leg Element	0.5	m
G Forces	0.14	-
Mass of 1st Leg Element	2:0.5:7	kg
Mass of 2nd Leg Element	6.5:0.5:11	kg
Joint Damping	5	Nm/rad/s

Table 6.7: Landing system elements for V3 of sensitivity analysis 3, done by changing both the mass of the first and second leg elements.

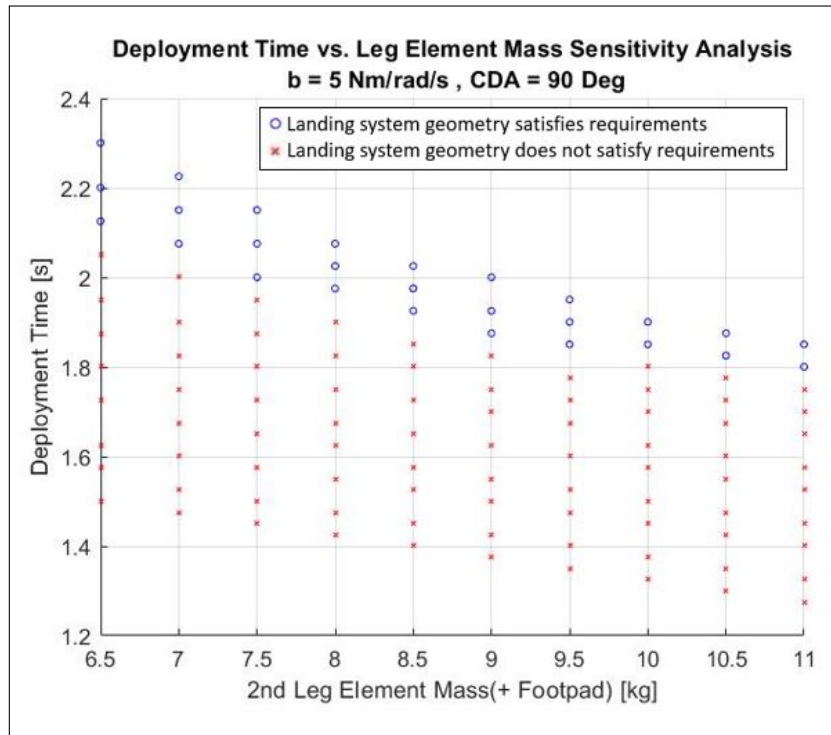


Figure 6.13: Variation of deployment time when masses of both leg elements is changed in the V3 of sensitivity analysis 3.

In Figure 6.13 it can be seen that, if the damping and the CDA are both low, also deployment time gets very low. On top of that, geometries developed by the deployment model start also becoming unsuccessful due to either the requirement on soil clearance or the fact that leg tips are higher than the joint in between leg elements.

Property	Value	Unit
CDA	90	Degrees
Length of 1st Leg Element	0.5	m
Length of 2nd Leg Element	0.5	m
G Forces	0.14	-
Mass of 1st Leg Element	2:0.5:7	kg
Mass of 2nd Leg Element	6.5:0.5:11	kg
Joint Damping	30	Nm/rad/s

Table 6.8: Landing system elements for V4 of sensitivity analysis 3, done by changing both the mass of the first and second leg elements.

Which results in the deployment time vs. leg element mass relation shown in Figure 6.14:

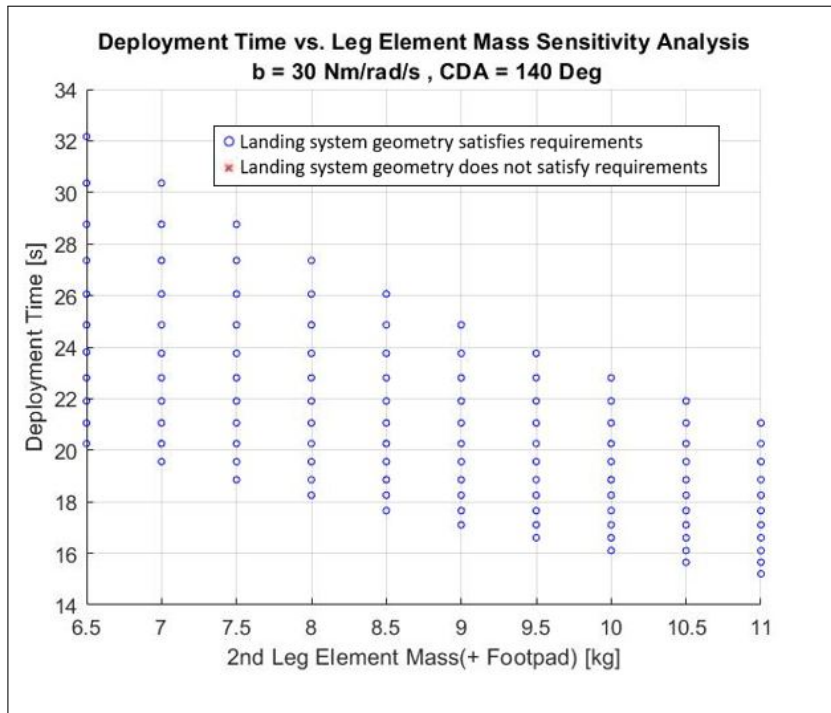


Figure 6.14: Variation of deployment time when masses of both leg elements is changed in the V4 of sensitivity analysis 3.

The higher the mass of the second leg elements, the lower the deployment time. The same can be said when increasing the mass of the 1st leg element. This means that the fastest deploying lander configuration is the one that has the heaviest legs.

With the above 4 sensitivity analyses it can be said that low masses for leg elements don't lead to successful geometries when damping and CDA are low, as seen in Figure 6.13. Then all leg element masses are allowed when the damping is high and CDA is low, as seen in Figure 6.14, same thing for when damping is low and CDA is high. On the other hand, when the damping and CDA are high, high masses are also required to make sure that the deployment time is within the required amount. Now the domain of possible mass values has been lowered to values between 2 and 7 kg. The second leg element mass is always 4.5 kg heavier than the first one because this one includes the footpad mass in it. Because of the fact that a leg element mass of 2 kg (for the first leg element) and one of 6.5 (for the second leg element plus footpad) is always possible (as seen with the top left point in all of the 4 success maps of this section), these are the mass choices for the next analyses.

6.5. Sensitivity Analysis 4: Leg Element Length vs. Deployment Time

In this section of the deployment analyses chapter, leg element lengths are changed and the changes in deployment time are tracked. First it is done with a low CDA:

Property	Value	Unit
CDA	90	Degrees
Length of 1st Leg Element	0.1:0.1:0.8	m
Length of 2nd Leg Element	0.1:0.1:0.8	m
G Forces	0.14	-
Mass of 1st Leg Element	2	kg
Mass of 2nd Leg Element	6.5	kg
Joint Damping	10	Nm/rad/s

Table 6.9: Landing system elements for V1 of sensitivity analysis 4, done by changing both the leg element lengths.

Which results in the following relation between leg length and deployment time:

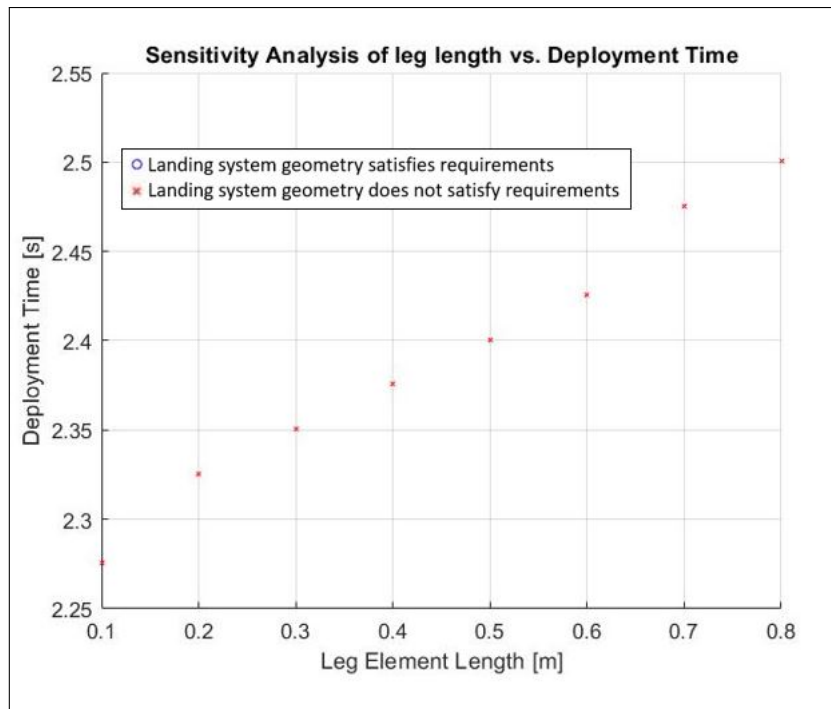


Figure 6.15: Variation of deployment time when leg element lengths are changed in the V1 of sensitivity analysis 4.

And the resulting geometries:

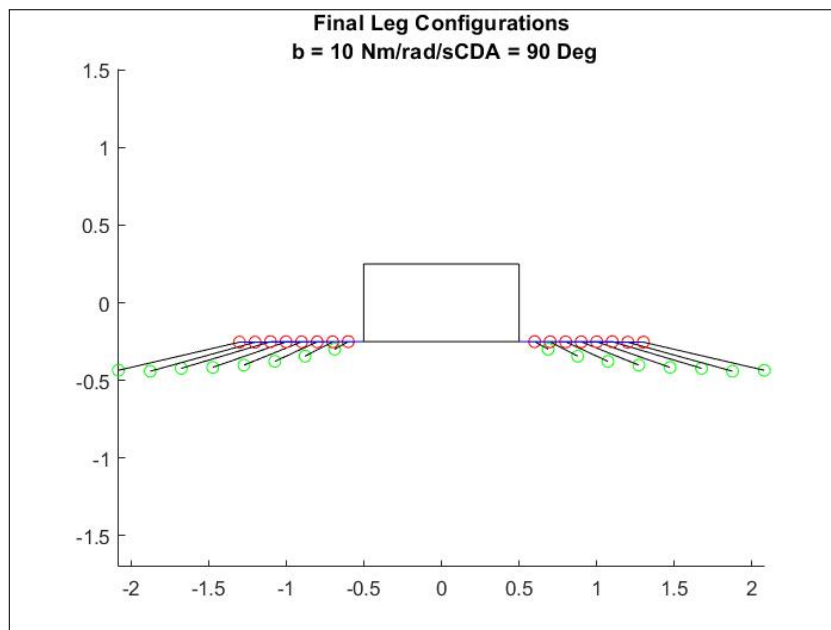


Figure 6.16: Leg configurations output in V1 of sensitivity analysis 4.

By looking at Figure 6.15, it can be said that, at that no geometry is feasible with all calculated leg element lengths. Furthermore, by looking at Figure 6.15, it can be seen that deployment time changes by not much. Specifically, the difference between deployment time with leg elements at 0.1 m and the same quantity with leg element length at 0.8 m is of 10 % when the leg element lengths become 8 times the size of the original.

Because of the fact that no feasible geometry is produced with the analysis shown in Figure 6.15 due to the soil clearance requirement not being fulfilled, now it is tried to slightly increase the CDA:

Property	Value	Unit
CDA	100	Degrees
Length of 1st Leg Element	0.1:0.1:0.8	m
Length of 2nd Leg Element	0.1:0.1:0.8	m
G Forces	0.14	-
Mass of 1st Leg Element	2	kg
Mass of 2nd Leg Element	6.5	kg
Joint Damping	20	Nm/rad/s

Table 6.10: Landing system elements for V2 of sensitivity analysis 4, done by changing both the leg element lengths.

The damping is also increased to 20 *Nm/rad/s* to make sure that the lower leg elements have time to deploy more towards the soil, in order to then raise the lander body with respect to the ground. Therefore leading to the following relation between deployment time and landing leg element lengths:

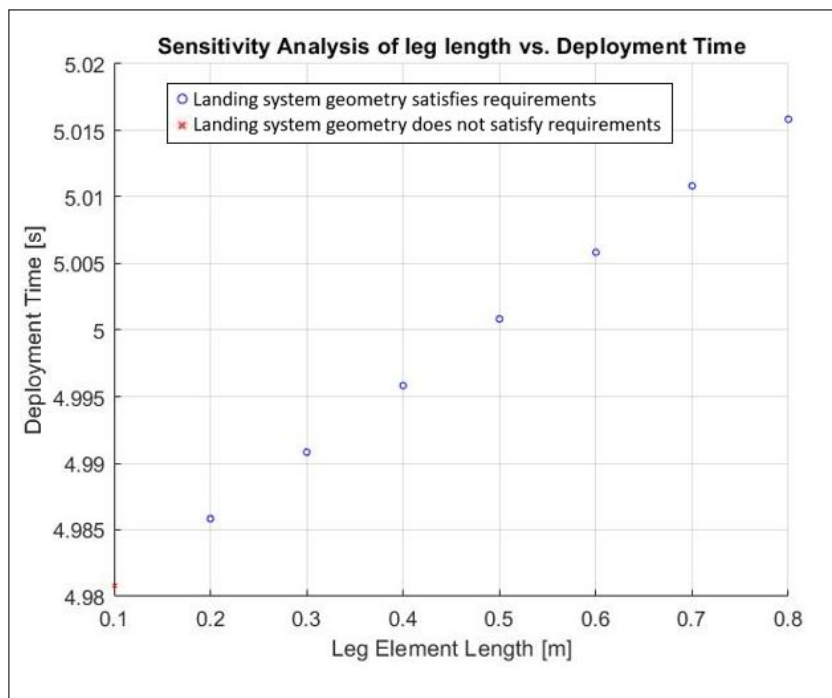


Figure 6.17: Variation of deployment time when leg element lengths are changed in the V1 of sensitivity analysis 4.

Only the first point is a red cross (in the bottom left section of Figure 6.17), this is because at this low leg element length, the geometry doesn't satisfy soil clearance requirements. All the other geometries are acceptable because it takes them less than 45 seconds to deploy and because they satisfy soil clearance requirements. The developed geometries for this sensitivity analysis are shown in Figure 6.18:

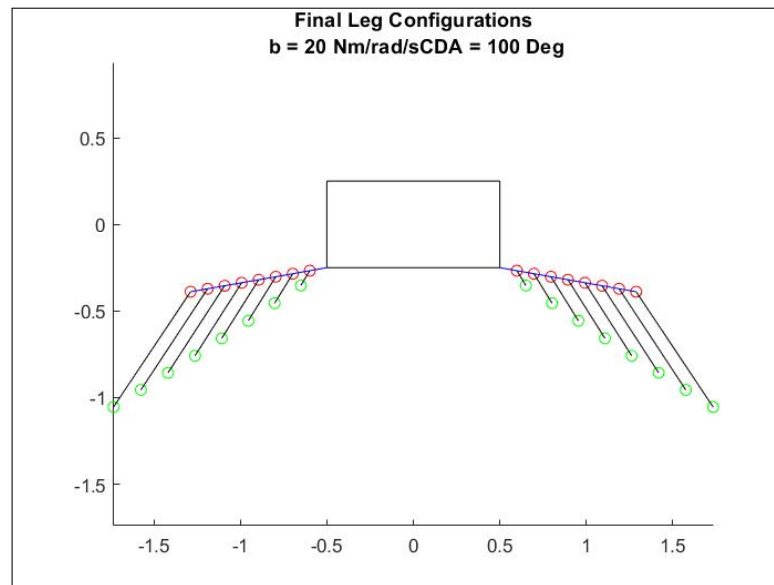


Figure 6.18: Leg configurations output in V2 of sensitivity analysis 4.

Also in this case, as seen in Figure 6.17, deployment time doesn't change by much between shortest leg element length and longest (percentage difference is of 0.5 %). What changes more, when inputting different values of leg element lengths is the footprint, as seen by the large array of different geometries in Figure 6.18. Because of the fact that leg length doesn't change deployment time and it is desired to keep the length of the leg at 0.5 m in order to package the legs as seen in Figure 3.6, for the following analyses the length will be kept at this size. This section shows the desired choice of CDA. It was in fact hypothesised after looking at Figure 6.7 that a suitable CDA would be of 90 degrees. However, looking at Figure 6.17, if the CDA is increased to 100 Degrees, all the geometries are feasible.

The quantity of interest that has been looked at so far is the deployment time, however also the landing stability has a requirement that is potentially limiting the value of footprint and COM height, which will be looked at in the following 2 sensitivity analyses.

6.6. Sensitivity Analysis 5: Footprint vs. Landing Stability

Landing stability is modelled, in this thesis, as the capability of the spacecraft of not toppling down in an inclined hill. The aim of this analyses is to find a relation that gives a maximum allowable value footprint with respect to the required landing stability at 15 degrees.

Footprint is changed, in this analysis, by varying the value of CDA:

Property	Value	Unit
CDA	90:10:170	Degrees
Length of 1st Leg Element	0.5	m
Length of 2nd Leg Element	0.5	m
G Forces	0.14	-
Mass of 1st Leg Element	2	kg
Mass of 2nd Leg Element	6.5	kg
Joint Damping	20	Nm/rad/s

Table 6.11: Landing system elements for V1 of Sensitivity analysis 5, done by changing the CDA.

Which leads to the results as seen in Figures 6.19 and 6.20 :

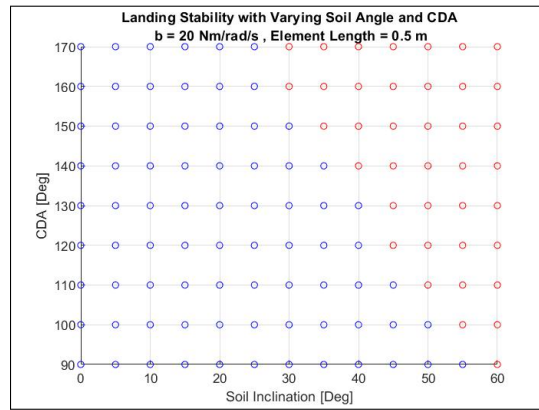
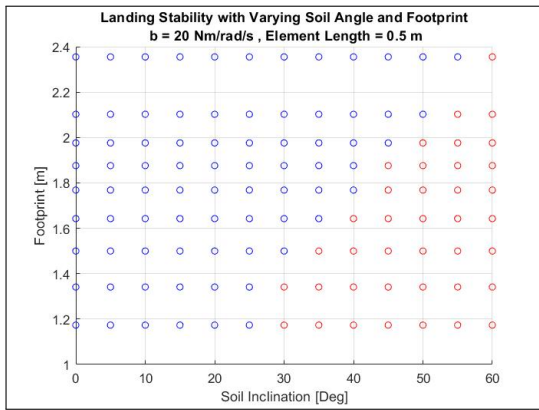


Figure 6.19: Stability plot of lander at different soil inclinations and footprint values. Figure 6.20: Stability plot of lander at different soil inclinations and CDA values.

The 2 figures above, showcase a high change in landing stability when some of the parameters of the landing system change. It should be noted that 3 different outcomes are present in the stability plots. A red cross signifies a landing system geometry that does not satisfy requirements, however this is not present in Figures 6.19 and 6.20. A red dot symbolises a landing system geometry that passes all requirements coded into the Matlab deployment model, but that doesn't lead to a stable landing. A blue dot symbolises a successful landing system geometry that also leads to a stable landing. It is clear by looking at Figure 6.19 that a smaller footprint leads to a less stable landing. Because a higher CDA leads to a smaller footprint, then it can be inferred that a higher CDA also leads to less stable landing. Nevertheless, all of the output geometries seen in Figure 6.21 fulfil requirements as they are all stable below and including 15 degrees of soil inclinations. The two charts in question show landing stability until 60 degrees, this is 4 times higher than required, however the fact that landing stability is shown in these graphs until here is not a performance parameter of value for the landing system. What is important is that the landing system is stable below at soil inclinations of 15 degrees or lower. The array of developed geometries for this study are presented in Figure 6.21:

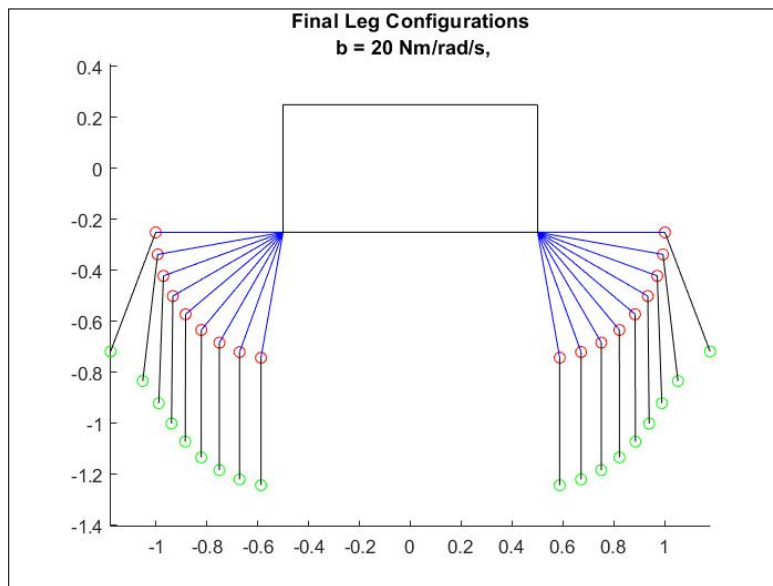


Figure 6.21: Output geometries for V1 of sensitivity analysis 5.

6.7. Sensitivity Analysis 6: COM Height vs. Landing Stability

Also in this sensitivity analysis, the height of the lander's COM is changed by changing the input for CDA:

Property	Value	Unit
CDA	90:10:170	Degrees
Length of 1st Leg Element	0.5	m
Length of 2nd Leg Element	0.5	m
G Forces	0.14	-
Mass of 1st Leg Element	2	kg
Mass of 2nd Leg Element	6.5	kg
Joint Damping	20	Nm/rad/s

Table 6.12: Landing system elements for V1 of Sensitivity analysis 6, done by changing the CDA.

The relation between COM height and landing stability is as follows:

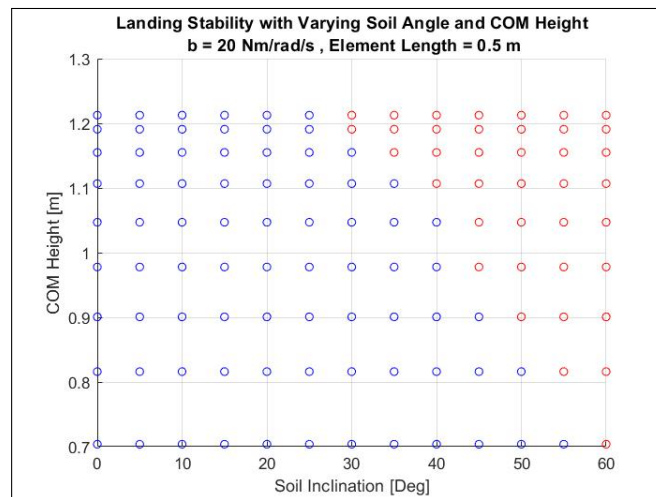


Figure 6.22: Variation of landing stability when COM height is changed in the V1 of sensitivity analysis 6.

And the developed landing system geometries are found in Figure 6.21.

By looking at Figure 6.22 that, as the height of the center of mass is increase, the landing stability decreases. This is noticeable because the red circles, representing non stable landings, become higher in number at lower soil angles (x-axis) the higher the center of mass is.

6.8. Conclusions Drawn from Sensitivity Analyses

These sensitivity analyses have made it possible to understand the deployment trends. Deployment trends help with the design by making it possible to understand how an input affects an output. These deployment trends are as follows:

- Damping and cutoff deployment angle increase the deployment time of the landing legs.
- Changing the landing leg masses doesn't change much the footprint or the center of mass height because it doesn't change much of the geometry in general. However, increase the leg mass decreases the deployment time.
- As expected, changing leg element length greatly affects the footprint size and the height of the lander's COM. However, focus has to be kept on the fact that the legs don't taper inwards and so damping can be changed to make sure that the second leg element doesn't displace further than the perpendicular direction before the first leg element locks itself into the desired position dictated by the CDA.
- COM height greatly affects landing stability. Similarly to what was seen with the footprint size in the first set of sensitivity analyses.

6.8.1. Choice of Landing System Parameters Based on Sensitivity Analyses

It was thought, before running the sensitivity analyses, that they would clearly lead to precise values of landing system characteristics. However this was not the case, the beneficial aspect of the deployment sensitivity analyses is that they pointed out at the trends that are present between inputs and outputs and the fact that they pointed out to ranges of possible numerical values that can be reached by the deployment inputs. These ranges are:

Property	Range [Min-Max]	Unit
Damping	5-30	Nm/rad/s
CDA	100-110	Deg
Leg Element Length	0.2-0.8	m
Leg Element Mass	2-4	kg

Table 6.13: Feasible ranges for deployable landing system elements.

The ranges can be made even smaller if more requirements are introduced, for example an horizontal landing velocity requirement. The geometry to be moved to the next stage within the process of this thesis, has the following landing system characteristics, chosen in between the ranges laid out in Table 6.13:

- Damping is at 20 *Nm/rad/s*. This is because it was found that the acceptable range of damping was between 5 and 30 *Nm/rad/s*. Furthermore, looking at the available rotary dampers in [21], a value of 20 *Nm/rad/s* is feasible for a damper the same size of the diameter of the joint in between legs, which is of 80 mm of diameter.
- CDA is at 100 Degrees. As explained in Section 6.5, this leads to a slightly higher capsule and therefore to soil clearance requirements being satisfied. A higher value of CDA would also be accepted, however this is chosen as a value for CDA to move to the rest of the analyses.
- Leg length is at 500 mm for each leg element. This is still feasible as a length with the hypothesised initial value of 500 still leads to a deployment that is within the required maximum time. Furthermore, as seen in Figure 6.20, this also leads to a satisfactory landing stability.
- Leg element mass is at 2 kg for each leg element. Knowing that the leg element mass is at 2 kg, length is at 0.5 metres and outer diameter is at 80 mm, assuming the section of the landing system is a tube, inner and outer radii can be produced:

$$2 = 2810 * A * 0.5 \rightarrow A = 1423.5 \text{ mm}^2$$

Which is the value of cross sectional area to reach a 2 kg mass for a 0.5 metre long tubular pipe. The chosen inner and radius is:

$$R_{Inner} = 33 \text{ mm}$$

These landing system parameters are checked in the next section in order to prove the fulfilment of the requirements on maximum deployment time and landing stability. If they satisfy requirements, then the project will move to landing analyses.

6.9. Detailed Deployment Analyses

This section is used to showcase more in details the capabilities of the deployment tool and to show requirements acceptance for the recently developed landing system geometry.

Table 6.14 shows the landing system characteristics needed to reach the desired geometry:

Property	Value	Unit
Cutoff Deployment Angle	100	Deg
Length of 1st Leg Element	0.5	m
Length of 2nd Leg Element	0.5	m
G forces	0.14	-
Mass of 1st Leg Element	2	kg
Mass of 2nd Leg Element	6.5	kg
Damping	20	Nm/rad/s

Table 6.14: Landing system elements for the aluminum design of the landing system.

In order to prove the fulfilment of requirement MDL-DEP-001, the first 2 timesteps of deployment will be shown in Figures 6.23 and 6.24:

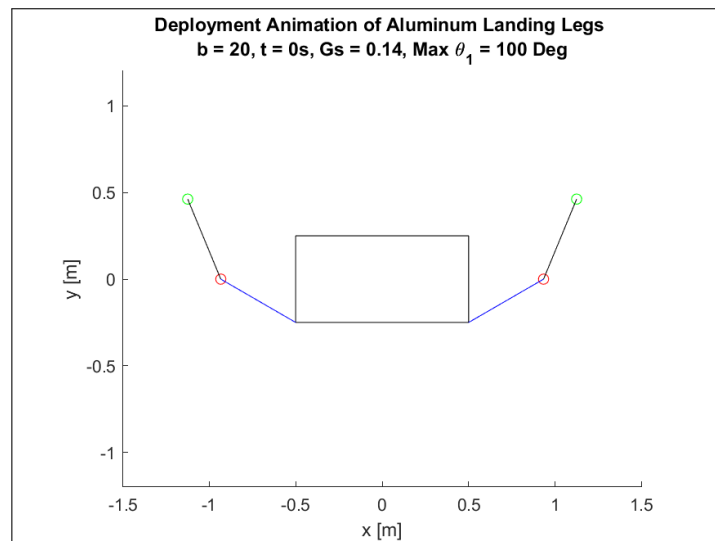


Figure 6.23: 1st timestep of deployment of aluminum landing leg.

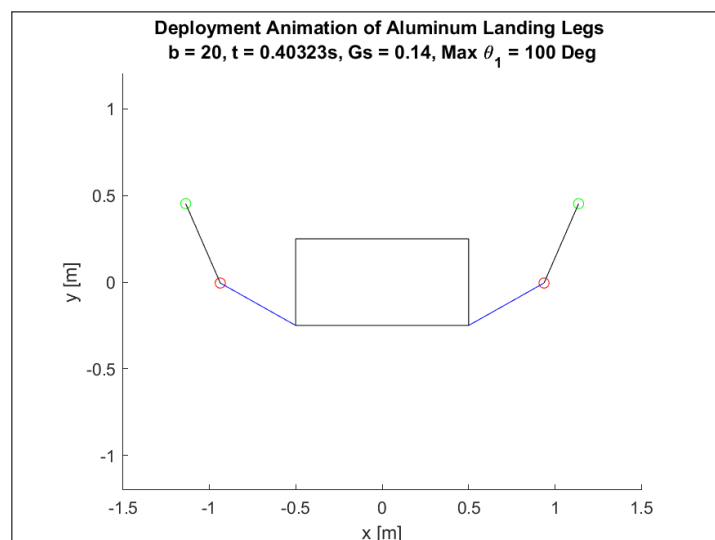


Figure 6.24: 2nd timestep of deployment of aluminum landing leg.

It can be seen that the first 2 timesteps show the dynamics of the deployment of the landing system at 0 seconds and at around 0.4 seconds. Although it should be noted that at this point within deployment

the angular rate of both elements is low, so the changes between the first two timesteps is barely noticeable. The last 2 timesteps are shown in Figures

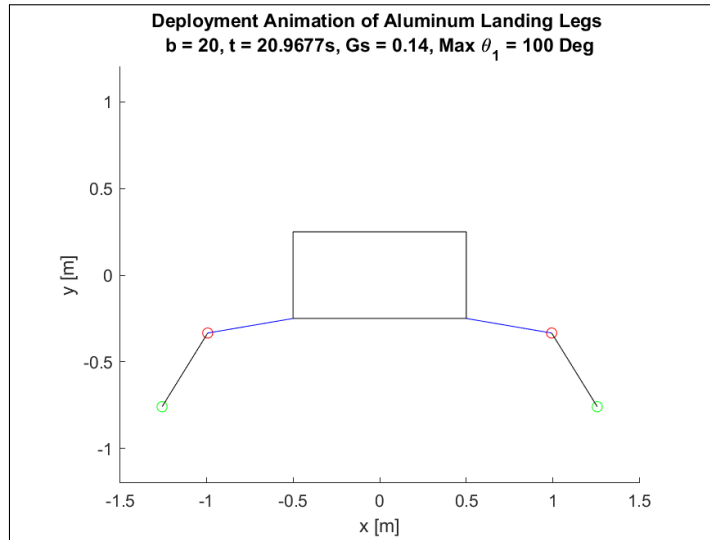


Figure 6.25: Second to last timestep of deployment of aluminum landing leg.

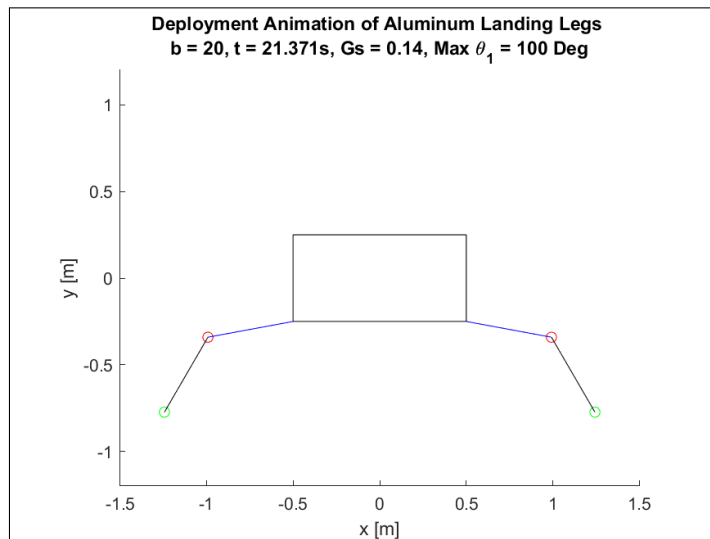


Figure 6.26: Last timestep of deployment modelling of aluminum landing leg.

The developed landing system geometry seen in Figure 6.26 leads to the following coordinates (taking as origin the centroid of the payload rectangle) for the landing leg geometric design:

$$[x_{1-1} \ x_{1-2} \ y_{1-1} \ y_{1-2}] = [-0.992 \ -1.246 \ -0.339 \ -0.770]$$

The aluminum landing system has a deployment time of $t_{dep} = 21.37 \text{ s}$. Therefore satisfying the requirement on deployment time.

The CFRP landing system, as seen in the deployment analyses in the second half of section A.2, has a deployment time of 42.57 s. Therefore also satisfying the requirement on deployment time.

This landing system leads to a stable landing until 55 degrees, as seen in Figure 6.27. 55 degrees is higher than 15 degrees, therefore the landing system is stable at any angle below this value, therefore satisfying the 15 degrees of soil inclination required for a stable landing on Europa.

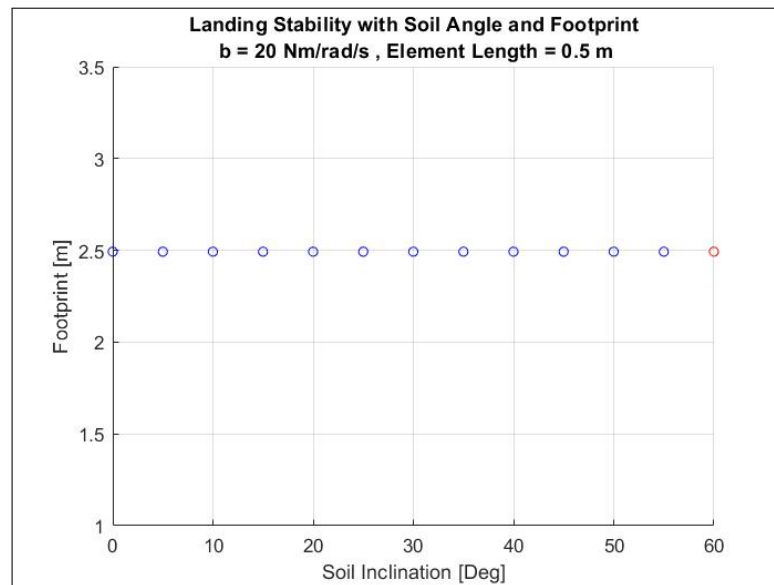


Figure 6.27: Landing stability at different soil inclination angles for developed geometry.

6.10. Conclusion and Limitations on Deployment Analyses

In this chapter, sensitivity analyses have been performed in order to understand the relation that there is between some inputs of the Matlab pendulum deployment model like, for example, length and mass of the leg elements, and some outputs of the same model, like the deployment time or the landing stability. Furthermore, from these analyses, ranges of values for the landing system elements have been found to then come up with a geometry of the landing system. In the following chapter, it will be seen, that the coordinates output by the model will be used to actually design on CAD a landing system geometry to be placed in FEA software Abaqus. In the chapter of which this is the conclusion, the capabilities of the deployment modelling tool to track the deployment dynamics of a self deploying landing system have also been proven. These capabilities show fulfilment of requirements that dictate the design of the tool as laid out in chapter 2. Furthermore, in Section 6.9, a geometry to be used for landing analysis is produced.

The deployment model is successful at showing the deployment dynamics of the deploying landing system, partially shown by Figures from 6.23 to 6.24. This makes it useful because then an indication of deployment time can be given. Furthermore, the deployment model is successful because it can output a large number of landing system geometries, which would give a designer an indication of the trends that are present in between the deployment inputs and outputs.

However one limitation that this approach to modelling has is the fact that it is not able to reach to precise value for each of the deployment inputs. Nevertheless, ranges for feasible values for each of the deployment inputs were reached and, from those, values for these characteristics were chosen and the requirements acceptance was also checked.

Another limitation that the deployment algorithm has is that, being based on penduli, the landing legs have to face outwards, as written in section 3.2. This is seen in, for example, in Figure 3.5. Therefore, with the landing system modelled in this thesis, the configuration found in Figure 3.6 cannot be reached. If an algorithm is developed where the landing legs, even if they face inward, but their center of mass' projection of the legs is still outside of the lander's body, this would mean that the landing legs can be packed in an even more efficient configuration inside the coasting module and, in turn, inside the launch vehicle. An example of inward facing legs with the COM of the left, right legs and the 2nd leg elements is provided in Figure 6.28:

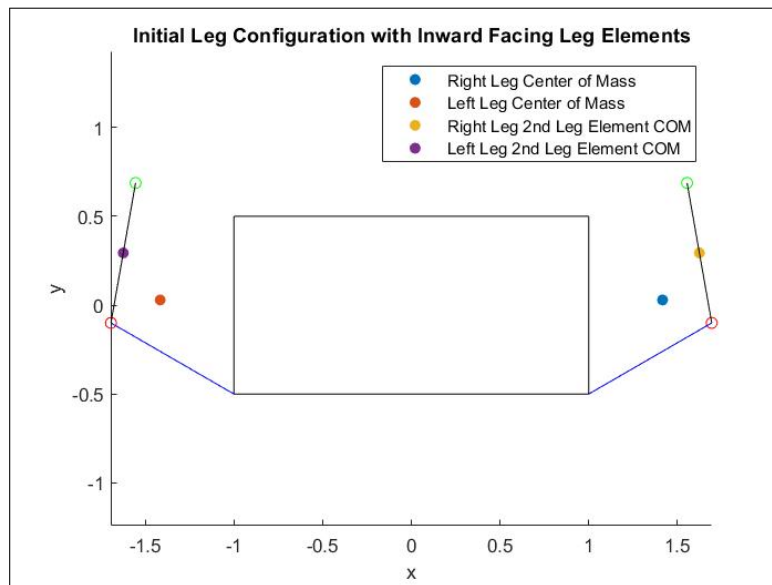


Figure 6.28: Initial leg configuration with inward facing legs.

Therefore, a further development in deployment modelling of the landing system can be in the form of an algorithm that uses rotational springs at the 2 joints for each leg (the first one between first leg element and payload rectangle, the second one between leg elements) to give an initial "push" to the landing legs. This "push" would move the landing legs from a stowed configuration to one that follows a pendulum like deployment as the ones that have been modelled in this chapter of the thesis. The advantage of having springs that push the landing legs outward is that the landing system can be stowed in an more packed an efficient way, like the one shown in Figure 3.6. With the springs, the first few seconds of deployment would be dictated by the springs pushing outward and then, when the 2nd leg elementCOM projection sits further outside (in the horizontal direction) from the position of the leg joint in between leg elements, the deployment would, at that point, be dictated by the pendulum like deployment dynamics.

7

Landing Analyses Results

In the following section, the results of the landing modelling explained in chapter 4 are laid out. The purpose of this chapter is to help making the design decision of whether going for aluminum or CFRP leg elements. If it is seen that the landing stresses don't exceed the UTS of the material with a safety factor of 1.4 or higher, then they will either be considered as reliable. Also, if it will be seen that the CFRP landing legs don't exceed the prescribed maximum value of strain of 5000 microstrains, then they will also be considered as reliable. Furthermore, the purpose of this chapter is also to verify the requirement related to maximum g forces imparted to the lander body. Success, regarding imparted g forces, means that the lander body COG does not experience G forces higher than 10 Earth gs in the vertical direction.

7.1. Types of Analyses

The list of analyses that will be done on the landing model is given as follows:

- Mesh convergence analysis to make sure that the number of mesh elements is not too low (or too high),
- Detailed time dependant landing analysis to see the phenomena happening within the landing leg in the seconds (or fractions) before, during and after landing. This is important to show that, at no point throughout the landing of the lander, the stresses and strains inside the landing legs do not exceed the UTS of the metallic material or the maximum allowable strains in the composite one.

An analysis that is not looked at one where the geometry of the landing system is changed (for example by changing the length or the thickness of the aluminum tube) and the changes in structural performance are then checked. It is expected nevertheless to see higher stresses when the wall thickness is reduced.

Furthermore, another analysis that is left for future work is one with all the 4 landing legs landing at the same time. This nominal case is not looked at in this thesis because of the fact that a landing with a single leg leads to higher values of stresses, therefore to a more conservative design.

7.2. Geometry

The geometry for the landing system is moved from the coordinates of the points of the landing system geometry that are output as part of the Matlab model and are found in Subsection 6.9 to CAD software SolidWorks, the result is shown in Figure 7.1:

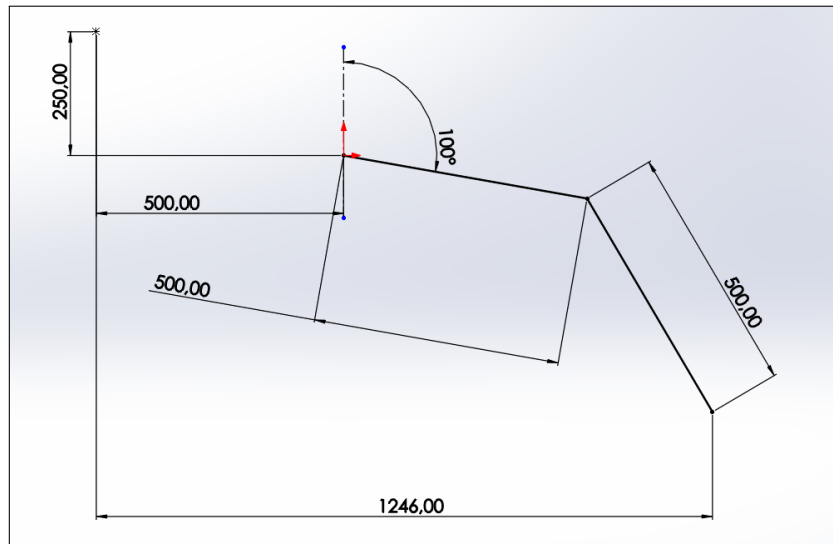


Figure 7.1: Geometry of landing system as developed by Matlab at the end of chapter 6 as a sketch.

And the resulting 3-dimensional shell geometry is shown in Figure 7.2



Figure 7.2: 3D Geometry of landing system.

The geometry is sketched as a shell geometry. Values of internal and outer diameters are input when modelling cross section properties in Abaqus. This is done because the cross section values are different between the aluminum leg and the CFRP. The first one, in fact, has a higher wall thickness than the latter.

7.3. Mesh Convergence Analysis

When working with FEA software, the validity of the mesh used has to be investigated. This is done by looking at the same result at the same location throughout the design and, because of the fact that this type of analysis is a dynamic one, at the same timestep. To do this, static simulations, where a 100 N force that pulls down the top of the leg, while the footpad is clamped, are performed. These simulations are not representing a result useful for the answer to the research question of this thesis, they are done in order to verify the quality of the mesh. The mesh convergence result is shown Figure 7.3:

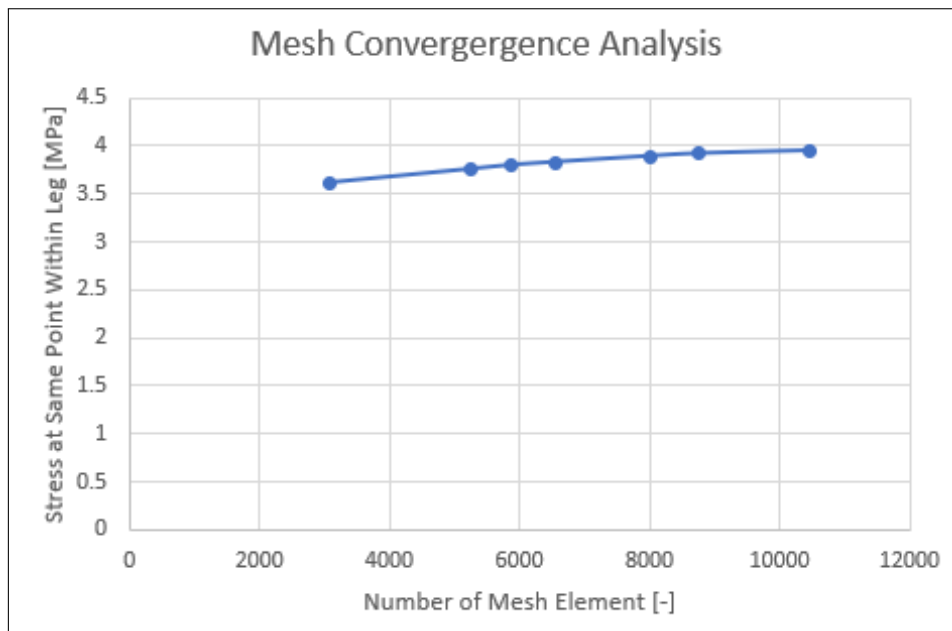


Figure 7.3: Mesh convergence analysis.

The change in quantity of interest between the first and second refinement is around 4 %. This is noticeable because the first line connecting the points with number of elements at 3067 and 5260. After the first refinement, all changes are within 1 % compared to the previous refinement's quantity of interest. Furthermore, after the 8000 elements mesh configuration is hit, the quantity of interest for this mesh convergence study starts plateauing. Therefore, a mesh size of 32, which corresponds to exactly 8002 elements in the model is chosen.

7.4. Detailed Landing Analyses

In this section of the report, the process of landing of a single landing leg, with initial velocity of 5 m/s and with a payload of 575 kg minus the mass of a single landing leg is analysed by looking at the below 2 performance indicators and by looking at the highlights of landing through the Abaqus Visualisation window.

The results are classified in terms of:

- Maximum stress for metal structures and strain for composite ones reached by the landing leg at the different moments throughout the landing. The reason for this is because it needs to be checked that the layup doesn't experience a value of strain that is higher than required. The same is to be said about metallic structures, but with regards to the stress and not the strain. If the stress in the legs is higher than the UTS, than it is safe to say that this will lead to damage appearing in the landing legs. Checking that the maximum experienced stress stays within limits is mandatory to assess therefore whether the legs will break or not.
- Variation of deceleration happening from the perspective of the lander body. The reason for this is because the acceleration experienced by the point mass is equal to the deceleration that is experienced by the internal components of the lander such as the payload and the electronics.

Because of the fact that these components have a requirement on the maximum G forces experienced by them (as written in section 2.1), it is important to check that in this final design the G forces experienced by the payload are within the dictated limits.

5 simulations are run in this section, these are:

1. No dashpot, aluminum landing leg and deformable soil.
2. With dashpot, aluminum landing leg and deformable soil.
3. With dashpot, CFRP landing leg and deformable soil,
4. With dashpot, aluminum landing leg and stiff soil,
5. With dashpot, CFRP landing leg and stiff soil.

7.4.1. Landing with No Dashpot, Aluminum Leg and Deformable Soil

The first analysis is brought forward in order to show what is the effect on the decelerations and stresses of landing of the developed landing leg when there is no dashpot, or shock absorber.

The moment of maximum stress experienced by the leg is shown:

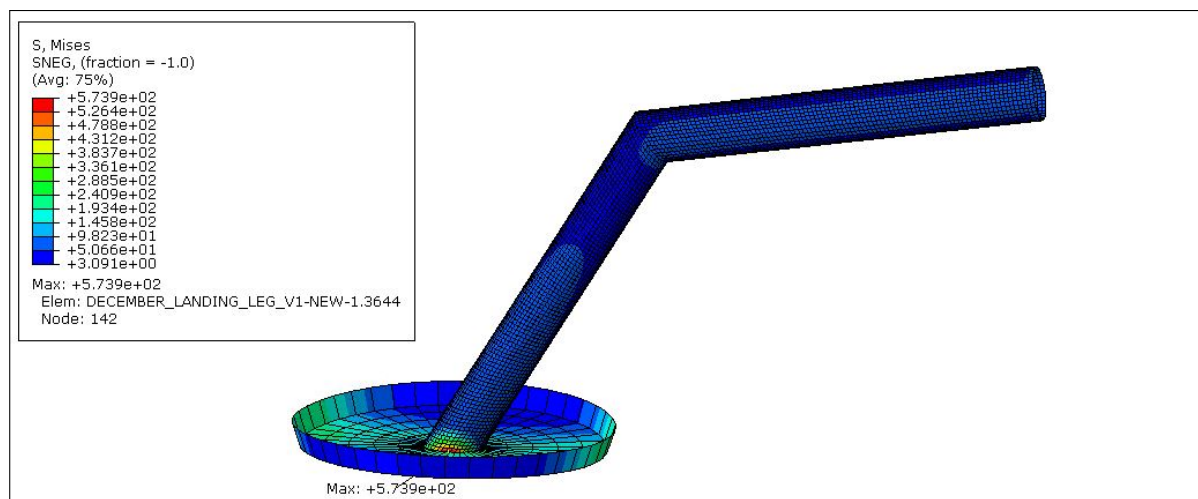


Figure 7.4: Max Von Mises stress experienced by aluminum leg during landing with no dashpot and deformable soil (soil has been suppressed for better viewing of the landing leg).

The value of Von Mises stress at this point is of 573.9 MPa and it leads to a safety factor of:

$$SF_1 = \frac{572}{573.9} \approx 1$$

This safety factor is not only slightly below 1, but it is also below the 1.4 required safety factor following the NASA handbook of space structures safety factors. Because of this, now a dashpot is attached to the connection between the lander body COG and the top of the landing leg.

The deceleration profile is shown in Figure 7.5:

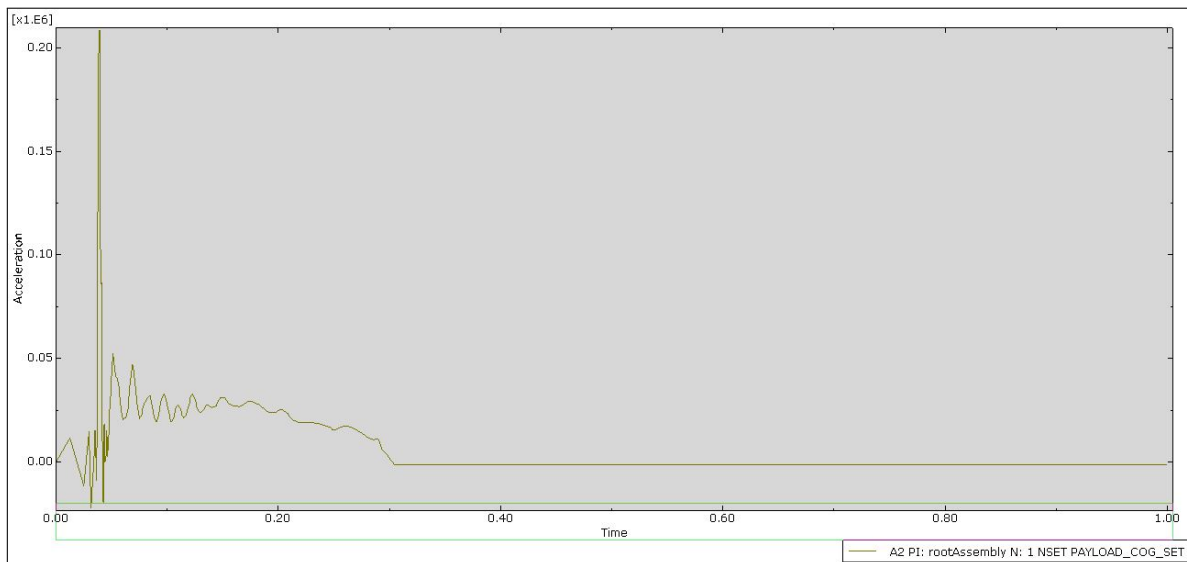


Figure 7.5: Vertical deceleration profile (in mm/s^2) over time in landing of aluminum leg with no dashpot and deformable soil.

Peak deceleration is at a value of 21.25 gs (208500 mm/s^2). This is twice as much as what is required from the lander. Making it clear that either a design change is needed, or the addition of a dashpot as a shock absorber is required. At this point, the soil clearance requirement is going to be checked. this is done by looking on the FEM model to only the deformed soil model at its highest compression point, for example in the case of this simulation:

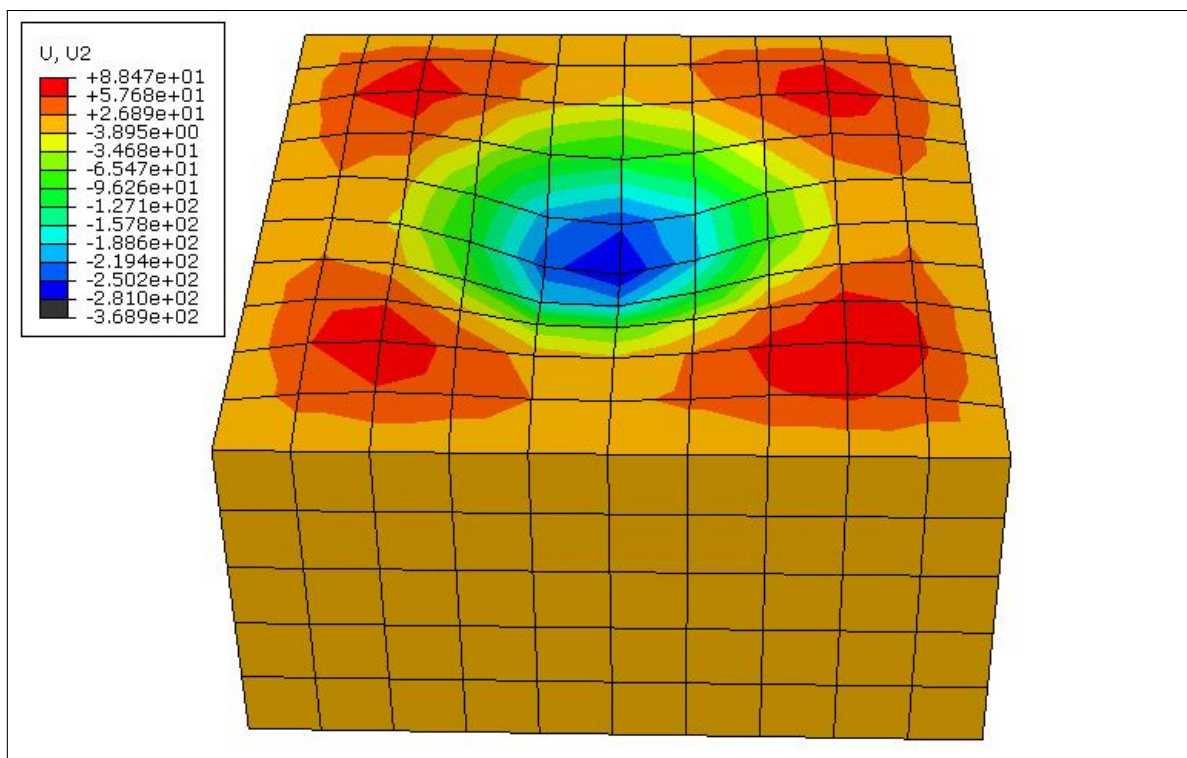


Figure 7.6: Deformation in vertical direction at moment of max sinking (landing leg has been suppressed for better viewing of the deformed floor).

Soil sinking, in this case, is of:

281.67 mm

Because of the fact that the vertical distance between the bottom and top of the leg is:

$$770 - 250 = 520 \text{ mm}$$

In which 770 mm is the vertical position of the bottom of the landing leg with respect to the COG of the lander body, as output in the landing system coordinates at the end of Section 6.9. 250 mm is the vertical distance between the lander COG and the bottom of the lander body. Therefore 520 mm is the vertical distance between the bottom of the lander body and the lower footpad, in the vertical direction. Therefore, the minimum clearance that there is between the deformed soil and the lower side of the lander body is of:

$$520 - 281.76 = 238.33$$

Therefore fulfilling the soil clearance requirement by slightly more than 38 mm since LS-DES-002 states that the required soil clearance shall be of 200 mm.

7.4.2. Landing with Dashpot, Aluminum Leg and Deformable Soil

A dashpot of coefficient 20 N/mm/s is added between the lander body COG and the top of the landing leg. The result in terms of maximum Von Mises stress at touchdown when touching only with one leg is as follows:

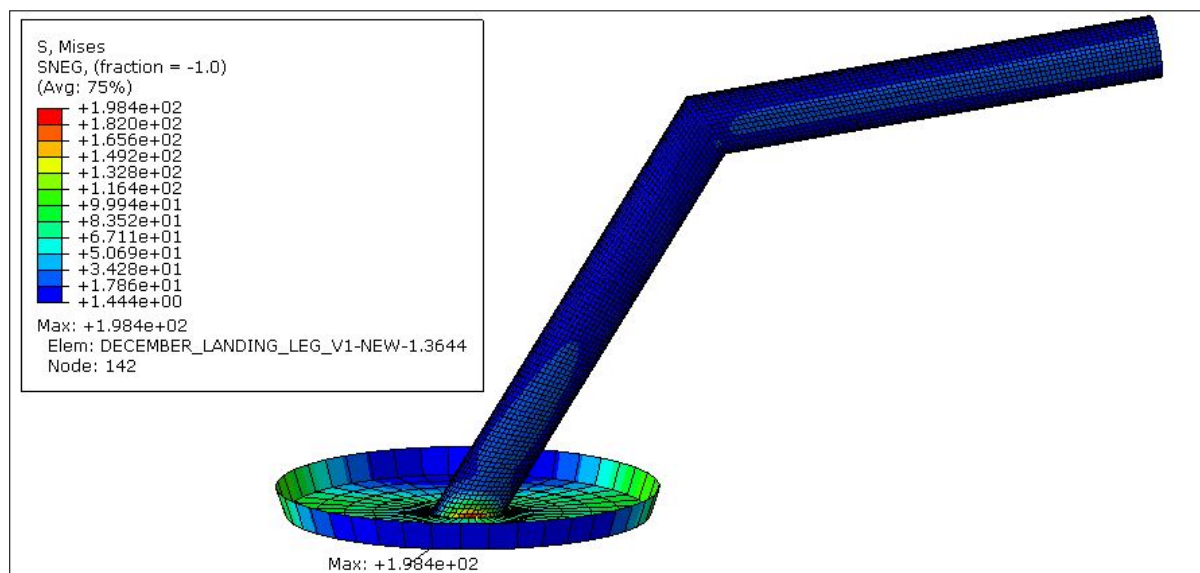


Figure 7.7: Max Von Mises stress experienced by aluminum leg during landing with dashpot and deformable soil (soil has been suppressed for better viewing of the landing leg).

The maximum stress experienced by the leg with a dashpot and with deformable soil is of 198.4 MPa. This stress leads to a safety factor of:

$$SF_2 = \frac{572}{198.4} = 2.88$$

It should be noted how in both simulations, the one shown in Figure 7.4 and the one in Figure 7.7, the maximum stresses pile up in the same location.

The result seen in Figure 7.7 serves to show that a dashpot is needed.

The deceleration profile is shown as follows:

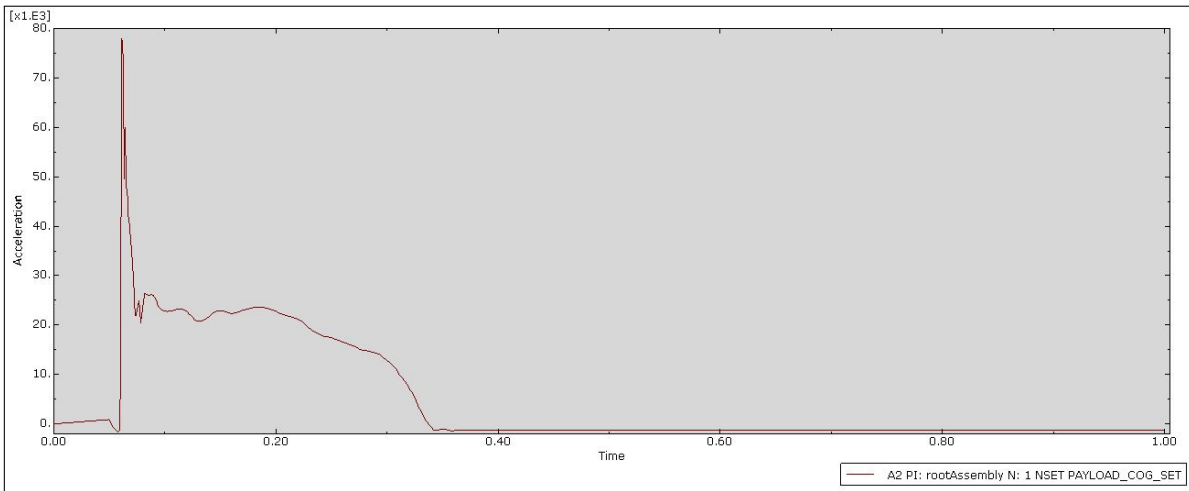


Figure 7.8: Vertical deceleration profile (in mm/s^2) over time in landing of aluminum leg with dashpot and deformable soil.

With the addition of a dashpot of $20 N/mm/s$, the peak deceleration is lowered down to $7.47 g$ s ($73233.6 mm/s^2$). This is a reduction in g forces imparted to the lander body COG of around 66 % or 2/3 compared to the case of the landing without a dashpot.

Sinking is, in this case, of:

$$225.46 \text{ mm}$$

Which, when calculated against the position of the lower side of the lander’s body leads to a value of clearance of:

$$520 - 225.46 = 294.54 \text{ mm}$$

Therefore exceeding the soil clearance criteria by 94 mm.

7.4.3. Landing with Dashpot, CFRP Leg and Deformable Soil

Now the material is changed from aluminum to CFRP using the material properties and layup written in chapter 4. The geometry stays the same because, as seen in figures like 6.9 or 6.12.

The moment of maximum strain experienced by the leg is shown:

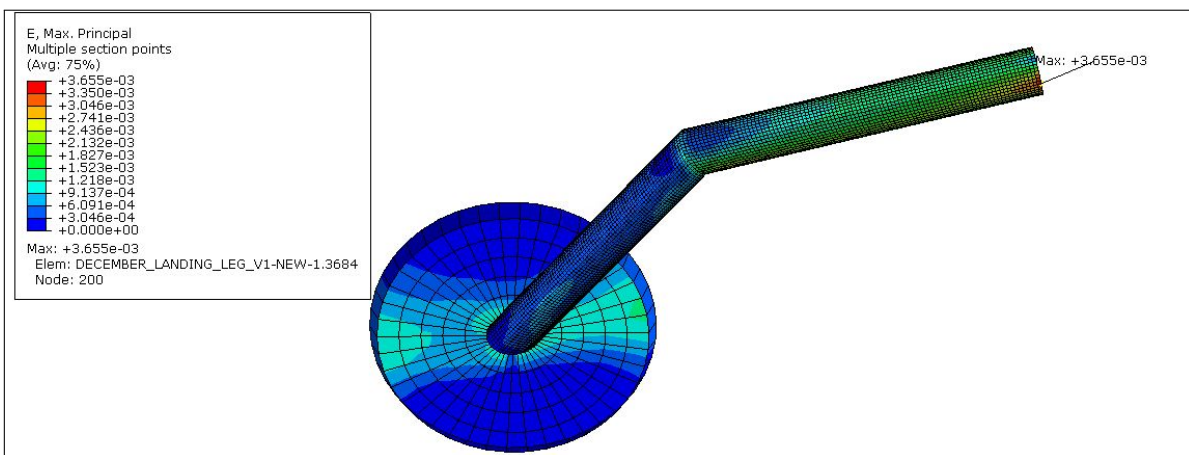


Figure 7.9: Max principal strain experienced by CFRP leg during landing with dashpot and deformable soil (soil has been suppressed for better viewing of the landing leg).

The design limit when it comes to composite structure is 5000 micro strains. The structure, as seen by looking at Figure 7.9 reaches a value of 3655 micro strains, therefore showing that it can survive a landing with a single leg on deformable soil and with a shock absorber dissipating some landing energy. The deceleration profile is shown as follows:

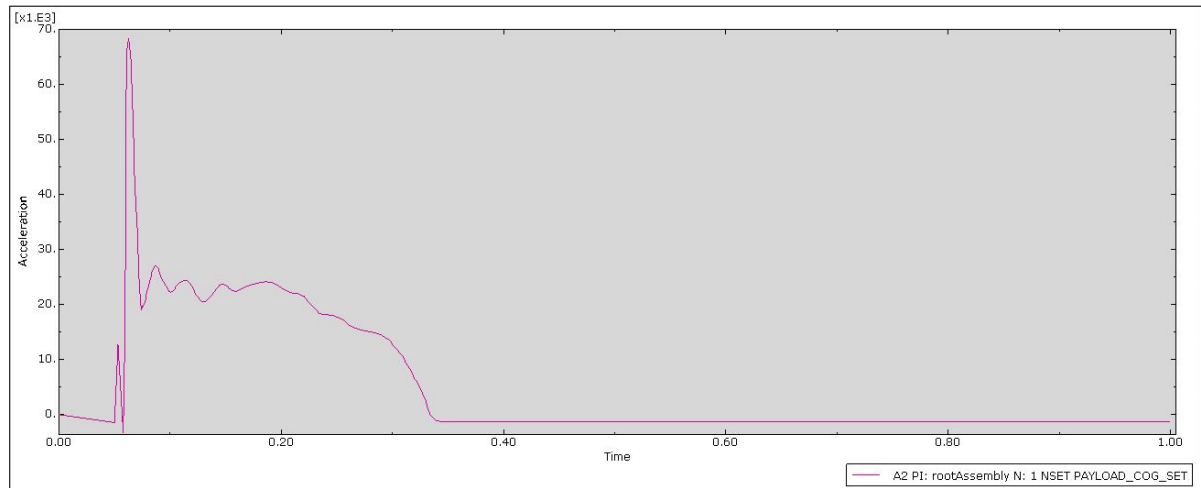


Figure 7.10: Vertical deceleration profile (in mm/s^2) over time in landing of CFRP leg with dashpot and deformable soil.

Peak deceleration is of a value of 7 gs ($68337.8 mm/s^2$). This is well within the limit set by requirement LS-PAY-002.

Soil sinking is, in this case, of:

$$227.24 mm$$

Which, when calculated against the position of the lower side of the lander's body leads to a value of clearance of:

$$520 - 227.24 = 292.76 mm$$

Therefore exceeding the soil clearance criteria by slightly less than 93 mm.

7.4.4. Landing with Dashpot, Aluminum Leg and Stiff Soil

Now the material of the landing leg body is returned to aluminum with the properties found in Table 4.1. The moment of maximum stress experienced by the leg is shown:

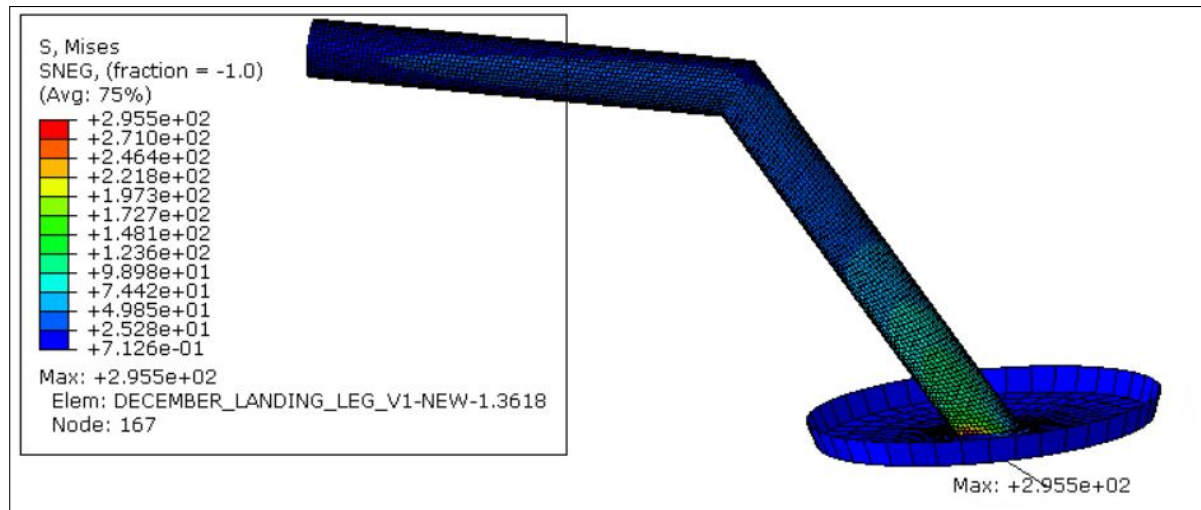


Figure 7.11: Max Von Mises stress experienced by aluminum leg during landing with dashpot and stiff soil (soil has been suppressed for better viewing of the landing leg).

The maximum stress experienced by the landing leg made of aluminum with rigid soil is of 295.5 MPa. This leads to a safety factor:

$$SF_3 = \frac{572}{295.5} = 1.94$$

The deceleration profile is shown in Figure 7.12:

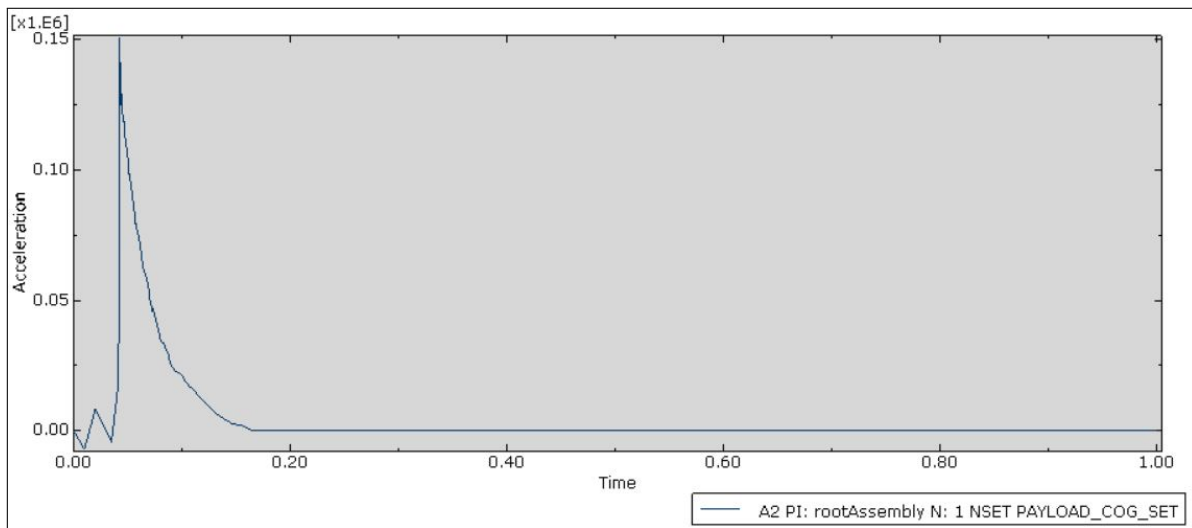


Figure 7.12: Vertical deceleration profile (in mm/s^2) over time in landing of aluminum leg with dashpot and stiff soil.

Peak deceleration has a value of 15.37 gs ($150813 mm/s^2$). Furthermore, similarly to the deceleration profile of the CFRP leg with stiff soil, the deceleration is not spread out through a longer amount of time.

This last landing leg satisfies the maximum stress and safety factor requirement, but not the maximum g forces load requirement.

7.4.5. Landing with Dashpot, CFRP Landing Leg and Stiff Soil

Now for this analysis and the one after, the soil cuboid is substituted with an analytical rigid soil. The moment of maximum strain within the landing of the CFRP landing leg on a stiff soil is shown in Figure 7.13:

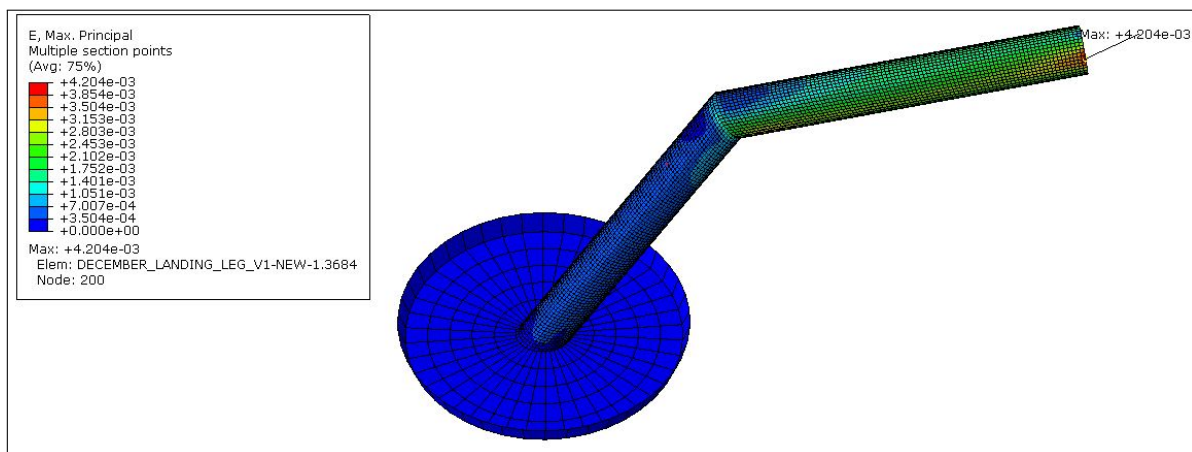


Figure 7.13: Max principal strain experienced by CFRP leg during landing with dashpot and stiff soil (soil has been suppressed for better viewing of the landing leg).

The maximum value of maximum principal strain reached by the composite layup is of 4204 micro strains. This is still below the design limit placed on landing system structures by NASA researchers as found in [27] and [19].

The deceleration profile is shown as follows:

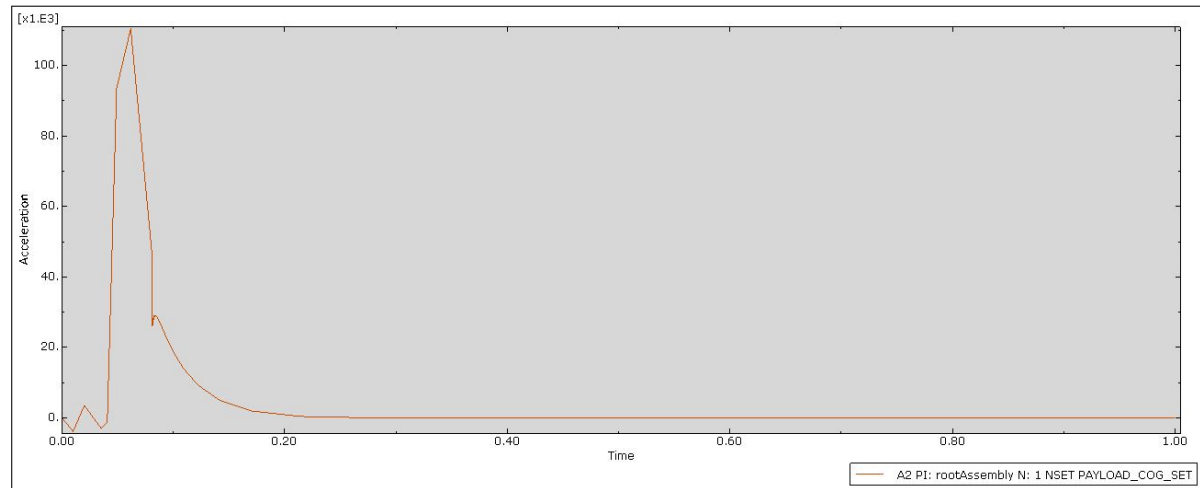


Figure 7.14: Vertical deceleration profile (in mm/s^2) over time in landing of CFRP leg with dashpot and stiff soil.

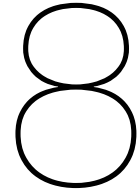
As can be seen in the deceleration profile of Figure 7.14, the deceleration peak of 11.3 gs ($110429 mm/s^2$), is higher compared to the other 2 peaks, but also it is spread throughout a smaller amount of time.

The soil clearance requirement in this simulation is not taken into account because the lower side of the lander's body is already clear of 520 mm from the bottom of the landing leg. Since, with a stiff soil, no soil deformation is present, this clearance is also the clearance between the soil and the bottom of the lander body.

7.5. Conclusion and Findings on Landing Analyses

By performing the 5 analyses written above, some conclusions can be drawn about the suitability of the landing leg geometry in landing the Europa Lander with a higher velocity compared to that of the Skycrane concept. Specifically, it can be said that a shock absorber is needed in order to lower down the stress experienced by the legs at touchdown and also the g forces experienced by the lander body. The shock absorber (or dashpot), can lower down stresses by around 60 % and the g forces by 67 %. When it comes to landing on Lunar like soil, both the CFRP and aluminum designs perform well within the margins of maximum stress, strain and g forces. On the other hand, landing on rigid soil, but keeping the same shock absorber value as the landings on deformable soil, leads to stress and strain values that are within the required margins, but g forces loads that are 10 to 50 % higher than prescribed. This shows that the changing of this parameter could help even further to lower down these 2 performance indicators (maximum stresses and strains and G forces experienced by the lander payload). Further analyses can help coming up with a better value for this parameter. However, due to lack of time, the comparison that was brought forward in this chapter of the thesis was the comparison between materials (aluminum and CFRP) and stiffness of the soil. Of which the conclusion is that CFRP is better because both for the case of landing on rigid and stiff soils it leads to less G forces.

One limitation that the landing case with only 1 leg leads to is the fact that not enough landing energy absorption is achieved by 1 damper. It was noticed, in the simulations, that a rebound after landing happens. Nevertheless, because of the fact that only 1 landing leg is modelled into the FEA software, landing stresses and strains shown in Subsections from 7.4.1 to 7.4.4 are much higher than the real ones because, in a case where multiple legs touch the ground at the same time, the weight is distributed through multiple legs. Therefore the conclusion to this chapter is that, while the landing case with a single leg leads to conservative values of stresses, strains, G forces and sinking, landing simulations with all 4 legs touching down shall be performed in future works.



System Design Guidelines

This section of the report lays out guidelines on how it is possible to design the system modelled so far. Therefore, assumptions taken in the modelling, limitations discovered through the sensitivity analyses and the aspects discovered while modelling, are put together to come up with a series of advices and suggestions over how to make the deployable landing system concept applied to the Europa Lander. Furthermore, an indication of the preliminary architecture, and therefore the mass, is also given in this chapter. This is done in order to prove for satisfaction of the mass fraction requirement (labelled as LS-DES-001).

8.1. Systems to Be Selected and Tradeoff Methodology

The deployment and landing models tell a few numerical parameters about the design and behaviour of a deployable landing system. What the numbers don't say are the real world implications that are inevitably present when designing such a system. The known matters so far of the design are the geometry, which is the one that is seen in Figures 7.1 and 7.2. Another known matter is that it is preferable to have the leg elements made of CFRP because it is better at sustaining G forces as seen by the analyses in the previous chapter.

The subsystems within the landing system that need to be designed using concept generation and selection are:

- The leg joints,
- The damping system for the leg deployment,
- The damping system for the leg landing,
- The locking mechanism to lock the legs at the required CDA.

For each subsystem, concepts are introduced. These concepts are either generated specifically for this thesis, or they are based off COTS components or existing solutions that have flown on previous missions or are used in other industries. Regarding the selection process of each concept, the chosen method is the graphical one. Meaning that each concept is going to be ranked based on the satisfaction of so called performance criteria. Graphical representations give a colour to rank the performance of each concept when acting on a specific performance indicator, colours represent the following performance satisfaction:

- Red: concept does not satisfy the performance required,
- Orange: Concept can satisfy the performance required, if minor adjustments are applied to it,
- Green: Concept satisfies the performance required,
- Blue: Concept exceeds the performance required.

8.2. Leg Joints

This section gives an overview on how to properly implement the requirements and the modelling done so far on the leg joint in a real life scenario. The information, requirements and constraints so far encountered during the thesis that dictate the design of a leg joints are:

1. **Design Constraint 1:** The leg joints shall be 2 per legs. This is because, for each landing leg, 1 leg joint shall connect the payload body to the first leg element and the second leg joint shall connect the 1st and 2nd leg element together. This aspect was taken as an assumption during the deployment modelling section of the thesis in section 3.2.
2. **Design Constraint 2:** The 2 leg joints shall only make it possible for rotation to happen around only 1 axis, the one parallel to the angular momentum axis.

8.2.1. Design Options for Leg Joints

Based on the requirements and design constraints contained above, the following list contains some of the design options that were either preliminarily designed for this thesis or found in literature:

- **Universal Joint:** A universal joint has 2 co-rotating parts. It's generally used for applications where 2 beams that have different rotation axes have to rotate at the same rate. However, if one constrains the rotation of an end, the other would be free to rotate along the axis of interference between the 2 components. A picture of a universal joint is given in Figure 8.1:



Figure 8.1: Example of universal joint [7].

- **Ball Joint:** A ball joint, similar to what is between the strut and the footpad in the Apollo, and many other, landers:

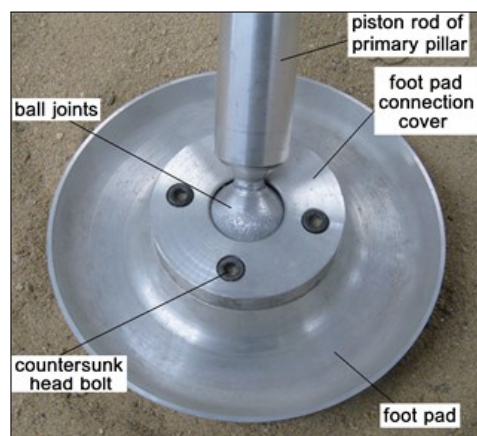


Figure 8.2: Ball joint in Lunar lander model of footpad [23].

Pin Joint: This design is similar to a universal joint, but this one only has 1 degree of freedom.

8.2.2. Tradeoff of Leg Joint Options

The performance indicator to characterise a ranking of the best concepts are listed as follows:

- Technology Readiness Level (TRL), because it is desired to use a system that has already been flow to space, which corresponds to a TRL level of 8-9 [18]. It is required that the technology has a TRL of 5-6, meaning that the technology is not completely new and its working principles have been proven in a relevant environment [18].
- Mass added to the already existing system. Because of the fact that the analysis have already been done, adding more mass with non-structural (but yet required) components makes the results less reliable. Because of this, it is desired to choose a component or subsystem that adds the least amount of mass to the already existing landing system design.
- Changes to geometry to the already existing system. When it comes to adding components, some accommodations have to be made, for example some holes have to be placed in order to fasten components or brackets have to be added or welded in order to brace new subassemblies to the already existing landing system design. This qualitative performance criteria wants to minimize the amount of accommodations to be made to the already existing landing system design when adding new components or assemblies that were not there during the analyses.
- Satisfaction of design constraints.

The tabular methodology used to solve the tradeoff of this section of the thesis is shown Figure 8.3:

Concept	TRL	Mass added to system	Accommodations to be made	Satisfaction of design constraints
Universal Joint	High (8-9)	Low	Extra housing and sealing, but small. Threading at end of each leg element	Satisfies all of them
Ball Joint	High (8-9)	Low	Extra housing and sealing. Threading at end of each leg element	Doesn't satisfy rotational axis constraint
Pin Joint	High (9)	Lowest	Extra housing and sealing, but small. Threading at end of each leg element	Satisfies all of them

Figure 8.3: Tradeoff table for leg joint concept selection.

By looking at the table in 8.3, it is clear that employing a pin joint is the best option. This is because, while other solutions perform well when it comes to mass or TRL, the pin joint only allows the second leg element to rotate around one axis. This can also be achieved by a universal joint, if the first component is rotationally locked with the upper leg element or the lander body, however the universal joint has more moving parts than the pin one. Therefore, the pin joint is chosen.

A preliminary design for a pin joint is sketched in SolidWorks and the mass is as follows:

2.44 kg

The pin joint subassembly as designed in SolidWorks is as follows:

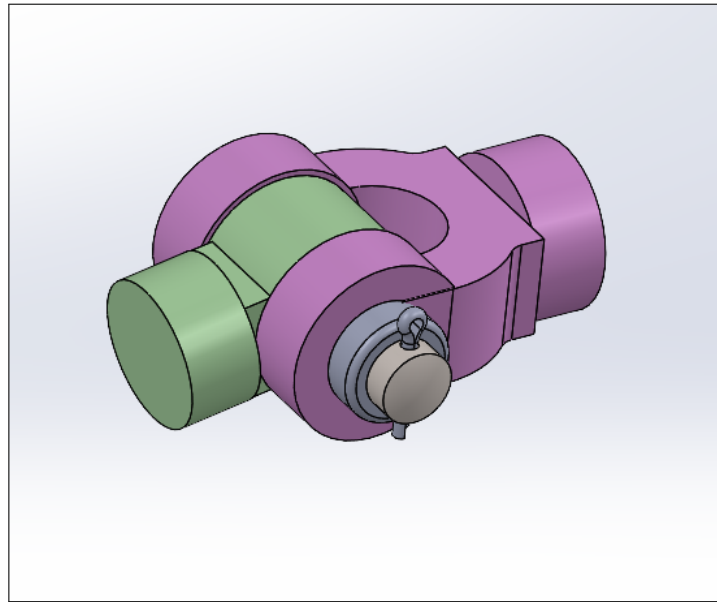


Figure 8.4: Visualisation on SolidWorks of pin joint subassembly.

8.3. Damping

8.3.1. Damping to Control Deployment of Legs

The first type of damping encountered in this thesis is the one that is used to control the rotational deployment of the landing legs. The design constraints that dictated the deployment damping, stemming from the deployment analyses results, are listed as follows:

1. **Design Constraint 1:** the deployment damping shall be of the rotational type, therefore measured in $Nm/rad/s$. This is the type of damping that offers a torque when counteracting angular rate.
2. **Design Constraint 2:** The values of damping for the deployment damping shall be contained between 5 and 30 $Nm/rad/s$. This is because, it has been shown by the deployment results that the allowed values of damping for the deployment legs are within that range. Although accommodations to the other landing system parameters can also be made in case those values of rotary damping are impossible to be achieved and they have to be raised (or lowered).
3. **Design Constraint 3:** The minimum travel angle allowed within the deployment damper is of 110 degrees. This is because the chosen CDA is 110, therefore a damper that can rotate from a position of 0 degrees to one of the CDA has to be found. If the damper is only allowed for example, to rotate 45 degrees, than the deployment would stop before, which is not a desired outcome.

Following is a list of options based on real life space missions that used damping solutions in their landing systems (or other deployable structures) or solutions from other industries that employed damping in a similar way:

- Use an active control damper, such as a magnetorheological one. In this case, current is let go through a magnet that induces a magnetic field that actively introduces a resistance to the co-rotation of 2 components, similarly to what was used as a landing damping strategy for rosetta [56].
- Damping during rotational deployment of the leg can be achieved with so called dashpots such as the ones as made by Kinetrol [21], that have a variety of applications such as pneumatic valves. One of the envisioned applications of their so called "dashpots" is indeed to control the motion of a pendulum like structure:

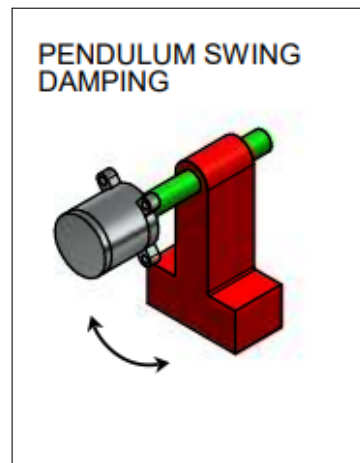


Figure 8.5: Envisioned application example of a rotary damper [21].

Looking at the catalogue of products of Kinetrol, it can be seen that dimensions are applicable only in the case of the *Model LA1* [21]. The specifications are as follows:

- Damping offered: 25 Nm/rad/s or lower,
- Angle of travel: $215 \text{ Degrees} \pm 5$,
- Mass: 1.61 kg .

The only problem with all dashpots offered by Kinetrol and found in [21] is the temperature range, which is very small compared to the one met when in orbit and around Europa: between 0 and $60 \text{ }^\circ\text{C}$.

- A hinge-like design where the 2 flaps co-rotate with respect to one another, similar to what is presented in Figure 8.6:



Figure 8.6: Hinge-like design for a rotational passive damper [1].

The above 3 deployment damping techniques are going to be compared in a tradeoff using the following performance criteria:

- TRL,
- Mass added to the already existing system,
- Need of control strategy. Because of the fact that Europa is far from Earth, and therefore no direct commands can be sent to the lander, and because of the fact that the environment around

Jupiter is rich in radiation [14], adding a control strategy adds complicacy to the system. Due to the radiation rich environment, in fact, it is possible that the software or electronics inside equipment needing a control strategy becomes faulty. Because of this, adding components that use material properties or physical phenomena (such as the addition of G forces during the landing process) is preferable compared to parts that use electricity or control strategies to function.

- Adjustments needed for fitting the concepts in the landing system,
- Satisfaction of design constraints.

The tabular methodology used to solve the tradeoff of this section of the thesis is shown Figure 8.7:

Concept	TRL	Mass added to system	Need of control strategy	Adjustment to Landing System for Fitting	Satisfaction of design constraints
Active magnetorheological	Low (2-3)	Highest	Control strategy is needed	Bigger housing and sealing	Can be designed to satisfy constraints
Dashpot	Not high for space applications (5-6)	Medium	No control strategy	Small housing and sealing	Solutions that satisfy the constraints exist
Hinge-like design	Not high for space applications (5-6)	Lowest	No control strategy	Threading of leg elements, plus brackets to fit to bolt holes	High values of damping have not been found

Figure 8.7: Tradeoff table for deployment damping concept selection.

By looking at the table in 8.7, it is clear that the best option to be employed to offer damping in the landing system is a dashpot. This is because the accommodations that would need to be made in order to fit a hinge-like design inside the already made landing system geometry would be too big. On the other hand, fitting a dashpot to control the deployment around the pin joint would require minimum adjustments to the joint's housing.

8.3.2. Damping to Control Landing Decelerations

As seen by the landing analyses, there is quite a lot of rebound energy that is not dissipated by the displacement of the soil regardless of the landing speed and the payload mass. Because of this, it is clear that damping components have to be placed in the landing system in order to make sure that the spacecraft reached a complete stop in a landing with all 4 legs.

Following in the list are a series of methods that are used in Space hardware in order to dissipate the landing energy:

- Shock alleviation with viscous methods. In which a plunger goes through a liquid (either oil or a very fine dust) and the frictional energy forming between the plunger and the particles of the liquid gets rid of the excess landing kinetic energy.
- Shock alleviation through plastic deformation. With this method, either the whole leg or a section of the landing leg goes through plastic deformation so that the landing energy doesn't bounce back in the form of an elastic rebound. This is also reached by adding crushable materials at the connection between the leg and the lander.
- Shock alleviation through means of creating a shock in the opposite direction. This is implemented by having a weight ejected from the top of the spacecraft as soon as the ground is touched. This is a novel an active method as a sensor and motor have to be present to eject the material to dissipate the landing shocks [17].

The above 3 shock alleviation techniques are going to be compared in a tradeoff using the following performance criteria:

- TRL,
- Mass added to the already existing system,
- Need of control strategy.

The tabular methodology used to solve the tradeoff of this section of the thesis is shown Figure 8.8:

Concept	TRL	Mass added to system	Need of control strategy
Viscous Damping Based Damper	High (8-9)	Medium	No control strategy
Plastic Deformation Based Damper	Medium (5-6)	Lowest	No control strategy
Shock Based Damper	Low (3-4)	High	Control strategy is needed

Figure 8.8: Tradeoff table for landing damping concept selection.

From the table in 8.8 it is clear that the plastic deformation damper and viscous dampers have the same outcome when it comes to choosing the method to dissipate the landing energies. Therefore both are possible options.

If it is desired to go with the viscous based dampers, the value of 20 N/mm/s is attainable by using automotive grade type of dampers [45]. In this paper it is stated that a damper of that value is used for damping the vibrations on the driver on a bus. While a bus is much heavier than the Europa Lander, a bus is not envisioned to dissipate shocks coming from a fall from 10 metres of vertical distance, therefore it can be said that this value is attainable in real life. Although, when designing viscous dampers for space applications, attention has to be placed on the fact that liquids in microgravity behave differently than on Earth [13]. Therefore a viscous damper that uses a fine particulate instead of a liquid preferable, similar to the one developed in [34].

Using a plastic deformation based damper is also an acceptable option. This is because, for this lander, only 1 landing is envisioned and the plastic deformation based solution is the most suitable one for single landing landers.

An example of a plastic deformation based damper is offered in Figure 8.9 [38]:

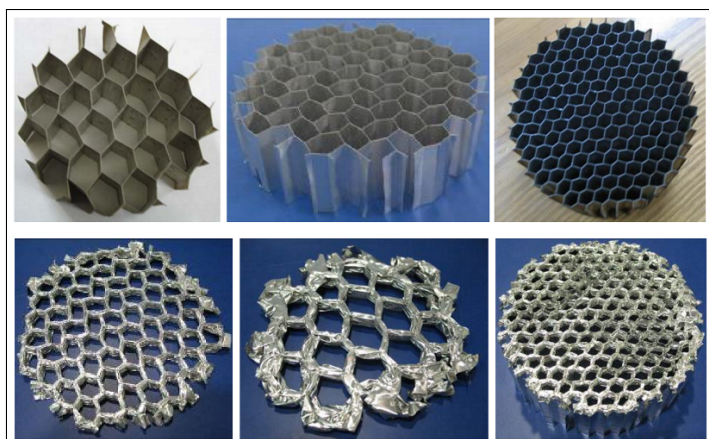


Figure 8.9: Dampers based on plastic deformation of aluminum honeycomb [38].

Using the same procedure used by [38] to size an aluminum foam plastic deformation damper can lead to values of diameter, length and mass for the application envisioned in this thesis. The article

is chosen because the input parameters are similar, in fact, in this article, a lander of mass 500 kg and a landing speed of 5 m/s leads to a cylinder of aluminum foam of height 0.241 m and area 0.0176 m^2 . Furthermore, the design of this lander also has a constraint of maximum g forces imparted by the landing to the rest of the body of 10 g.

For the application of this thesis, only the lander mass is different (575 kg). This leads to the design of a damper of the same area as the one in the article (0.0176 m^2) and a height of 0.28 m or 280 mm. According to SolidWorks, aluminum honeycomb that is this height and length has a mass of:

$$0.53 \text{ kg}$$

The cartridge shall be inserted at the interface between the upper pin joint and the lander body and a slider mechanism shall be incorporated in this interface. This way, when the lander lands, the joint is free to slide in the vertical direction, which then results in the crushing of the aluminum damper. A CAD model of the damper is provided in Figure 8.10:

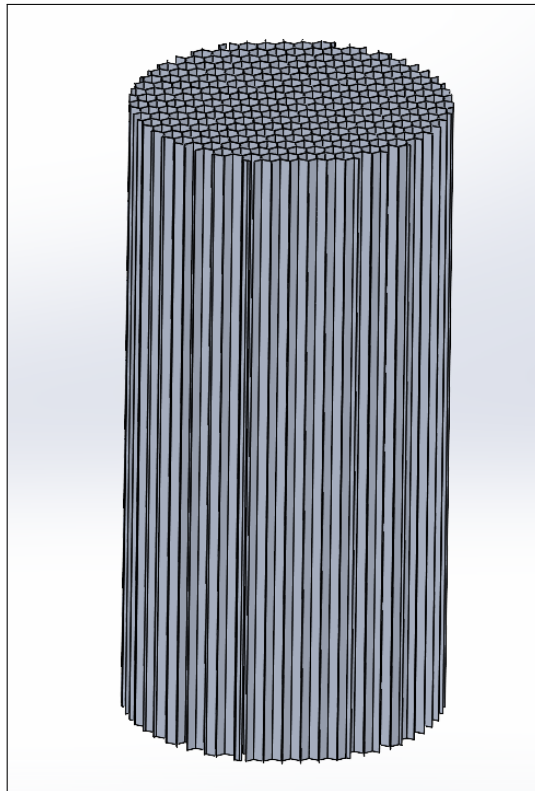


Figure 8.10: CAD model of honeycomb damper.

8.4. Locking Mechanism

The locking mechanism is what drives the deployment of the landing legs to a complete stop. This is dictated by the so called CDA, which is a design input that dictates the maximum angular displacement between the vertical wall of the payload body and the first leg element. The same mechanism shall be placed in order to stop the angular displacement between the first and second leg elements. However the angle at which to stop the deployment of the second leg element is an output of the deployment model.

8.4.1. Design Options for Locking mechanism

This system is not one that is generally publicly available, not as much as the geometry of the landing legs, the footpad etc. Therefore, 2 options are briefly introduced, all of them that are high level options and more detail can be looked at in a future project:

- A ratchet with pin mechanism. Similar to a bicycle wheel mechanism, where rotation is only possible in one direction (the desired direction of rotation) and it is not possible in the opposite

one. Plus the addition of a pin at the desired angle where angular deployment is supposed to stop will make sure that the leg element's rotation is ended. An example of a ratchet mechanism is provided in Figure 8.11:

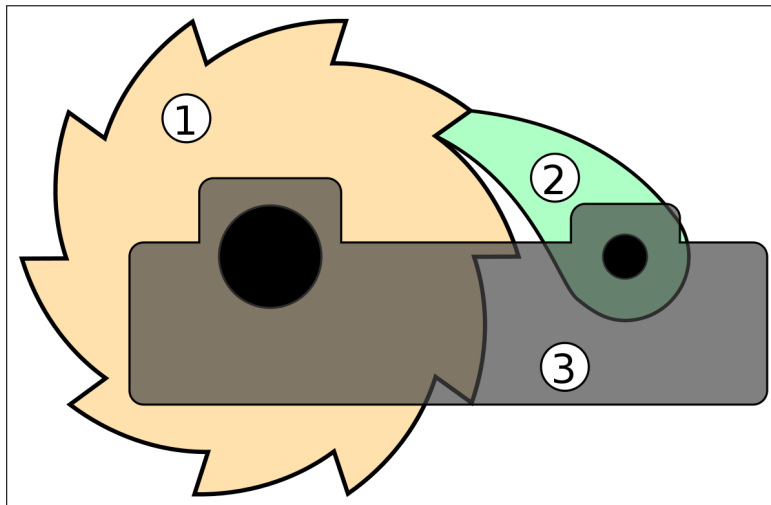


Figure 8.11: Diagram of simplified ratchet mechanism.

Ratchet mechanisms have been used before to stop for the retraction of deployable structures [48], albeit space based ones rather than landing system.

- Use of a motor or actuator that linearly deploys a rubber head in order for friction to stop the deployment to happen inside the pin joint while the leg element are co-rotating with respect to one another. Actuators are sometimes used in the deployment of space based structures, for example solar arrays, as presented in [53], therefore TRL shall be medium high.

8.4.2. Tradeoff for Locking Mechanism

The above 2 locking mechanisms are going to be compared in a tradeoff using the following performance criteria:

- TRL,
- Mass added to the already existing system,
- Need of control strategy.

The tabular methodology used to solve the tradeoff of this section of the thesis is shown in Figure 8.12:

Concept	TRL	Mass added to system	Need of control strategy
Ratchet and Pin Mechanism	High (7-8)	Lowest	No control strategy
Actuator	Medium-high (6-7)	Medium	Control strategy is needed

Figure 8.12: Tradeoff table for locking mechanism concept selection.

As seen in in the table in 8.12, the best concept is the ratchet and pin mechanism due to its simplicity and reliability. This mechanism can be designed as incredibly small, for example by taking inspiration from small ratchets that are used for house or bike repairs. This mechanism is also to be designed in a way that stops the deployment of the landing legs at the right angle. For the joint between the lander

body and the first leg element the angle is the CDA. For the joint in between leg elements, the angle between the leg elements at the moment when the deployment model stops the calculation is taken as a design input and a locking mechanism is designed keeping this constraint in mind. For example, if CDA is of 100 degrees, teeth for the ratchet can only extend of 100 degrees around its center and after that a small wall could be extended to make sure that the pin does not extend further.

8.5. Preliminary Landing System Design

As referred in the landing analyses section of the thesis, the landing legs at that point didn't have a design of the leg joints and other considerations embedded into them. However, taking into account the previous points of system design guidelines, a more detailed CAD design was made that can be used as a starting point for future analyses. The model of the landing leg with metallic elements is seen in Figure 8.13:

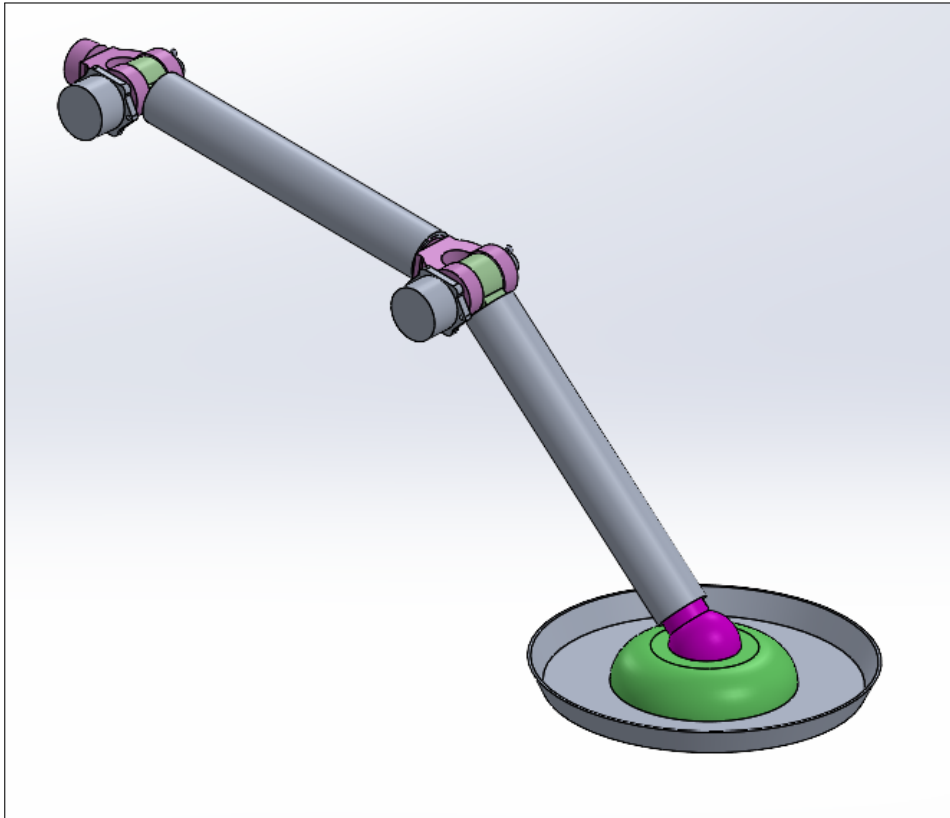


Figure 8.13: Detailed CAD model of aluminum leg design.

The plastic aluminum damper is not placed in Figures 8.13 and 8.14 because of the fact that this is placed inside the lander body. A preliminary mass breakdown for the landing leg made of aluminum elements is given in Table 8.1:

Item	Mass [kg]	Quantity	Total Mass [kg]
Aluminum Damper	0.53	1	0.53
Aluminum Leg Element	2.07	2	4.14
Rotary Damper	1.61	2	3.22
Pin Joint	2.44	2	4.88
Ball Joint	2.01	1	2.01
Footpad	4.50	1	4.50
Total			19.28

Table 8.1: Mass breakdown of landing leg with aluminum leg elements.

With this total mass, 4 landing legs are about 13 % of the whole lander mass. Meaning that, in the case of aluminum landing leg elements, the landing system surpasses mass fraction requirements.

The CFRP landing leg design is seen in Figure 8.14:

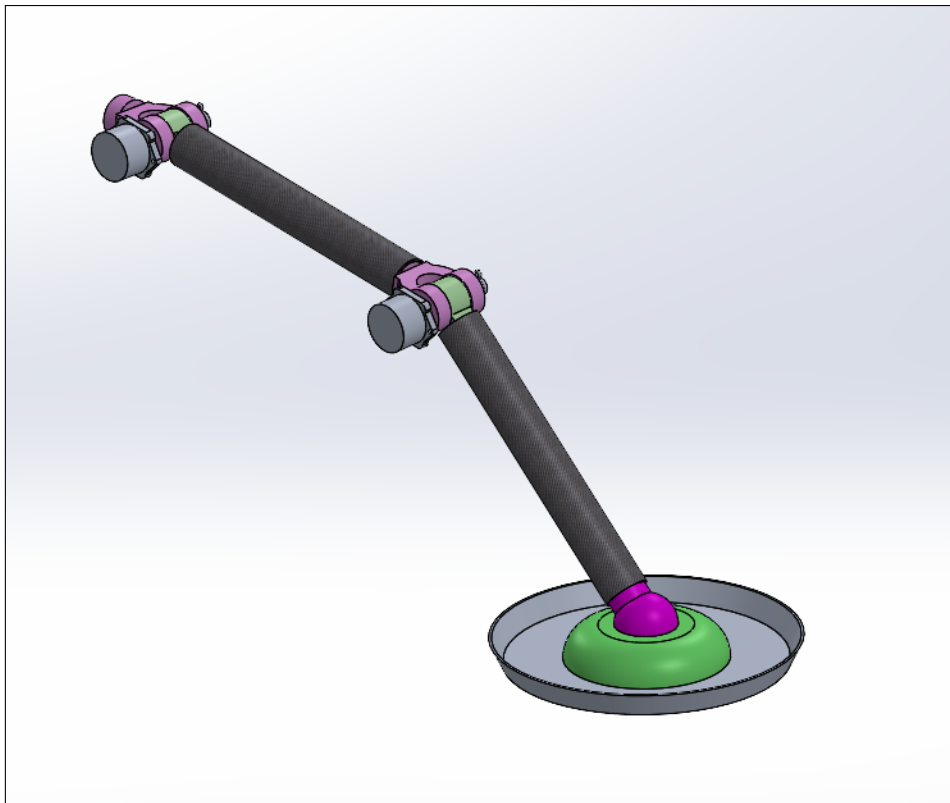


Figure 8.14: Detailed CAD model of CFRP leg design.

The mass breakdown of a single landing leg made of CFRP leg elements is contained in Table 8.2:

Item	Mass [kg]	Quantity	Total Mass [kg]
Aluminum Damper	0.53	1	0.53
Aluminum Leg Element	0.94	2	1.88
Rotary Damper	1.61	2	3.22
Pin Joint	2.44	2	4.88
Ball Joint	2.01	1	2.01
Footpad	4.50	1	4.50
Total			17.02

Table 8.2: Mass breakdown of landing leg with CFRP leg elements.

With this mass, 4 landing legs correspond to 11.8 % of the whole lander mass. This means that, also in the case of the landing system made of CFRP leg elements, the landing system does not pass mass fraction requirements. However, a lot of space for optimization remains through the mass optimization of, for example, the footpad. The difference between this landing leg and the aluminum one is that this one has 2 leg elements made of CFRP which weigh 0.94 kg each.

No detailed analysis has been done on this model, however it is expected to see a high stress concentration at the location where the pin joints are, specifically where the bolts are, as highlighted in Figure 8.15:

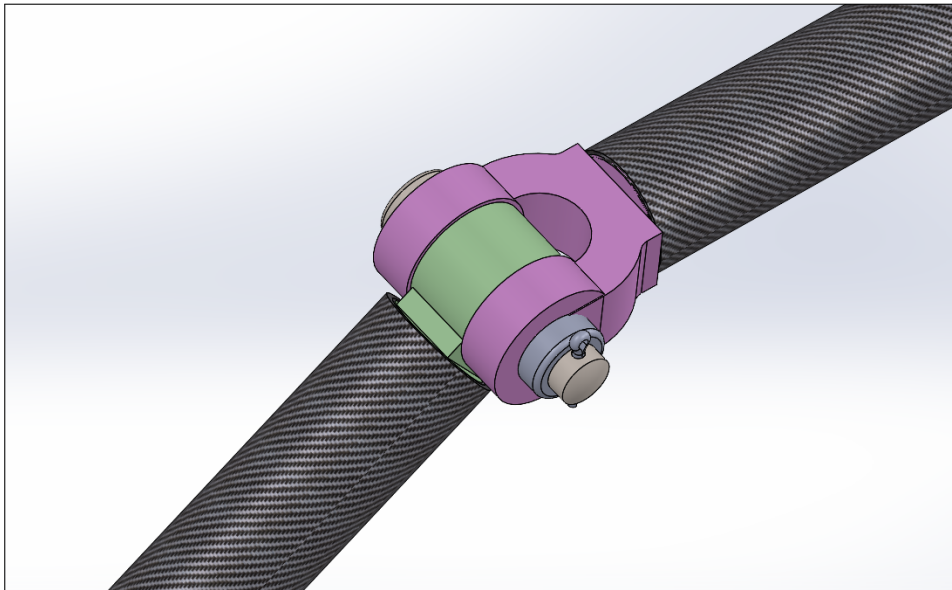


Figure 8.15: Particular of pin joint (without rotary dashpot) between leg elements in detailed CFRP CAD model of the landing leg.

One way to avoid the stresses piling up in either the cross pin or in the bolts of the joint is to use materials with a high strength such as a titanium alloy. Otherwise, another solution is to add cross bracing in between the 2 leg elements in order to add a further load path to decrease stress in this section. However in this case, the deployment modelling has to be done with another model, differently from how it was done in this project.

8.6. Conclusions on System Design Guidelines

Regarding the system design guidelines given here, these are suggestions based on the modelling that was gathered in the previous chapters of this thesis. Because of the fact that each subsystem (i.e. locking subsystem, damping subsystem and so on) hasn't been looked at extensively, the designs need maturation. This can come in the form of future work to be done on each subsystem to allow for the proper re-design of the ELLS.

In this chapter, the landing leg masses were computed with the subsystems making the whole landing system. The added masses coming from the other components such as the dampers don't affect the deployment time negatively. In fact, as seen by the success maps found in section 6.4, adding mass decreases deployment time. Furthermore, adding more mass doesn't change the final developed geometry, as seen in the "Final Leg Configurations" charts also found in section 6.4. This means that, if the deployment analyses would be performed again, it would be found that the deployment time of both the aluminum and CFRP designs would be lower. In the end it was found out that also the CFRP landing leg does not fulfil the mass fraction requirement.

The approach of first gathering numerical characteristics related to the deployment and landing mechanics of this landing system, then using systems engineering practises to limit the amount of design options and come up with a preliminary architecture, is possible because of the fact that a feasible design is reached as shown in section 8.5. On top of that, finding ranges of values was also beneficial because it made it possible to choose the manufacturer based on numerical parameters output by the models used for this thesis. The downside of this approach is the overlooking of some of the aspects that are encountered in this chapter, for example the masses of the components that are not part of deployment and landing analyses. As seen in section 8.5 in fact, the addition of these masses adds to a value that is beyond the limits prescribed by the mass fraction requirement. Nevertheless, choosing the CFRP option is best because this is lighter and it leads to lower amounts of maximum decelerations as seen in the analyses at the end of chapter 7. Furthermore, it can be said that optimisation on this type of leg can be achieved by, for example, lowering the mass of the footpad. This can be achieved by either keeping this component made of aluminum, but lower its thickness of 1 cm, or by making it entirely of CFRP.

9

Conclusions and Recommendations

9.1. Conclusions

In this section of the thesis, first the work done in the previous chapters is wrapped and the answers to the research questions are laid out, secondly, suggestions for further work to either refine the modelling or to mature the design further are going to be laid out.

The project started with the laying out of a novel way to track the deployment dynamics of a specific type of interplanetary landing system undergoing passive deployment using the decelerating forces of landing. The model made it possible to discover that, in order to accurately model landing legs subject to decelerating G forces, their initial position has to point towards the outward direction from the center of the lander. Other matters that were discovered were that, in order to reach a specific value of footprint, which is important when computing landing stability, the angle at which deployment is stopped is the most important parameter to be edited. Furthermore, another important performance parameter with regards to the deployment of a landing system is its deployment time. Through the deployment model it has been found out that changing the joint damping between leg joints has the biggest effect with the control of the deployment time. The proper implementation of the pendulum algorithms has been verified through comparison with existing literature, however a validation of the deployment model was not possible throughout this project due to time and availability constraints. In the future it is suggested to make a deployable landing system model rig where deployment experiments can be brought forward to make sure that the modelling performed in this thesis has a real life correlation. If this path is followed, this thesis can work as a reference on how to make those validation experiments, for example by picking a joint damper with the same values as the ones input throughout the sensitivity analyses. The only difference would be the G forces so some analysis would have to be re-performed, because of this, the Matlab code used for this project has been attached in section A.1.

This thesis also entailed an initial estimation of the landability of this landing system. This was done by looking at a specific landing scenario of 1 leg touching the ground in the case of that leg touching a rock or icy boulder that is higher than the rest of the ground. Also some simplifications were used in here, for example by the use of a Lunar or stiff soil because of lack of soil data for the European soil. Nevertheless, it was shown that the chosen geometry can still lead to a successful landing without leading to damages to the landing leg itself (in the case UTS or maximum strain would have been overtaken) or to the instruments inside the payload (in the case the 10 Gs of shocks of the lander COM would have been hit) in the case of the landing on deformable Lunar soil. In the case of landing on the stiff soil, the landing leads to peak g forces on the lander body that are higher than the minimum required of 10 gs, but the legs are not damaged.

And, in the end guidelines on how the modelling is implemented to actually make the landing system have been given. In order to successfully come up with a concept, the modelling was used as a starting point for the design. The modelling outputs gave design constraints which were then turned into design options by using systems engineering practices. Design options were then laid out and selected based on performance indicators such as mass addition and TRL. In the end a preliminary design was made that uses pin joints as a way to co-rotate leg elements, a ratchet mechanism to lock and prevent the

rotation of the landing leg elements in the opposite direction, dashpots to control the legs' deployment and aluminum honeycomb cartridges to dissipate the shocks of landing.

9.1.1. Answer to Research Questions

To answer the first research question, the acceptance of requirements has to first be laid out. In this section of the report, the acceptance of all the requirements set in chapter 2 is verified. Regarding the acceptance of design requirements of the ELLS:

Design Requirement Code	Fulfilled?	Proof
LS-PAY-001	Partially	Not fulfilled with stiff soil landing
LS-PAY-002	Partially	Not fulfilled with stiff soil landing
LS-LAN-001	Partially	Not fulfilled with stiff soil landing
LS-LAN-002	Yes	As seen in Section 6.9
LS-LAN-003	Yes	As seen in Section 7.4
LS-LAN-004	Yes	For deformable and stiff soil landings
LS-LAN-005	Yes	For deformable and stiff soil landings
LS-DEP-001	Yes	As seen in Section 6.9
LS-DEP-002	Yes	One of the inputs of the deployment model
LS-DEP-003	Yes	One of the inputs of the deployment model
LS-DES-001	No	Although the CFRP landing leg does better than the aluminum one
LS-DES-002	Yes	As seen in Subsections 7.4.1 to 7.4.3

Table 9.1: Design requirements acceptance.

Regarding modelling requirements, they are placed in Table 9.2:

Requirement Code	Fulfilled?	Proof
MDL-DEP-001	Yes	As seen in Section 7.4
MDL-DEP-002	Yes	As seen in Section 7.4
MDL-DEP-003	Yes	Within 10 % when compared to original paper results
MDL-LAN-001	Yes	Stress is one of the field outputs in FEM
MDL-LAN-002	Yes	G forces is a history output in FEM
MDL-LAN-003	Yes	They take around 15 minutes
MDL-LAN-004	Yes	As seen in Section 7.4
MDL-LAN-005	Yes	Within 10 % when compared to NASA results

Table 9.2: Modelling requirements acceptance.

The first research question entailed the possibility of modelling the deployment dynamics for a landing system that uses the decelerating g forces to deploy itself and that scraps the Skycrane system, therefore leading to higher landing velocities. This question was only partially fulfilled. While the modelling in Chapter 3 shows that it is possible to track the deployment dynamics of a self deployable landing system that uses a pendulum like motion, not all the requirements were, as seen in Table 9.1, fulfilled. Specifically, the ones related to the landing on stiff soil. Because of this, it is suggested to look into the design of a shock absorbing system that can lead to a more spread out deceleration when landing on stiff soil, rather than the sudden and very short deceleration that can be found in Figures like 7.14 and 7.12. In the end, it was written in the Introduction that the mass saved by taking out the Skycrane concept could have been used to increase the mass allocated to internal lander components, such as more scientific instruments or more power for existing ones. However this has not been proven because of the fact that the value of Skycrane mass (or a value for Skycrane mass fraction) was not found. Nevertheless, if mass is added to the payload because the 1235 kg combined mass (between Descent Stage and Lander) is kept after taking out the Skycrane concept, maximum G forces would decrease, as Figure A.2 shows. Stresses and strains in the landing legs, on the other hand, would increase with an increase in payload. However, their value would increase by around 5 % with an increase in 100 kg between a payload mass of 500 and 600 kg. This is seen by calculating the increase in stress in the

legs when payload is increased by 100 kg between 500 and 600 payload mass as seen in Figure A.1.

The second research question entailed the implementation of the modelling in order to come up with design guidelines, options and selection for different subsystems of the ELLS. System engineering practices were performed to select the options on the joint damping, the locking mechanism etc. This was a partial success as, on one side, using numerical inputs from the models to come up with subsystems' preliminary designs is possible (for example knowing from the analyses that joints should only rotate with 1 degree of freedom and choosing pin joints consequently). On the other side though, the mass additions that were added through the coming up with the concepts were larger than expected. This is not a problem for changes in landing system geometries, as shown by the analyses in section 6.4, or for the changes in deployment time, as a higher landing leg mass decreases the deployment time. This is a problem for the mass fraction requirement, which ended up not being fulfilled for either landing system design, the CFRP one or the aluminum one. Nevertheless, optimisation of the footpad or the joints can be performed, as is explained in the following section.

The final choice between the CFRP design and the aluminum one lands on the CFRP one because it has a lower mass and because it leads to lower G forces when landing with the same landing scenario as the aluminum leg.

9.2. Further Work

This thesis used 3 different software as part of the pipeline to go from deployment model, to 3D design, to 3D landing simulations: Matlab for the first one, SolidWorks for the second matter and Abaqus for the last one. A recommendation would be to avoid using Matlab and SolidWorks and perform all the relevant analyses (deployment and landing) on Abaqus. This will greatly increase efficiency since it avoids the time wasted to move between software. The reason for this to be placed on further work is because, while the Matlab deployment model allowed for a high degree of design iterations of the deployable landing system to be produced, it was noted that moving the geometry from a 2-dimensional set of coordinates developed by Matlab, to a geometry placed in FEM software was time consuming. Further work can also be done with regards to the design maturation of single components and subsystems laid out in Chapter 8. It is in fact also suggested to perform more detailed analyses on single components of the landing systems to see if they are all suitable for surviving landing. One of the biggest unknowns yet is, in fact, whether the leg joints would safely transfer loads from the landing shocks without damages. This was not possible to be analysed during the thesis as the joint in between leg elements was modelled as a rigid component as simplification. This type of project can also look into optimizing the mass of the landing system by either changing the shape of the pin joints or, more importantly, looking into weight savings coming from the footpad. This thesis could also look into other landing scenarios, for example a type of landing with multiple legs touching the ground at the same time or a type of landing with an horizontal velocity.

In the end, the last recommended area of research for the design of the Europa Lander Landing System is the design of the system by making it adaptable to unknown terrains. This was already started in this project by choosing the landing case over a single landing leg in the case one leg lands on a platform that is higher than the other legs. However more work can be done by looking into the design of an adaptable mechanism that unlocks the joint in between leg elements or in between the leg and the lander body in order to re-stabilize the lander body over uneven terrains. Because adaptability is something that is performed by the landing legs after landing and deployment happens before, the deployment model doesn't necessarily have to be changed.

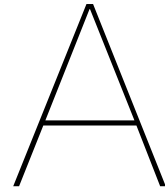
Bibliography

- [1] Acorn Bearings. *Ace Rotary Dampers*. 2007. URL: <https://www.acornbearings.co.uk/downloads/catalogues/aerospace/struts-and-dampers/ace-rotary-dampers.pdf> (visited on 10/10/2021).
- [2] Aerospace Specification Metals. *Aluminum 7075-T6 Datasheet*. 2019. URL: <http://asm.matweb.com/search/SpecificMaterial.asp?bassnum=MA7075T6> (visited on 09/22/2021).
- [3] Altair University. *CAE and Multi Body Dynamics*. 2014. URL: <https://altairuniversity.com/wp-content/uploads/2014/02/cae-and-multi-body-dynamics.pdf> (visited on 12/03/2021).
- [4] H. O. Alvidres. *A Probe to Europa*. University of Texas. 1997. URL: <http://www.tsgc.utexas.edu/archive/design/europa/> (visited on 01/14/2022).
- [5] T. Amamoto, H. Sakamoto, H. Furuya, N. Okuizumi, A. Watanabe, and N. Kawabata. "Modeling of Composite Booms' Deployment Dynamics under Microgravity Based on Ground Tests". In: *2018 AIAA Spacecraft Structures Conference*. American Institute of Aeronautics and Astronautics. URL: <https://arc.aiaa.org/doi/abs/10.2514/6.2018-1435>.
- [6] F. Bagenal and V. Dols. "The Space Environment of Io and Europa". In: *Journal of Geophysical Research: Space Physics* 125.5 (2020). ISSN: 2169-9402. DOI: 10.1029/2019JA027485. URL: <https://onlinelibrary.wiley.com/doi/abs/10.1029/2019JA027485>.
- [7] Bahco. *3/8" Square Drive Universal Joints*. 2021. URL: https://www.bahco.com/int_en/3-8--square-drive-universal-joints-pb_7766_.html (visited on 10/14/2021).
- [8] A. Cammarata, R. Sinatra, A. Rigano, M. Lombardo, and P. D. Maddio. "Design of a Large Deployable Reflector Opening System". In: 8.1 (2020), p. 7. URL: <https://www.mdpi.com/2075-1702/8/1/7>.
- [9] J. Chen. *An Introduction to the Double Pendulum*. 2008. URL: https://ir.canterbury.ac.nz/bitstream/handle/10092/12659/chen_2008_report.pdf;sequence=1.
- [10] R. Christy. *USSR - Luna 9*. The Mission of Luna 9. 2019. URL: <https://www.zarya.info/Diaries/Luna/Luna09.php> (visited on 11/04/2021).
- [11] S. Contant. "Design and Optimization of a Small Reusable Launch Vehicle Using Vertical Landing Techniques". MSc Thesis. Delft: TU Delft, 2019. URL: <https://repository.tudelft.nl/islandora/object/uuid%3A58cb0a6e-e9ac-4ce5-9051-5ddd863e98a8?collection=education>.
- [12] H. Doiron and G. A. Zupp. *A Mathematical Procedure for Predicting the Touchdown Dynamics of a Soft-Landing Vehicle*. 19710007293. Houston, TX, USA: NASA, 1971. URL: <https://ntrs.nasa.gov/citations/19710007293>.
- [13] R. L. Fusaro. "Lubrication of Space Systems". In: (1994), p. 28. URL: <https://ntrs.nasa.gov/api/citations/19940024896/downloads/19940024896.pdf>.
- [14] R. Gershman, E. Nilsen, and R. Oberto. "Europa Lander". In: *Acta Astronautica*. Selected Proceedings of the 4th IAA International conference on Low Cost Planetary Missions 52.2 (2003), pp. 253–258. ISSN: 0094-5765. DOI: 10.1016/S0094-5765(02)00164-9. URL: <http://www.sciencedirect.com/science/article/pii/S0094576502001649>.
- [15] M. R. Grover, B. D. Cichy, and P. N. Desai. "Overview of the Phoenix Entry, Descent, and Landing System Architecture". In: *Journal of Spacecraft and Rockets* 48.5 (2011). Publisher: American Institute of Aeronautics and Astronautics. eprint: <https://doi.org/10.2514/1.46548>, pp. 706–712. ISSN: 0022-4650. DOI: 10.2514/1.46548. URL: <https://doi.org/10.2514/1.46548>.

- [16] K. Hand, E. Maize, C. Phillips, R. Crum, and J. Krajewski. "Europa Lander Mission Concept Update". Jet Propulsion Laboratory, 2020. URL: https://www.lpi.usra.edu/opag/meetings/opag2020fall/presentations/Hand_6014.pdf.
- [17] S. Hara, R. Ito, M. Otsuki, Y. Yamada, T. Kubota, T. Hashimoto, H. Matsuhisa, and Keisuke Yamada. "Momentum-Exchange-Impact-Damper-Based Shock Response Control for Planetary Exploration Spacecraft". In: *Journal of Guidance, Control, and Dynamics* 34.6 (2011). Publisher: American Institute of Aeronautics and Astronautics, pp. 1828–1838. DOI: 10.2514/1.53786. URL: <https://arc.aiaa.org/doi/10.2514/1.53786> (visited on 10/13/2020).
- [18] Horizon 2020 Europe. *Technology readiness levels (TRL)*. 2014. URL: https://ec.europa.eu/research/participants/data/ref/h2020/wp/2014_2015/annexes/h2020-wp1415-annex-g-trl_en.pdf (visited on 11/19/2021).
- [19] D. C. Jegley, K. C. Wu, J. E. Phelps, M. J. McKenney, and L. Oremont. "Structural Efficiency of Composite Struts for Aerospace Applications". In: *Journal of Spacecraft and Rockets* 49.5 (2012), pp. 915–924. ISSN: 0022-4650. DOI: 10.2514/1.A32085. URL: <https://doi.org/10.2514/1.A32085>.
- [20] G. W. Kim, S. B. Choi, and J. Kang. "Dynamic Modeling and Spin Control for Deployment of Spin-Type Heliogyro Solar Sail". In: *Journal of Spacecraft and Rockets* 57.3 (2020), pp. 464–472. ISSN: 0022-4650, 1533-6794. DOI: 10.2514/1.A34582. URL: <https://arc.aiaa.org/doi/10.2514/1.A34582>.
- [21] Kinetrol. *Precision Rotary Dampers for Smooth Motion Control*. 2017. URL: https://www.kinetrol.com/pdf/cat/Rotary_Damper_2013_LR.pdf (visited on 06/30/2021).
- [22] D. Liang, H. Chai, and Tianzhi Chen. "Landing dynamic analysis for landing leg of lunar lander using Abaqus/Explicit". In: *Proceedings of 2011 International Conference on Electronic Mechanical Engineering and Information Technology*. Proceedings of 2011 International Conference on Electronic Mechanical Engineering and Information Technology. Vol. 8. 2011, pp. 4364–4367. DOI: 10.1109/EMETT.2011.6023924.
- [23] Q. Lin, Z. Kang, J. Ren, Q. Zhao, and H. Nie. "Investigation on soft landing impact test of scale lunar lander model". In: *Journal of Vibroengineering* 16.3 (2014). Number: 3 Publisher: JVE International Ltd., pp. 1114–1139. ISSN: 1392-8716. URL: <https://www.jvejournals.com/article/14949>.
- [24] C. Mallikarachchi and S. Pellegrino. "Deployment Dynamics of Ultrathin Composite Booms with Tape-Spring Hinges". In: *Journal of Spacecraft and Rockets* 51.2 (2014), pp. 604–613. ISSN: 0022-4650. DOI: 10.2514/1.A32401. URL: <https://arc.aiaa.org/doi/abs/10.2514/1.A32401> (visited on 10/13/2020).
- [25] Mars.nasa.gov. *Entry, Descent and Landing (EDL)*. NASA Science. URL: <https://mars.nasa.gov/mars2020/timeline/landing/entry-descent-landing/> (visited on 09/17/2021).
- [26] Mars.nasa.gov. *Mars 2020 Perseverance Rover*. NASA Science. URL: <https://mars.nasa.gov/mars2020/> (visited on 11/04/2021).
- [27] B. H. Mason, A. Zahn, K. Gould, and A. Przekop. "Design of a Manufacturing Demonstration Unit for a Composite Lunar Landing Gear Strut". In: *AIAA Scitech 2021 Forum*. 0 vols. AIAA SciTech Forum. American Institute of Aeronautics and Astronautics, 2021. DOI: 10.2514/6.2021-0569. URL: <https://arc.aiaa.org/doi/10.2514/6.2021-0569>.
- [28] S. Morikawa, H. Eguchi, Y. Maru, T. Kawano, M. Nohmi, and Shujro Sawai. "Evaluation of Landing Stability of Two-step Landing Method for Small Lunar-planetary Lander". In: *30th International Symposium on Space Technology and Sciences* (2017), p. 6. URL: https://issfd.org/ISSFD_2017/paper/ISTS-2017-d-069__ISSFD-2017-069.pdf.
- [29] NASA Space Science Data Coordinated Archive. *Viking 1 Lander*. NASA. 2021. URL: <https://nssdc.gsfc.nasa.gov/nmc/spacecraft/display.action?id=1975-075C> (visited on 09/22/2021).
- [30] National Aeronautics and Space Administration. *Structural Design and Test Factors of Safety for Spaceflight Hardware*. 2016. URL: https://standards.nasa.gov/sites/default/files/nasa-std-5001b_w_change_1.pdf (visited on 12/03/2021).

- [31] M. Nohmi and A. Miyahara. "Modeling for Lunar Lander by Mechanical Dynamics Software". In: *AIAA Modeling and Simulation Technologies Conference and Exhibit*. AIAA Modeling and Simulation Technologies Conference and Exhibit. San Francisco, California: American Institute of Aeronautics and Astronautics, 2005. ISBN: 978-1-62410-057-4. DOI: 10.2514/6.2005-6416. URL: <http://arc.aiaa.org/doi/10.2514/6.2005-6416>.
- [32] M. Orr. "Development of a Finite Element Model to Predict the Behaviour of a Prototype Wheel on Lunar Soil". PhD thesis. Clemson University, 2010. URL: https://www.researchgate.net/publication/258699047_Development_of_a_finite_element_model_to_predict_the_behavior_of_a_prototype_wheel_on_lunar_soil.
- [33] R.T. Pappalardo, S. Vance, F. Bagenal, B.G. Bills, D.L. Blaney, D.D. Blankenship, W.B. Brinckerhoff, J.E.P. Connerney, K.P. Hand, T.M. Hoehler, J.S. Leisner, W.S. Kurth, M.A. McGrath, M.T. Mellon, J.M. Moore, G.W. Patterson, L.M. Prockter, D.A. Senske, B.E. Schmidt, E.L. Shock, D.E. Smith, and K.M. Soderlund. "Science Potential from a Europa Lander". In: *Astrobiology* 13.8 (2013), pp. 740–773. ISSN: 1531-1074, 1557-8070. DOI: 10.1089/ast.2013.1003. URL: <http://www.liebertpub.com/doi/10.1089/ast.2013.1003>.
- [34] J.G. Park and L. Oliva. "Design and Analysis of a Damping System for Landing in Microgravity". PhD thesis. Milan: Politecnico di Milano, July 27, 2017. URL: <https://www.politesi.polimi.it/handle/10589/135615> (visited on 10/13/2020).
- [35] S. Pellegrino, S. Kukathasan, G. Tibert, and A. Watt. *Small Satellite Deployment Mechanisms*. 2000. URL: <http://www-civ.eng.cam.ac.uk/dsl/publications/TR190.pdf>.
- [36] J. C. Pohlen, B. D. Maytum, I. W. Ramsey, and U. J. Blanchard. *The Evolution of the Viking Landing Gear*. 1976. URL: <https://ntrs.nasa.gov/citations/19760021205> (visited on 10/15/2020).
- [37] W.F. Rogers. *Apollo Lunar Module Landing Gear*. 1972. URL: https://www.hq.nasa.gov/alsj/LM_Landing%20Gear1973010151.pdf.
- [38] L. Rongqiang, L. Changjie, D. Zongquan, and W. Chuang. "Design and selection of aluminum foam for impact damper of legged lunar Lander". In: *2008 2nd International Symposium on Systems and Control in Aerospace and Astronautics*. 2008 2nd International Symposium on Systems and Control in Aerospace and Astronautics. 2008, pp. 1–6. DOI: 10.1109/ISSCAA.2008.4776270.
- [39] M. Rozemeijer. "Launch Vehicle First Stage Reusability: a study to compare different recovery options for a reusable launch vehicle". In: (2020). URL: <https://repository.tudelft.nl/islandora/object/uuid%3A5cf403e0-5621-486c-8f41-6d0dbbe0f37f>.
- [40] A. Sahinoz. "Landing Gear Design and Stability Evaluation of a Lunar Lander". MSc Thesis. Sabanci University, 2012. DOI: 10.13140/RG.2.2.13160.83202. URL: https://www.researchgate.net/publication/338209202_Landing_Gear_Design_and_Stability_Evaluation_of_a_Lunar_Lander.
- [41] A. M. San Martin, E. D. Skulsky, N. Trawny, and A. Katake. "A Hazard Detection Sensor for Landing on Europa". In: (2018). URL: <https://trs.jpl.nasa.gov/handle/2014/48609>.
- [42] G. A. Scheglov and R. O. Lukovkin. "Dynamic crushing of spacecraft landing gear with crash legs". In: *Journal of Physics: Conference Series* 1348 (2019). Publisher: IOP Publishing, p. 012080. ISSN: 1742-6596. DOI: 10.1088/1742-6596/1348/1/012080. URL: <https://doi.org/10.1088%2F1742-6596%2F1348%2F1%2F012080>.
- [43] P.M. Schenk. "Slope Characteristics of Europa: Constraints for Landers and Radar Sounding". In: *Geophysical Research Letters* 36 (2009). URL: <https://agupubs.onlinelibrary.wiley.com/doi/full/10.1029/2009GL039062>.
- [44] T. M. Schmidt and P. Bhandari. "Thermal Design of a Europa Lander Mission Concept". In: *49th International Conference on Environmental Systems*. Boston: ICES, 2019. URL: <https://ttu-ir.tdl.org/bitstream/handle/2346/84424/ICES-2019-4.pdf?sequence=1>.
- [45] D. Sekulić and V. Dedović. "The Effect of Stiffness and Damping of the Suspension System Elements on the Optimisation of the Vibrational Behaviour of a Bus". In: *International Journal for Traffic and Transport Engineering* (2011), p. 14.

- [46] S.W. Sell, B.T. Cook, and M. E. Greco. "Touchdown System for a Europa Lander Concept". 14th International Planetary Probe Workshop. The Hague, 2017. URL: <https://trs.jpl.nasa.gov/bitstream/handle/2014/47973/CL%2317-2462.pdf?sequence=1&isAllowed=y>.
- [47] S. Seriani. "A New Mechanism for Soft Landing in Robotic Space Exploration". In: *Robotics 8.4* (2019). Number: 4 Publisher: Multidisciplinary Digital Publishing Institute, p. 103. DOI: 10.3390/robotics8040103. URL: <https://www.mdpi.com/2218-6581/8/4/103> (visited on 11/12/2020).
- [48] R. Slade and C. Brown. "A Large Self-Deploying Structure Concept For Space Telescope Missions". In: 14th European Space Mechanisms & Tribology Symposium. Constance, 2011, p. 8. URL: <https://www.esmats.eu/esmatspapers/pastpapers/pdfs/2011/slade.pdf>.
- [49] B. Szabó and I. Babuška. *Introduction to Finite Element Analysis: Formulation, Verification and Validation*. John Wiley & Sons, 2011. 412 pp. ISBN: 978-1-119-99348-3.
- [50] G. Tan-Wang and S. Sell. "Europa Lander Mission Concept Overview". Bellevue, WA, 2019. URL: <https://trs.jpl.nasa.gov/handle/2014/50950>.
- [51] Toray Composite Materials America. *Toray T800S Technical Datasheet*. Apr. 13, 2018. URL: <https://www.toraycma.com/wp-content/uploads/T800S-Technical-Data-Sheet-1.pdf> (visited on 09/14/2021).
- [52] S. Ulamec and J. Biele. "Surface elements and landing strategies for small bodies missions – Philae and beyond". In: *Advances in Space Research* 44.7 (2009), pp. 847–858. ISSN: 0273-1177. DOI: 10.1016/j.asr.2009.06.009. URL: <http://www.sciencedirect.com/science/article/pii/S0273117709003858>.
- [53] Y. Wang, R. Liu, H. Yang, Q. Cong, and H. Guo. "Design and Deployment Analysis of Modular Deployable Structure for Large Antennas". In: *Journal of Spacecraft and Rockets* (2015). DOI: 10.2514/1.A33127. URL: https://www.researchgate.net/publication/279805403_Design_and_Deployment_Analysis_of_Modular_Deployable_Structure_for_Large_Antennas.
- [54] R.G. Weixiong. "Preliminary Design of Reusable Lunar Lander Landing System". MSc Thesis. Lulea University of Technology, 2017. URL: <https://www.diva-portal.org/smash/get/diva2:1159285/FULLTEXT01.pdf>.
- [55] W.A.R. Wildvank. "Launch Vehicle Structural Mass Prediction Model". MSc Thesis. Delft: TU Delft, 2018. URL: <https://repository.tudelft.nl/islandora/object/uuid%3A3Abb943ec1-1a2a-462d-873e-05338b29235f?collection=education>.
- [56] L. Witte, R. Roll, J. Biele, S. Ulamec, and E. Jurado. "Rosetta Lander Philae – Landing Performance and Touchdown Safety Assessment". In: *Acta Astronautica* (2016). DOI: 10.1016/j.actaastro.2016.02.001.
- [57] X. Zhang and C. Zhou. "Dynamic analysis of spinning solar sails at deployment process". In: *Chinese Journal of Aeronautics* 30.5 (2017), pp. 1719–1728. ISSN: 1000-9361. DOI: 10.1016/j.cja.2017.08.006. URL: <http://www.sciencedirect.com/science/article/pii/S1000936117301838>.



Matlab Deployment Modelling Code and Extra Figures

A.1. Matlab Deployment Modelling and Landing Stability Tool

```
1 % Pietro Squillace, 5011116, Spaceflight, TU Delft %
2 % V6 MAIN Thesis Script, %
3 % With verified double pendulum algorithm for results gathering %
4 % 27/07/2021 %
5 %-----%
6 tic
7 clear all, close all, clc
8 format short g
9 %% Initialize output tables
10 T = []; % Table of outputs
11 P = []; % Table of leg coordinates
12 T_stability = []; % Table of stability
13 T_stress = []; % Table of stresses
14 T_deployment = []; % Table of Deployment
15 T_f7 = []; % Table of values for making the chart in figure 7
16 T_f9 = []; % Table of output values for figure 9
17 T_footprint=[];
18 %% Input parameters

20 m_pay = 517; % Payload mass, kg

22 rho_al = 2810; % Density of aluminium, kg/m^3

25 % Calculated area values
26 Ra = 40*10^(-3); % Outer radius of first leg element cylinder
27 ra = 33*10^(-3); % Inner radius of first leg element cylinder
28 A_l1 = pi*((Ra)^2-(ra)^2); % Calculated area of first leg element
29 A_l2 = A_l1;

31 g_eur = 1.315; % Gravitational force of Europa [m/s^2]

33 m_f = 0; % Footpad mass [kg]

35 max_dep_time = 45; % Maximum deployment time, a design constraint depending
   on burn time [s]
36 %% Deployment Modelling
37 % Starting with V5 of Deployment Modelling or a version of it with a smaller lander
38 %% Initialise Geometry (Design)
39 % Payload geometry (a fixed rectangle)
40 payload_x = [-0.5 0.5 0.5 -0.5 -0.5]; % X coordinates of 4 points
   making the payload rectangle
41 payload_y = [-0.25 -0.25 0.25 0.25 -0.25]; % Y coordinates of 4 points making
   the payload rectangle

43 sp_leg = [payload_x(1); payload_y(1)]; % Left leg starting point (bottom left
   corner of payload square)
44 sp_right_leg = [payload_x(2); payload_y(2)]; % Right leg starting point, bottom right
   corner of payload square

46 %% Deployment Modelling Inputs
47 % For Loops to be activated to find out model connections through
48 % sensitivity analyses
```

```

49     % for b = 10:5:60                                     % For loop for Joint damping [Nm/rad/
        s]
50     %for max_theta_1_1 = 270:5:350;                       % For loop for Cutoff deployment
        angle [rads]
51     % for l = 0.1:0.1:0.8
52     % for m2 = 6.5:0.5:11
53     % for m1 = 2:0.5:7
54     %for mul = 0.5:0.5:1

56     % Constants
57     max_theta_1_1 = 100 +180 ;                             % Cutoff deployment angle for joint
        between payload and 1st leg element[deg]
58     max_theta_1_1 = max_theta_1_1*pi/180;
59     max_theta_1_1_Deg = max_theta_1_1*180/pi;
60     %max_theta_1_2 = 290;                                 % Cutoff deployment angle for joint
        between leg elements [deg]
61     b = 20;                                               % Damping, [Nm/rad/s = kg/s]
62     n = 0.14;                                             % G forces [-]
63     g = n*9.81;                                           % Gravity acceleration [m/s^2]
64     l = 0.5;                                              % Length of leg element [m]

66     %m1 = l * A_l1 * rho_al;                               % Mass of each leg element, kg
67     m1 = 2;
68     m2 = m1+m_f;
69     %m2 = 8;
70     m_SC = m_pay + 8*m1;                                  % Whole SC mass, kg
71     %I = (1/3)*m1*l^2;                                     % Moment of inertia of cylindrical legs
        around the bob [kg mm^2]
72     mul1 = 0.5;                                           % Multiplier for position of COM
        throughout the leg assumption analysis
73     mul2 = 1-((m2-m_f)*l/2)/(m2));

75     % Starting angles [rad] and velocities [rad/sec]
76     theta0 = [240*pi/180 ; 0 ; 202.5*pi/180 ; 0 ; 120*pi/180 ; 0 ; 157.5*pi/180 ; 0 ]; % Left
        leg 1st element initial angle, initial velocity [rad/sec];

79     % Timeframe of deployment analysis
80     max_t = 130;                                           % Seconds after which
        computation finishes
81     n_intervals = (2.5*max_t);
82     tspan = linspace(0,max_t,n_intervals);                 % Timeline

84     % Legs computations
85     [t,results] = ode45(@(t,theta) chen_Odefunc(t,theta,b,g,l,m1,m2,mul1,mul2),tspan,theta0);

87     results_deg = round(180/pi*results);
88     % Plot of Initial leg configuration

90     % Left leg position
91     x1_1 = sp_leg(1) + l*sin(results(1,1));                % Horizontal position of first joint
        of first leg (left)
92     y1_1 = sp_leg(2) - l*cos(results(1,1));              % Vertical position of first joint of
        first leg (left)
93     x1_2 = x1_1 + l*sin(results(1,3));                   % Horizontal position of second joint
        of first leg (left)
94     y1_2 = y1_1 - l*cos(results(1,3));                   % Vertical position of second joint of
        first leg (left)
95     % Right leg position
96     x2_1 = sp_right_leg(1) + l*sin(results(1,5));        % Horizontal position of first joint
        of second leg (right)
97     y2_1 = sp_right_leg(2) - l*cos(results(1,5));        % Vertical position of first joint of
        second leg (right)
98     x2_2 = x2_1 + l*sin(results(1,7));                   % Horizontal position of second joint
        of second leg (right)
99     y2_2 = y2_1 - l*cos(results(1,7));                   % Vertical position of second joint of
        second leg (right)

101    figure(1)
102    hold on

104    plot(payload_x, payload_y,'k-')                       % Payload
        rectangle plot

106    plot(x1_1,y1_1,'Marker','O','color','r')              % Plot of 1st
        joint of left leg
107    plot([sp_leg(1) x1_1],[sp_leg(2) y1_1],'linewidth',0.5,'color','b') % Plot of 1st
        element of left leg
108    plot(x1_2,y1_2,'Marker','O','color','g')              % Plot of 2nd
        joint of left leg
109    plot([x1_1 x1_2],[y1_1 y1_2],'linewidth',0.5,'color','k') % Plot of 2nd
        element of left leg

```

```

111     plot(x2_1,y2_1,'Marker','O','color','r') % Plot of 1st
        joint of right leg
112     plot([sp_right_leg(1) x2_1],[sp_right_leg(2) y2_1],'linewidth',0.5,'color','b') % Plot of 1st
        element of right leg
113     plot(x2_2,y2_2,'Marker','O','color','g') % Plot of 2nd
        joint of right leg
114     plot([x2_1 x2_2],[y2_1 y2_2],'linewidth',0.5,'color','k') % Plot of 2nd
        element of right leg

116     xlabel('x')
117     ylabel('y')
118     title('Initial Leg Configuration With Legs Stowed Inside Lander Body')
119     axis equal
120     xlim([-0.6 0.6])
121     % hold off
122 }
123 %% Set while loop that shows a stop motion animation for the deployment of the landing legs
124 % Set conter (ct)

126 ct = 1;
127 i = ct;
128 ct_max = 1.5*n_intervals; % Maximum amount of iterations

130 while ct <= ct_max && results(i,1) <= max_theta_1_1

132     %|| results(i,3) <= max_theta_1_2 % Stopping criteria are maximum amount of counter
        steps and cutoff deployment angle
133     i=ct;
134 % Left leg loop
135     x1_1 = sp_leg(1) + l*sin(results(i,1)); % Horizontal position of first joint
        of first leg (left)
136     y1_1 = sp_leg(2) - l*cos(results(i,1)); % Vertical position of first joint of
        first leg (left)
137     x1_2 = x1_1 + l*sin(results(i,3)); % Horizontal position of second joint
        of first leg (left)
138     y1_2 = y1_1 - l*cos(results(i,3)); % Vertical position of second joint
        of first leg (left)

140 % Right leg loop
141     x2_1 = sp_right_leg(1) + l*sin(results(i,5)); % Horizontal position of first joint
        of second leg (right)
142     y2_1 = sp_right_leg(2) - l*cos(results(i,5)); % Vertical position of first joint of
        second leg (right)
143     x2_2 = x2_1 + l*sin(results(i,7)); % Horizontal position of second joint
        of second leg (right)
144     y2_2 = y2_1 - l*cos(results(i,7)); % Vertical position of second joint
        of second leg (right)

149 %% Plot of final leg configuration
150 %%{
151     figure(3)

153     hold on

155     plot(payload_x, payload_y,'k-') % Payload
        rectangle plot

157     plot(x1_1,y1_1,'Marker','O','color','r') % Plot of 1st
        joint of left leg
158     plot([sp_leg(1) x1_1],[sp_leg(2) y1_1],'linewidth',0.5,'color','b') % Plot of 1st
        element of left leg
159     plot(x1_2,y1_2,'Marker','O','color','g') % Plot of 2nd
        joint of left leg
160     plot([x1_1 x1_2],[y1_1 y1_2],'linewidth',0.5,'color','k') % Plot of 2nd
        element of left leg

162     plot(x2_1,y2_1,'Marker','O','color','r') % Plot of 1st
        joint of right leg
163     plot([sp_right_leg(1) x2_1],[sp_right_leg(2) y2_1],'linewidth',0.5,'color','b') % Plot of 1st
        element of right leg
164     plot(x2_2,y2_2,'Marker','O','color','g') % Plot of 2nd
        joint of right leg
165     plot([x2_1 x2_2],[y2_1 y2_2],'linewidth',0.5,'color','k') % Plot of 2nd
        element of right leg
166     title(['Final Leg Configurations'; [...
167         ' b = ',num2str(b),' Nm/rad/s', ...
168         ' CDA = ',num2str(max_theta_1_1_Deg-180),' Deg', ...
169         ' l = ',num2str(l),' m'...
170         ]
171     )
172     axis equal

```

```

173 %}
174 %% Reset counter in order to show path of landing legs deployment
175 % {
176 ct = 1;
177 i = ct;
178 while ct <= ct_max && results(i,1) <= max_theta_1_1
179 % || results(i,3) <= max_theta_1_2
180 i = ct;
181 % Left leg loop
182 x1_1 = sp_leg(1) + l*sin(results(i,1)); % Horizontal position of
183 % first joint of first leg (left)
184 y1_1 = sp_leg(2) - l*cos(results(i,1)); % Vertical position of
185 % first joint of first leg (left)
186 x1_2 = x1_1 + l*sin(results(i,3)); % Horizontal position of
187 % second joint of first leg (left)
188 y1_2 = y1_1 - l*cos(results(i,3)); % Vertical position of
189 % second joint of first leg (left)
190
191 % Right leg loop
192 x2_1 = sp_right_leg(1) + l*sin(results(i,5)); % Horizontal position of
193 % first joint of second leg (right)
194 y2_1 = sp_right_leg(2) - l*cos(results(i,5)); % Vertical position of
195 % first joint of second leg (right)
196 x2_2 = x2_1 + l*sin(results(i,7)); % Horizontal position of
197 % second joint of second leg (right)
198 y2_2 = y2_1 - l*cos(results(i,7)); % Vertical position of
199 % second joint of second leg (right)
200
201 % {
202 % Plot of Landing Legs path
203 figure(4)
204
205 hold on
206
207 plot(payload_x, payload_y, 'k-') % Payload
208 % rectangle plot
209
210 plot(x1_1, y1_1, 'Marker', 'O', 'color', 'r') % Plot of 1st
211 % joint of left leg
212 plot([sp_leg(1) x1_1], [sp_leg(2) y1_1], 'linewidth', 0.5, 'color', 'b') % Plot of 1st
213 % element of left leg
214 plot(x1_2, y1_2, 'Marker', 'O', 'color', 'g') % Plot of 2nd
215 % joint of left leg
216 plot([x1_1 x1_2], [y1_1 y1_2], 'linewidth', 0.5, 'color', 'k') % Plot of 2nd
217 % element of left leg
218
219 plot(x2_1, y2_1, 'Marker', 'O', 'color', 'r') % Plot of 1st
220 % joint of right leg
221 plot([sp_right_leg(1) x2_1], [sp_right_leg(2) y2_1], 'linewidth', 0.5, 'color', 'b') % Plot of 1st
222 % element of right leg
223 plot(x2_2, y2_2, 'Marker', 'O', 'color', 'g') % Plot of 2nd
224 % joint of right leg
225 plot([x2_1 x2_2], [y2_1 y2_2], 'linewidth', 0.5, 'color', 'k') % Plot of 2nd
226 % element of right leg
227
228 xlabel('x')
229 ylabel('y')
230 title({'Path of Landing Legs'; [' b = ', num2str(b), ', Gs = ', num2str(n), ', Max \theta_1 = ', num2str
231 (180/pi * max_theta_1_1 - 180)]})
232 %}
233 ct = ct+1;
234 %axis equal
235 %pause(0.05)
236 %hold off
237 %clf('reset')
238
239 end
240 %}
241 %% Deployment shock calculator
242 Final_Angular_Rates = results(ct, [2 4]) ; % rad/s, Angular rate of
243 % First and second deployment angles at end of deployment, when CDA is reached
244 Final_Angular_Accs = Final_Angular_Rates/tspan(2) ; % rad/s^2, Angular
245 % deceleration from previous state to 0
246 Acc_At_Tip_m_s2 = l*Final_Angular_Accs; % m/s^2, axial
247 % acceleration obtained by multiplying length with the above calculated angular deceleration
248 Acc_At_Tip_G = Acc_At_Tip_m_s2/9.81;
249 %% Outputs of Deployment Modelling
250 % Can be commented out if input is a table for sensitivity analyses
251 disp('-----')
252 fprintf('Inputs: gravity is %4.2f m/s^2, damping is %4.2f, m1 = %4.2f kg, m2 = %4.2f kg \n', g, b, m1, m2)
253 fprintf('Outputs: Deployment time = %4.4f s , theta1 = %4.2f degrees, theta2 = %4.2f degrees \n', tspan(
254 i), 180/pi*results(i,1)-180, 180/pi*results(i,3)-(180/pi*results(i,1)-180))
255
256 % Table to see different geometries when the maximum allowable angle is

```

```

235 % changed
236 P = [P; b max_theta_1_1 x1_1 x1_2 x2_1 x2_2 y1_1 y1_2 y2_1 y2_2]; % Table of
    coordinates of leg elements

238 % Table to see deployment time and footprint distance with differing max
239 % allowable deployment angles
240 T = [T; b max_theta_1_1 tspan(i) x2_2-x1_2];

243 %% Estimation of geometry parameters of spacecraft Landing System
244 % Estimation of physical parameters
245 % Payload centroid
246 [x_c_pay,y_c_pay] = centroid(polyshape(payload_x,payload_y)); % Estimation of centroid
    payload square [x,y]
247 %scatter(x_c_pay,y_c_pay,'filled','k','DisplayName','Payload Centroid')

249 [x_c_legs,y_c_legs] = centroid(polyshape([x1_1 x1_2 x2_1 x2_2],[y1_1 y1_2 y2_1 y2_2]));
250 % Leg centroid for whole leg system
251 %scatter(x_c_legs,y_c_legs,'filled','Displayname','Legs Centroid')

253 % Center of mass fo whole Spacecraft (calculated with 4 legs overall and 8 leg elements)
254 COM_x = (m_pay*x_c_pay + 8*m1*x_c_legs)/(m_pay + 8*m1); % horizontal position of
    SC center of mass
255 COM_y = (m_pay*y_c_pay + 8*m1*y_c_legs)/(m_pay + 8*m1); % vertical position of SC
    center of mass from origin of chart
256 COM_height = abs(y2_2 - COM_y); % COM height from lowest
    point of landing system

258 % Horizontal distances between leg tips and centroid (will then be used to calculate the stability
    criterion)
259 COM_leg1_tip_dist_x = COM_x - x1_2;
260 COM_leg2_tip_dist_x = x2_2 - COM_x;

262 % Store a value for footprint
263 footprint = x2_2-x1_2;
264 T_footprint = [T_footprint; footprint];

267 figure(2)
268 hold on
269 plot(payload_x, payload_y,'k-') % Payload
    rectangle plot

271 plot(x1_1,y1_1,'Marker','o','color','r') % Plot of 1st
    joint of left leg
272 plot([sp_leg(1) x1_1],[sp_leg(2) y1_1],'linewidth',0.5,'color','b') % Plot of 1st
    element of left leg
273 plot(x1_2,y1_2,'Marker','o','color','g') % Plot of 2nd
    joint of left leg
274 plot([x1_1 x1_2],[y1_1 y1_2],'linewidth',0.5,'color','k') % Plot of 2nd
    element of left leg

276 plot(x2_1,y2_1,'Marker','o','color','r') % Plot of 1st
    joint of right leg
277 plot([sp_right_leg(1) x2_1],[sp_right_leg(2) y2_1],'linewidth',0.5,'color','b') % Plot of 1st
    element of right leg
278 plot(x2_2,y2_2,'Marker','o','color','g') % Plot of 2nd
    joint of right leg
279 plot([x2_1 x2_2],[y2_1 y2_2],'linewidth',0.5,'color','k') % Plot of 2nd
    element of right leg

283 xlabel('x')
284 ylabel('y')
285 axis equal
286 title({'Deployment Stop Motion Animation of Landing Legs ';['b = ',num2str(b),' t = ',num2str(
    tspan(i)), 's, Gs = ',num2str(n),' Max \theta_1 = ',num2str(180/pi*max_theta_1_1-180),' Deg'
    ]})

288 %}

290 ct = ct+1;

292 saveas(gcf,['December_New_LS' num2str(i) '.png']);

294 % pause(0.08);
295 clf('reset')

299 end
300 %% Plots for Deployment Modelling Sensitivity Analyses
301 % 1) Angle Thetal variation wrt to time

```

```

302 % {
303     figure(5)
304
305     plot(t(1:ct),results((1:ct),1)); % Plot of angle
306         variation Theta1 wrt time
307
308     title('Theta1 Variation Over Deployment Time')
309     ylabel('Theta1 [rad]')
310     xlabel('time [s]')
311
312 % 2) Angle Theta2 variation wrt to time
313     figure(6)
314
315     plot(t(1:ct),results((1:ct),3)); % Plot of angle
316         variation Theta2 wrt time
317
318     title('Theta2 Variation Over Deployment Time')
319     ylabel('Theta2 [rad]')
320     xlabel('time [s]')
321 % }
322
323 % 3) Model connection #1 plot with scatter plot of deployment time variation when damping is changed
324 % {
325     figure(7)
326
327     hold on
328
329     if t(ct) > max_dep_time || y1_1 < y1_2 || 1000*(payload_y(1)-y1_2) < 200
330         scatter(b,t(ct-1),20,'r','x')
331     else %y1_1 > y1_2
332         scatter(b,t(ct-1),20,'b')
333     % else
334     %     scatter(b,t(ct),20,'r','x')
335     end
336
337     title('Joint Damping vs. Deployment Time Sensitivity Analysis')
338     ylabel('Deployment Time [s]')
339     xlabel('Joint Damping b [Nm/rad/s]')
340     grid on
341     T_f7 = [T_f7; b t(ct-1)];
342     %legend([max(ct) 1],'Output LS does not satisfy requirements','Output LS satisfies requirements')
343
344 % }
345 % 4) Model connection #2 plot with scatter plot of deployment time variation when Cutoff Deployment
346 % Angle is changed
347 % {
348     figure(8)
349
350     hold on
351     if t(ct) > max_dep_time || y1_1 < y1_2 || 1000*(payload_y(1)-y1_2) < 200
352         scatter(max_theta_1_1*180/pi-180,t(ct),20,'r','x')
353     else %y1_1 > y1_2
354         scatter(max_theta_1_1*180/pi-180,t(ct),20,'b')
355     % else
356     %     scatter(b,t(ct),20,'r','x')
357     end
358
359     title('CDA vs. Deployment Time Sensitivity Analysis')
360     ylabel('Deployment Time [s]')
361     xlabel('Cutoff Deployment Angle (CDA) [deg]')
362     grid on
363 % }
364
365 % 4) Model connection #3 plot with scatter plot of deployment time variation with footprint
366 % {
367     figure(9)
368     hold on
369     if t(ct) > max_dep_time || y1_1 < y1_2 || 1000*(payload_y(1)-y1_2) < 200
370         scatter(x2_2-x1_2,t(ct-1),10,'r','x')
371     else %y1_1 > y1_2
372         scatter(x2_2-x1_2,t(ct-1),10,'b')
373     % else
374     %     scatter(b,t(ct),20,'r','x')
375     end
376
377     title({'Deployment Time vs. Footprint Variation when changing CDA and Damping'; ...
378         [' l = ',num2str(1),' m']})
379     ylabel('Deployment Time [s]')
380     xlabel('Footprint [m]')
381     grid on
382 % }

```

```

383 % Model connection #2.1 plot with scatter plot of deployment time
384 % variation wrt leg mass
385 % {
386 figure(9)
387 hold on
388 if t(ct) > max_dep_time || y1_1 < y1_2 || 1000*(payload_y(1)-y1_2) < 200
389 scatter(m2,t(ct),10,'r','x')
390 else %y1_1 > y1_2
391 scatter(m2,t(ct),10,'b')
392 % else
393 % scatter(b,t(ct),20,'r','x')
394 end
395 title('Deployment Time vs. Leg Element Mass Sensitivity Analysis'; ...
396 [' b = ',num2str(b),' Nm/rad/s , CDA = ',num2str(180/pi * max_theta_1_1 - 180),' Deg'])
397 ylabel('Deployment Time [s]')
398 xlabel('2nd Leg Element Mass(+ Footpad) [kg]')
399 grid on

401 T_f9 = [T_f9; m1 m2 t(ct-1)];
402 % }

404 % Model connection #2.2 V1 plot with scatter plot of CDA
405 % variation wrt COM height (vertical) and footprint
406 % {
407 figure(10)
408 hold on
409 if t(ct) > max_dep_time || y1_1 < y1_2 || 1000*(payload_y(1)-y1_2) < 200
410 scatter(180/pi*max_theta_1_1-180,COM_height,10,'r','x')
411 else %y1_1 > y1_2
412 scatter(180/pi*max_theta_1_1-180,COM_height,10,'b')
413 % else
414 % scatter(b,t(ct),20,'r','x')
415 end

417 title('Sensitivity Analysis of CDA vs. COM Height')
418 ylabel('COM Height [m]')
419 xlabel('Cutoff Deployment Angle')

421 % V2 plot of model connection 2.2
422 figure(11)
423 hold on
424 if t(ct) > max_dep_time || y1_1 < y1_2
425 scatter(180/pi*max_theta_1_1-180,x2_2-x1_2,10,'r','x')
426 else %y1_1 > y1_2
427 scatter(180/pi*max_theta_1_1-180,x2_2-x1_2,10,'b')
428 % else
429 % scatter(b,t(ct),20,'r','x')
430 end

432 title('Sensitivity Analysis of CDA vs Footprint')
433 ylabel('Footprint [m]')
434 xlabel('Cutoff Deployment Angle')
435 % }

437 % Model connection #2.3 V1 plot with scatter plot of Leg length
438 % variation wrt COM height (vertical) and footprint
439 % {
440 figure(12)
441 hold on
442 if t(ct) > max_dep_time || y1_1 < y1_2 || 1000*(payload_y(1)-y1_2) < 200
443 scatter(l,t(ct),10,'r','x')
444 else %y1_1 > y1_2
445 scatter(l,t(ct),10,'b')
446 % else
447 % scatter(b,t(ct),20,'r','x')
448 end

450 title('Sensitivity Analysis of leg length vs. Deployment Time')
451 ylabel('Deployment Time [s]')
452 xlabel('Leg Element Length [m]')
453 grid on

455 % }
456 % {
457 % V1 of Model connection 2.3, with footprint variation wrt leg length
458 figure(13)
459 hold on
460 if t(ct) > max_dep_time || y1_1 < y1_2 || 1000*(payload_y(1)-y1_2) < 200
461 scatter(l,x2_2-x1_2,10,'r','x')
462 else %y1_1 > y1_2
463 scatter(l,x2_2-x1_2,10,'b')
464 % else
465 % scatter(b,t(ct),20,'r','x')
466 end

```

```

468     title('Sensitivity Analysis of leg length vs. Footprint')
469     ylabel('Footprint [m]')
470     xlabel('Leg length [m]')
471 }

473 % Model connection #2.3 V2 plot with scatter plot of Leg element mass
474 % variation wrt COM height (vertical) and footprint
475 %{
476 figure(14)
477 hold on
478 if t(ct) > max_dep_time || y1_1 < y1_2 || 1000*(payload_y(1)-y1_2) < 200
479     scatter(m1,COM_height,10,'r','x')
480 else %y1_1 > y1_2
481     scatter(m1,COM_height,10,'b')
482 % else
483     % scatter(b,t(ct),20,'r','x')
484 end

486     title('Sensitivity Analysis of leg element mass vs. COM Height')
487     ylabel('COM height [m]')
488     xlabel('Leg element mass [kg]')

490 % V2 of Model connection 2.3, with footprint variation wrt leg mass
491 figure(15)
492 hold on
493 if t(ct) > max_dep_time || y1_1 < y1_2 || 1000*(payload_y(1)-y1_2) < 200
494     scatter(m1,x2_2-x1_2,10,'r','x')
495 else %y1_1 > y1_2
496     scatter(m1,x2_2-x1_2,10,'b')
497 % else
498     % scatter(b,t(ct),20,'r','x')
499 end

501     title('Sensitivity Analysis of leg element mass vs. Footprint')
502     ylabel('Footprint [m]')
503     xlabel('Leg element mass [kg]')
504 }

506 % Sensitivity analysis (or assumption analysis #1 to prove the effect of
507 % the position of the leg element center of mass when it comes to
508 % deployment time
509 %{
510 figure(19)
511 hold on
512 scatter(mul,tspan(i))
513 title('Sensitivity Analysis of Deployment Time wrt Leg Center of Mass Position')
514 xlabel('Position of center of mass wrt to Total Length of Leg Element [-]')
515 ylabel('Deployment Time [s]')
516 legend('Center of mass in Geometric Center','Center of Mass at end of the Element')
517 ylim([3 5])
518 xlim([0 1.1])
519 grid on

521 }

523 %% Save matrix P of leg coordinates in an Excel table
524 P = double(P);
525 writematrix(P,'P.csv')

528 % end
529 %% Upload Landing System Geometry from Deployment Modelling
530 %Load geometry points from V5 Deployment modelling script (based on double
531 %penduli)
532 %{
533 for j = 1:height(P)
534 % Update matrix P for stability and landing analyses by from now on using the matrix Q
535 Q = P(j,3:10);

538 x1_1 = Q(1);
539 x1_2 = Q(2);
540 y1_1 = Q(5);
541 y1_2 = Q(6);

543 x2_1 = Q(3);
544 x2_2 = Q(4);
545 y2_1 = Q(7);
546 y2_2 = Q(8);
547 }

550 %% Sketch of geometry for visual checking of whether this is the same as V5 Deployment Modelling

```

```

551 % Sketcher of leg configuration when landing starts, or when deployment finishes

554 %{
555     figure(10)
556
557     hold on
558
559     plot(payload_x, payload_y, 'k-', 'DisplayName', 'Payload')
560                                     % Payload rectangle plot
561
562     scatter(x1_1, y1_1, 'r', 'DisplayName', '1st joint of left leg')
563                                     % Plot of 1st joint of left leg
564     plot([sp_leg(1) x1_1], [sp_leg(2) y1_1], 'linewidth', 0.5, 'color', 'b', 'DisplayName', '1st element of
565         left leg')
566                                     % Plot of 1st element of left leg
567     scatter(x1_2, y1_2, 'g', 'DisplayName', '2nd joint of left leg')
568                                     % Plot of 2nd joint of left leg
569     plot([x1_1 x1_2], [y1_1 y1_2], 'linewidth', 0.5, 'color', 'k', 'DisplayName', '2nd element of left leg')
570                                     % Plot of 2nd element of left leg
571
572     scatter(x2_1, y2_1, 'r', 'DisplayName', '1st joint of right leg')
573                                     % Plot of 1st joint of right leg
574     plot([sp_right_leg(1) x2_1], [sp_right_leg(2) y2_1], 'linewidth', 0.5, 'color', 'b', 'DisplayName', '1st
575         element of right leg')
576                                     % Plot of 1st element of right leg
577     scatter(x2_2, y2_2, 'g', 'DisplayName', '2nd joint of right leg')
578                                     % Plot of 2nd joint of right leg
579     plot([x2_1 x2_2], [y2_1 y2_2], 'linewidth', 0.5, 'color', 'k', 'DisplayName', '2nd element of right leg')
580                                     % Plot of 2nd element of right leg
581
582 }%
583
584 %scatter(COM_x, COM_y, 'filled', 'p', 'DisplayName', 'SC Center of Mass')
585
586 %legend
587 %{
588     xlabel('x')
589     ylabel('y')
590     title('Lander Configuration(s) for Stability Analysis')
591     axis equal
592     hold off
593 }%
594
595 %% Calculate stability of Landing System based on footprint size and inclination of the lander
596 for th = 0:5:60;
597
598     crit = abs((y2_2-COM_y)*tand(th));
599                                     % mm, Projected distance on horizontal axis of
600     COM Height,
601     crit1 = abs(x2_2);
602                                     % mm, Projected distance on vertical axis of
603     Footprint,
604
605     % If this distance is negative then the landing is impossible, therefore leading to failure
606     if crit1 > crit;
607         Y1stability = 1;
608                                     % Y1 = 1, landing
609         is stable based on trigonometry
610
611     else crit1 < crit;
612         Y1stability = 0;
613                                     % Y1 = 0, landing
614         is unstable based on trigonometry
615
616     end
617
618     T_stability = [T_stability; max_theta_1_1 th Y1stability];
619
620 }%
621 %% Landing Stability Plots
622 % This section will be used to output the plots for Model connections 4 and 6
623
624 % Following plot outputs the stability of different LS geometries at the
625 % angles from 0 to 80 degrees (on the x axis) and the different cutoff
626 % deployment angles (in the y axis)
627 %{
628     figure(11)
629
630     hold on
631     if Y1stability == 1 && y1_1 > y1_2 && 1000*(payload_y(1)-y1_2) > 200 ;
632                                     % If
633         stable at that soil inclination angle and possible as LS geometry
634         scatter(th, max_theta_1_1*180/pi-180, 25, 'b', 'DisplayName', 'S')
635     elseif Y1stability == 0 && y1_1 > y1_2 && 1000*(payload_y(1)-y1_2) > 200 ;
636                                     % If
637         unstable at that soil inclination angle but still possible as LS geometry
638         scatter(th, max_theta_1_1*180/pi-180, 25, 'r', 'DisplayName', 'X')
639     else
640         scatter(th, max_theta_1_1*180/pi-180, 20, 'r', 'x', 'DisplayName', 'Q') ;
641                                     % If
642         unstable and impossible as LS geometry

```

```

620     end
621     title('Landing Stability with Varying Soil Angle and CDA'; ...
622           [' b = ',num2str(b),' Nm/rad/s , Element Length = ',num2str(1),' m'])
623     ylabel('CDA [Deg]')
624     xlabel('Soil Inclination [Deg]')
625     grid on
626     %}
627 % Following plot outputs the stability of different LS geometries at the
628 % angles from 0 to 80 degrees (on the x axis) and the Footprint (in the y axis)

630 figure(12)

632     hold on
633     if Y1stability == 1 && y1_1 > y1_2      && 1000*(payload_y(1)-y1_2) > 200      ;           % If
        stable at that soil inclination angle and possible as LS geometry
634         scatter(th,footprint,25,'b')
635     elseif Y1stability == 0 && y1_1 > y1_2      ;           % If unstable at that soil inclination
        angle but still possible as LS geometry
636         scatter(th,footprint,25,'r')
637     else      ;           % If unstable and impossible as LS geometry
638         scatter(th,footprint,20,'r','x')

640     end

642     title('Landing Stability with Soil Angle and Footprint'; ...
643           [' b = ',num2str(b),' Nm/rad/s , Element Length = ',num2str(1),' m'])
644     ylabel('Footprint [m]')
645     xlabel('Soil Inclination [Deg]')
646     grid on
647     %}

649 %Following plot outputs the stability of different LS geometries at the
650 % angles from 0 to 80 degrees (on the x axis) and the Decelerating G forces (in the y axis)
651 % {
652 figure(13)

654     hold on
655     if Y1stability == 1 && y1_1 > y1_2      ;           % If stable at that soil inclination angle
        and possible as LS geometry
656         scatter(th,n,25,'b')
657     elseif Y1stability == 0 && y1_1 > y1_2      ;           % If unstable at that soil inclination
        angle but still possible as LS geometry
658         scatter(th,n,25,'r')
659     else;
660         scatter(th,n,20,'r','x')           % If unstable and impossible as LS geometry

662     end
663     title('Landing Stability with Varying Soil Angle and decelerating G forces')
664     ylabel('G Forces [-]')
665     xlabel('Soil Inclination [deg]')

667     %}

669 %Following plot outputs the stability of different LS geometries at the
670 % soil inclination angles (on the x axis) and the damping (in the y axis)
671 % {
672 figure(17)

674     hold on
675     if Y1stability == 1 && y1_1 > y1_2      ;           % If stable at that soil inclination angle
        and possible as LS geometry
676         scatter(th,b,25,'b')
677     elseif Y1stability == 0 && y1_1 > y1_2      ;           % If unstable at that soil inclination
        angle but still possible as LS geometry
678         scatter(th,b,25,'r')
679     else;
680         scatter(th,b,20,'r','x')           % If unstable and impossible as LS geometry

682     end
683     title('Landing Stability with Varying Soil Angle and Damping')
684     ylabel('Damping [Nm/rad/s]')
685     xlabel('Soil Inclination [deg]')
686     %}

688 %Following plot outputs the stability of different LS geometries at the
689 % soil inclination angles (on the x axis) and the Height of COM (in the y axis)

691 % {
692 figure(17)

694     hold on
695     if Y1stability == 1 && y1_1 > y1_2      && 1000*(payload_y(1)-y1_2) > 200      ;           % If
        stable at that soil inclination angle and possible as LS geometry

```

```

696         scatter(th,COM_height,25,'b')
697     elseif Ylstability == 0 && y1_1 > y1_2           ;           % If unstable at that soil inclination
        angle but still possible as LS geometry
698         scatter(th,COM_height,25,'r')
699     else;
700         scatter(th,COM_height,20,'r','x')           % If unstable and impossible as LS
        geometry

702     end
703     title({'Landing Stability with Varying Soil Angle and COM Height'; ...
704           [' b = ',num2str(b),' Nm/rad/s , Element Length = ',num2str(1),' m']})
705     ylabel('COM Height [m]')
706     xlabel('Soil Inclination [Deg]')
707     grid on
708 }

710 % Stability map of landing systems able to landing at values less than 15
711 % degrees and no more depending on COM height and Footprint
712 % {
713 crit15
714 figure(17)

716     hold on
717     if Ylstability == 1 && y1_1 > y1_2           ;           % If stable at that soil inclination angle
        and possible as LS geometry
718         scatter(footprint,COM_height,25,'b')
719     elseif Ylstability == 0 && y1_1 > y1_2           ;           % If unstable at that soil inclination
        angle but still possible as LS geometry
720         scatter(footprint,COM_height,25,'r')
721     else;
722         scatter(fooptint,COM_height,20,'r','x')           % If unstable and impossible as LS
        geometry

724     end
725     title('Landing Stability with Varying Soil Angle and COM Height')
726     ylabel('COM Height [m]')
727     xlabel('Footprint [m]')

729 }

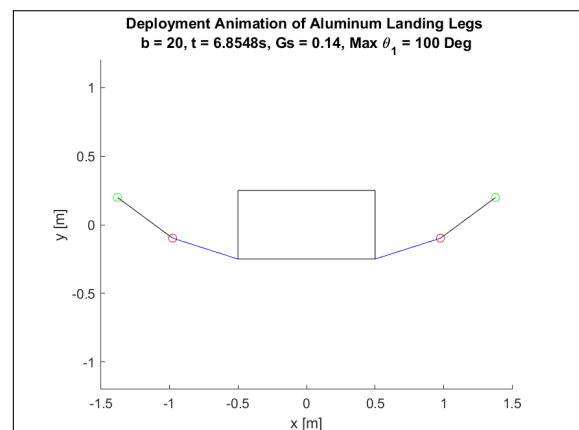
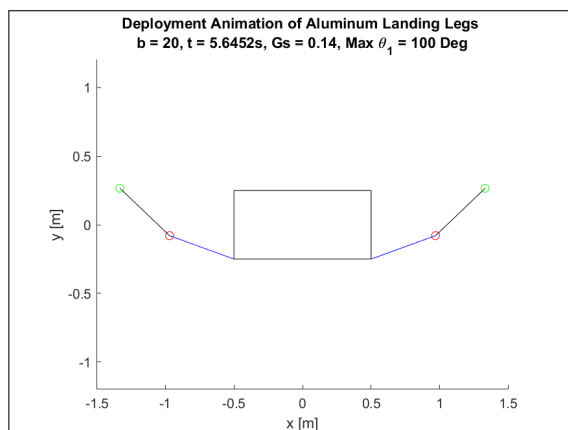
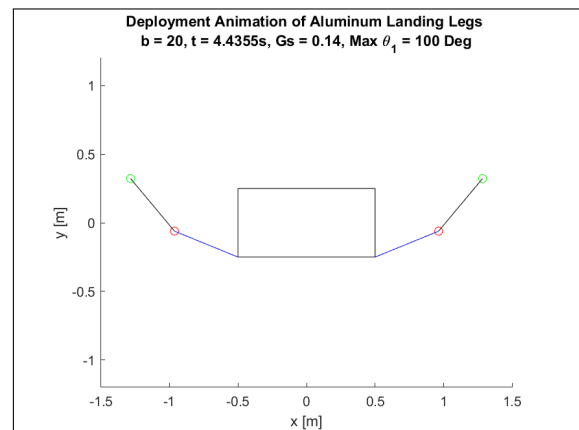
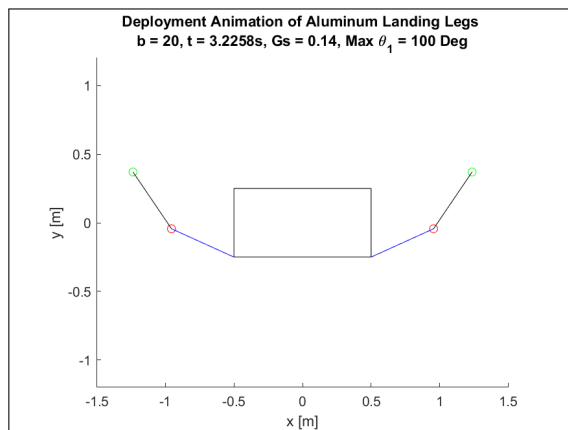
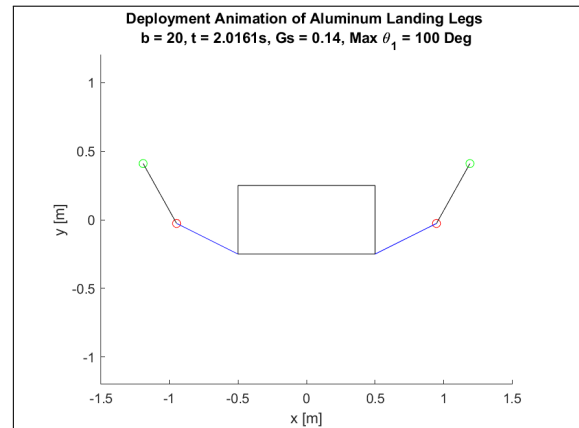
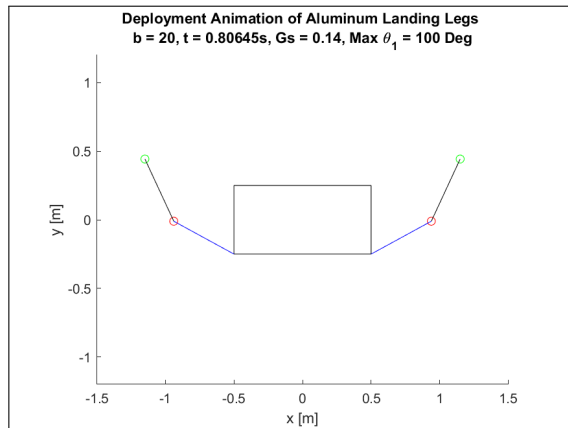
731 % }

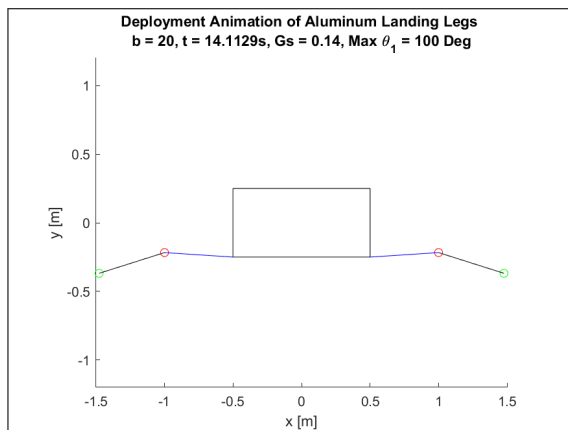
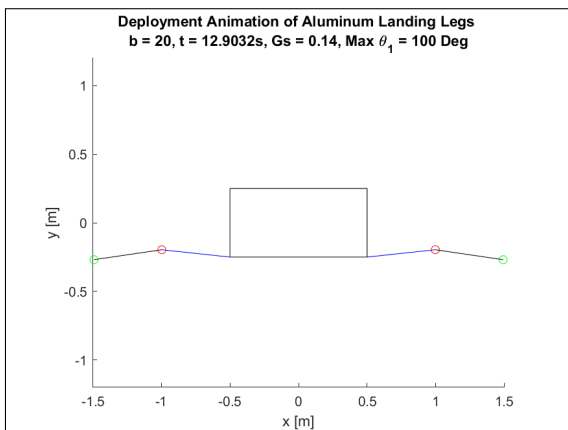
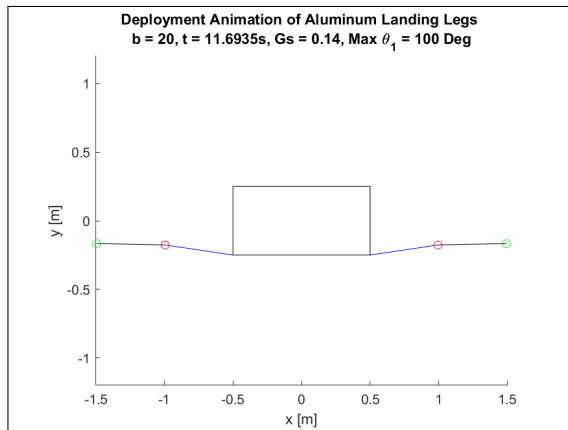
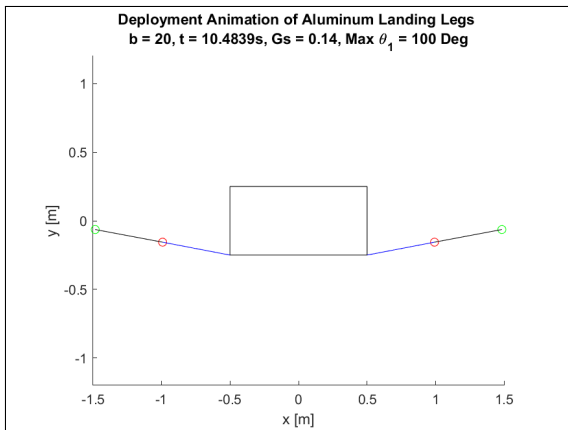
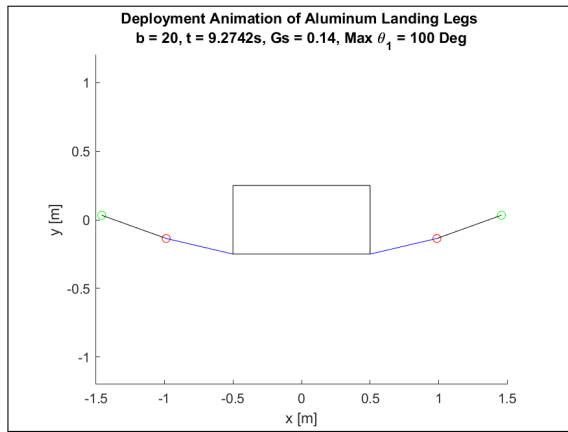
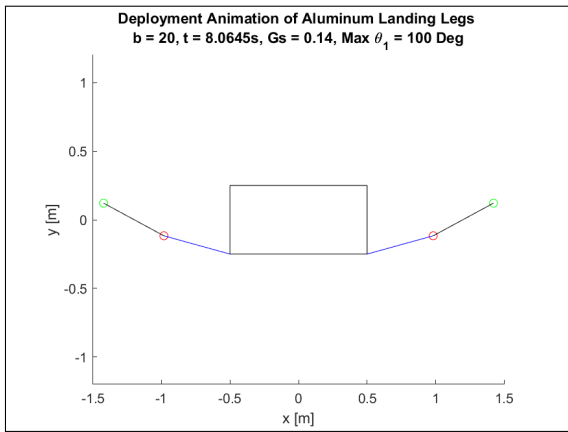
733 end
734 %end
735 % end
736 toc

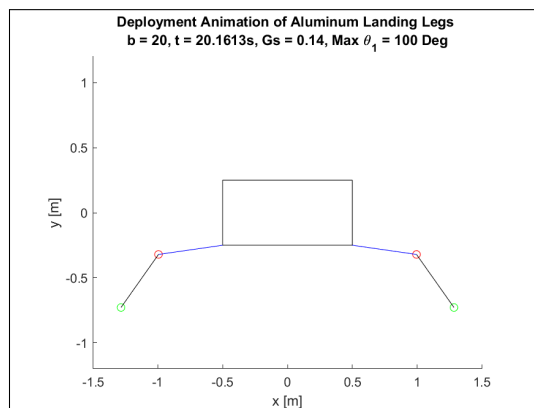
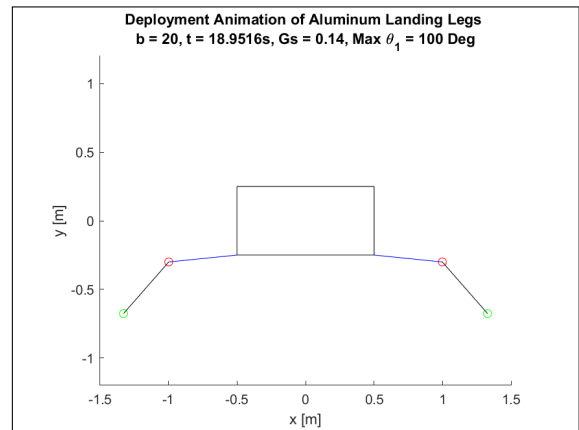
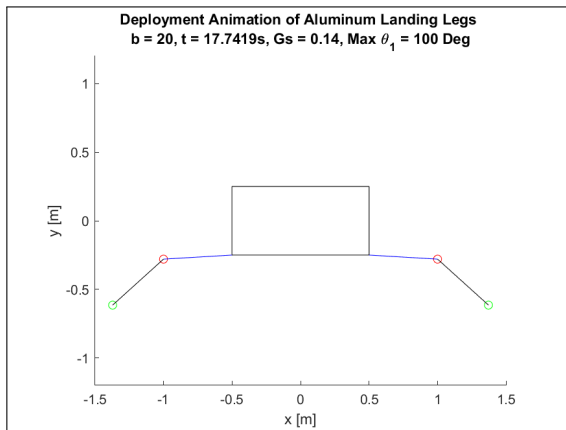
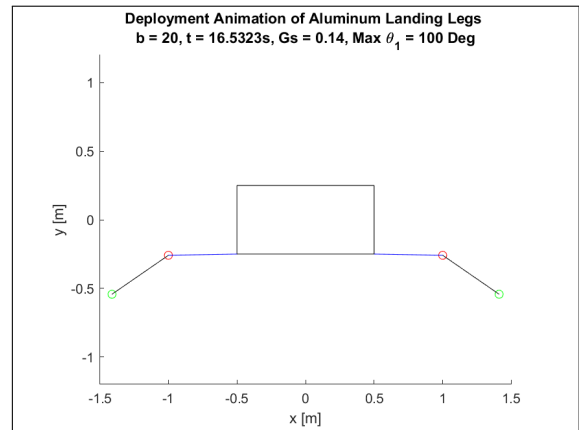
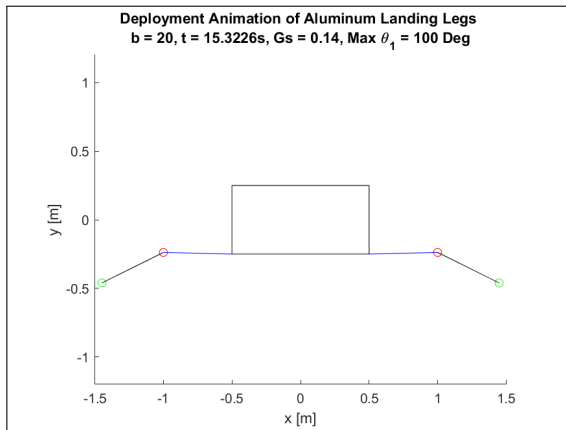
```

A.2. Detailed Deployment Modelling Figures

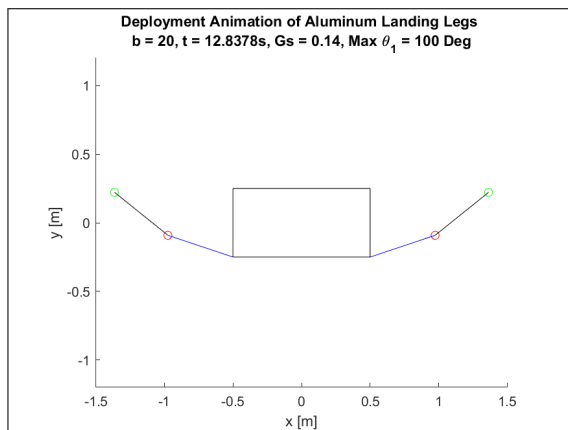
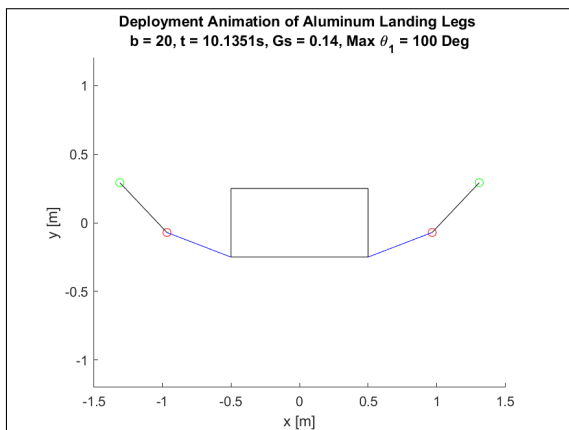
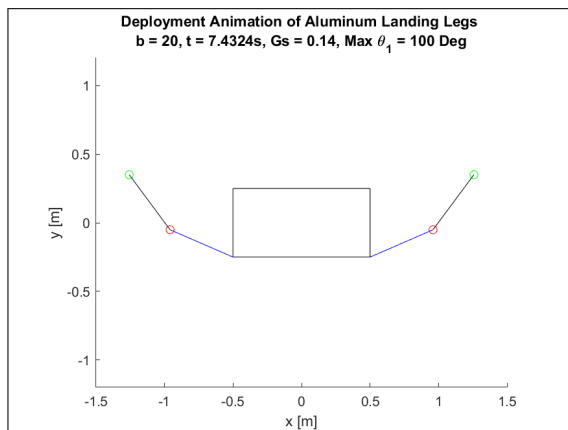
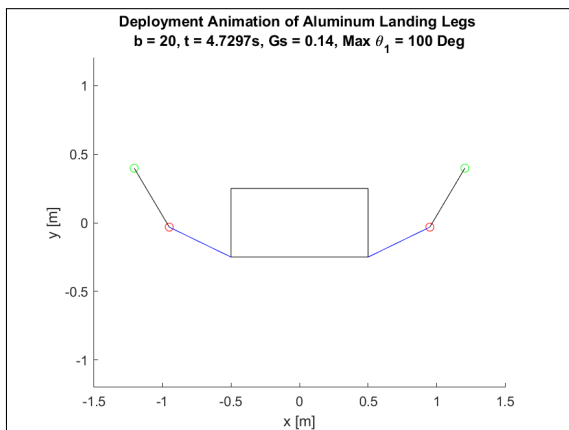
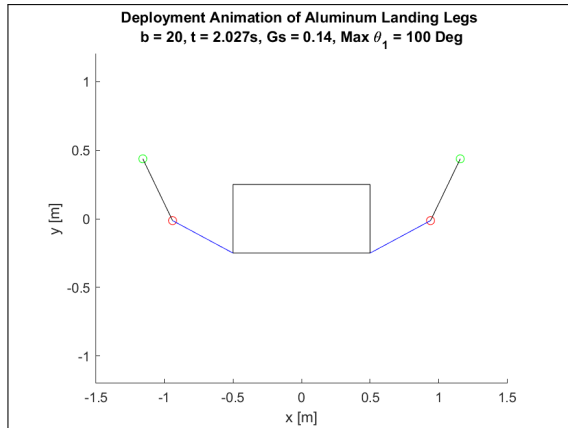
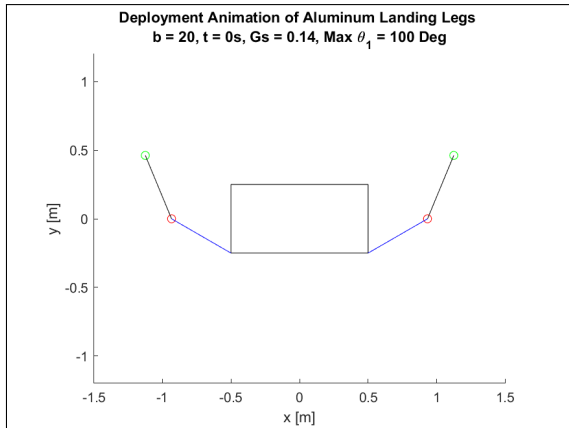
The following figures refer to the detailed deployment analysis studies performed and found the deployment modelling results section before the size change of the Europa Lander body was applied. They are placed in the appendix because they show the capability of the deployment to track the deployment dynamics of the landing system. However, in order not to fill these pages with images, they are filtered since the requirement of tracking positions of the landing legs every 0.5 seconds has already been fulfilled section 6.9. The following figures refer to the aluminum landing leg deployment:

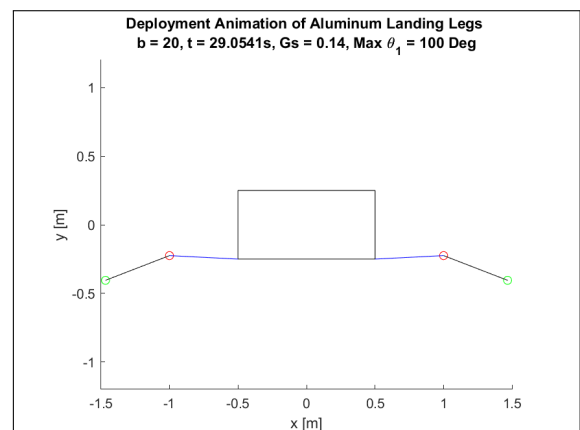
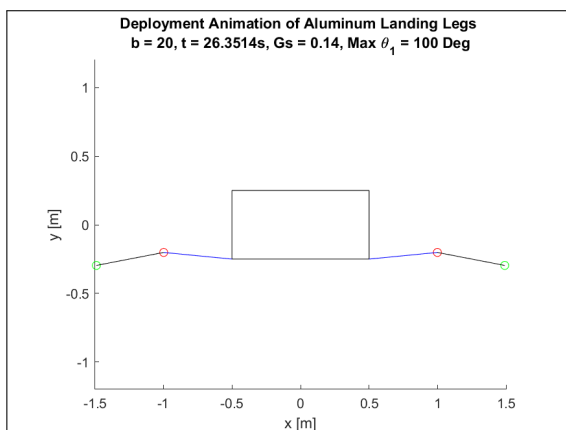
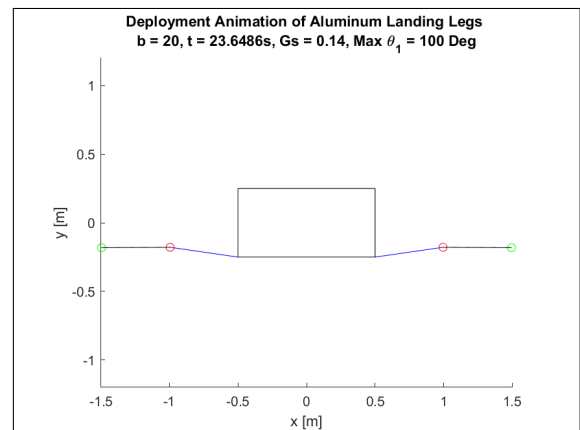
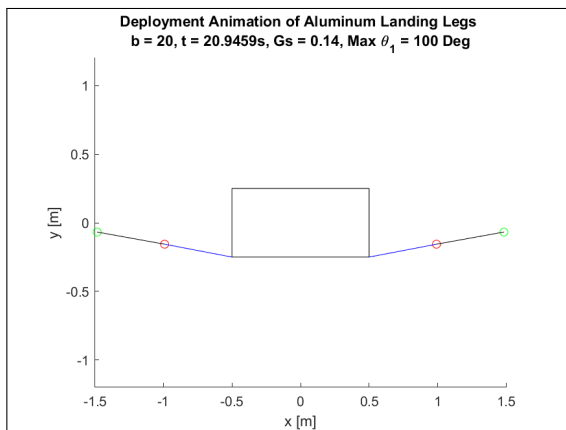
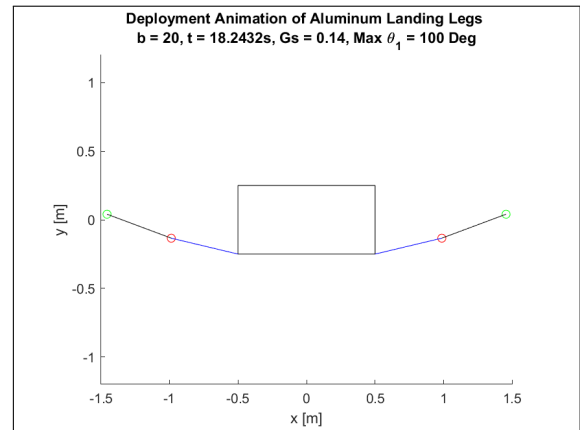
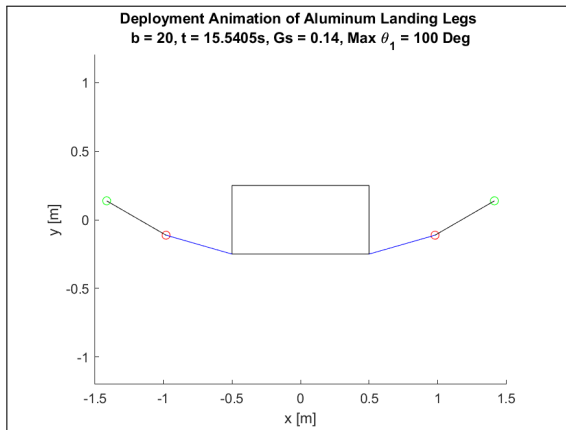


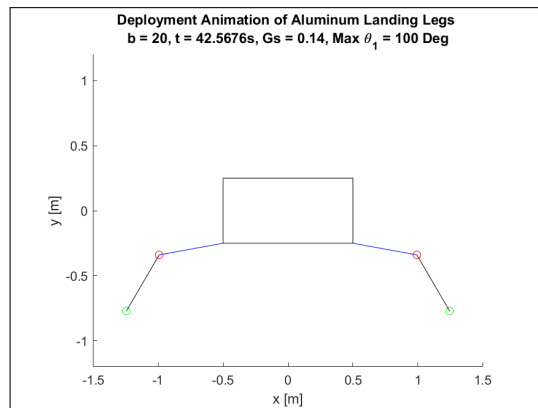
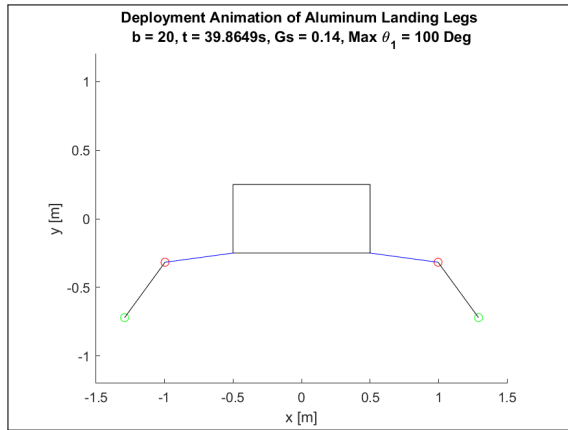
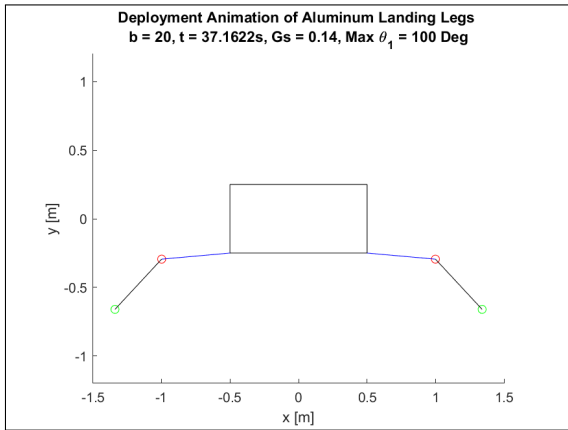
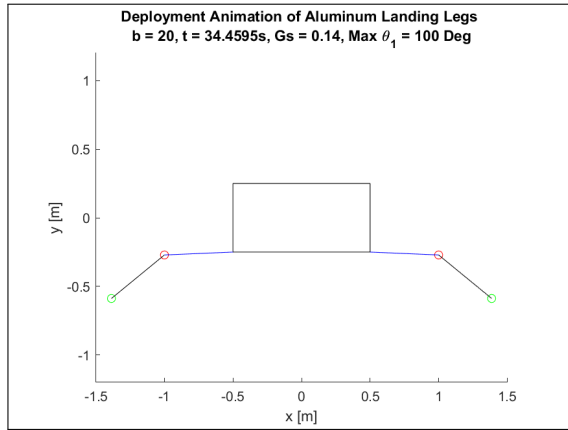
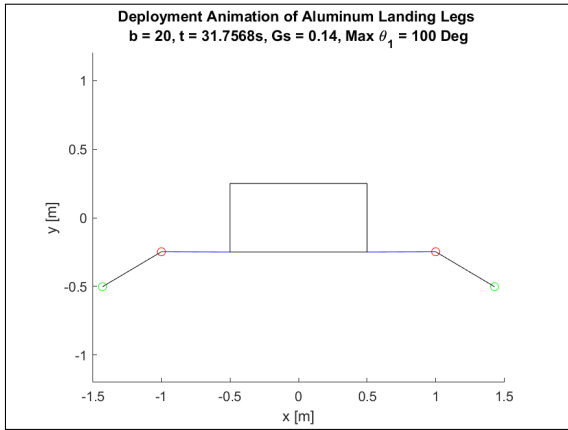




The following figures show the timeline of deployment of the CFRP landing legs:







A.3. Landing Performances vs. Increasing Payload Mass

Landing sensitivity analyses have also been performed. Because of the fact that these analyses have been performed on another design iteration of the landing system, that is not shown in the main matter of thesis, the values are not to be taken as related to the final values reached by the landing system geometry chosen for this thesis. What is important in the analyses of the following charts are the trends between inputs (lander mass) and outputs. The outputs visualised in the landing analyses with changing lander mass are listed as follows:

- Variation of maximum stress at the same location throughout one leg.

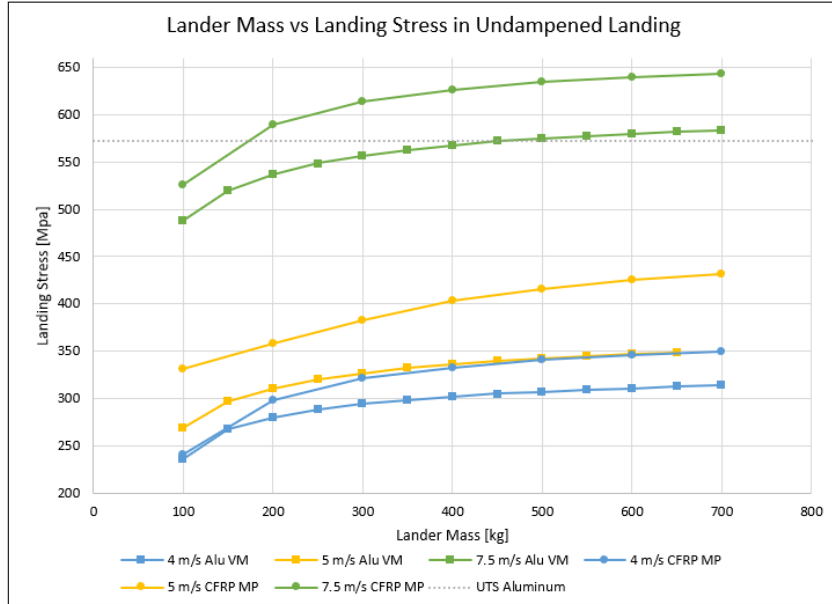


Figure A.1: Variation of internal stresses experienced by the landing leg with varying payload mass.

- Variation of maximum G forces experienced by the spacecraft COM.

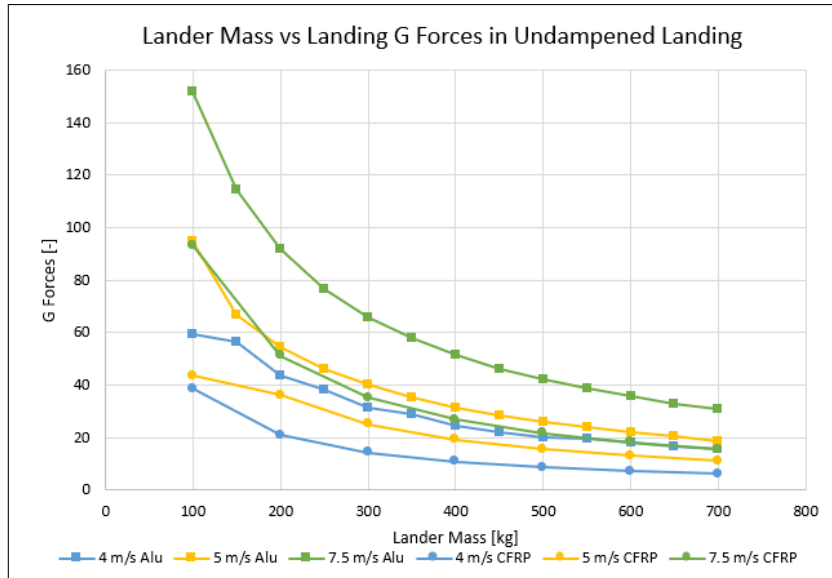


Figure A.2: Variation of G forces experienced by the lander COM with varying payload mass.

- Variation of amount of sinking inside the deformable soil experienced by the footpad (and the whole leg itself).

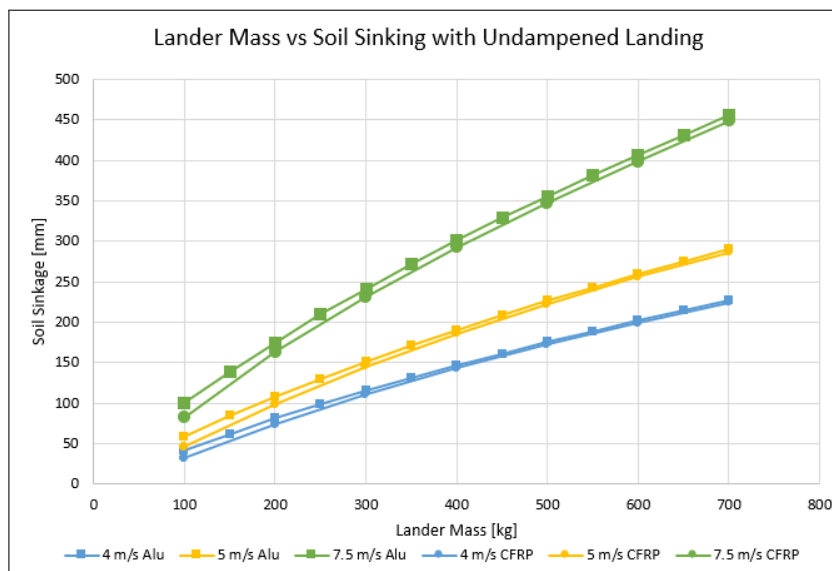


Figure A.3: Variation of soil sinkage experienced by the footpad with varying payload mass.

For these sensitivity analyses, the lander mass is varied from 100 to 700 kg, while keeping the structure of the legs (therefore keeping their mass) constant. The materials used are first Aluminum 7075 T6 and then the CFRP material and layup used by [27].

In Figure A.1, the variation of stresses with varying material, landing speed and payload mass is presented.

Stresses, in Figure A.1, are measured as Von Mises stresses for the aluminum legs and Maximum Principal stress in the case of the composite one. As can be seen by looking at Figure A.1, the stresses in the CFRP and aluminum landing legs increase in a non linear way when the payload mass is added to them. Furthermore, the stresses increase with an increase in landing velocity, which is expected due to the fact that the shock is higher at this setting. By looking at the same figure, furthermore, it can be seen that the only unsuitable designs from a load bearing point of view are the ones with the aluminum landing leg landing at 7.5 m/s and with a payload mass higher than 500 kg. The compressive strength of CFRP is not included in Figure A.1 as its value is way above the graph, at around 1490 MPa [51]. Because of this, all payload masses input in the simulations done to output Figure A.1 are suitable to be landed by the CFRP legs with the fixed geometry without exceeding the value of UTS of the composite layup.

The variation of G forces experienced by the lander's COM is found in Figure A.2.

In general, by looking at the trends of each of the curves in Figure A.2, it can be seen that, at all landing speeds and different materials, an increase in payload mass leads to a decrease in G forces. This is due to the fact that, as payload masses increase, also inertia increases and the higher amount of soil sinking, seen in the following graph means that energy is absorbed by the ground, rather than by shocks to the payload COM.

The variation of soil sinking with increasing payload masses is seen in Figure A.3.

As expected, the sinking in the soil increases with an increase in payload mass. Furthermore, it also increases with an increase in landing speed. This is because the inertia increases with increase in lander mass and increase in landing velocity and, the higher the inertia, the more the spring like deformable soil will be compressed, which is why a high soil sinkage happens in the cases of heavy and fast approaching landers.

B

Thesis proposal

DELFT UNIVERSITY OF TECHNOLOGY

MASTER THESIS AEROSPACE - SPACEFLIGHT

Thesis Proposal - Design and Analysis of a Deployable Landing System Concept for the Europa Lander

Author:

Pietro Squillace (5011116)

January 8, 2021



Contents

1	Introduction	2
2	Needs for the Europa Lander Landing System Deployable Concept	2
3	Research Questions and Project Goals	2
4	Stakeholders	3
5	Thesis Planning	4
A	Gantt Chart	11
B	Work Breakdown Structure	12

1 Introduction

In Space vehicles, a landing system is used by the spacecraft in order to decelerate, in the final stage of descent, on the target body until full stop. On top of that, a landing system needs to make sure that the decelerations imparted by hitting the planet's surface at a certain velocity don't damage internal components and also needs to make sure that the landed spacecraft is in a position that is upright so that it doesn't run the risk of tipping over.

Most of the landers that have been sent to other planetary bodies use landing legs [8]. The alternative is to use airbags, but this solution offers less accuracy over the landing spot because the bouncing is less predictable. When the lander is inside the launch vehicle and on its way to the planet, landing legs are in a stowed state in order to minimize the volume that they occupy. Once they are close to reaching the target of landing, the legs are deployed. Because of this, landing legs can be considered as deployable structures. One of the main aspects defining deployable structures is the mean of actuation. This is done by either unlocking the energy stored inside components, which is called the "passive" way. An example of how this is designed by unlocking the energy inside a pre-loaded spring or inside a coiled up Carbon Fibre Reinforced Polymer (CFRP) tape spring hinge [8]. Another way to deploy such a structure is by using actuators. This is called the "active" way because it uses energy from the power subsystem of the spacecraft and it uses a control strategy. The missions in which deployable structures are usually employed for are for orbiters and, in these, the spacecraft are subject to almost no forces when operations start. Because of this, it makes sense that the energy needed to actuate the deployables comes from within the spacecraft itself. On the other hand, the unique advantage that landers have is that they will have forces acting upon them because of their mission profile. These forces will be due to the decelerations imparted by the retro-rockets when the lander is slowing down to land on the target body's surface. This deceleration can be used to the lander's advantage when actuating the deployable landing system. The thesis will focus, as will be explained later, on the structural modelling and the deployment dynamics of the Europa Lander Landing System (ELLS) whose deployment is aided by the decelerating force of landing. The goal of this is to also show whether weight savings can be achieved compared to using a metallic structure and one that doesn't use the retro rockets to aid with the deployment actuation of the structure itself. In fact, it is hypothesized that if the landing system does not use the negative g forces of the retro rockets, then a thicker layout for the landing legs or actuators are needed in order to deploy them because more force to actuate the deployment will be needed. With the use of the negative g forces, some of the actuating force can still come from the material properties of composites and some of the force can come from the deceleration of the lander itself [5] [8]. From the modelling, design guidelines as to how to design such a structure, will be given.

2 Needs for the Europa Lander Landing System Deployable Concept

The needs as of why such a deployable structure shall be applied to an interplanetary lander's landing systems and the needs for the modelling that will be performed in the project will be explained in this section.

Using novel composite materials in order to design the Europa Lander Landing System will likely yield to a lighter design, since the current design envisions aluminum landing legs. A lighter landing system, in turn, makes it possible to have more mass allocated to the the payload of the lander which, in turn, leads to more scientific output coming from the mission. The problem with lighter landing legs is that the center of mass of the spacecraft is raised, which leads to a slightly less stable landing configuration. This is why, although not the main goal of this thesis, some degree of landing stability analyses will be done. According to [7], weight savings that can be reached by using composites in interplanetary structures can reach 20 %, this will be the goal of this study as well.

The landing system is the section of a lander that provides the capability of dissipating the shocks due to the touchdown of the lander with the planetary body. The ability of dissipating shocks and bring the spacecraft to rest is to be found in damping. Damping can be employed in different ways, for example by using viscous dampers or by using components that crush plastically. A compliant landing system design with parts that move relatively from each others, as is the case for a deployable concept, makes it more suitable for the landing shocks to be absorbed when compared to a rigid design. This is because each member making the landing system can contribute in a small way to by dissipating energy and, when combined, full dissipation of landing shocks can be reached.

3 Research Questions and Project Goals

In this section of the proposal, the research questions will be stated. A short description of the questions will

be added with some remarks of the goals envisioned for the project.
The main research question is as follows:

Is it possible to model the mechanics of deployment of a Soft Landing System for Interplanetary Landers where the deployment is actuated by the decelerating force of the engine module?

This research question makes it clear that the landing method taken in consideration is of the "soft" type, meaning that spacecraft models like penetrators are not part of the analysis that will be performed in this project. The other matter that needs to be highlighted about this research question is what is meant by the word "possible". It can be argued, in fact, that something that works in a model in a computational program does not necessarily work in real life. It is because of this that the modelling employed has to be verifiable and validatable. Verification and validation of the modelling will therefore be an important part of the project, as will be explained in Section 5. The model has to also be "landable" (only to a certain extent as this is not the focus of the project) so simplified landing analyses will be attached to the project as well. Therefore, if the model is verified and validated, if it is shown that indeed the landing system geometry and predicted structural performance makes it clear that it is possible to use the decelerating forces of the lander's boosters and if it is shown, with the landing modelling, that the lander will be able to stably land, this research question will be considered as fulfilled. Furthermore, it needs to be shown that no component within the ELLS will experience damages throughout deployment and landing. Because of this, the component within the landing system (which can be a straight element, a joint or an entire landing leg) that will experience the highest amount of stresses as will be shown by the modelling, will be input in Abaqus for a detailed Finite Element Analysis (FEA).

A sub-research question stemming from the previous research question will also be attached to the project:

What are the design guidelines that can be gathered from the model to then be used as inputs for the actual design of this specific type of deployable landing system concept that can achieve a 20 % weight decrease compared to the metal baseline and to a baseline that does not use negative g forces for deployment actuation?

Purely performing modelling of the deployment and landing of the ELLS is not enough for the project to be successful. If such a project would be made in a company, the stakeholder would want to see what types of design choices shall be employed in order to come up with a design that behaves in an identical fashion as the one in the mode. Because of this, the other goal of the project is to offer a series of design information needed to manufacture the structure modelled computationally.

The concept that will be studied is the articulated mast design. In this, a truss like structure with parts moving and sliding relative to each others and that open up like a pantograph is going to be designed in Matlab using a similar approach to that used in [10]. After the midterm review, the concept will be either refined or a new concept is going to be studied. This new structure is going to be idealised as a series of rotational springs and dampers and a series of straight beams. The rotational spring simulate the deploying moment of tape spring hinges while, the straight beams, simulate the presence of non deformable straight elements. This model is also called Multiple Particle Approximation Method as it was used in [1].

The 20 % weight saving goal comes from the need for more scientific output as written in Section 2. The weight saving comes from using a composite structure and not metal as is the case with the current ELLS concept [8] and by having no actuators or a thinner layout by using the negative g forces of deceleration as aid for the actuation of deployment.

4 Stakeholders

In this section of the thesis proposal, the interests in the thesis project from different parties is going to be laid out and the parties themselves are going to be listed. The stakeholders are:

- The structural Engineer. Which, for the thesis, can be identified in Prof. Chiara Bisagni. Since this is a project that will involve a high amount of structural modelling, Prof. Bisagni will be the one to review the matters related to the deployment modelling. Furthermore, the interest from ASM department in deployable structures will be fulfilled by the giving out of the design guidelines to design a lighter, self deployable landing system.
- The System Engineer. Which, for the thesis, can be identified with Prof. Barry Zandbergen. The System Engineer is interested in the application, in this case the Europa Lander and what are the steps to be taken to design the best solution for the ELLS. One way to understanding what is the best solution is by

comparison with other solutions. Which is why, throughout the thesis, 3 models are going to be made. The first one will be a truss like articulated mast similar to that used for the modular synthetic aperture radar antenna design in [10]. The second one, which will be considered as the baseline, will represent the current version of the ELLS with non self deployable but compliant aluminum landing legs [6]. And the last one, which will be decided at the midterm review whether it will be done, is one that uses CFRP tape spring hinges to deploy the landing legs, similar to how it was done in [1] for the design of a deployable solar sail. Performance indicators that will be used to compare these are found in Section 5. If time allows it, it is also desired to come up with a model that relates the mass of the landing system with the mass of the landable payload. This is done in the case it is desired to scale up (or down) the Europa Lander.

A preliminary list of requirements identified for the Landing System of the Europa Lander are listed in Table 1.

ID	Requirement
LS-PAY-001	The landing system shall support a payload of maximum 520 kg
LS-PAY-002	The decelerations imparted by the LS to the Payload shall not exceed 20 g
LS-PAY-003	The payload segment of the rover shall be simplified to a square (for 2D simulations) and to a cube (for 3D ones)
LS-LAN-001	The Landing System shall bring the lander to a stop from a maximum vertical velocity of 10 m/s
LS-LAN-002	The landing system shall provide a stable landing for slopes in between -15 and 15 degrees
LS-LAN-003	The landing system shall provide a stable landing on a soil that has comparable properties (stiffness and damping) to that of ice
LS-LAN-004	The stress due to landing in all landing system members made of composite materials shall never exceed the UTS of the material
LS-LAN-005	The peak deceleration of landing shall happen within the first second of shutdown
LS-LAN-006	The horizontal maximum velocity of the lander shall be of maximum 2 m/s without which tipping happens
LS-LAN-007	Landing success maps shall show a 99% success rate for all possible conditions offered by the simplified European Surface Model
LS-DEP-001	The deployment time of the landing system shall be of maximum 1 minute
LS-DEP-002	The landing system deployment shall not make use any actuator to aid in its motion
LS-DEP-003	The shocks due to landing system locking itself in position after deployment shall not exceed 20 Gs
LS-DEP-004	Deployment of the landing system shall be started by the retro rockets of the lander firing to slow down during the approach to the designated landing spot on Europa
LS-DEP-005	Deployment of the LS shall not be actuated by the loads, vibrations and accelerations of the launch vehicle at launch
LS-DEP-006	Deployment of the LS shall not be actuated by any possible attitude and trajectory adjustment that the spacecraft will go through on its way to Jupiter's SOI and then Europa
LS-DES-001	The landing system shall not exceed 6% of the whole lander mass.

Table 1: Preliminary ELLS requirements table. Abbreviations stand for: Landing System (LS), Payload (PAY), Landing (LAN), Deployment (DEP) and Design (DES).

5 Thesis Planning

Regarding the project planning in general, the project will work in 2 rounds. The first one will be about showing in a high level and simplified way that the articulated concept for the deployable ELLS can indeed be actuated by the decelerations imparted by the retrorockets before landing. In this section of the work, simplified 2-dimensional deployment and landing analyses can be done. This should last all January and February.

Once there is a good understanding of the simplified deployment and landing models, a review session can be agreed upon between all stakeholders of the project to review preliminary results. The review session can happen at the beginning of March and can be the so called "Midterm Review", as envisioned by the Aerospace MSc Thesis guidelines.

After this review session, the analyses can become more refined by either switching to 3-dimensions or by refining the simplified analyses performed before the review or by adding a new concept to be analysed that uses the

CFRP tape spring hinges as landing legs. This should last for all March and April. May will be used to perform the analysis of results and FEA until mid June. The second half of June will be used to finalise the writeup of the report and hand it in.

In this section of the proposal, the different work packages envisioned to be needed for the success of the project will be listed and explained. An estimation of working and buffer time for each work package will also be included. Buffer time can be used to both account for unpredictable matters (for example longer than predicted modelling time) and to write documentation on the steps taken in that work package in order to simplify the final project writeup.

A Gantt Chart and a Work Breakdown Structure are provided respectively in Sections A and B.

The planning above is divided in sections which are chronologically in order. The following list divides the planning in work packages:

1. **WP1: Come up with requirements that dictate and constrain the design of the deployable landing system and the capabilities of the script.** Structural requirements can be based on the real requirements identified by the Europa Lander missions team in [3] or from previous lander missions. Performance parameters such as deployment time, stresses during deployment and other matters will be part of capabilities of the script and will be dictated by requirements.
Approximate time for this work package: 1 week + 0.5 buffer time.
Percentage of time allotted with respect to total time for the project: 5 %.

2. **WP2: Find suitable models for the deployment script and landing scripts.** As written before, it will be likely that 2 concepts of the Europa Lander Landing System will be analysed in the project: the truss like articulated mast and the CFRP tape spring hinges concepts. For these 2 concepts, suitable matlab models have to be used. By looking at literature, 2 models have been identified that can be input in Matlab and can simulate the behaviour of these types of concepts. For the articulated concept, the so called "Stickman model" found in [11] will be used. In the article, the model is used to assess the differences in landing stability when different leg geometries and stiffness parameters are loaded into the simulation environment. An example of a landing system geometry loaded in the article is seen in Figure 1:

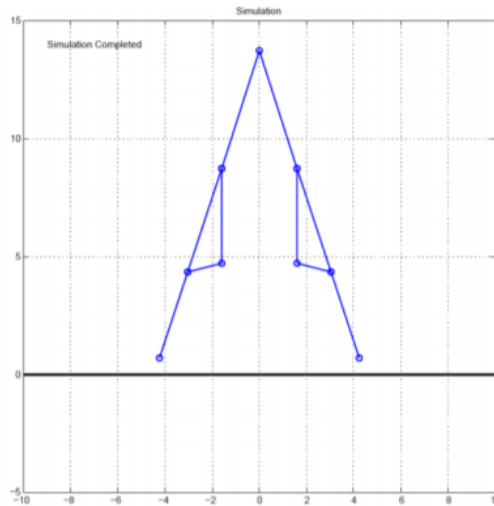


Figure 1: Simplified model of a lander used for landing analyses in [11].

This model is useful for the landing stability section of the project. However this does not fulfill the requirements that would be needed for the deployment modelling section of the project. To make it useful for the deployment modelling section of the project, the geometry will have to be tweaked and made moveable. The way the geometry is edited and made moveable is found in [10]. In this article, a 28 metres long modular synthetic aperture radar antenna is developed and the deployment modelling of this is explained. The modelling of deployment, in this article, is done by kinematically constraining the movement of the beam elements and joints. This can be done by developing a Matlab algorithm for which the inputs are

the length of the members of the truss structure and the angles that the elements have relatively between each others. Some of the angles will be variables in order to allow for deployment to happen.

After the review, it is possible that a new concept will be made. This concept will be a legged landing system that uses CFRP tape spring hinges in order to have the legs folded when stowed. When released, the legs will open up in a similar way to the bending of a carpenter's tape. The modelling that will be used will be similar to that employed by the JAXA Ikaros mission to model the deployment of the composite booms guiding the solar sail deployment [1]. In other words, the boom will be designed using a multiple-particle-approximation method. In here, the leg will be divided into multiple elements that will be idealised as linear springs, in order to have a way to model the leg stiffness, and as rotary springs, in order to have a way to model their behaviour with regards to the relation between straightening moment and angle of deployment. A diagram that shows how one of these booms was modelled is shown in Figure 2.

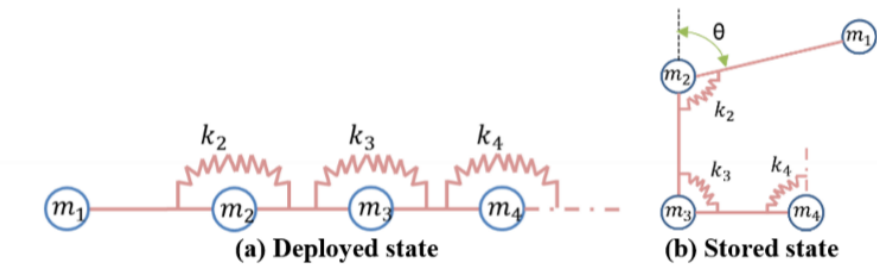


Figure 2: Multi Particle Approximation Method (MPAM) used to model the deployment mechanics of a composite solar sail foldable boom [1]

The way this model will be implemented in Matlab will be by using the *Simscape* toolbox [9]. This toolbox is used to model multi body systems, as will be the case for the latter landing system concept. Other models to be chosen are: 1 for the modelling of the CFRP material properties, for which stiffness and strength properties will be the focus of the model; and the other one for the Europa surface conditions, for which only terrain angles and soil properties can be the focus of the model.

Approximate time for this work package: 1 week of work + 0.5 weeks of buffer time.

Percentage of time allotted with respect to total time for the project: 5 %.

- WP3: Simplified deployment modelling.** The first matter that will be embedded in the script will be the landing system geometry. This will be done using the kinematically locked model found in [10] and it will be shown using the stickman model in [11] and both discussed in the work package description. The articulated landing system can be simplified as a series of beams that are attached by joints with selectable degrees of freedom. Joints with translational degrees of freedom will lead two connected beams to slide on each others. Joints with rotational degrees of freedom will lead to beams rotating in from one another as if they are connected with a pin. For legged landers, simple composite landing legs that can bend similarly to a carpenter tape will be designed using the multi particle approximation method. Subsequently, a section on modelling the deployment of the structure due to the negative g forces will be present. In order to implement the fact that the landing system will have to follow the direction of a deceleration imparted upon them, a simple gravity model will be employed. For a simple gravity model, it is meant one with a constant gravity acting on the lander. In this model, the spacecraft body will remain stationary and the landing system components, which will have their own masses, will be subject to gravity. Because of this, they will "fall" from a stowed (or packed) configuration around the lander's body to the final, desired configuration. The simplified landing system model will be made of slender members (or beams) which will correspond, in real life, to the landing struts. Struts will have connections in between them and also with other components such as with the lander's body and with the footpad. These connections will be modelled as joints.

In this section of the work, a script to track the change of position of the lander's COM due to the change in shape of the landing system during deployment will also be added. Furthermore, a section to track the amount of stresses present in each member of the LS will also be added.

The inputs in this section are:

- Accelerations imparted by retrorockets, assumed to be at 800N as seen in the actual concept of the Europa Lander [3],
- Stowed configuration of the LS,
- Material making the LS, in the case of this project, a space grade carbon fibre,
- Length of each member making the LS,
- Angles in between different members of the LS.

The outputs desired from the deployment modelling script will be:

- Stress in all components making the LS,
- Deployment time,
- Undesired clashing of components,
- Configuration of LS once deployment is done,
- Mass of the landing system,
- Calculator for change in COM with the deployment of the landing system.

In [10], the antenna reflector is deployed with the use of actuators. In the case of this project the structure will be deployed through the use of negative g forces. The simplified deployment model that will be developed in this section of the thesis will help answering the research question because first it will show whether it is possible to deployable a landing system using negative g forces and, secondly, the weight of the landing system without actuators will represent the save in weight achieved with this novel approach to deployable landing systems. However, the project must still go through other steps because the design has to be "landable", which will be proven with some of the following work packages.

Approximate time for this work package: 3.5 weeks of work + 1 week of buffer time.

Percentage of time allotted with respect to total time for the project: 15 %.

4. **WP4: Simplified landing modelling.** After making the preliminary deployment modelling script, a section will be added on landing stability analyses. This section will be simplified since, at this point, only terrain angles and soil stiffness are going to be taken into analysis to virtually simulate the Europa surface environment. The stability criterion that will be applied is the one devised in [2]. The same models used for inputting the deployable geometry for the previous section will be used in this script as well. The only difference will be that, for the landing stability analyses, the LS will already be in the deployed state rather than in a deploying state. Which means that the LS will be stiff and not subject to high degrees of deformation, as it happened during deployment. Furthermore, also in this section, a calculator to compute stresses in each member of the LS due to landing shocks will be attached.

The inputs in this step are as follows:

- Europa surface conditions: terrain angles in between ± 15 degrees and soil stiffness of 182 MPa [4],
- Landing velocities, both vertical and horizontal,
- Lander's mass,
- Landing system deployed geometry: footprint, height, angle between lander and LS, stiffness and damping properties of the LS.

The outputs from the landing stability and analysis script will be:

- Landing success/failure maps. These are indicators of how often does a certain LS geometry lead to landing success at 2 certain landing conditions, for example landing velocity and terrain angle.
- Stresses due to landing shocks in each component.

Approximate time for this work package: 2 weeks + 1 week of buffer time.

Percentage of time allotted with respect to total time for the project: 10 %.

5. **WP5: Validation & Verification of simplified modelling.** For landing analyses, the behaviour encountered in previous landings is going to be compared to the behaviour that will be encountered in the self made algorithm. If data related to previous landers' landings is not publicly available online, then the data found in [11] will be used. The parameter to be used for comparison in the validation of the landing analyses is landing stability performance. This will be done by inputting the same physical characteristics of the lander in [11] in the self made, simplified, landing algorithm, and differences in landing stability, which can be seen by looking at landing success maps, should tell whether the simplified landing algorithm is reliable. For deployment analyses, the deployment mechanics of a simple joint with movable elements that are subject to gravity can be input on abaqus. The deployment behaviour of the joint in Abaqus should be representative of those modelled in Matlab for the articulated mast design, meaning that dimensions, g forces acting upon them and material inputs will be the same. Therefore, parameters related to their deployment performance, such as final locked configuration and deployment time will be compared. If they show similarities, then the model can be considered as validated. At the end of this section of the work, the midterm review session can be done.

Approximate time for this work package: 2 weeks + 1 week buffer time.

Percentage of time allotted with respect to total time for the project: 10 %.

6. **WP6: Model refinement.** After the review, it can be decided how the model can be refined. One possible way the modelling can get refined is by moving to a 3-dimensional environment. Another way would be to analyse another concept for the deployable landing system. In this concept, the structure is going to be idealised as a series of rotational springs and dampers and a series of straight beams. The rotational spring simulate the deploying moment of tape spring hinges while, the straight beams, simulate the presence of non deformable straight elements. The modelling of this concept, as explained in the description of WP3, is taken from [1]. To model the tape spring hinges of this concept, data on the relation between deployment moment and deployment angle can be found online in validated articles such as [5] or even the JAXA paper itself [1]. Comparison of deployment and landing performances between the 2 concepts can be performed in this section. The comparisons will focus on the following performance indicators:

- Mass of the system,
- Maximum stresses reached during deployment and landing, one (or two) components that experience the highest amounts of stresses will be put through FEA for the next work package.
- Deployment time,
- Weight saving achieved compared to a concept that doesn't use the negative g forces of deceleration. The calculation for weight saving in the articulated mast concept has already been explained in WP3. In order to calculate the weight saving for the tape spring hinge LS, it will be simulated first with the negative g forces and secondly without. The model without will need more force given by the properties of CFRP and therefore a thicker layup. The change in weight due to the thicker layup will give an indication on the amount of weight saved by the concept that uses negative g forces.

If enough time is available to investigate on the scalability of the ELLS, another output is a model that relates the relation that there is between that mass of the landing system and the mass of the landed payload. This can be done by keeping the geometry the same once this is validated as a successful one (both in deploying and in landing) and inputting an array of payload masses into the script and seeing the change in landing system mass that achieves a full deployment and the same degree of landing stability as the original solution.

Approximate time for this work package: 5 weeks + 1 week buffer time.

Percentage of time allotted with respect to total time for the project: 20 %.

7. **WP7: FEA of critical components.** Through the algorithm implemented on Matlab, the components that will undergo the highest amounts of stresses will be highlighted. The stresses can come from both the deployment of the landing system and the shocks due to landing, but the landing stresses will be higher than the ones experienced during deployment. These components (a maximum of 2) will be designed in using CAD software SolidWorks and they will be placed in FEM software Abaqus in order to further prove, using detailed finite element analyses, that they will not fail.

As said before, the component that will go through FEA will be the one that experiences the highest amount of stress during either deployment or landing. Verification of FEA results will happen differently

depending on why the component has been put through FEA for this project. If it is due to the highest stresses happening during deployment, the results can be verified by comparing them with those found in one of the articles that detail the stresses reached by a tape spring hinge (since these are the types of deployable that are analysed in this thesis) in, for example, [5]. If the component, more likely, will experience the maximum stress during landing, then the analysis will also be performed using LS-Dyna, since this software is more suitable for shock analyses. If the results in between the 2 software converge, then the results are verified. *Approximate time for this work package:* 3.5 weeks of work + 1 week of buffer time.

Percentage of time allotted with respect to total time for the project: 15 %

8. **WP8: Design guidelines writeup.** From all the analyses above, gather a series of design guidelines that can be employed if a stakeholder would have to manufacture the landing system for the Europa Lander mission. An example of this would be to give a value of leg stiffness that can be reached through the tweaking of the leg's layup in order to be able to land a certain amount of mass while, at the same time, the leg would still be able to be deployable.

Approximate time for this work package: 2 weeks of work + 1 week of buffer time

Percentage of time allotted with respect to total time for the project: 10 %

9. **WP9: Write thesis report and prepare thesis defense.**

Approximate time for this work package: 2 weeks of work + 1 week of buffer time

Percentage of time allotted with respect to total time for the project: 10 %

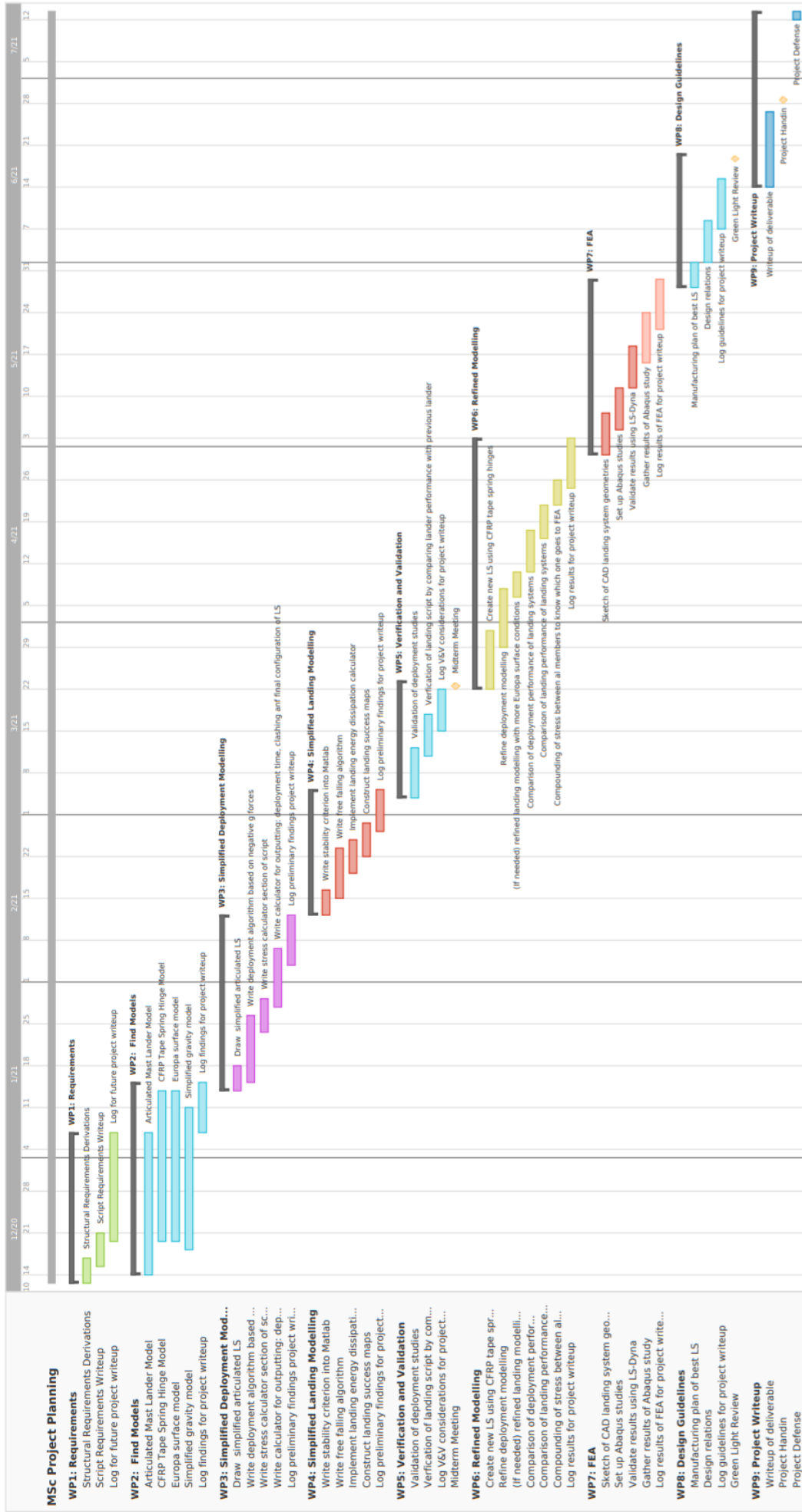
Total time for the project: 30 weeks.

References

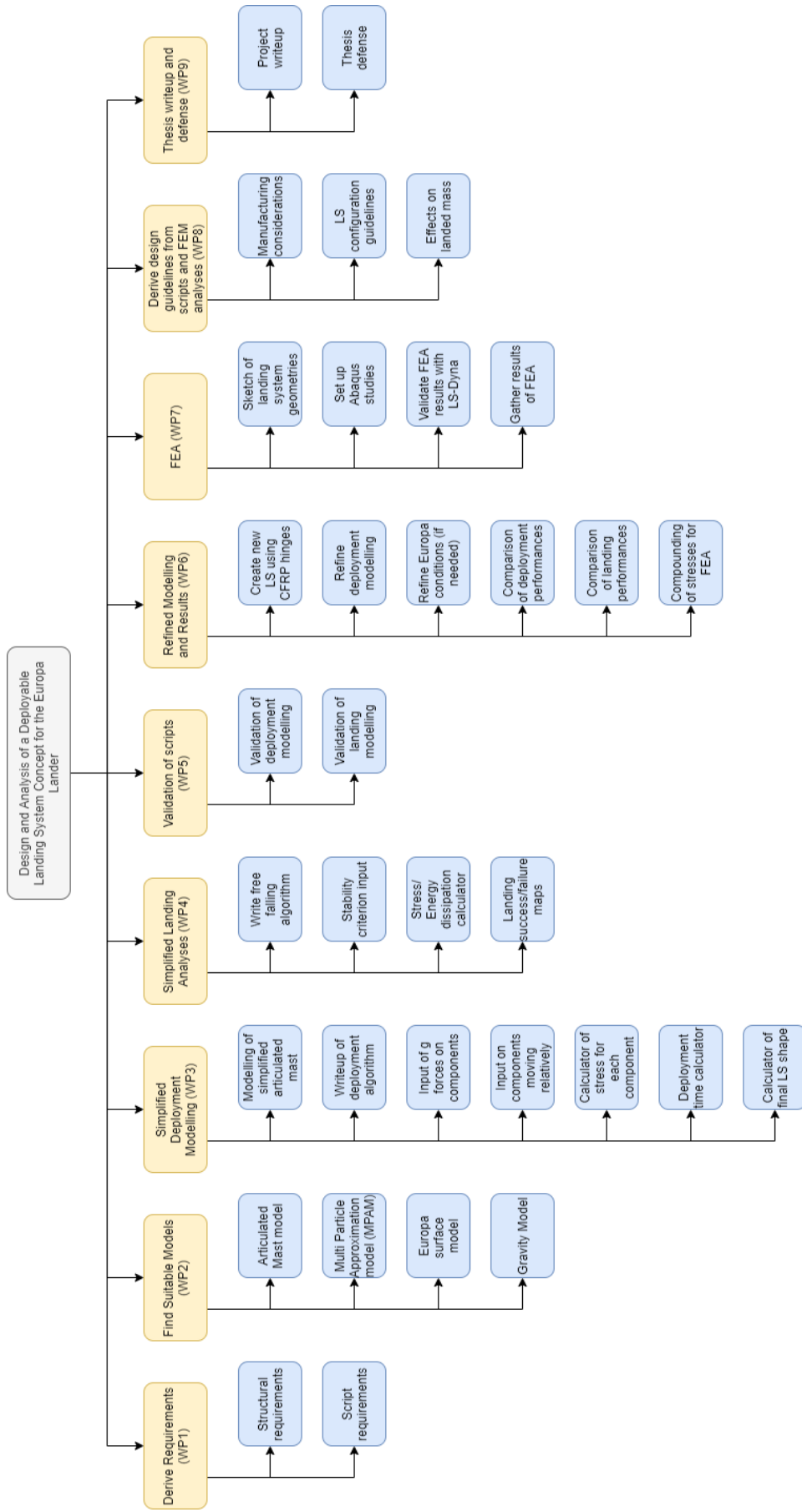
- [1] T. Amamoto, H. Sakamoto, H. Furuya, N. Okuizumi, A. Watanabe, and Nobuyuki Kawabata. "Modeling of Composite Booms' Deployment Dynamics under Microgravity Based on Ground Tests". In: *2018 AIAA Spacecraft Structures Conference*. _eprint: <https://arc.aiaa.org/doi/pdf/10.2514/6.2018-1435>. American Institute of Aeronautics and Astronautics. DOI: [10.2514/6.2018-1435](https://doi.org/10.2514/6.2018-1435). URL: <https://arc.aiaa.org/doi/abs/10.2514/6.2018-1435> (visited on 10/13/2020).
- [2] H. Doiron and G. A. Zupp. *A Mathematical Procedure for Predicting the Touchdown Dynamics of a Soft-Landing Vehicle*. 19710007293. Houston, TX, USA: NASA, Mar. 1, 1971. URL: <https://ntrs.nasa.gov/citations/19710007293>.
- [3] Europa Lander Science Definition Team. *Europa Lander Study 2016 Report*. NASA, Aug. 10, 2017, p. 264. URL: <https://europa.nasa.gov/resources/58/europa-lander-study-2016-report> (visited on 11/17/2020).
- [4] D. Liang, H. Chai, and Tianzhi Chen. "Landing dynamic analysis for landing leg of lunar lander using Abaqus/Explicit". In: *Proceedings of 2011 International Conference on Electronic Mechanical Engineering and Information Technology*. Proceedings of 2011 International Conference on Electronic Mechanical Engineering and Information Technology. Vol. 8. Aug. 2011, pp. 4364–4367. DOI: [10.1109/EMEIT.2011.6023924](https://doi.org/10.1109/EMEIT.2011.6023924).
- [5] C Mallikarachchi and S. Pellegrino. "Deployment Dynamics of Ultrathin Composite Booms with Tape-Spring Hinges". In: *Journal of Spacecraft and Rockets* 51.2 (2014), pp. 604–613. ISSN: 0022-4650. DOI: [10.2514/1.A32401](https://doi.org/10.2514/1.A32401). URL: <https://arc.aiaa.org/doi/abs/10.2514/1.A32401> (visited on 10/13/2020).
- [6] Alex McCalmont. *Europa Lander*. Alex McCalmont. URL: <http://www.alexmcclmont.com/portfolio/europa-lander/> (visited on 01/06/2021).
- [7] Matthew A Simon, Lemuel Carpenter, Glenn Hrinda, Andrew Bergan, Jamshid Samareh, and Anatoli Mitrou. "Application of Composite Materials to Reduce Mass of Internal and External Exploration Habitat Structures". In: (), p. 19.
- [8] Pietro Squillace. *Literature Review: Design and Analysis of a Deployable Landing System Concept for the Europa Lander*. Nov. 22, 2020.
- [9] The Mathworks, Inc. *Simscape Documentation*. URL: <https://www.mathworks.com/help/physmod/simscape/> (visited on 12/11/2020).

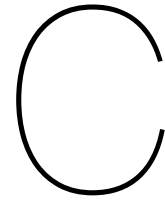
- [10] Y. Wang, R. Liu, H. Yang, Q. Cong, and H. Guo. “Design and Deployment Analysis of Modular Deployable Structure for Large Antennas”. In: *Journal of Spacecraft and Rockets* (July 3, 2015). DOI: [10.2514/1.A33127](https://doi.org/10.2514/1.A33127). URL: https://www.researchgate.net/publication/279805403_Design_and_Deployment_Analysis_of_Modular_Deployable_Structure_for_Large_Antennas.
- [11] R.G. Weixiong. “Preliminary Design of Reusable Lunar Lander Landing System”. MSc Thesis. Lulea University of Technology, 2017. URL: <https://www.diva-portal.org/smash/get/diva2:1159285/FULLTEXT01.pdf>.

A Gantt Chart



B Work Breakdown Structure





Tabulated Data for Future Verification Purposes

In this appendix, the tabulated data used to formulate the verification charts in the thesis is found. The purpose of this section is to simplify the verification process in case it is desired to compare the results found in these thesis with future study ones.

The data used to make Figure 5.4 is found in Table C.1:

Beginning of Table for Data for Figure 5.4			
θ_1 [rad]	$\dot{\theta}_1$ [rad/s]	θ_1 [rad]	$\dot{\theta}_1$ [rad/s]
2.09	0	0.01	0.19
2.05	-0.94	0.03	0.17
1.91	-1.81	0.04	0.14
1.68	-2.61	0.06	0.11
1.38	-3.42	0.06	0.07
0.99	-4.57	0.07	0.03
0.45	-5.89	0.07	-0.01
-0.07	-4.28	0.07	-0.05
-0.44	-3.14	0.06	-0.08
-0.5	-3.02	0.06	-0.09
-0.7	-1.97	0.05	-0.11
-0.83	-0.57	0.04	-0.13
-0.81	0.88	0.02	-0.14
-0.67	1.68	0.01	-0.15
-0.52	1.3	0	-0.14
-0.5	1.24	-0.01	-0.13
-0.4	1.03	-0.02	-0.13
-0.3	0.95	-0.03	-0.11
-0.21	0.87	-0.04	-0.09
-0.13	0.66	-0.05	-0.06
-0.08	0.26	-0.05	-0.03
-0.08	-0.23	-0.05	0.01
-0.12	-0.31	-0.05	0.04
-0.12	0.29	-0.05	0.06
-0.06	0.92	-0.04	0.08
0.06	1.31	-0.03	0.1
0.2	1.42	-0.02	0.11
0.33	1.24	-0.01	0.11

Continuation of Table for Data for Figure 5.4			
θ_1 [rad]	$\dot{\theta}_1$ [rad/s]	θ_1 [rad]	$\dot{\theta}_1$ [rad/s]
0.44	0.8	0	0.11
0.49	0.25	0.01	0.1
0.49	-0.28	0.02	0.08
0.44	-0.7	0.03	0.07
0.35	-0.97	0.04	0.04
0.25	-1.06	0.04	0.02
0.14	-1.01	0.04	0
0.05	-0.87	0.04	-0.02
-0.03	-0.71	0.03	-0.04
-0.1	-0.57	0.03	-0.06
-0.15	-0.49	0.02	-0.07
-0.19	-0.43	0.01	-0.08
-0.23	-0.36	0.01	-0.08
-0.27	-0.26	0	-0.08
-0.29	-0.12	-0.01	-0.07
-0.29	0.04	-0.02	-0.06
-0.28	0.21	-0.02	-0.05
-0.25	0.38	-0.03	-0.03
-0.2	0.51	-0.03	-0.02
-0.15	0.61	-0.03	0
-0.08	0.65	-0.03	0.02
-0.02	0.65	-0.03	0.03
0.05	0.61	-0.02	0.04
0.1	0.53	-0.02	0.05
0.15	0.43	-0.01	0.06
0.19	0.3	-0.01	0.06
0.21	0.17	0	0.06
0.22	0.04	0.01	0.06
0.22	-0.09	0.01	0.05
0.21	-0.2	0.02	0.04
0.18	-0.3	0.02	0.03
0.15	-0.37	0.02	0.01
0.11	-0.43	0.02	0
0.06	-0.45	0.02	-0.01
0.02	-0.46	0.02	-0.02
-0.03	-0.44	0.02	-0.03
-0.07	-0.4	0.01	-0.04
-0.11	-0.33	0.01	-0.04
-0.14	-0.25	0	-0.05
-0.16	-0.16	0	-0.05
-0.17	-0.05	0	-0.04
-0.17	0.05	-0.01	-0.04
-0.16	0.14	-0.01	-0.03
-0.14	0.22	-0.01	-0.02
-0.11	0.28	-0.02	-0.01
-0.08	0.32	-0.02	0
-0.05	0.35	-0.02	0.01
-0.01	0.35	-0.01	0.02
0.02	0.33	-0.01	0.02
0.05	0.3	-0.01	0.03
0.08	0.25	-0.01	0.03
0.1	0.19	0	0.03

Continuation of Table for Data for Figure 5.4			
θ_1 [rad]	$\dot{\theta}_1$ [rad/s]	θ_1 [rad]	$\dot{\theta}_1$ [rad/s]
0.12	0.12	0	0.03
0.12	0.05	0	0.03
0.13	-0.03	0.01	0.03
0.12	-0.1	0.01	0.02
0.11	-0.16	0.01	0.02
0.09	-0.21	0.01	0.01
0.07	-0.24	0.01	0
0.04	-0.26	0.01	-0.01
0.01	-0.26	0.01	-0.01
-0.01	-0.25	0.01	-0.02
-0.04	-0.23	0.01	-0.02
-0.06	-0.19	0.01	-0.02
-0.07	-0.15	0	-0.03
-0.09	-0.09	0	-0.03
-0.09	-0.04	0	-0.02
-0.09	0.02	0	-0.02
-0.09	0.07	-0.01	-0.02
-0.08	0.12	-0.01	-0.01
-0.07	0.15	-0.01	-0.01
-0.05	0.18	-0.01	0
-0.03	0.19	-0.01	0
-0.01	0.2	-0.01	0.01

Table C.1: Tabulated and filtered data for Figure 5.4 .

The data used to make Figure 5.5 is found in Table C.2:

Beginning of Table for Data for Figure 5.5			
Time [s]	θ_1 [rad]	Time [s]	θ_1 [rad]
0	2.09	10.05	0.01
0.1	2.05	10.15	0.03
0.2	1.91	10.25	0.04
0.3	1.68	10.35	0.06
0.4	1.38	10.45	0.06
0.5	0.99	10.55	0.07
0.6	0.45	10.65	0.07
0.7	-0.07	10.75	0.07
0.8	-0.44	10.85	0.06
0.9	-0.7	10.95	0.05
1.01	-0.83	11.06	0.04
1.11	-0.81	11.16	0.02
1.21	-0.67	11.26	0.01
1.31	-0.52	11.36	0
1.41	-0.4	11.46	-0.02
1.51	-0.3	11.56	-0.03
1.61	-0.21	11.66	-0.04
1.71	-0.13	11.76	-0.05
1.81	-0.08	11.86	-0.05
1.91	-0.08	11.96	-0.05
2.01	-0.12	12.06	-0.05
2.11	-0.12	12.16	-0.05
2.21	-0.06	12.26	-0.04

Continuation of Table for Data for Figure 5.5			
Time [s]	θ_1 [rad]	Time [s]	θ_1 [rad]
2.31	0.06	12.36	-0.03
2.41	0.2	12.46	-0.02
2.51	0.33	12.56	-0.01
2.61	0.44	12.66	0
2.71	0.49	12.76	0.01
2.81	0.49	12.86	0.02
2.91	0.44	12.96	0.03
3.02	0.35	13.07	0.04
3.12	0.25	13.17	0.04
3.22	0.14	13.27	0.04
3.32	0.05	13.37	0.04
3.42	-0.03	13.47	0.03
3.52	-0.1	13.57	0.03
3.62	-0.15	13.67	0.02
3.72	-0.19	13.77	0.01
3.82	-0.23	13.87	0.01
3.92	-0.27	13.97	0
4.02	-0.29	14.07	-0.01
4.12	-0.29	14.17	-0.02
4.22	-0.28	14.27	-0.02
4.32	-0.25	14.37	-0.03
4.42	-0.2	14.47	-0.03
4.52	-0.15	14.57	-0.03
4.62	-0.08	14.67	-0.03
4.72	-0.02	14.77	-0.03
4.82	0.05	14.87	-0.02
4.92	0.1	14.97	-0.02
5.03	0.15	15.08	-0.01
5.13	0.19	15.18	-0.01
5.23	0.21	15.28	0
5.33	0.22	15.38	0.01
5.43	0.22	15.48	0.01
5.53	0.21	15.58	0.02
5.63	0.18	15.68	0.02
5.73	0.15	15.78	0.02
5.83	0.11	15.88	0.02
5.93	0.06	15.98	0.02
6.03	0.02	16.08	0.02
6.13	-0.03	16.18	0.02
6.23	-0.07	16.28	0.01
6.33	-0.11	16.38	0.01
6.43	-0.14	16.48	0
6.53	-0.16	16.58	0
6.63	-0.17	16.68	0
6.73	-0.17	16.78	-0.01
6.83	-0.16	16.88	-0.01
6.93	-0.14	16.98	-0.01
7.04	-0.11	17.09	-0.02
7.14	-0.08	17.19	-0.02
7.24	-0.05	17.29	-0.02
7.34	-0.01	17.39	-0.01
7.44	0.02	17.49	-0.01

Continuation of Table for Data for Figure 5.5			
Time [s]	θ_1 [rad]	Time [s]	θ_1 [rad]
7.54	0.05	17.59	-0.01
7.64	0.08	17.69	-0.01
7.74	0.1	17.79	0
7.84	0.12	17.89	0
7.94	0.12	17.99	0
8.04	0.13	18.09	0.01
8.14	0.12	18.19	0.01
8.24	0.11	18.29	0.01
8.34	0.09	18.39	0.01
8.44	0.07	18.49	0.01
8.54	0.04	18.59	0.01
8.64	0.01	18.69	0.01
8.74	-0.01	18.79	0.01
8.84	-0.04	18.89	0.01
8.94	-0.06	18.99	0.01
9.05	-0.07	19.1	0
9.15	-0.09	19.2	0
9.25	-0.09	19.3	0
9.35	-0.09	19.4	0
9.45	-0.09	19.5	-0.01
9.55	-0.08	19.6	-0.01
9.65	-0.07	19.7	-0.01
9.75	-0.05	19.8	-0.01
9.85	-0.03	19.9	-0.01
9.95	-0.01	20	-0.01

Table C.2: Tabulated and filtered data for Figure 5.5 .

The data used to make Figure 5.9 is found in Table C.3:

Beginning of Table for Data for Figure 5.9					
θ_1 [rad]	$\dot{\theta}_1$ [rad/s]	θ_1 [rad]	$\dot{\theta}_1$ [rad/s]	θ_1 [rad]	$\dot{\theta}_1$ [rad/s]
2.09	0	0.24	0.58	0.06	0.16
1.9	-1.92	0.23	-0.6	0.08	0.05
1.33	-3.77	-0.01	-1.73	0.07	-0.19
0.23	-6.72	-0.33	-0.99	0.01	-0.31
-0.79	-4.12	-0.37	0.47	-0.04	-0.22
-1.34	-0.99	-0.14	1.79	-0.07	-0.02
-1.1	3.53	0.22	1.37	-0.06	0.09
-0.5	2.42	0.36	0.03	-0.04	0.05
0.04	3.22	0.22	-1.35	-0.04	-0.02
0.75	3.45	-0.07	-1.14	-0.04	0.03
1.24	0.99	-0.19	-0.08	-0.02	0.18
1.09	-2.53	-0.09	1.03	0.03	0.26
0.17	-4.28	0.14	0.91	0.07	0.15
-0.5	-3.02	0.21	-0.27	0.08	-0.05
-1.07	-2.44	0.05	-1.29	0.06	-0.18
-1.38	-0.43	-0.23	-1.12	0.02	-0.15
-1.22	1.99	-0.33	0.17	0	-0.06
-0.47	6.06	-0.17	1.34	-0.01	-0.05
0.44	3.46	0.11	1.19	-0.02	-0.12
1.06	2.55	0.24	0.09	-0.05	-0.14

Continuation of Table for Data for Figure 5.9					
θ_1 [rad]	$\dot{\theta}_1$ [rad/s]	θ_1 [rad]	$\dot{\theta}_1$ [rad/s]	θ_1 [rad]	$\dot{\theta}_1$ [rad/s]
1.36	0.31	0.15	-0.98	-0.07	-0.04
1.15	-2.55	-0.05	-0.73	-0.07	0.13
0.3	-4.3	-0.11	0.17	-0.03	0.23
-0.41	-3.17	0.01	0.95	0.02	0.18
-0.95	-1.86	0.19	0.52	0.04	0.07
-1.03	1.21	0.18	-0.55	0.05	0
-0.39	3.82	-0.01	-1.26	0.05	0.01
0.16	2.22	-0.23	-0.68	0.05	0.02
0.59	2.05	-0.25	0.42	0.05	-0.05
0.9	0.84	-0.08	1.08	0.03	-0.16
0.85	-1.47	0.09	0.54	-0.01	-0.21
0.18	-4.93	0.11	-0.32	-0.05	-0.14
-0.45	-2.02	-0.01	-0.71	-0.07	-0.01
-0.76	-1.13	-0.09	-0.04	-0.06	0.09
-0.89	-0.05	-0.02	0.7	-0.04	0.09
-0.75	1.43	0.15	0.77	-0.02	0.07
-0.22	4.48	0.22	-0.08	-0.01	0.08
0.55	2.24	0.12	-0.9	0.02	0.13
0.83	0.66	-0.08	-0.85	0.04	0.14
0.84	-0.52	-0.17	-0.06	0.06	0.06
0.63	-1.64	-0.11	0.62	0.06	-0.08
0.11	-4.02	0.01	0.43	0.04	-0.16
-0.64	-2.13	0.03	-0.19	0.01	-0.15
-0.86	-0.22	-0.05	-0.56	-0.02	-0.09
-0.77	1.05	-0.13	-0.1	-0.03	-0.05
-0.45	2.14	-0.08	0.6	-0.04	-0.05
0.2	4.55	0.08	0.8	-0.05	-0.03
0.78	1.4	0.19	0.21	-0.05	0.04
0.88	-0.33	0.15	-0.52	-0.04	0.13
0.68	-1.62	0.02	-0.64	0	0.18
0.21	-3.37	-0.06	-0.14	0.03	0.14
-0.56	-2.67	-0.04	0.34	0.05	0.05
-0.87	-0.65	0.03	0.21	0.05	-0.02
-0.85	0.85	0.02	-0.3	0.04	-0.05
-0.53	2.5	-0.07	-0.57	0.03	-0.06
0.21	3.71	-0.16	-0.19	0.02	-0.09
0.7	1.48	-0.13	0.44	0	-0.13
0.85	0.02	-0.01	0.68	-0.03	-0.14
0.68	-1.75	0.1	0.29	-0.05	-0.07
0.07	-3.81	0.1	-0.23	-0.06	0.03
-0.46	-1.74	0.04	-0.32	-0.04	0.1
-0.68	-0.5	0	0.02	-0.02	0.12
-0.63	1.19	0.04	0.31	0	0.1
-0.12	3.47	0.1	0.13	0.02	0.08
0.35	1.42	0.07	-0.35	0.03	0.08
0.52	0.37	-0.03	-0.58	0.05	0.05
0.48	-0.89	-0.12	-0.29	0.05	-0.01
0.08	-3.22	-0.13	0.21	0.04	-0.1
-0.39	-1.22	-0.06	0.42	0.02	-0.14
-0.49	0.1	0.01	0.18	-0.01	-0.13
-0.37	1.17	0.01	-0.13	-0.03	-0.08
0.03	3.02	-0.02	-0.11	-0.04	-0.03

Continuation of Table for Data for Figure 5.9					
θ_1 [rad]	$\dot{\theta}_1$ [rad/s]	θ_1 [rad]	$\dot{\theta}_1$ [rad/s]	θ_1 [rad]	$\dot{\theta}_1$ [rad/s]
0.51	1.22	-0.01	0.21	-0.04	0
0.58	-0.39	0.05	0.4	-0.04	0.04
0.37	-1.74	0.12	0.19	-0.03	0.08
-0.16	-3.18	0.12	-0.24	-0.01	0.12
-0.58	-1.08	0.04	-0.46	0.02	0.13
-0.63	0.47	-0.04	-0.27	0.04	0.09
-0.37	2.26	-0.06	0.05	0.05	0.01
0.19	2.35	-0.04	0.14	0.05	-0.05
0.49	0.79	-0.02	-0.04	0.03	-0.08
0.51	-0.68	-0.05	-0.2	0.01	-0.09
0.17	-2.6	-0.09	-0.08	0	-0.1
-0.23	-1.22	-0.07	0.25	-0.02	-0.1
-0.36	-0.08	0	0.42	-0.04	-0.07
-0.25	1.28	0.08	0.26	-0.05	-0.01
0.15	2.01	0.1	-0.07	-0.04	0.06
0.36	0.26	0.06	-0.23	-0.03	0.11
0.3	-0.92	0.03	-0.12	0	0.11
-0.02	-2.29	0.02	0.05	0.02	0.09
-0.42	-1.12	0.03	0.01	0.03	0.06
-0.48	0.45	0.01	-0.2	0.04	0.03
-0.24	1.98	-0.04	-0.31	0.04	-0.01
0.22	1.93	-0.09	-0.16	0.04	-0.06
0.45	0.4	-0.1	0.13	0.02	-0.11
0.38	-1.15	-0.05	0.3	0	-0.12
0.02	-1.95	0	0.21	-0.03	-0.09
-0.24	-0.67	0.03	0.03	-0.04	-0.04
-0.26	0.51	0.02	-0.02	-0.04	0.01
-0.02	1.77	0.03	0.08	-0.04	0.05

Table C.3: Tabulated and filtered data for Figure 5.9 .

The data used to make Figure 5.10 is found in Table C.4:

Beginning of Table for Data for Figure 5.10					
Time [s]	θ_1 [rad]	Time [s]	θ_1 [rad]	Time [s]	θ_1 [rad]
0	2.09	20.07	0.24	40.13	0.06
0.2	1.9	20.27	0.23	40.33	0.08
0.4	1.33	20.47	-0.01	40.54	0.07
0.6	0.23	20.67	-0.33	40.74	0.01
0.8	-0.79	20.87	-0.37	40.94	-0.04
1	-1.34	21.07	-0.14	41.14	-0.07
1.2	-1.1	21.27	0.22	41.34	-0.06
1.4	-0.5	21.47	0.36	41.54	-0.04
1.61	0.04	21.67	0.22	41.74	-0.04
1.81	0.75	21.87	-0.07	41.94	-0.04
2.01	1.24	22.07	-0.19	42.14	-0.02
2.21	1.09	22.27	-0.09	42.34	0.03
2.41	0.17	22.47	0.14	42.54	0.07
2.61	-0.5	22.68	0.21	42.74	0.08
2.81	-1.07	22.88	0.05	42.94	0.06
3.01	-1.38	23.08	-0.23	43.14	0.02
3.21	-1.22	23.28	-0.33	43.34	0

Continuation of Table for Data for Figure 5.10					
Time [s]	θ_1 [rad]	Time [s]	θ_1 [rad]	Time [s]	θ_1 [rad]
3.41	-0.47	23.48	-0.17	43.55	-0.01
3.61	0.44	23.68	0.11	43.75	-0.02
3.81	1.06	23.88	0.24	43.95	-0.05
4.01	1.36	24.08	0.15	44.15	-0.07
4.21	1.15	24.28	-0.05	44.35	-0.07
4.26	1.01	24.33	-0.08	44.41	-0.06
4.41	0.3	24.48	-0.11	44.55	-0.03
4.62	-0.41	24.68	0.01	44.75	0.02
4.82	-0.95	24.88	0.19	44.95	0.04
5.02	-1.03	25.08	0.18	45.15	0.05
5.22	-0.39	25.28	-0.01	45.35	0.05
5.42	0.16	25.48	-0.23	45.55	0.05
5.62	0.59	25.69	-0.25	45.75	0.05
5.82	0.9	25.89	-0.08	45.95	0.03
6.02	0.85	26.09	0.09	46.15	-0.01
6.22	0.18	26.29	0.11	46.35	-0.05
6.42	-0.45	26.49	-0.01	46.56	-0.07
6.62	-0.76	26.69	-0.09	46.76	-0.06
6.82	-0.89	26.89	-0.02	46.96	-0.04
7.02	-0.75	27.09	0.15	47.16	-0.02
7.22	-0.22	27.29	0.22	47.36	-0.01
7.42	0.55	27.49	0.12	47.56	0.02
7.63	0.83	27.69	-0.08	47.76	0.04
7.83	0.84	27.89	-0.17	47.96	0.06
8.03	0.63	28.09	-0.11	48.16	0.06
8.23	0.11	28.29	0.01	48.36	0.04
8.43	-0.64	28.49	0.03	48.56	0.01
8.63	-0.86	28.7	-0.05	48.76	-0.02
8.83	-0.77	28.9	-0.13	48.96	-0.03
9.03	-0.45	29.1	-0.08	49.16	-0.04
9.23	0.2	29.3	0.08	49.36	-0.05
9.43	0.78	29.5	0.19	49.57	-0.05
9.63	0.88	29.7	0.15	49.77	-0.04
9.83	0.68	29.9	0.02	49.97	0
10.03	0.21	30.1	-0.06	50.17	0.03
10.23	-0.56	30.3	-0.04	50.37	0.05
10.43	-0.87	30.5	0.03	50.57	0.05
10.64	-0.85	30.7	0.02	50.77	0.04
10.84	-0.53	30.9	-0.07	50.97	0.03
11.04	0.21	31.1	-0.16	51.17	0.02
11.24	0.7	31.3	-0.13	51.37	0
11.44	0.85	31.51	-0.01	51.57	-0.03
11.64	0.68	31.71	0.1	51.77	-0.05
11.84	0.07	31.91	0.1	51.97	-0.06
12.04	-0.46	32.11	0.04	52.17	-0.04
12.24	-0.68	32.31	0	52.37	-0.02
12.44	-0.63	32.51	0.04	52.58	0
12.64	-0.12	32.71	0.1	52.78	0.02
12.84	0.35	32.91	0.07	52.98	0.03
13.04	0.52	33.11	-0.03	53.18	0.05
13.24	0.48	33.31	-0.12	53.38	0.05
13.44	0.08	33.51	-0.13	53.58	0.04

Continuation of Table for Data for Figure 5.10					
Time [s]	θ_1 [rad]	Time [s]	θ_1 [rad]	Time [s]	θ_1 [rad]
13.65	-0.39	33.71	-0.06	53.78	0.02
13.85	-0.49	33.91	0.01	53.98	-0.01
14.05	-0.37	34.11	0.01	54.18	-0.03
14.25	0.03	34.31	-0.02	54.38	-0.04
14.45	0.51	34.52	-0.01	54.58	-0.04
14.65	0.58	34.72	0.05	54.78	-0.04
14.85	0.37	34.92	0.12	54.98	-0.03
15.05	-0.16	35.12	0.12	55.18	-0.01
15.25	-0.58	35.32	0.04	55.38	0.02
15.45	-0.63	35.52	-0.04	55.59	0.04
15.65	-0.37	35.72	-0.06	55.79	0.05
15.85	0.19	35.92	-0.04	55.99	0.05
16.05	0.49	36.12	-0.02	56.19	0.03
16.25	0.51	36.32	-0.05	56.39	0.01
16.45	0.17	36.52	-0.09	56.59	0
16.66	-0.23	36.72	-0.07	56.79	-0.02
16.86	-0.36	36.92	0	56.99	-0.04
17.06	-0.25	37.12	0.08	57.19	-0.05
17.26	0.15	37.32	0.1	57.39	-0.04
17.46	0.36	37.53	0.06	57.59	-0.03
17.66	0.3	37.73	0.03	57.79	0
17.86	-0.02	37.93	0.02	57.99	0.02
18.06	-0.42	38.13	0.03	58.19	0.03
18.26	-0.48	38.33	0.01	58.39	0.04
18.46	-0.24	38.53	-0.04	58.6	0.04
18.66	0.22	38.73	-0.09	58.8	0.04
18.86	0.45	38.93	-0.1	59	0.02
19.06	0.38	39.13	-0.05	59.2	0
19.26	0.02	39.33	0	59.4	-0.03
19.46	-0.24	39.53	0.03	59.6	-0.04
19.67	-0.26	39.73	0.02	59.8	-0.04
19.87	-0.02	39.93	0.03	60	-0.04

Table C.4: Tabulated and filtered data for Figure 5.10 .